Junctional remodeling during angiogenesis: The role of Claudin5 during ISV formation in Zebrafish

Inauguraldissertation

zur

Erlangung der Würde eines Doktors der Philosophie

vorgelegt der

Philosophisch-Naturwissenschaftlichen Fakultät

der Universität Basel

von

Alice Krudewig

aus

Bocholt, Deutschland

Basel, im Mai 2012

Originaldokument gespeichert auf dem Dokumentenserver der Universität Basel**edoc.unibas.ch**

Dieses Werk ist unter dem Vertrag „Creative Commons Namensnennung-Keine kommerzielle Nutzung-Keine Bearbeitung 2.5 Schweiz“ lizenziert. Die vollständige Lizenz kann unter **creativecommons.org/licences/by-nc-nd/2.5/ch**eingesehen werden.

creative commons

Namensnennung-Keine kommerzielle Nutzung-Keine Bearbeitung 2.5 Schweiz

---

Sie dürfen:

das Werk vervielfältigen, verbreiten und öffentlich zugänglich machen

Zu den folgenden Bedingungen:

Namensnennung. Sie müssen den Namen des Autors/Rechteinhabers in der von ihm festgelegten Weise nennen (wodurch aber nicht der Eindruck entstehen darf, Sie oder die Nutzung des Werkes durch Sie würden entlohnt).

Keine kommerzielle Nutzung. Dieses Werk darf nicht für kommerzielle Zwecke verwendet werden.

Keine Bearbeitung. Dieses Werk darf nicht bearbeitet oder in anderer Weise verändert werden.

- Im Falle einer Verbreitung müssen Sie anderen die Lizenzbedingungen, unter welche dieses Werk fällt, mitteilen. Am Einfachsten ist es, einen Link auf diese Seite einzubinden.
- Jede der vorgenannten Bedingungen kann aufgehoben werden, sofern Sie die Einwilligung des Rechteinhabers dazu erhalten.
- Diese Lizenz lässt die Urheberpersönlichkeitsrechte unberührt.

Die gesetzlichen Schranken des Urheberrechts bleiben hiervon unberührt.

Die Commons Deed ist eine Zusammenfassung des Lizenzvertrags in allgemeinverständlicher Sprache: http://creativecommons.org/licenses/by-nc-nd/2.5/ch/legalcode.de

Haftungsausschluss:
Die Commons Deed ist kein Lizenzvertrag. Sie ist lediglich ein Referenztext, der den zugrundeliegenden Lizenzvertrag übersichtlich und in allgemeinverständlicher Sprache wiedergibt. Die Deed selbst entfaltet keine juristische Wirkung und erscheint im eigentlichen Lizenzvertrag nicht. Creative Commons ist keine Rechtsanwaltsgesellschaft und leistet keine Rechtsberatung. Die Weitergabe und Verlinkung des Commons Deeds führt zu keinem Mandatsverhältnis.

Quelle: http://creativecommons.org/licenses/by-nc-nd/2.5/ch/ Datum: 3.4.2009

Genehmigt von der Philosophisch-Naturwissenschaftlichen Fakultät auf Antrag von

Prof. Dr. Markus Affolter (Dissertationsleiter)	Prof. Dr. Rolf Zeller (Koreferent)

Basel, den 20.09.2011

Prof. Dr. Martin Spiess
(Dekan)

1. LIST OF ABBREVIATIONS 1

2. ABSTRACT 4

3. INTRODUCTION 5

3.1 Vascular development 9
3.1.1 Vasculogenesis – formation of the dorsal aorta and posterior cardinal vein 9
3.1.1.1 Differentiation of endothelial cells 9
3.1.1.2 Aorta and venous tube formation 10
3.1.1.3 Arterial-venous differentiation 12
3.1.2 Angiogenic network formation 13
3.1.2.1 ISV formation via the process of angiogenesis 13
3.1.2.2 Molecular regulation of sprout formation and outgrowth 15
3.2.2.4 Tip cell selection 17
3.2.2.3 Environmental cues and endothelial pathfinding 19
3.2 Junctional proteins in development 21
3.2.1 Junctional proteins in endothelial cells 21
3.2.2 The formation of an epithelium 23
3.2.3 Junctional remodeling as a driving force for morphogenesis 25
3.2.4 The role of VE-Cadherin in morphogenesis 26
3.2.5 Claudins seal epithelia 27
3.2.6 The role of Claudins in morphogenesis 29
3.3 Aim of the thesis 30

4. MATERIALS AND METHODS 31

4.1 Companies 31
4.2 Buffer, Media and Solutions 31
4.3 Molecular Biology Protocols 35
4.3.1 Bacteria strains 35
4.3.2 Plasmids and cDNA clones 35
4.3.3 PCR amplification 37
4.3.4 Restriction enzyme digestion and gel extraction 37
4.3.5 Ligation and transformation 37
4.3.6 Generation of plasmids via the Gateway system 38
4.3.6.1 Generation of Entry clones 38
4.3.6.2 Generation of Expression clones 38
4.3.6.3 Generation of Tol2 mRNA 38
4.3.7 Generation of mRNA 39
4.3.8 Genotyping 39
4.3.8.1 Fin clips 39
4.3.8.2 Genomic DNA extraction 39
4.3.8.3 PCR on genomic DNA 40
4.3.8.4 Restriction enzyme digestion 40
4.4 Immunohistochemistry and in situ hybridization 40
4.4.1 Immunofluorescence whole mount antibody staining 40
4.4.1.1 Primary antibodies 40
4.4.1.2 Secondary antibodies (all Invitrogen) 41
4.4.1.3 Immunofluorescence whole mount antibody staining 41
4.4.2 Vibratom Sectioning and Antibody Stainings on Sections 42
4.4.3 Whole-Mount in situ Hybridization 43
4.4.4 Double whole-mount FISH using Alexa Tyramides 45

4.5 Fish lines, maintenance and handling....46
4.5.1 Fish maintenance....46
4.5.2 Fish lines....46
4.5.3 DNA/RNA and morpholino injection....47
4.5.4 Generation of transgenic fish lines....47
4.6 Confocal microscopy....48
4.6.1 Mounting and confocal microscopy of fixed embryos....48
4.6.2 Mounting and confocal live imaging of living embryos....48

5. RESULTS....49

5.1 Contributions to publications....49
5.1.1 49
Distinct cellular mechanisms contribute to vessel anastomosis and lumen formation in the zebrafish DLAVs....49
5.1.2 72
Semaphorin-PlexinD1 Signaling Limits Angiogenic Potential via the VEGF Decoy Receptor sFlt1....72
5.1.3 74
The novel transmembrane protein Tmem2 is essential for coordination of myocardial and endocardial morphogenesis....74
5.2 Generation of transgenic fish lines using the Gateway®/Tol2 system....76
5.3 *Cldn5b* is a vascular-specific gene....83
5.4 Analysis of the effects of *cldn5b* knock-down on angiogenesis....88
5.4.1 Leaky vessels in *cldn5b* knock-down embryos cause hemorrhages....95
5.4.2 *Cldn5b* is required for vessel outgrowth and stability....100
5.4.3 *Cldn5b* and *cldn5a* do not function redundantly during ISV formation....106
5.5 Normal cellular rearrangement in *cldn5b* morphants....110
5.6 Expression of Cldn5b:EGFP does not rescue the morphant phenotype....111
5.7 Reduced cell number and cell proliferation in *cldn5b* morphants – a cause for ISV formation defects?....118
5.8 VE-cadherin is necessary for cell rearrangement during ISV formation....121
5.8.1 *VE-cadherin* and *Claudin5* function non-redundantly during ISV formation....123
5.8.2 VE-cadherin does not influence Cldn5 expression and localization *in vivo*....125
5.9 Generation and analysis of a *cldn5b* mutant....127
5.9.1 Efficient knock-out in *cldn5b* mutants....129
5.9.2 *Cldn5b* mutant embryos show an overall normal anatomy....130
5.9.3 ISVs develop normally in *cldn5b* mutants....133
5.9.4 *Cldn5b* is not required for the organization of ZO-1....137
5.9.5 The *cldn5b* mutant phenotype cannot be enhanced by additional *cldn5b* MO knock-down....139
5.9.6 *Cldn5a* knock-down does not cause any angiogenesis phenotype in *cldn5b* mutants....142

6. DISCUSSION....146

6.1 Dynamics of Cldn5b protein expression correlate with the need for adhesion during ISV outgrowth....146
6.2 Cldn5b and VE-cadherin have different expression patterns and functions....151
6.3 *Cldn5b* mutants lack a clear angiogenesis phenotype....154
6.4 Conclusions....158

7. CONTRIBUTION TO FURTHER PUBLICATION....159

Vascular morphogenesis in the zebrafish embryo....159

8. SUPPLEMENTARY DATA 161

8.1 Supplementary Figures 161
8.2 Supplementary Lists 166
8.2.1 Supplementary list 1 of primers 166
8.2.2 Supplementary list 2 of morpholinos 166

9. APPENDIX 167

9.1 Generation of the *fli1ep*:gal4ff construct 167
9.2 Generation of the *fli1ep*:nlsmCherry construct 168
9.3 Generation of the UAS:*cldn5b*:EGFP construct 169

10. REFERENCES 170

1. List of abbreviations

A	Adenin
AJ	adherens junctions
attB	bacterial attachment site
attP	phage attachment site
BCIP	5-bromo-4-chloro-3`-indolyphosphate p-toluidine salt
BSA	bovine serum albumine
C	Cytosin
Cldn	Claudin
CV	caudal vein
DA	dorsal aorta
ddH_2O	double-destilled water
DIG	digoxigenin
DLAV	dorsal longitudinal anastomotic vessel
DMSO	dimethylsulfoxid
DNA	deoxyribonucleic acid
dNTP	deoxyribonucleotide
dpf	days post fertilization
EC	endothelial cell
EDTA	ethylenediaminetetraacetic acid
EGFP	enhanced green fluorescent protein
EVL	enveloping layer
FITC	fluorescein isothiocyanate
fli	Friend leukemia integration
flk	Fetal liver kinase
flt	Fms related tyrosin kinase
G	Guanosine
h	hours
HMF	horizontal myoseptum
hpf	hours post fertilization
Hyb	hybridization
ISV	intersegemental vessel

kdr	Kinase insert domain receptor
LB medium	lysogeny-broth medium
LDA	lateral dorsal aorta
mg	milligram
µg	microgram
ml	milliliter
µl	microliter
MO	morpholino
mRNA	message Ribonucleic acid
NBT	nitro-blue tetrazolium chloride
NEB	New England Biolab
ON	over night
PBDT	phosphate-buffered saline-DMSO-Tween20
PBS	phosphate-buffered saline
PBST	phosphate-buffered saline-Tween 20
PBSTX	phosphate-buffered saline-Tween 20- Triton-X 100
PCR	polymerase chain reaction
PCV	posterior cardinal vein
PFA	paraformaldehyde
PTU	propylthiouracil
RNA	ribonucleic acid
RT	room temperature
SA	segmental artery
SDS	sodium dodecyl sulfate
SJ	septate junctions
SSC	saline sodium citrate
SSCT	SSC with
SV	segmental vein
SV40	simian virus 40
T	Thymin
TER	trans epithelial resistance
TJ	tight junctions
TSA	Tyramide Signal Amplification
TSS	Transformation and Storage Solution

VE-cadherin (VE-cad)	Vascular endothelial cadherin
VEGF	Vascular endothelial growth factor
VEGFR	Vascular endothelial growth factor receptor
Wnt	Wingless-type MMTV integration site family member
ZO	Zonula occludens
ZONAB	ZO-1–associated nucleic acid binding proteins

2. Abstract

During sprouting angiogenesis several cellular activities are required such as cell shape changes, cell migration, cell proliferation and cell rearrangement. These processes have to be tightly regulated in order to allow cellular dynamics on one side and maintain tissue integrity on the other side. Cell-cell contacts are the main mediators of dynamic cell behaviors during morphogenesis. These contacts are composed of adherens and tight junctions.

To better understand the role of tight junctions during the morphogenetic events of angiogenesis, I have analyzed the function of the endothelial specific Cldn5b during the process of intersegmental vessel (ISV) formation. Although MO-mediated knock-down of *cldn5b* does not alter the initial outgrowth of endothelial cells (ECs) from the dorsal aorta (DA), it does lead to a halt of EC migration at the level of the horizontal myoseptum (HMS). Furthermore, neighboring ISVs do not connect within the dorsal-longitudinal-anastomotic vessel (DLAV) and detach from the DA. In contrast, the adherens junction specific protein VE-cadherin rather exerts a cell rearrangement function. The different expression pattern of Cldn5b and VE-cadherin support these findings. While VE-cadherin is expressed in every EC of the ISV, Cldn5b is temporally downregulated in early sprouting ECs. Furthermore, a clear reduction of cell number in the ISVs was observed in *cldn5b* morphants. The latter observation, together with a possible reduction in adhesion between ECs, is suggested to cause the phenotypes observed in *cldn5b* knock-down embryos. Together, this study suggests for the first time a possible role of a Cldn during a morphogenetic event.

Additionally, I generated mutant fish lacking *cldn5b* gene function by using Zinc-Finger Nucleases. The analysis of these mutant fish will help to understand the functional role of a core component of tight junctions during vertebrate blood vessel development. However, the preliminary analysis shows only a very weak ISV phenotype compared to *cldn5b* morphants. I will discuss several ideas explaining the discrepancy between *cldn5b* morphants and mutants.

3. Introduction

The development of specialized organs is a hallmark of multicellular animal evolution. The development of tubular organs brought the advantage of improved physiological processes and environmental adaptation. Tubular organs like the tracheal system in *Drosophila melanogaster* (*Drosophila*), the kidney, lung, mammary gland and the vasculature of vertebrates serve the transport of liquids and gases throughout the body. During development, these organs increase their surface area in a process known as branching morphogenesis, which in turn leads to the optimization of exchange between these organs and the body. The branching of some tubular organs is very stereotypical with branches always at the exact same positions. For instance, although the branchial tree in the mammalian lung consists of thousands of airway branches, it was shown that early the mouse lung has a reproducible architecture (Metzger et al., 2008). In other organs branching is rather stochastic as for example in the mammary gland (Watson and Khaled, 2008).
Several studies have started to address interesting questions regarding the nature of branch formation. What drives branch formation? Where and when are branches initiated? How do branches extend in length? Which molecules are required for branch formation? Some aspects of branch formation were found to be similar among many branched tubular organs including the initiation of branch formation. Here, local extrinsic signaling cues are involved. For example, in the tracheal system of *Drosophila*, the epithelial cells express the fibroblast-growth factor receptor Breathless (Btl), which senses its ligand Branchless (Bnl) expressed in the surrounding tissue (Ghabrial and Krasnow, 2006; Klambt et al., 1992; Sutherland et al., 1996). The formation of the vasculature or the branchial trees of the lung also depends on extrinsic signaling cues like Vascular endothelial growth factor (Vegf) and Fibroblast-growth factor 10 (Fgf10), respectively (Bellusci et al., 1997; Cardoso and Lu, 2006; Coultas et al., 2005; Leung et al., 1989). Upon activation of the respective signaling pathways, some epithelial cells send out filopodia and start to migrate towards the ligand source. Some cells adopt the identity of a tip cell and drive the migration and elongation processes forward. The other

cells become stalk cells, which are less responsive to the signaling cue. Such behavior can be observed in the fly tracheal system during the highly stereotypic process of dorsal branch intercalation. In this case tip cells at the top of the branch create the pulling force driving dorsal migration (Caussinus et al., 2008; Ribeiro et al., 2004). Although the details of branch formation in every tubular organ are different, all of these organs have several cellular activities in common. These are the migration of cells, their proliferation as well as the cell shape changes and the rearrangement of cells within the branch.

One branched tubular organ, which is especially well suited for the analysis of branch formation is the vascular system. It consists of different kind of tubes of certain architecture that are highly ramified and interconnected. The vascular system is the first organ to arise in vertebrates. It serves the transport of nutrients, gases and metabolic wastes, but it is also required for hormonal communication and immune responses of the body. Furthermore, the functionality of the vasculature is crucial for the development and function of most other organs. Defects in the vasculature often lead to a delay and abnormal development of other organs, which can lead to embryonic death.

In humans the cardiovascular system is divided into the pulmonary circulation and the systemic circulation. In the pulmonary circulation, oxygen deprived blood from the body enters the heart through the *vena cava* and flows from there through the pulmonary arteries to the lung. From here the oxygenated blood goes back to the heart through the pulmonary veins, from where it flows to the rest of the body through the aorta. In the systemic circulation oxygenated blood is pumped through the body vessels. The oxygen depleted blood flows then back to the heart. Certain prerequisites are needed for the different vessels to function properly. The aorta, which has to stand high pressure and carries large volumes of blood, consists of a wall of many cell layers in thickness and is outlined by many cells in diameter. Also the *vena cava* has a big diameter. The second biggest vessels are the arteries and veins followed by the arterioles and venules, which consist of a few cells in diameter. The smallest vessels, the capillaries form the connection between arterioles and venules. They are made of one cell only, which allows for exchange of gases and nutrients between the blood and surrounding tissue.

The wall of all blood vessels of the vasculature is made up of endothelial cells (ECs). They are surrounded by a basal lamina on the outer surface. While arteries are often ensheathed by a dense layer of smooth muscle cells and pericytes to ensure dilation and constriction of the vessels, veins are rather free of these cells.

The development and anatomy of the embryo vasculature is highly conserved among vertebrates. In both the mouse and the zebrafish embryos the DA and PCV constitute the main vessels of the body, which are connected by intersegmental vessels (ISVs) and dorso-longitudinal anastomotic vessels (DLAV) (Fig. 1A, B, D). The pattern and development of the vasculature are also conserved in terms of genetic determination (Thisse and Zon, 2002). An example of this is the expression of *gata-1* in all cells that will become blood cells during both mouse and zebrafish embryogenesis (Heicklen-Klein et al., 2005; Whitelaw et al., 1990). Another example of conservation comes from the transcription factor *scl*, which is expressed in the common progenitors for cells making the blood and blood vessels (Gering et al., 1998; Kallianpur et al., 1994). Furthermore, the heart determining factor *nkx2.5* can be found in zebrafish as well as mouse embryos *(Lints et al., 1993; Tu et al., 2009)*.

Several model organisms are used to study the complex development of the vasculature system such as mice (*Mus musculus*), chicken (*Gallus gallus*) and frogs (*Xenopus laevis*). Zebrafish (*Danio rerio*) has become a more relevant model system over time. It belongs to the ray-finned fishes (*Actinopterygii*) and is a suitable model organism to study vertebrate development. Compared to mice and chick, zebrafish can be kept in high stock densities. Fertilization takes place externally and embryos develop rapidly. Most importantly, zebrafish embryos are optically clear, which allows easy visualization of developmental processes. In recent years, imaging techniques for live observation have been especially developed. The vasculature can now be visualized by the expression of reporter genes encoding enhanced green fluorescent protein (EGFP) in endothelial cells (ECs) (Lawson and Weinstein, 2002). The functional circulatory loop within the vasculature can be observed by microangiography, the injection of fluorescent dye into the functional circulation (Weinstein et al., 1995). Studying specific gene functions in vascular development by gene knock-down/ knock-out can not only lead to

defects in blood vessel formation but also in heart development leading to a lack of blood flow. In mice this would lead to embryonic lethality. Because zebrafish embryos can live without blood flow until the end of embryogenesis, gene knock-down/ knock-out analysis can be easily performed.

The vasculature of the zebrafish embryo is relatively simple. The heart pumps the blood directly into the main aortae of the head, the lateral dorsal aortae (LDA). These aortae merge in the cranial trunk to one big vessel, the dorsal aorta (DA), which carries the blood to the posterior part of the embryo (Fig. 1 B, D). The posterior cardinal vein (PCV) carries the blood back to the heart and to the major vein of the head, the primordial hindbrain channel (PHBC). In the trunk two smaller vessels connect the DA and PCV: the intersegmental vessels (ISVs), which later differentiate into segmental arteries (SA) and segmental veins (SV) and the dorsolongitudinal anastomotic vessel (DLAV) (Fig. 1 D). The capillaries of the head form a very complex network of arteries and veins (Fig. 1 C) (Isogai et al., 2001).

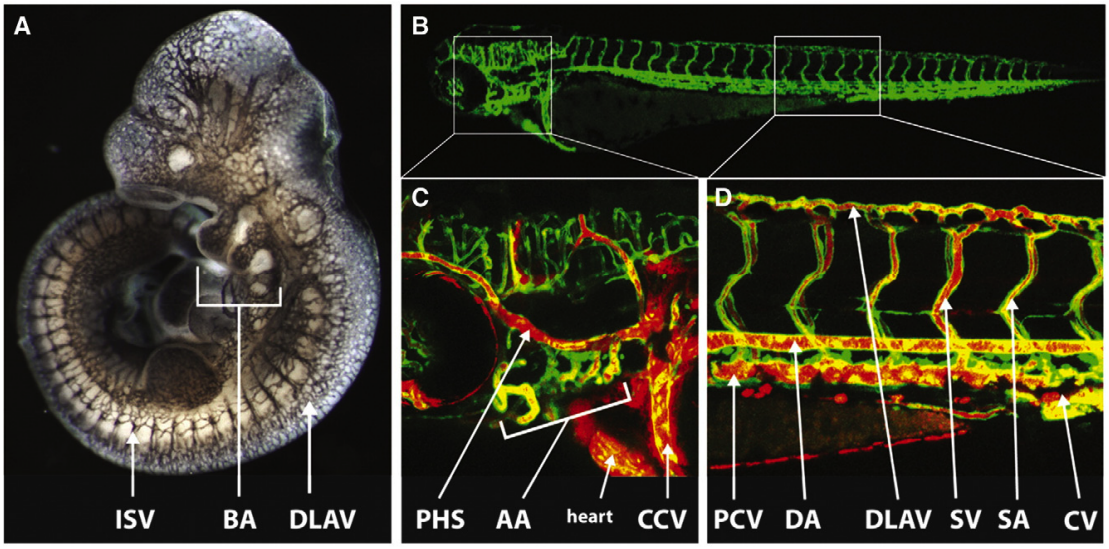

Figure 1: The vasculature in mouse and zebrafish embryos. (A) Immunohistochemichal staining for PECAM-1 visualizing the vascular system in a 10 day old mouse (photo Ralf Adams). (B-D) Transgenic reporter gene expression of flk1:EGFP (green) and visualization of the blood vessel lumen by quantum dot injection (red in C and D). ISV: intersegmental vessel, BA: branchial arches, DLAV: dorso-longitudinal anastomotic vessel, PHS: primary head sinus, AA: aortic arches, CCV: common cardinal vein, PCV: posterior cardinal vein, DA: dorsal aorta, SV: segmental vein, SA: segmental artery, CV: caudal vein. Images taken from (Ellertsdottir et al., 2010).

The primary vascular network (the DA and PCV) is formed by the process of vasculogenesis, which is the coalescence of individual endothelial cells and the subsequent vessel formation of a lumenized vessel. Further expansion of the vascular network is brought about by the process of angiogenesis, where new capillary vessels are formed out of an already existing vessel {Ellertsdottir, 2010 #7}. This process can be divided into sprouting angiogenesis and intussusceptive angiogenesis {Patan, 2000 #356}. The latter is defined by the division of an existing vessel along its longitudinal axis into two separate vessels {Makanya, 2009 #355}. During and after the formation of the primary and secondary vessels this primitive network is remodeled extensively. This leads to the rearrangement of vascular segments in number and location allowing for a functional adaptation of the network. One example of remodeling is the process of anastomosis, whereby previously branched blind-ending vessels connect to each other to form a new circulatory loop. At the same time vascular fusion results in the formation of larger vessels and concomitantly larger vessels can disappear by the process of pruning and/or remodeling to create smaller vessels.
In the following chapters I will describe the process of vasculogenesis and sprouting angiogenesis and how a patterned vascular network is put together during development.

3.1 Vascular development

3.1.1 Vasculogenesis – formation of the dorsal aorta and posterior cardinal vein

3.1.1.1 Differentiation of endothelial cells

The development of blood vessels and cellular blood components is highly connected. Endothelial cells (ECs), which make up the vasculature and hematopoietic cells, such as erythrocytes descend partially from a common progenitor, the hemangioblast, but also from distinct progenitors, the angioblast and hematopoietic stem cells, respectively (Risau and Flamme,

1995; Vogeli et al., 2006; Warga et al., 2009). These progenitors arise from the lateral plate mesoderm from where they migrate towards the midline. Here they assemble into a cord that adopts the form of a tube making the first main vessel of the embryo. The first progenitors that are determined to become endothelial cells or hematopoietic cells express several transcription factors like *fli1*, *flk1*, *scl*, *gata2* and an unknown factor called *cloche* (Brown et al., 2000; Detrich et al., 1995; Liao et al., 1998; Liao et al., 1997; Liu et al., 2008; Pham et al., 2007). While these cells migrate to the midline they start to separate spatially and differentiate into two different cell types. On one hand, the dorsal cells become hematopoietic cells and express *fli1* and *scl*, but no *flk1*. On the other hand, the ventral cells are the endothelial cells that express *fli1*, *flk1*, but no *scl*. A driving factor for the migration of ECs towards the midline is *vascular endothelial growth factor* (*vegf*), the key growth factor in vascular development. Vegf expression is induced by *shh*, which is expressed in the notochord. The deletion of *vegf* in mouse and Xenopus results in the lack of angioblast migration and the abnormal formation of axial vessels (Carmeliet et al., 1996; Cleaver and Krieg, 1998). In zebrafish embryos however, VEGF, although inducing angioblast cell fate, is not responsible for angioblast migration (Jin et al., 2005). So far only the endoderm was found to influence the temporal regulation of primary tube formation, as it is thought to be a substrate for migrating angioblasts (Jin et al., 2005). The anterior endoderm of the head, however, has an even stronger impact on angioblast migration. Here, the angioblasts migrate towards the chemokine signal *cxcl12*, which is expressed in the anterior endoderm and which they sense through the receptor *cxcr4*. Knock-down of both of these genes or the whole endoderm lead to a total lack of lateral dorsal aorta (LDA) formation (Siekmann et al., 2009).

3.1.1.2 Aorta and venous tube formation

Angioblast migration towards the midline occurs in two waves. The first wave of cells starts to migrate at 14 hpf, the second wave of cells migrates at 16 hpf (Fig. 2 A). At 18 hpf the cells assemble into a cord-like structure at the midline between the hypochord and the underlying mesoderm (Fig. 2 B) (Eriksson and Lofberg, 2000; Jin et al., 2005). Shortly after this, the cells start to get

polarized shown by the localization of Zonula Occludens-1 (ZO-1) and Claudin 5 (Cldn5) to cell-cell contacts. At this point cells start to rearrange. Through the process of cord hollowing an aortic lumen is formed, which is apparent at 20 hpf and is lined by a wall of one cell layer (Jin et al., 2005). The aortic lumen enlarges by cells changing from a spherical to an elongated shape. The endothelial cells are polarized by now and Fibronectin is localized at the basal sides of the vessel. At this timepoint the PCV has not formed yet. At 17 hpf *ephrinB2a*, a marker for arterial cell fate, gets expressed in the dorsal cells of the vascular cord. Therefore the first wave contains some angioblasts that differentiate into arterial and venous cells. The second wave, however, contains cells that contribute to the formation of the PCV only (Jin et al., 2005). Additionally, Herbert et al., (2009) found that the PCV forms by ventral sprouting of angioblasts from the DA. This process is called selective cell sprouting and is blocked when arterial-venous differentiation is impaired (Herbert et al., 2009). The lumen of the PCV also starts to form by a cord hollowing mechanism, but unlike the aorta expands by erythrocyte invasion (Herbert et al., 2009) (Fig. 2 C). At 28 hpf both main vessels are fully luminized (Fig. 2 D).

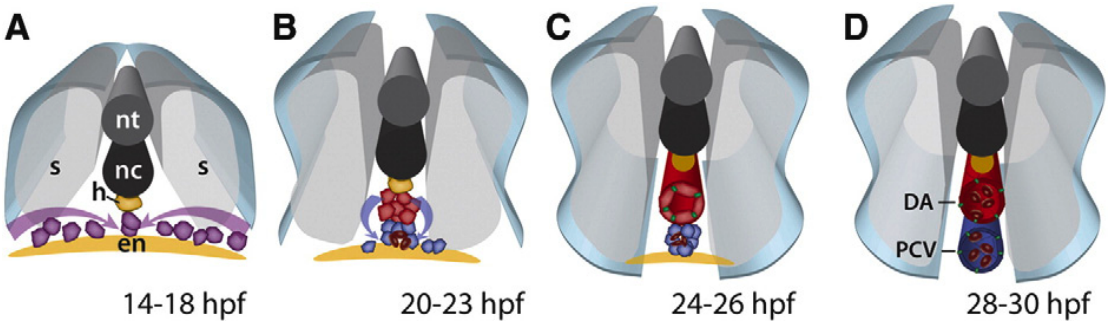

Figure 2: Model for vasculogenesis stages in the zebrafish embryo. Angioblasts originating from the lateral plate mesoderm migrate in two waves towards the midline of the embryo (A). They assemble into a vascular cord between the hypochord and the underlying endoderm (B). While *ephrinB2a* expressing cells become the DA, *Ephrinb4a* expressing cells sprout ventrally to form the PCV (B). The DA lumen forms by cord hollowing, while venous ECs sprout ventrally, coalesce around the blood cells and eventually form a tube (C). At 28 hpf both the DA and PCV are fully functional (D). nt: neural tube, nc: notochord, h: hypochord, s: somites, en: endoderm, DA: dorsal aorta, PCV: posterior cardinal vein. Taken from (Ellertsdottir et al., 2010).

3.1.1.3 Arterial-venous differentiation

At first, with the help of tracer injection experiments it was thought that arterial or venous cell fates can be assigned by the direction of blood flow in an existing blood vessel (Jargiello and Caplan, 1983). However, several recent studies prove that arterial and venous cell fate determination is already established before the onset of blood flow and is therefore genetically determined (Herzog et al., 2005; Zhong et al., 2001). In the zebrafish embryo the notochord expresses *sonic hedgehog* (*shh*) (Stemple et al., 1996), which induces the expression of *vegf-a* in the somites (Lawson et al., 2002). Vegf-a binds to the vascular endothelial growth factor receptor-2 (VEGFR-2/fetal liver kinase (flk)-1) on angioblasts leading to the activation of *notch5* signaling and the subsequent induction of arterial cell fate. In mouse knock-out studies, the deletion of one *VEGF* allele leads to a decrease in aorta diameter; deletion of both alleles abolished aorta formation completely (Carmeliet et al., 1996). It is thought that cells located in the dorsal part of the vascular cord are exposed to a higher level of Vegf, therefore express more *notch5* and become arterial cells. The more ventral cells however receive very little Vegf signal and therefore do not express *notch5* and adopt a venous cell fate (Lawson et al., 2002). Notch5 induces the expression of *ephrinB2 (efnB2a)*, an arterial marker, and suppresses the induction of EphrinB4 (*EphB4)*, a venous marker, via the bHLH transcription factor *gridlock* (Lawson et al., 2001; Zhong et al., 2001; Zhong et al., 2000). Although *ephrinB2* knock-out experiments in mice reveal a normal development of the main vessels (Wang et al., 1998), in zebrafish morpholino knock-down experiments all ECs clearly adopt venous identity (Herbert et al., 2009). Transplantation experiments showed that the differential expression of *EphB4* and *efnb2a* leads to a repulsion of arterial and venous cells (Herbert et al., 2009).

Another gene specifically expressed in venous cells and repressed by *notch* signaling is *fms-related tyrosine kinase (flt)-4*. *Mind-bomb* mutants, in which *notch* signaling is defective, present an expanded *flt-4* expression into the aorta (Lawson et al., 2001).

Moreover, it was shown that not only does the aorta suppress venous cell fates, but also vice versa. Knock-out studies of the transcription factor

COUPTFII in mice showed its role in repressing *notch* in the vein and therefore ensuring vein identity (You et al., 2005).

3.1.2 Angiogenic network formation

As mentioned above several remodeling and rearrangement processes lead to the formation of a complex vascular network. This network does not only ensure blood supply to all possible organs and distant places of the body, but is also a prerequisite for other developmental processes such as the formation of other organs that arise later during development. Therefore, the vascular network has to be highly organized, which is exactly what can be observed in the developing fish embryo. All embryos have the same kind of vessels arising at the same position and at the same timepoint. This remarkably stereotyped formation and patterning of blood vessels between embryos is ensured by genetic hardwiring.

3.1.2.1 ISV formation via the process of angiogenesis

One type of vessel, which develops in a highly stereotypical manner, is the ISV. Its morphogenesis is reproducible from vessel to vessel and from embryo to embryo.

The ISVs form via the process of sprouting angiogenesis, the sprouting and growth of new vessels out of preexisting vessels (Childs et al., 2002; Isogai et al., 2003; Risau, 1997). Temporally, ISVs develop from anterior to the posterior end of the trunk. At 20 hpf, on each lateral side of the embryo primary sprouts emerge from the aorta adjacent to the somite boundaries (Fig. 3 A). They grow out dorsally between notochord and somites or neural tube and somites at later stages (Fig. 3 B). During the dorsal outgrowth, the ECs send out extensive filopodial extensions, especially at the tip of the branch. While the sprout grows along the somite boundary until it reaches the level of the horizontal myoseptum (HMS), it commences to grow perpendicular to the body axis from there onwards. As the sprouts reach the dorsal roof of the neural tube, they ramify anteriorly and posteriorly, elongate further and connect and fuse to the neighboring ISV (Fig. 3 C). This process starts at around 27 hpf and ultimately leads to the formation of the dorso-

longitudinal anastomotic vessel (DLAV). At this stage the two parallel DLAVs of each lateral side are distinct vessels. At the end of this primary network formation only the anterior-most ISVs have started to make a lumen (Isogai et al., 2003) and a connection to the PCV is lacking completely (Fig. 3 D).

The completion of the circulatory loop is brought about by the connection of some of the ISVs to the PCV. For this to happen, from 32 hpf onwards, secondary sprouts emerge from the PCV (Fig. 3C). These sprouts grow dorsally in very close proximity to the already existing ISV. Half of these secondary sprouts make a connection to the ISV, which always occurs in the first third of the ISV above the DA (personal communication, Anna Lenard) (Fig. 3 D). Several remodeling processes lead to the formation of a functional vessel including the regression and disappearance of the ventral part of the old connection between DA and ISV (personal communication Anna Lenard) (Isogai et al., 2003). This new vessel, connected to the PCV, is called an intersegmental vein (SV), a vessel connected to the DA is called intersegmental artery (SA) (Fig. 3 E).

The other half of the secondary sprouts also elongates dorsally, but does not connect to the ISVs. These sprouts stop to grow dorsally at the level of the horizontal myoseptum and grow towards the anterior and posterior where they connect to the neighboring sprouts. Together, they form the parachordal chain, which will later give rise to a part of the lymphatic system (Hogan et al., 2009; Yaniv et al., 2006).

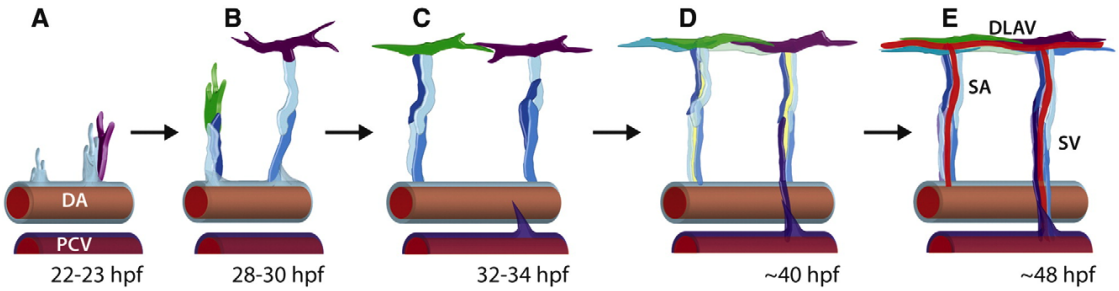

Figure 3: Model of intersegmental vessel formation in the zebrafish trunk. First sprouts emerge from the aorta at 22 hpf (A). While growing dorsally, the ECs send out filopodial extensions. When reaching the dorsal roof of the neural tube, the sprouts grow anteriorly and posteriorly, where they connect to the neighboring ISVs (B,C). Between 32 hpf and 42 hpf a lumen is formed (D). Secondary sprouts emerge from the PCV from 32 hpf onwards and connect to the primary vessel, which will become a segmental vein (C,D). Eventually the blood flows through this circulatory loop (E). DA: dorsal aorta, PCV: posterior cardinal vein, DLAV: dorso-longitudinal anastomotic vessel, SA: segmental artery, SV: segmental vein. Taken from (Ellertsdottir et al., 2010).

The anterior-posterior order of arteries and veins occurs at random. Only the anterior most ISVs in the head show a stereotypic distribution (Bussmann et al., 2010; Isogai et al., 2001; Isogai et al., 2003).

Several studies have investigated the morphology of a growing ISV in detail (Blum et al., 2008; Childs et al., 2002; Isogai et al., 2003; Lawson and Weinstein, 2002). Earlier studies assumed that the ISV consists of three endothelial cells: one being a reverse T-shaped cell embedded in the aorta, the second one being a T-shaped cell embedded in the DLAV and the third one being the connection between the two (Childs et al., 2002). A more recent study proposed that a sprout consists of three to four cells, one tip and two to three stalk cells (Abb. 4 B). Cell divisions during ISV formation lead to a final number of 3-7 endothelial cells per ISV, the majority of which consists of 4 or 5 cells, though (Blum et al., 2008). This study has further used mosaic analysis and immunohistochemical analysis of cell junctions to show the paired assembly of ECs along the dorsal-ventral axis of the ISV (Blum et al., 2008). A region of the ISV containing no or one line of junctional staining perpendicular to the body axis, resembles a unicellular vessel; a region with more than one line of junctional staining resembles a multicellular vessel.

3.1.2.2 Molecular regulation of sprout formation and outgrowth

In line with the hardwiring of the morphogenetic events during ISV formation, the regulation of these events on the genetic level is also very stereotypical.

As mentioned earlier the primary function of blood vessels is the transport of oxygen and nutrients to various places in the body. Interestingly, the lack of oxygen in a body region also regulates the formation of new blood vessels (reviewed in (Fraisl et al., 2009)). In particular, genes of the family of *hypoxia-inducible transcription factors (HIF)* are capable of responding to changes in oxygen level. When activated they induce the expression of *vascular endothelial growth factor (VEGF)* in target areas and its receptor, vascular endothelial growth factor receptor (VEGFR)-2 (fetal-liver kinase-1 (flk-1)), in endothelial cells (Elvert et al., 2003; Gerhardt et al., 2003).

VEGFs and their receptors are the main driving forces of vasculogenesis, angiogenesis and lymphangiogenesis (reviewed by (Lohela et al., 2009)). While the receptors are expressed by the ECs (Liao et al., 1997), *VEGFs* itself

are expressed by the surrounding tissue such as the somites (Pollard et al., 2006).

The main factors for the induction of angiogenesis are VEGF-A (VEGF) and its receptor VEGFR-2. Upon binding of the ligand, the receptor dimerizes and autophosphorylation occurs (Guo et al., 1995). The phospholipase C (PLC) γ/protein kinase C (PKC) pathway gets activated and leads to the generation of inositol trisphosphate. This in turn activates the c-Raf-MEK-MAP kinase cascade (Takahashi et al., 2001; Xia et al., 1996), which induces EC growth, migration and proliferation (Wang et al., 2008). Knock-down experiments in mice showed that *flk-1* is necessary for vasculogenesis, blood island formation and organized blood vessel formation (Carmeliet et al., 1996; Ferrara et al., 1996; Shalaby et al., 1995). Endothelial cells send out filopodia and migrate towards a VEGF gradient. Studies in the mouse retina could show, that disruption of this gradient by interfering with the interaction between VEGF and the extracellular matrix (ECM) inhibited vascular branch formation (Ruhrberg et al., 2002). How VEGF and other factors drive angiogenesis by inducing filopodia and tip cell formation will be discussed in section 1.2.2.4.

Signaling via the ligands *VEGF-B* and *PlGF* has a different impact on angiogenesis. Knock-out of these two ligands does not cause any phenotype during development (Bellomo et al., 2000; Carmeliet et al., 2001). Deletion of their receptor VEGFR-1 (*fms-like tyrosine kinase 1*, *Flt1*), however, leads to embryonic lethality due to excessive angioblast and endothelial cell proliferation (Fong et al., 1995; Fong et al., 1999; Kearney et al., 2002). Therefore it was assumed and shown that VEGFR-1 and especially the secreted form sFlt-1 functions as a negative regulator of VEGFR-2 by acting as a ligand sink to modulate the amount of VEGF-A (Kendall and Thomas, 1993; Roberts et al., 2004). The relatively weak tyrosine kinase activity of VEGFR-1 and the high affinity to VEGF-A support this idea (Autiero et al., 2003; Hiratsuka et al., 2005; Park et al., 1994).

3.2.2.4 Tip cell selection

The determination of patterning within a vessel is also genetically hard-wired. The most prominent features of migrating endothelial sprouts are the filopodial extensions of the tip cells. The stalk cells do not possess any or only few filopodia, pointing to a specialized role of tip cells during sprout outgrowth. It was shown, for example, during retinal angiogenesis that tip cells respond differently to VEGF-A than do stalk cells. While tip cells respond by sending out filopodia and migrating towards the VEGF-A source, stalk cells respond by proliferating (Gerhardt et al., 2003). It has been found that endothelial tip cells express different genes than stalk cells allowing for the response to guidance cues more readily than stalk cells. Several studies in zebrafish, mouse retina, tumor angiogenesis and 3D endothelial cell culture found the most important factor in determining tip cell specification to be the Notch pathway (Phng and Gerhardt, 2009). In mammalian endothelial cells the ligand Dll4 binds to the receptor Notch. Upon proteolytical cleavage of Notch the resulting Notch intracellular domain (NICD) activates several target genes with the help of basic helix-loop-helix (bHLH) transcription factors. While *dll4* is expressed in the tip cells, Notch signaling is most prominent in the stalk cells (Hellstrom et al., 2007; Jakobsson et al., 2010; Lobov et al., 2007). Inhibition of the *notch* signaling pathway by deleting *notch1* or *dll4* function results in excessive branching in the mouse retina as well as in the zebrafish ISVs (Hellstrom et al., 2007; Leslie et al., 2007; Lobov et al., 2007). Overexpression of Notch on the other hand leads to a total lack of endothelial sprouts (Siekmann and Lawson, 2007). Several studies found that the excessive sprouting in *notch* knock-down scenarios is accompanied by the upregulation of endothelial tip cell markers like *Pdgfb*, *Unc5b*, *flk* and *flt4* and is therefore caused by an increased tip cell formation (Hellstrom et al., 2007; Suchting et al., 2007; Tammela et al., 2008). This is supported by transplantation experiments in zebrafish ISVs, which showed that *notch* deficient cells more readily become the tip cell, while *notch* overexpressing cells contributed to the aorta and did not migrate (Siekmann and Lawson, 2007).

A few lines of evidence support the idea that Notch signaling influences VEGFR signaling during tip cell selection. The knock-down of *notch* cause *flt4* expression to increase in all endothelial cells (Siekmann and Lawson, 2007;

Tammela et al., 2008). Also, is the expression of *VEGFR-1* and *2* is altered in *Notch* deprived cells. In wt conditions, *VEGFR-2* is expressed more abundantly in the tip cell, while *VEGFR-1* is expressed stronger in the stalk cells. Jakobson et al. (2010) showed by knock-down experiments that VEGF induces Dll4 expression in the tip cell, which in turn activates Notch signaling in the adjacent stalk cell (Fig.4). Here *VEGFR-2* expression is downregulated and *VEGFR-1* expression upregulated. This leads to a decreased VEGF response in the stalk cells (Fig. 4 green cell). Cells with the highest *dll4* and therefore *VEGFR-2* expression sense more VEGF and become tip cells (Fig. 4 red cell) (Jakobsson et al., 2010). However, time-lapse imaging showed the shuffling of cells between the tip and stalk both in vitro and in vivo. This suggests that a constant re-evaluation of signaling circuits occurs, as cells meet new neighbors during vessel outgrowth and remodeling (Jakobsson et al., 2010).

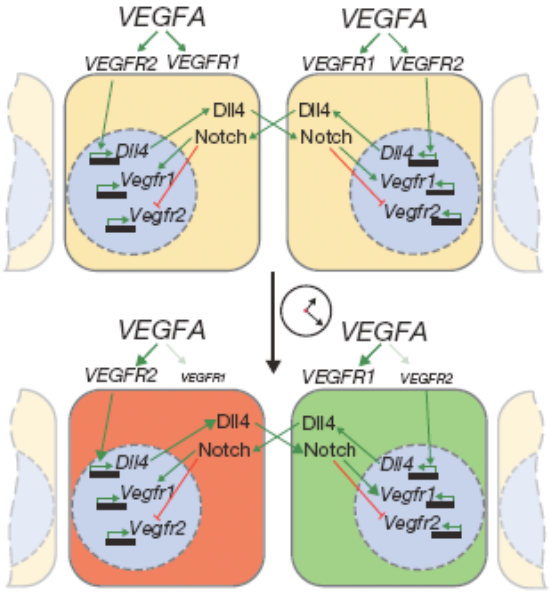

Figure 4: Model of VEGF-Notch/Delta signaling in endothelial cells of the branching tip. A cell expressing by chance more Dll4 enhances *VEGFR-2* expression and reduces *VEGF-R1* expression. This cell responds stronger to the extracellular VEGF signal than its neighboring stalk cell and leads the migration process. In the stalk cell *notch* expression is induced via the tip cell, which leads to reduction of *VEGFR-2* expression and enhancement of *VEGFR-1* expression. Therefore this cell does not respond to VEGF signaling as strongly as the tip cell. Taken from (Jakobsson et al., 2010).

Additional evidence comes from the upregulation of soluble Flt-1 (sFlt-1) by Notch activation (Harrington et al., 2008). Furthermore, deletion of *flt-1* results in misguided emerging sprouts, which can be rescued by the expression of *sFlt-1* immediately adjacent to the endothelial sprout (Chappell et al., 2009). This indicates a role for sFlt-1 in guiding the tip cell away from the parent vessel by sequestering extracellular VEGF and the response to VEGF adjacent to the tip cell.

3.2.2.3 Environmental cues and endothelial pathfinding

Intrinsic cues are not the only factors determining the patterning of the vascular network. Extrinsic guidance cues also regulate the pathfinding of endothelial sprouts.

As mentioned above, ISV sprouting and outgrowth always occur at the same position – the somite boundary - in zebrafish and mice vessel. ISVs also grow stereotypically at the same time. Several factors that are known to provide positional cues for axonal outgrowth have been found to influence the guidance of endothelial cells along their path (Eichmann et al., 2005; Gelfand et al., 2009; Weinstein, 2005).

The PlexinD/Semaphorin system represents one of these guidance cues. The Semaphorin (Sema) receptor PlexinD1 is almost exclusively expressed in endothelial cells. The *out-of-bounds* (*obd*) zebrafish mutant that lacks PlexinD1 function shows premature sprout formation and abnormal positioning of these sprouts along the axis of the aorta (Childs et al., 2002; Torres-Vazquez et al., 2004). Mouse mutants for *PlexinD1* also have a strong disorganization of the somitic vasculature (Gitler et al., 2004; Gu et al., 2005). The role for the ligand Sema is not as well understood (Gu et al., 2005; Torres-Vazquez et al., 2004; Yee et al., 1999). While the knock-out of *sema3E* in mice phenocopies the effect of *PlexinD1* mutants, the same molecule in zebrafish has the opposite effect. Here the knock-down of *sema3E* causes a delayed outgrowth of ISVs (Lamont et al., 2009). Therefore, different semaphorin ligand/receptor pairs show antagonistic effects on the timing of sprout formation during zebrafish development.

Another neuronal signaling pathway known to regulate angiogenic outgrowth is the Netrin/Unc5b system. The receptor Unc5b is expressed in arterial cells. The ligand Netrin1, on the other hand, is expressed at the neural keel and the horizontal myoseptum in zebrafish embryos (Park et al., 2005). Netrin1 was found to be an angiogenic factor due to its capability to induce the proliferation and migration of ECs and vascular smooth muscle cells (Park et al., 2004). However, other studies however showed that inhibition of Unc5b/Netrin1 signaling causes the formation of an excess of filopodial extensions and vessel branches leading to the conclusion that Netrin1 is an anti-angiogenic factor (Bouvree et al., 2008; Larrivee et al., 2007; Lu et al., 2004). The

different outcomes of these experiments most likely represent the bipotential ability of Netrins to work as repulsive as well as attractive signals.

Next to guidance cues that determine the path and timing of sprout outgrowth, another prerequisite is needed for proper angiogenic behavior of ECs. Space has to be generated to allow for EC migration, tissue invasion and vascular lumen formation. This is brought about by the degradation of basement membrane and removal of ECM (van Hinsbergh and Koolwijk, 2008). In particular, the *membrane type1- matrix metalloproteinase* (*MT1-MMP*) and other MMPs are well known to degrade Collagen type IV and other ECM proteins (Chun et al., 2004). However, the fact that ECs most probably use their filopodia to generate an attachment site, points to a reason why proper angiogenesis also does not work completely without ECM proteins. In zebrafish, a role for CollagenIX was described in the formation of the vascular plexus in the caudal fin (Huang et al., 2009). Additionally, several genes encoding ECM components such as Laminins and Perlecan have been found to more active in tip cells (del Toro et al., 2010).

All of the conserved genetic pathways described so far determine the establishment of the circulatory system before the onset of blood flow. However, it was shown that also the blood flow itself is required for the modulation of the vascular network. A particular vessel called AAx connecting two aortic arches to the LDA in zebrafish only starts to develop after the onset of blood flow the inhibition of blood flow totally abolishes the formation of this vessel (Nicoli et al., 2010). They showed that in this case flow induces the expression of the transcription factor *klf2*α, which in turn drives expression of the micro RNA *miR-126*. This in turn allows for *Vegf*-mediated induction of angiogenesis and the formation of the AAx vessel (Nicoli et al., 2010).

Another study demonstrated a similar defect after the ablation of blood flow for the central arteries (CtA) of the brain. These vessels do form and connect to the basilar artery (BA) without blood flow. This is mediated by the chemokine signaling of *cxcl12b* and its receptor *cxcr4a*. Only after perfusion of these vessels, they loose their angiogenic potential through the downregulation of the receptor. Ablating blood flow in these vessels causes

the CtAs to keep their angiogenic behaviors like the formation of filopodial extensions (Bussmann et al., 2011).
Therefore, blood flow does not only induce the formation of new vessels, but also leads to the maturation of newly formed vascular connections.

3.2 Junctional proteins in development

Branched tubular organs are characterized by their composition of epithelial cells, which manifest an apical-basal polarity. The apical sides of these cells face the lumen and the basal sides face towards the surrounding tissues. Each of these sides usually fulfills special functions associated with the role of the specific organ. Therefore, the apical-basolateral diffusion of membrane components has to be restricted. The compartmentalization of the membranes is brought about by junctional proteins that connect to their equivalent junctions of neighboring cells. In addition to providing a membrane diffusion barrier, junctions allow the separation of the lumen and the surrounding tissue enabling the organ to function properly.

3.2.1 Junctional proteins in endothelial cells

Next to desmosomes and gap junctions, epithelial and endothelial cells harbor two major types of junctions, adherens junctions (AJs) and tight junctions (TJs) (Legan et al., 1992; Simon and Goodenough, 1998). The latter two consist of transmembrane proteins that hold adhesion functions. AJs are intracellular scaffolding proteins that mediate the connection with neighboring cells through homophilic interactions (Bazzoni and Dejana, 2004; Hartsock and Nelson, 2008). Epithelial cells are often cuboidal and have a long lateral membrane. Here the apically localized AJs and TJs are separate with TJs localizing more apically than AJs within the membrane. Endothelial cells however are elongated and have a thin spot of lateral membrane that contains TJs and AJs in an intermingled fashion (Simionescu et al., 1975). The main function of AJs is the establishment, maturation and maintenance of

endothelial cell-cell contacts. TJs on the other hand, are required for paracellular transport of solutes and for sealing the epithelium.

Some junctional proteins are specifically expressed in endothelial cells; these are the Vascular endothelial cadherin (VE-cadherin) at AJs and Claudin 5 at TJs (Fig. 5). Further transmembrane proteins help to build the AJ and TJ complexes. Vascular endothelial protein tyrosine phosphatase (VE-PTP), Platelet endothelial cell adhesion molecules (PECAMs) and N-Cadherin contribute to the AJ complex. Additional Claudins, Occludin, Junctional Adhesion Molecules (JAMs), ESAM and Nectin are further transmembrane components of TJs (Fig. 5).

All of the transmembrane proteins mentioned above bind to intracellular cytoskeletal and signaling proteins. The connection to the cytoskeleton ensures stability of the junction and is required for its dynamic rearrangement (see 1.2.3) (Dudek and Garcia, 2001; Lampugnani et al., 2002; Sheldon et al., 1993). Proteins like Afadin and Ponsin connect Nectin directly to F-actin (Fig. 5) (Takahashi et al., 1999). Other proteins like Zonula Occludens-1 (ZO-1) act as scaffolds, as they bind via their PDZ domain to the tight junction proteins Claudin, Occludin and JAMs, but also to cytoskeletal binding proteins like cortactin, cingulin and α-catenin (Fanning et al., 1998; Itoh et al., 1999a; Matter and Balda, 2003; Stevenson et al., 1986; Wittchen et al., 2000). ZO-1 also binds to other ZO proteins, namely ZO-2 and 3 and to the signaling molecule ZO1-associated nucleic-acid binding (ZONAB) (Fig. 5) (Balda and Matter, 2000; Haskins et al., 1998; Itoh et al., 1999b). ZONAB is one example of a junctional protein that can translocate to the nucleus and regulate transcription of specific genes, in this case ZONAB regulates the expression of genes involved in cell proliferation (Balda et al., 2003). The most studied example of a signaling molecule, however, is β-catenin, which is usually in tight association to VE-Cadherin (Fig. 5), but once it translocates to the nucleus as a result of Wnt pathway activation, it induces expression of *CyclinD1* or *TCF*. Thereby it regulates cell growth, apoptosis and cell differentiation (Ben-Ze'ev and Geiger, 1998; Bienz and Clevers, 2000).

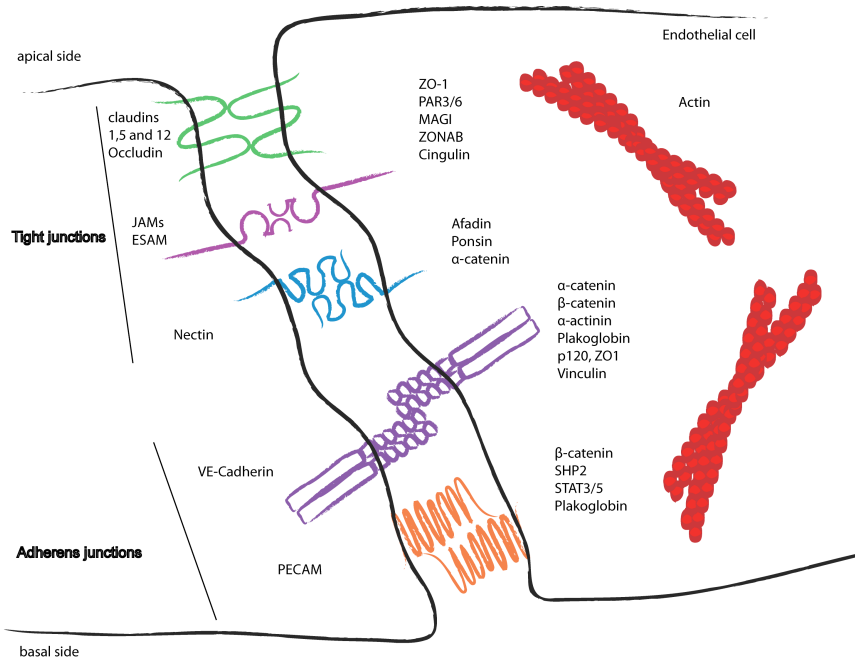

Figure 5: Schematic drawing of junctional proteins in endothelial cells. ECs harbor tight and adherens junctions. They contain transmembrane proteins that connect neighboring ECs via homophilic interactions. Proteins specifically expressed in ECs are Claudin5 (TJs) and VE-cadherin (AJs). Many junctional proteins bind to intercellular proteins like ZO-1 or α/β-catenin. These provide a connection to the cytoskeleton and are responsible for signaling into the nucleus. After (Dejana, 2004).

3.2.2 The formation of an epithelium

Cells that build blood vessels are not polarized from the start. Only while the vasculature develops, mesodermally derived cells become polarized and transform into endothelial cells. The formation of cell-cell contacts and the development of junctions in epithelial and endothelial cells occur in a series of events. In cell culture experiments, it was shown that while migrating towards an inductive signal, epithelial cells send out filopodia. These filopodial extensions connect to filopodia of neighboring cells and junctional proteins are deposited at contact sites forming the first primordial AJ (pAJ) (Adams et al., 1996; McNeill et al., 1993). Several of these pAJs result in a zipper-like appearance, which fuse upon further maturation and make a linear contact region (McNeill et al., 1993). During this maturation process more and more junctional proteins are recruited and localize to the junctions. A functional epithelium requires the formation of AJs and TJs. In cell culture the first junctional proteins to accumulate between cells are Nectins (Sato et al., 2006;

Takai et al., 2008). It was shown in epithelial cell culture experiments, that Partitioning-defective-3 (Par-3) binds to Nectins and recruits Cadherins as well as afadin, α-catenin, β-catenin to the junctional domain. Afterwards, TJ proteins such as ZO-1 and JAMs accumulate (Asakura et al., 1999; Ebnet et al., 2001; Ooshio et al., 2007). With further maturation Occludin and later Claudins localize to the junctions. PAR-3 and atypical protein kinase C (aPKC) are recruited to the tight junctions and ensure the initiation of the tight junction complex (Suzuki et al., 2002). Generally it is believed that AJs form first and initiate the generation of TJs. ZO-1 is one of the first scaffold proteins, because it localizes to early AJs and recruits other TJ proteins to this site. Later, the AJ proteins are sorted out from this spot and ZO-1 specifically localizes to TJs (Ando-Akatsuka et al., 1999). In some cell lines the AJ complex is indispensable for proper TJ formation (Gumbiner et al., 1988; Ikenouchi et al., 2007). However, also the PAR3-aPKC-PAR6 complex is crucial for TJ maturation from AJs. It probably regulates the localization of TJ components by phosphorylation or indirectly by inducing asymmetric distribution of other membrane components (Hurov et al., 2004; Suzuki et al., 2004). AJ proteins, however, are not only used as a scaffold for TJ formation, they also induce the expression of TJ proteins. Experiments with mouse endothelial cells revealed a direct link between the formation of VE-cadherin containing AJs and the upregulation of Claudin 5. Clustering of VE-cadherin leads to sequestration of β-catenin to the membrane, which causes the transcriptional repressor complex of FoxO1, TCF-4 and β-catenin not to form, therefore enabling the transcription of Claudin 5 (Taddei et al., 2008).

It is not known if the step-wise process of junction maturation also occurs during angiogenesis. However, immunohistochemical analysis of the first contact formation of neighboring ISVs reveal that VE-Cadherin and ZO-1 are among the first proteins to accumulate at contact sites of filopodia (Blum et al., 2008).

3.2.3 Junctional remodeling as a driving force for morphogenesis

A mature epithelium is not considered to be fixed and immobile. Cells within the epithelium remain mobile most of the time. The ability of junctions to be continually assembled and disassembled is crucial for tissue-reorganization, cell death or cell division and epithelial maintenance (Guo et al., 2007). Even more so is the development of an epithelial organ very dynamic. Constant junctional turnover in order to shorten or lengthen junctional strands is needed for the cellular processes occurring during organ development, such as cell shape changes, cell division, cell migration and cell rearrangement (Baer et al., 2009; Baum and Georgiou, 2011). On one hand, this is ensured by the internalization and recycling of junctional proteins (Le et al., 1999) (Shaye et al., 2008) (Matsuda et al., 2004) (Tiklova et al., 2010). E-Cadherin was shown to be endocytosed in a clathrin-dependent manner in epithelial cultured cells and *in vivo* its trafficking is required for intercalation processes occurring during tracheal development in *Drosophila* (Le et al., 1999) (Shaye et al., 2008). On the other hand, the dynamics of AJs and TJs is brought about by the potential of certain proteins to diffuse within the junctional strand. While AJ proteins or the tight junction proteins Occludin and ZO-1 diffuse rapidly, Claudin is rather stably localized at the membrane (Sasaki et al., 2003; Shen et al., 2008). These different diffusion properties might represent the specific functions of certain proteins within a junctional strand.

During morphogenetic processes in development, all kinds of junctional remodeling linked to cell rearrangement and cell shape changes can be observed. For example, in the *Drosophila* wing epithelium, cells change from an irregular to a hexagonal shape. This process is tightly linked to junctional rearrangement; some cell-cell contacts have to be enlarged and maintained, while others have to shorten or dissolve (Classen et al., 2005). Another example of junctional remodeling is seen in the formation of the dorsal branch during trachea development. While at the onset of dorsal branch formation cells are set up in a side-to-side arrangement with intercellular junctions only, at the end of the remodeling process cells have intercalated, they are elongated and most intercellular AJs have been replaced by autocellular AJs.

This junctional remodeling occurs throughout the process of intercalation, which requires cells to wrap around the lumen and initiate initial autocellular junctions (Ribeiro et al., 2004).

The dynamics of junctional remodeling during angiogenesis are less well understood, but were described for the process of anastomosis. Anastomosis is the connection of two separated vessels, which in this case are the neighboring ISVs. During this process ZO-1 and VE-Cadherin accumulate as a dot at the first contact between filopodia. This dot develops into a ring, which becomes bigger the more the neighboring cells crawl over each other and the bigger their contact area gets (Blum et al., 2008).

3.2.4 The role of VE-Cadherin in morphogenesis

Cadherins have been shown to play significant roles during cell rearrangement in morphogenetic processes like dorsal closure or tracheal tube formation in *Drosophila* (Gorfinkiel and Arias, 2007; Ribeiro et al., 2004; Tanaka-Matakatsu et al., 1996; Uemura et al., 1996). *Shotgun* mutants, that partially lack the DE-Cadherin protein, show severe morphological defects during the fusion of adjacent tracheal metamers. The fusion cells fail to accumulate junctional proteins at the contact point and do never adhere to each other (Tanaka-Matakatsu et al., 1996).

The role of VE-cadherin in angiogenesis has started to be studied in more detail. VE-cadherin mutations in mice lead to impaired vessel remodeling and maturation, which causes early death during embryogenesis (Carmeliet et al., 1999; Crosby et al., 2005). In cell culture VE-cadherin was shown to have pro- and anti-angiogenic functions. It is known to bind directly to VEGFR-2, which leads to the retension of the receptor at the membrane; thereby it is not internalized into signaling compartments leading to limited cell proliferation (Lampugnani et al., 2006). Furthermore, VE-cadherin suppresses angiogenic sprouting by inhibiting Rac1-dependent migration (Abraham et al., 2009). However, another study with mouse allantoids showed the pro-angiogenic function of VE-cadherin. In wt situations, ECs can crawl over an existing sprout to form a new tip. This highly motile behavior of migrating cells was blocked by inhibiting the function of VE-cadherin (Perryn et al., 2008). *In vivo*,

VE-cadherin also seems to have an angiogenic function. During zebrafish blood vessel formation morpholino (MO) knock-down of VE-cadherin causes a reduction in vascular integrity and the lack of lumen formation in segmental arteries (Wang et al., 2010). Furthermore, filopodial extensions of neighboring ISVs, although touching and retracting over a long period of time, never established a functional contact leading to impaired ISV formation (Montero-Balaguer et al., 2009).

3.2.5 Claudins seal epithelia

Claudin family members are the main components of epithelial/endothelial tight junctions and consist of at least 27 members in mammals (Furuse, 2010; Mineta et al., 2011). In transmission electron microscopy, TJs appear as attachments of opposing membranes without an intercellular gap (Farquhar, 1963; Goodenough and Revel, 1970). The main function of TJ proteins is the restriction of protein diffusion within the lateral membrane as well as the formation of a paracelllular diffusion barrier. Claudins are transmembrane proteins with four transmembrane domains, two extracellular domains and a cytoplasmic N- and C-terminus. Several studies identified the different roles of these domains in the capability of forming an epithelial barrier. The “tightness” of such a barrier is defined by different properties of paracellular transport. Determining the trans epithelial electrical resistance (TER), the charge selectivity and permeability of non-charged solutes as well as size discrimination provide information about the “tightness” of an epithelium (Powell, 1981). Leaky tight junctions do not support steep gradients of ions and therefore form a low TER (Van Itallie and Anderson, 2004b). These means of measure helped to find that the first extracellular domain of each of the Claudins defines their paracellular tightness and selective ion permeability of the junction (Colegio et al., 2003). With this domain Claudins form a pore by connecting to Claudins of neighboring cells. It is believed that when equally charged residues line this pore, the pore is open and it is permeable for either cations or anions as is the case for Claudin 2, 7 or 15 (Alexandre et al., 2005; Amasheh et al., 2002; Van Itallie et al., 2003). Unequally charged residues, however, lead to paracellular tightness like for Claudin 4, 5 or 8 (Krause et al.,

2008; Krause et al., 2009; Van Itallie et al., 2001; Wen et al., 2004; Yu et al., 2003). The second extracellular domain has the function to hold the opposing cell/Claudin and regulate the narrowing of the paracellular cleft (Krause et al., 2009; Piontek et al., 2008). Some Claudin subtypes, like Claudin 3 with Claudin 1 and 2, can connect in trans to each other in a heterotypic way, others cannot (e.g. Claudin 1 with Claudin 2) (Furuse et al., 1999). This heterogeneity of Claudin connections in cis and trans creates a diversity of channel and barrier properties for different cell types (Furuse et al., 1999). Connections to other tight junction proteins are brought about by the C-terminus of Claudins. The C-terminus contains a conserved sequence, which resembles a PDZ-binding domain through which Claudins bind to the PDZ-domains of ZO-1 – ZO-3 (Itoh et al., 1999a). For some Claudins the C-terminus was shown to be required for its apical membrane localization (Arabzadeh et al., 2006; Ruffer and Gerke, 2004). Furthermore, several phosphorylation sites and a palmitoylation site are required for the localization of Claudins to the junctions (Aono and Hirai, 2008; Ishizaki et al., 2003; Van Itallie et al., 2005).

The requirements of certain tissues for specific barrier functions is in part reflected by the expression pattern of different Claudins. *Claudin 2* is expressed in the leaky epithelia of the proximal renal tubule and in the Bowman`s capsule of the kidney (Kiuchi-Saishin et al., 2002; Reyes et al., 2002). *Claudin 1* is expressed in tissues that resemble tight epithelia like the epidermis and the distal nephron of the kidney (Furuse et al., 2002; Reyes et al., 2002). Several pathological conditions in humans and mice are attributed to mutations in *claudin* genes. In mice a deletion of *claudin 1* causes early death of new-borns due to extensive water loss over the epidermis (Furuse et al., 2002). Changes in the expression of *claudin 1*, *5* and *8* lead to barrier dysfunctions of the gut and cause Crohn`s disease (Zeissig et al., 2007). Furthermore, a mutation in *claudin 14* causes autosomal recessive deafness (Wilcox et al., 2001) (Ben-Yosef et al., 2003).

The endothelial specific gene *cldn5* was also found to cause barrier defects in mice, humans and zebrafish (Morita et al., 1999). In humans, *claudin 5* is one of 45 genes deleted in Velo-cardio-facial syndrome. This disease is characterized by several disorders like craniofacial anomalies or conotruncal

heart defects. How the deletion of *claudin 5* in particular contributes to the pathological condition is unknown (Sirotkin et al., 1997). *Claudin 5* most importantly has a function in forming the blood-brain-barrier (BBB). The BBB is made of ECs that restrict the diffusion of solutes from the blood into the extracellular fluid of the central nervous system (CNS). Deletion of *claudin 5* in mice leads to a size-selective loosening of the BBB. Neither the brain morphology nor the formation of TJs itself are impaired in these mutants. However, after perfusion of differently sized molecules into the blood system, only the mutant showed diffusion of the small molecules into the brain (Nitta et al., 2003). Zebrafish express two *claudin 5*, *claudin 5a* (*cldn5a*) and *claudin 5b* (*cldn5b*). *Cldn5a* is expressed in the neuroepithelium (http://zfin.org), where it is essential together with the Na,K-ATPase for the brain ventricular lumen expansion (Zhang et al., 2010). The role for *cldn5b* in zebrafish development is not known so far.

3.2.6 The role of Claudins in morphogenesis

Next to their role in barrier formation, some Claudins were also found to influence morphogenetic processes. The SJ proteins Megatrachea and Sinuous are not only known for their barrier function in all epithelial tissues of the Drosophila embryo (Behr et al., 2003; Stork et al., 2008; Wu et al., 2004). They are also important for normal development of the tracheal shape, as mutations in these genes reveal elongated and tortuous tracheal branches (Behr et al., 2003; Wu et al., 2004). In mice Claudin 4 and 6 are essential for blastocyst formation. Inhibition of their gene functions causes a lack of blastocoel cavity and an abnormally rounded shape of blastomeres (Moriwaki et al., 2007). In zebrafish, Claudins carry out functions in morphogenesis. MO knock-down of Claudin-15 results in a multiple lumen phenotype of the gut (Bagnat et al., 2007). A study of the zebrafish blastoderm revealed a function for Claudin-E during morphogenesis. Claudin-E is expressed by the enveloping layer (EVL), which moves vegetally over the yolk during epiboly. Knock-down of Claudin-E causes a slow and uneven advancement of the EVL and blastoderm resulting in delayed epiboly. This is probably caused by reduced tension on the EVL (Siddiqui et al., 2010).

3.3 Aim of the thesis

Cell-cell contacts mediate many dynamic cell behaviors during developmental processes like the formation of the vascular network. These cell-cell contacts contain among others tight junction proteins, whose role in the morphogenetic processes of angiogenesis remains largely unknown. Endothelial cells in mice specifically express Cldn5 as the key component of tight junctions. Therefore, I analyzed the role of Cldn5 during angiogenesis in zebrafish. For this purpose, I studied the effect of MO-mediated knock-down on the formation of ISVs using live-imaging techniques. Furthermore, I generated *cldn5b* mutant fish for the analysis of the gene function during angiogenesis.

4. Materials and Methods

4.1 Companies

All chemicals were obtained from the following companies:

Applichem	BD Biosciences
BioRad	Difco laboratories
Eurogentec	Fluka
Invitrogen	Machery-Nagel
Merck	Roche
Schwartz	Sigma-Aldrich

4.2 Buffer, Media and Solutions

0.1 M Glycin pH 2.2	75mg glycin in 10ml PBST
0.3 M Sucrose solution	102.69g/l sucrose in 1xPBS, heat until dissolved
0.3M Succrose-Solution	102,69g/l Succrose in 1x PBS
1% Agarose	Agarose in 1xTAE/TBE
10% (2mM) PTU (Phenylthiourea)	304 mg PTU (RT) in 1 l eggwater, stir on at 4°C, store at 4°C
10%SDS	10% sodium dodecyl sulfate in ddH_2O
1x SSCT	add Tween-20 to 0,1% final conc. in 1x SSC
2% Paraformaldehyde (PFA)	Dilute 4% PFA with 1x PBST
20mg/ml Proteinase K	Lyophilized powder is dissolved 20mg/ml in sterile 50mM Tris (pH8.0), 1.5mM calcium acetate. Divide stock solution into small aliquots and store at -20°C.
20x-SSC	NaCl 8,8g, NaCitrate 4,4g, H_20 to 1l Adjust to pH7.0
25x Tricaine	2g tricaine in 350 ml, set to pH 7.0 w TrisHCL (1M pH8.0). Fill up to 500ml. Aliquot. Store at -20°C.
2mM EDTA	93,05g EDTA (RT), add 400ml ddH_2O and

	10M NaOH to pH 8.0. Fill up to 500ml with ddH_2O. Autoclave.
4% PFA	550ml ddH_2O, warm under the hood to 60°C. Add 40g PFA, wear gloves, protection glasses, lab coat. Stir 5 – 40 min at 60°C. Add three to four drops of 2N NaOH, wait until cleared; if not, repeat. Take from heater, add 333,3 ml 10x PBS (pH 7.22). Fill up to 1l; filtrate
5% Bakto-Agar	5% Bakto-Agar in 0,3M Sucrose/PBS
50-70% glycerol	50-70% glycerol in ddH_2O
70% Ethanol	70% Ethanol in ddH_2O
Ampicillin stock solution (50mg/ml)	500mg Ampicillin (stored at 4°C) in 10ml H_2O. Sterilized with 0.2mm filter. Aliquot and store at -20°C.
Antibody solution in situs	Anti-dig IgG(FAB2)- alkaline phosphatase 1:3000 in blocking solution
Blocking solution antibody staining	2% goat serum and 5% BSA in PBST + 1:1000 NaAzid
Blocking solution in situs	2% sheep serum, 2mg/ml BSA in PBST + 1:1000 NaAzid
Blocking stock solution fluorescent in situ	10% (w/v) blocking reagent (Roche #1096176) dissolved in maleic acid buffer. Autoclave and store aliquots at –20 ˚C.
Chloramphenicol stock solution (34mg/ml)	340mg Chloramphenicol dissolved in 10ml 100% EtOH. Aliquot and store at -20°C.
DNA loading buffer (10x)	Dissolve 15ml glycerol in 40ml ddH_2O. Dissolve 100mg Orange G. Fill up to 50ml with water. Store at -20°C.
eggwater	6 g seasalt in 20 l autoclaved ddH_2O + 1% methylenblue
Equilibration buffer	0,1M Tris-HCL pH9.5 + 0,5M NaCl
Genomic DNA extraction	10mM Tris pH8

buffer	2mM EDTA 0.2% TritonX-100 0.5% SDS 200 µg/ml Proteinase K (keep cool!)
Hyb4	20x-SSC 250ml Torula-RNA 500mg Heparin 50mg Tween-20 1ml H_20 to 500ml Formamide 500ml
Kanamycin stock solution (10mg/ml)	100 mg Kanamycin dissolved in 10ml ddH_2O. Filter sterilize. Aliquot and store at -20°C.
LB (Lysogeny-broth) medium	10g peptone, 5g yeast extract, 10g NaCl in 950 ml ddH_2O. Shake until dissolved. Adjust to pH7.0 with 5N NaOH. Adjust to 1l with ddH_2O. Autoclave.
LB agar plates	Add 15g Bacto agar per liter LB medium. Autoclave and add antibiotics at 50°C. Pour into petridishes.
Maleic acid buffer	100mM maleic acid, 150mM NaCl, pH7.5
Methylcellulose	3% Methylcellulose in eggwater. Dissolve at 4°C.
Methylenblue	Dissolve 1g Methylenblue in 1l ddH_2O.
NaAzid	10% solution in ddH_2O. Store at -20°C.
PBDT	1x PBS, 1% DMSO, 0,1% Tween 20
PBS	NaCl 8 g KCl 0.2 g $Na_2HPO_4(2H_20)$ 1.8 g KH_2PO_4 0.24g Add H_2O to 1l Adjust to pH 7,2
PBST	10% PBS 0.1% Tween 20

PBSTX	0.5% TritonX-100 in PBST
SOB-Medium	10g Tryptone, 2.5g Yeast extract, 2.5mM KCl, 487 ml ddH_2O. Autoclave.
SOC	5ml of $MgSO_4$ (1M), 5ml $MgCl_2$ (1M) (both sterile filtered), 10ml Glucose (1M) + 500ml SOB.
SSC 20x	8.8g NaCl, 4.4g NaCitrate, H_2O to 1l, adjust to pH 7.0
SSCT	Dilute SSC 1/20, add Tween-20 to 0.1% final conc.
Staining solution (in situs)	200 µl NBT/BCIP stock solution (Roche) in 10ml equilibration buffer (or: 1 tablet NBT/BCIP in 10ml H_20 (Roche))
TAE (Tris-acetate-EDTA electrophoresis buffer)	242g Tris Base, 57.1ml Acetic Acid, 37.2g EDTA in 1l. Autoclave.
TBE (Tris-borate-EDTA electrophoresis buffer)	Dilute 200ml TBE (5x) in 800ml H_2O
TE (tris-EDTA) -buffer	10mM Tris HCl, 1mM EDTA in ddH_2O. Adjust to pH8.0.
TNT	100 mM Tris-HCl pH 7.5 150 mM NaCl 0.5% Tween20
TNTB	Blocking stock solution diluted 1:10 with TNT
TSS	5g PEG 6000, 1.5ml 1M $MgCl_2$, 2.5ml DMSO, add LB to 50ml. Filter sterilize (0.22µm). Store at 4°C.
Tris HCl	Dissolve 121.1g Tris base in 800ml ddH_2O. Adjust to desired pH by adding HCl.

4.3 Molecular Biology Protocols

4.3.1 Bacteria strains

strain	source
E.coli DH5α	Invitrogen
E.coli OneShot®Mach1™T1Rchemicaly competent cells	Invitrogen
E.coli OneShot®TOP10chemically competent cells	Invitrogen
E.coli OneShot®ccdB Survival™2T1Rchemically competent cells	Invitrogen
E.coli XL1blue	Invitrogen
E.coli TOP10 electrocompetent cells	Invitrogen

4.3.2 Plasmids and cDNA clones

plasmid	comment	source
pENTR/D-TOPO®	cloning vector, gateway cloning technology	Invitrogen
cldn5b cDNA	IRBOp991A1057D	ImaGenes
cldn5a cDNA	IRBOp991E0139D	ImaGenes
p5E-UAS	10xUAS element and basal promoter for Gal4 response, Gateway	Kwan et al., 2007
p5E-fli1ep	Fli1a enhancer promoter, Gateway	Driever, unpublished
pME-nlsmCherry	nuclear-localized mCherry	Kwan et al., 2007
pME-cldn5b wo stop	Cldn5b without stop, Gateway	this study
pME-gal4ff	Gal4ff	this study
p3E EGFP pA	EGFP for C-terminal	Kwan et al., 2007

	fusions, Gateway	
pDestTol2CG2	attR4-R3 gateway with SV40 polyA flanked by Tol2 inverted repeats with cmlc2:egfp transgenesis marker, Gateway	Kwan et al., 2007
pDONRP2R-P3	3`donor vector; attP2R-P3 flanking chlor/ccdB cassette	Invitrogen
pCS2FA-transposase	for in vitro transcription of capped Tol2 transposase mRNA	Kwan et al., 2007
pCS2+ cldn5b RNA expression vector	for in vitro transciption of capped cldn5b mRNA	this study
pTolUAScldn5bEGFP	C-terminal EGFP fusion to cldn5b under control of UAS	this study
pTolfliepnlsmCherry	nuclear localized mCherry under control of fliep	this study
pTolfliepgal4ff	Gal4ff expression under control of fliep	Zygmunt et al., 2011; Totong et al., 2011; this study
pCS2+	for in vitro transcription of mRNA	Rupp, Affolter lab
pCS2+ mKate	for in vitro transciption of capped mKate mRNA	this study
pmKate2-N	mKate2 expression, fusion	Evrogen

4.3.3 PCR amplification

1µl	template
1µl	10mM dNTPs
10µl	Phusion 5x buffer
2.5µl	10µM Primer
0.5µl	(2U/µl) Phusion DNA polymerase (Finnzymes)
32.5µl	H_2O

4.3.4 Restriction enzyme digestion and gel extraction

DNA		1µg – 5µg
Restriction buffer 10x		1x
Restriction enzyme		0,5 µl
add H_2O	to	20 – 100 µl

The digested DNA was separated by agarose gel electrophoresis and the desired bands were cut out of the gel. They were purified with the Sigma Gel Extraction Kit according to the manual.

4.3.5 Ligation and transformation

Vector	100 ng
PCR fragment	
T4 DNA ligase buffer (10x)	1,5 µl
T4 DNA ligase (NEB)	1 µl
Add H_2O to	15 µl

The reaction was incubated at 16°C overnight.

Chemically competent E. coli were thawed on ice for two min. 1µl of DNA solution was added to the tube (2µl for TOPO reaction cloning). The bacteria were incubated for 30 min. Meanwhile, the water bath was preheated to 42°C. The bacteria were heat shocked at 42°C for 40sec and kept on ice for 2 min. Then 0.5 ml prewarmed LB or SOC medium was added to the bacteria, which were then recovered by shaking (200rpm) at 37°C for 30 min. They were plated on selective LB medium and grown at 37°C ovn.

Clones were picked from the selective LB media plates and the plasmid isolated according to the manufacturers protocol (Sigma GenEluteTM Plasmid

Mini Kit). The constructs were tested by PCR or restriction enzyme digestion. For injection into fish or further use in Gateway reactions, larger bacterial cultures were inoculated and the plasmid isolated using the Sigma Plasmid Midi Kit. The isolated plasmid was sequenced.

4.3.6 Generation of plasmids via the Gateway system

4.3.6.1 Generation of Entry clones

For the generation of middle entry clones the gene of interest was PCR amplified with Phusion DNA Polymerase (Finzymes). The forward primer contains a CACC 5` overhang for directional TOPO cloning into pENTR/D-TOPO vector using the pENTR/D-TOPO cloning kit (Invitrogen). For further cloning the pENTR/D-TOPO manual (Invitrogen) was followed.

For the generation of 3` entry clones PCR amplification of the gene of interest was performed using the pDONR P2R-P3 vector. Here the forward primer contained an attB2 site (GGGGACAGCTTTCTTGTACAAAGTGGNN) 5`of the gene specific sequence. The reverse primer contained a reverse attB3 site (GGGGACAACTTTGTATAATAAAGTTGN). The PCR product was not purified. For further cloning the LR Clonase Gateway Enzyme Mix and the according manual (Invitrogen) was used.

After purification of the vectors (see midi preparation), they were verified by sequencing.

4.3.6.2 Generation of Expression clones

Multisite Gateway recombination reactions were performed as in the Invitrogen Multisite Gateway manual. All plasmids were diluted in TE buffer and reactions were performed with TE-buffer.

4.3.6.3 Generation of Tol2 mRNA

The pCS2FA-transposase plasmid was used as a template. 3 µg DNA was linearized with NotI and purified by ethanol precipitated (see section 4.3.9). RNA synthesis was performed using the mMessage mMachine SP6 Kit (Ambion). The RNA was purified by precipitation.

4.3.7 Generation of mRNA

cDNA was linearized and mRNA was transcribed according to the manufacturer`s protocol of mMESSAGEmMACHINE. The RNA was purified by precipitation.

4.3.8 Genotyping

4.3.8.1 Fin clips

materials:

- 200 ml beaker with 100ml egg water + 4ml tricaine (25x)
- 70% ethanol
- razor blades
- net
- sterile eppendorf tubes on ice
- plastic spoon
- plastic lid (single crossing cages)
- forceps
- genomic DNA extraction buffer

protocol:

Take one fish out of the tank with a net and put it into eggwater + tricaine. Wait until the fish is paralyzed, take it out carefully with a plastic spoon and put on a clean plastic lid. Take one razor blade and press on the tip of the fin. Use another razor blade to cut off the tip of the fin. Use forceps to put fin into eppendorf tube with 100 µl genomic DNA extraction buffer. Put the fish into a single fish cage with eggwater + methylenblue.

4.3.8.2 Genomic DNA extraction

- for fin clips:

Incubate Eppendorf tubes at 55°C at 800 rpm for 4 hrs to ovn and spin down liquid. Denature proteinase K at 94°C for 10` and spin down debris for 30`at 4°C. Dilute DNA 1:10 in H_2O.

- for embryonic pools:

Set up 30- 40 crossings (single female + single male). Let embryos grow until 1.5 – 2 dpf and pool 5 embryos per well (in total 80 embryos per crossing). Remove egg water (as much as possible) on ice and add 100 µl genomic DNA extraction buffer per well (on ice). Incubate at 50°C 4hrs to ovn (much better ovn), take lid off the wells before taking out of incubator. Put 50µl of

DNA prep into new PCR 96 well plate and cover well with sealing tape. Then denature proteinase K at 94°C, 10` and dilute DNA 1:10 in H_2O.

4.3.8.3 PCR on genomic DNA

- make master mix:

5 µl	primer (10µM)
5 µl	dNTPs (2mM)
5 µl	Titanium Taq Buffer
1 µl	Genomic DNA
0,5 µl	Titanium Tag
28,5 µl	H_2O

- protocol:

98°C 1`
98°C 30``
68°C 30`
68°C 10`
10°C f.e.

Add 50µl per well, then add genomic DNA and cover with sealing tape.

4.3.8.4 Restriction enzyme digestion

make master mix:

5 µl	10x NEB Buffer 4
0,5 µl	HinfI
20 µl	DNA
add to 50 µl	H_2O

When using genomic DNA of fixed embryos, use 30 µl DNA.

Digest at 37°C for 2hrs. Add 20µl H_2O to original PCR (for fixed embryos, do not add H_2O). Analyze on TBE agarose gel by loading 20µl of digestion and 10µl of PCR on gel.

4.4 Immunohistochemistry and in situ hybridization

4.4.1 Immunofluorescence whole mount antibody staining

4.4.1.1 Primary antibodies

Host	Specificity/ dilution	source
mouse αhuman / mono	ZO-1 / 1:200	Zymed
rabbit αzebrafish / poly	VE-cad /1:200	H.G. Belting
mouse αhuman / mono	Cldn5 / 1:150	Invitrogen
Rabbit αzebrafish / poly	Cldn5b	PickCell Laboratories

Rabbit αzebrafish / poly	Cldn5b	PickCell Laboratories
guineapig αzebrafish / poly	Cldn5b	PickCell Laboratories
guineapig αzebrafish / poly	Cldn5b	PickCell Laboratories

4.4.1.2 Secondary antibodies (all Invitrogen)

Conjugate	Specificity/ dilution	source
Alexa568	goat αrabbit IgG	Invitrogen
Alexa633	goat αrabbit IgG	Invitrogen
Alexa568	goat αmouse IgG	Invitrogen
Alexa633	goat αmouse IgG	Invitrogen
Alexa568	goat αguineapig IgG	Invitrogen
Alexa633	goat αguineapig IgG	Invitrogen

All Alexa conjugated antibodies were diluted 1:1000 in blocking solution.

4.4.1.3 Immunofluorescence whole mount antibody staining

All incubations were performed on a rocking platform.

For prehybridization of antibodies, Incubate antiserum at final dilution in blocking solution with fixed embryos ovn at 4°C. Use at least 100 embryos/5ml of antiserum solution. For antibody stainings fix embryos in 2%PFA for 2hr at RT or ovn at 4°C. Then wash three times in PBST, 5`at RT.

Permeabilize (depending on primary antibody) with PBSTX:

15` 1dpf 30` 1,5 dpf

60` 2dpf 90` 3dpf

Block in 500µl of blocking solution, 2hrs at RT. Incubate primary antibody in blocking solution, ovn at 4°C. Wash 3x 5`at RT with PBST. Wash every hour with PBST. Incubate with secondary antibody 2hrs at RT or ovn at 4°C. Wash 6x over 3-4hrs, even better: ovn.

4.4.2 Vibratom Sectioning and Antibody Stainings on Sections

Materials

- Cyanacrylat Glue (Roti®call1, Carl Roth GmbH)
- Succrose-Solution
- Bakto-Agar
- PBDT
- blocking solution

Sectioning:

1. Fixation of fish in 2%PFA 2hrs RT, on shaker, 3x5` washing in PBST
2. Incubation in Succrose solution, 30` 4°C (this will improve the connection of embryo and embedding medium)
3. Embedding in Bakto-Agar
   Keep this solution at 55°C, place embryos in 24well plate whole each, add Bakto-Agar, orient embryo so that anterior is down, posterior up and ventral away from you and dorsal towards you. Cut a square with embryo out of the agarose
4. Glue the solid block onto the round metal plates of the vibratom using special Cyanacrylat glue
5. Vibratom settings:
   Feed: 150-200µm Freq: 7.8
   Speed: 5.5
   Fill the sectioning box completely with PBS. Remove the sections using a cut brush; collect them in 24well plates in PBDT

Antibody-Stainings:

1. short wash with PBDT, this and all following steps in 24 well plate
2. Blocking 60-100 min in blocking solution
   Slow shaking at RT, Primary antibody incubation; ovn at 4°C
3. Removal of primary antibody; washes 6x10`in PBDT, Secondary antibody incubation; 1h RT; slow shaking; keep dark!
4. Removal of secondary antibody: washes 6x10`in PBDT (you can store these sections until analysis for 1-2 weeks at 4°C)

5. Mounting: single out the best sections, use whole agar slice or remove sections from agar, arrange them on a slide, remove liquid and add a few drops slow Fade, add cover slip without air bubble formation

4.4.3 Whole-Mount in situ Hybridization

Probes were generated using the DIG RNA labeling mix from Roche.

Fixation:

1. Fix embryos with 4% parformaldehyde in PBS overnight at 4°C, or for 3h RT (for 3 day old embryos). Over 20 somites dechorinate before fixing. 40 embryos or less in 1ml PFA. 3x wash with PBST, 5 min each, at RT.
2. Remove the embryos from their chorions using watchmaker forceps (easiest at this point, if they have not been dechorionated already).
3. Transfer embryos to vials with 100% methanol (MeOH), equilibrate for 5min with at least 4 changes of MeOH. **Note**: From this point on, the embryos remain in the same plastic tube until they are ready for rehybridization.
4. Cool the embryos to -20°C for at least 30 min (embryos can be stored that way for months; this step is necessary for permeabilization of embryos even if you do not want to store them).

Protocol A (0- bud stage):

5. Directly from storage, replace MeOH with 200µl preHyb+ (depending on no. of embryos)
6. Incubate for 1-3 h at 68°C (heat oven)
7. Replace preHyb+ with Hyb+RNA-probe, (0,5µl-4µl in 200µl, depending on the probe (1:50 to 1:200). Incubate overnight at 68°C

Protocol B (later stages, 24hpf onward):

6. Rehydrate embryos in PBST (2x5min). 1-3 h at 68°C (heat oven)
7. Replace PBST by proteinase K (20mg/ml stock solution) in PBST, dilution 1/2000 for 24 hpf and older, 200µl for each probe
8. Incubate: 25hpf: 8min, 28hpf: 10 min, 32hpf: 13min, 48pf: 30min
9. Wash 2x in PBST. Fix for 20min at RT in 4% PFA
10. Wash 1x5min in PBST, 1x1min in H_2O and 1x5min in PBST

Hybridization:

11. Incubate for 1-3h at 68°C (heat oven or water bath)
12. Replace preHyb+ with Hyb+RNA-probe, (0,5µl – 4µl in 200µl, depending on the probe; 1:50 to 1:200), incubate over night at 68°C

Probe removal and wash:

13. Next morning, remove probe (probes can be reused twice).

a) wash 1x20min in 0,5ml Hyb-, 68°C (all solutions should be 68°C)
b) wash 2x20min in 0,5ml 2xSSCT, 50%Formamid 68°C
c) wash 1x20min in 0,5ml 2xSSCT, 25% Formamid 68°C
d) wash 2x20min in 0,5ml 2xSSCT, 68°C
e) wash 3x30min in 0,5ml 0,2xSSCT, 68°C
f) wash 1x5min in 0,5ml PBST, 68°C

Incubation with anti DIG/FITC antiserum:

14. Block with blocking solution at RT, minimum 1h
15. Replace with 200µl of a 1/3000 dilution (0,375U/ml) of sheep anti-digoxygenin alkaline phosphatase conjugated Fab-fragments (+NaN 1:1000), incubate in antibody solution overnight with agitation at +4°C ON, or for 2h at RT

Staining:

16. Wash for at least 2h in PBST, changing solution 10 times (8x 15`, 2x30`). This is an important step to prevent background.
17. Equilibrate 2x5`in equilibration solution (to prevent precipitation of salt in buffer)
18. Stain with freshly made NBT/BCIP solution. Incubate embryos in staining solution at RT (if faster necessary at 37°C) in the dark and monitor with a dissecting microscope.
19. Stop the reaction by removing the staining solution and washing the embryos in PBST. Store the embryos in PFA at +4°C in the dark
20. Clearance for staining with high background:
    Stop staining only once in PBST, 2x5` glycin, 4x5` PBST

Mounting:

21. For observation using a dissecting microscope, mount embryos in glycerol, 50-100% depending on the tissue observed (70% for expression

in brain and vessels). For longer storage, store in 4% PFA at 4°C, as embryos tend to get dark in glycerol

4.4.4 Double whole-mount FISH using Alexa Tyramides

The FITC/DIG labeled probes were generated using the RNA Labeling Mix from Roche. Different probe concentrations were tested beforehand.

Solutions:

- Hyb
- 20X SSC
- 50% Formamide in 2x SSCT
- 25% Formamide in 2x SSCT
- TNT
- TNTB
- Blocking Stock Solution 10x

Fixation, Rehydration and Hybridization:

- See section 4.4.3

Washes and blocking:

- Wash see section 4.4.3 (probe removal and wash)

5' TNT (this wash at RT). Block in TNTB at RT, at least 1 h.

Detection of the FITC-labeled probe:

- Mix a 1:500 dilution of the HRP-coupled anti-FITC (Roche) in TNTB. Replace TNTB from the previous step with the antibody mix and incubate ON at 4 ˚C.
- Remove the antibody mix and wash 8x 15' with TNT.

Staining:

- Spin down TSA substrate before making staining solution. For the reaction, dilute tyramide reagent 1:50 in Perkin Elmer amplification diluent buffer.
- Incubate 30-60 minutes in TSA Plus Fluorescein Solution. During this incubation, we lay the microcentrifuge on its side. Reaction time must be determined empirically for each probe. Unfortunately, the staining reaction cannot be visually monitored as the substrate is fluorescent, and one will see ubiquitous green fluorescence throughout the staining reaction.
- Wash 3x5`with TNT.

Bleaching:

- Bleach with 1% hydrogen peroxide in TNT, 30', to inactivate the peroxidase conjugated to the first antibody (for early stages 20' are enough).
- Wash 5x 5' with TNT (big volumes! Hydrogen peroxide must be completely washed out). Block in TNTB at RT, at least 1 h.

Detection of the DIG-labeled probe:

- Mix a 1:1000 dilution of the HRP-coupled anti-DIG in TNTB (Roche). - Replace TNTB from the previous step with the antibody mix and incubate ON at 4 ˚C. Remove the antibody mix and wash 8x 15' with TNT.

Staining:

- Spin down TSA substrate before making staining solution. For the reaction, dilute tyramide reagent 1:50 in Perkin Elmer amplification diluent buffer.
- Incubate 30-60 minutes in TSA Plus TMR Solution. During this incubation, we lay the microcentrifuge on its side. Reaction time must be determined empirically for each probe. Unfortunately, the staining reaction cannot be visually monitored as the substrate is fluorescent, and one will see ubiquitous green fluorescence throughout the staining reaction.
- Wash 3x 5' with TNT.

DON'T POSTFIX.

Note: Use FITC before TMR reaction, develop week probe before strong probe

4.5 Fish lines, maintenance and handling

4.5.1 Fish maintenance

Fish were maintained and bred according to standard protocols (Westerfield, 2000).

4.5.2 Fish lines

Wildtype lines:

Fish line	Source/reference
AB/EK	W. Driever, Freiburg
EK/TL	W. Driever, Freiburg

Transgenic lines:

Fish line	Source/reference
Tg(UAScldn5bEGFP)	this study
Tg(fliep:GFF)	(Asakawa and Kawakami, 2008) Lukas Herwig, this study
Tg(fliep:GFF;UASmRFP)	Zygmunt et al., 2011; Totong et al., 2011; Lukas Herwig, this study
Tg(fli1a:EGFP)	(Lawson and Weinstein, 2002)
Tg(fli1a:EGFP; gata1:dsRed)	(Chico et al., 2008)
Tg(fli1a:EGFP;fliep:nlsmCherry)	this study
Tg(fli1a:EGFP)cldn5b^{ubs11}	this study
Tg(fli1a:EGFP)cdh5^{ubs8}	Heinz-Georg Belting

4.5.3 DNA/RNA and morpholino injection

Microinjection needles were pulled with a Sutter Instrument Co. Agarose plates were made by pouring 1% agarose into petridishes and putting a plastic mold with striations on the surface. After polymerization the mold was removed. Eggwater was poured over the agarose and the plates were stored at 4°C. The microinjection needles were loaded with DNA/RNA with the help of a microloader (Eppendorf). Needles were connected to a FemtoJet microinjector (Eppendorf) or a hand injector. The tips of the needles were cut of with forceps. The DNA/RNA was injected into the yolk close to the cell or into the cell.

4.5.4 Generation of transgenic fish lines

Approximately 200 eggs (one cell stage) were injected with 60 pg DNA and 60 pg Tol2 RNA. Embryos were screened for transient reporter gene expression between 24 hpf and 48 hpf. Fish transiently expressing the reporter gene were raised separately from the others. Founders were screened for germline transmission by screening at least 100 embryos for expression of the transgene.

4.6 Confocal microscopy

4.6.1 Mounting and confocal microscopy of fixed embryos

The trunk and tail of the embryo were cut off the head and yolk with a razorblade. The tail was embedded in vectashield (Vector Laboratories, Inc.) on an objective slide (ThermoScientific) and covered with a cover slip (Marienfeld Laboratory Glassware). Images were taken with the Leica SP5 confocal microscope with the 20x objective, 20x objective with 2x zoom or the 63x objective. A frame size of 512x512 pixel and 512x1024 pixel and a step size of 0.8 µm – 1 µm was used. Pictures were processed with Imaris® (Bitplane) and ImageJ.

4.6.2 Mounting and confocal live imaging of living embryos

0.7% low melting agarose was dissolved in egg water. For mounting it was melted in the microwave. After addition of 0.01% tricaine (pH7.5) and 1x PTU the agarose was kept at 55°C during mounting. Reporter gene expressing embryos were selected under the fluorescent binocular microscope (brand) and anesthesized with 0.01% tricaine in egg water. A big drop of agarose was put on the 10mm microwell of a 35mm petridish (No. 1.5 coverglass, 0.16-0.19 mm thickness; Glass Bottom Culture Dishes from MatTek). Embryos were mounted in the agarose and covered with egg water containing 0.01% tricaine and 1x PTU. The Leica SP5 confocal microscope was used for imaging. The heating chamber was set to 28.5°C. All movies were taken with a frame size of 512x512 pixel and a stack thickness of between 80 – 110 µm. For Tg(fli1a:EGFP) fish, the 20x objective was used with a 2x zoom. For Tg(UAScldn5bEGFP) fish, the 63x objective was used. Movies were processed with Imaris® (Bitplane) and ImageJ.

5. Results

5.1 Contributions to publications

5.1.1

Distinct cellular mechanisms contribute to vessel anastomosis and lumen formation in the zebrafish DLAVs

Lukas Herwig[1], Yannick Blum[1], Alice Krudewig, Elin Ellertsdottir, Anna Lenard, Heinz-Georg Belting and Markus Affolter

1 – contributed equally to this work

Current Biology – submitted

Contribution:
Together with Lukas Herwig I generated the pTol(*fli1ep*:Gal4ff)^{ubs4} transgenic zebrafish line using the Gateway® system (Invitrogen™). I contributed to discussions during writing of the manuscript.

Distinct cellular mechanisms contribute to vascular anastomosis and lumen formation in zebrafish DLAVs

Lukas Herwig[1], Yannick Blum[1], Alice Krudewig, Elin Ellertsdottir, Anna Lenard, Heinz-Georg Belting[2] and Markus Affolter[2]

Running Title: Cellular Mechanisms of Vascular Anastomosis

Biozentrum der Universität Basel, Klingelbergstrasse 70, CH-4056 Basel

[1] these authors contributed equally to this work

[2] corresponding authors

email: heinz-georg.belting@unibas.ch

markus.affolter@unibas.ch

Summary

While many of the cellular and molecular mechanisms of angiogenesis have been intensely studied, very little is known about the processes that underlie vascular anastomosis. We have generated transgenic fish lines expressing an EGFP tagged version of the junctional protein ZO-1 to visualize cellular behaviors that occur during vessel fusion and lumen formation *in vivo*. These life observations of cell junctions during anastomosis and lumen formation show that endothelial cells perform distinct morphogenetic mechanisms, cell hollowing and cord hollowing to generate different types of vascular tubes. In the case of cell hollowing, the vascular lumen is formed by extension of the proximal lumen of the ISV and gives rise to a seamless, unicellular tube. This process is primarily driven by cell membrane invagination rather than vacuole formation. In the case of cord hollowing, new apical membrane compartments are brought together by cell rearrangements, which result in lumen coalescence and formation of a multicellular tube. Thus, DLAVs and ISVs consist of two different types of tubes: multicellular tubes that arise by cord hollowing and unicellular tubes that are generated by cell hollowing.

Results and Discussion

Generation and expansion of vascular beds by vascular remodeling involves a variety of morphogenetic mechanisms such as angiogenic sprout and lumen formation, as well as blood vessel fusion (anastomosis) and their removal (pruning). Anastomosis is the essential process that converts otherwise non-productive dead-end sprouts into a functional vascular network. Angiogenic sprouts are guided by so-called tip cells, which are more motile and send out more filopodia than the trailing stalk cells [1]. During the first step of anastomosis, tip cells from neighboring sprouts establish contact with each other [2, 3]. Subsequently, endothelial cells (ECs) from neighboring sprouts form a continuous epithelium and their lumens are connected. How these events are achieved and coordinated at the cellular level is not known. We have used the zebrafish dorsal anastomotic vessels (DLAV) as a model to analyze the cellular mechanisms that underlie vascular anastomosis *in vivo*. To this end we generated transgenic reporter lines that label endothelial cell junctions (*fli1ep:GAL4ff*$^{ubs2\text{-}4}$ and *UAS:EGFP-ZO1*$^{ubs5\text{-}7}$, see supplementary material). These lines allowed us to follow individual cell junctions and, consequently, relative cell movements and cell shape changes, as they occur during vascular remodeling.

The DLAV is formed in a seemingly stereotypic pattern by the anastomosis of neighboring segmental arteries (SA) [4]. Tip cells of individual SA that have reached the roof of the neural tube extend processes laterally both in rostral and caudal direction. Some of these filopodia emanating from neighboring tip cells eventually contact each other, stabilize and integrate into the DLAV. During further development, a lumen extends through the SA and the DLAV (see Fig. 1A, S1A). We first examined the cellular architecture of DLAVs to determine whether this vessel is made of unicellular (intracellular) or multicellular (extracellular) tubes. By photoconversion of the fluorophore KAEDE in *fli1ep:GAL4ff*^{ubs2}*;UAS:KAEDE*^{rk8} embryos we labeled single cells within the DLAV and determined whether these spanned the circumference of the DLAV either entirely or partially (Fig. 1B,C). In 16 out of 24 cases, we found cells enclosing the entire lumen representing a unicellular tube, whereas in 8 out of 24 cases labeled cells covered the vessel only partially, which is indicative for multicellular tubes. To test whether the different cellular arrangements correspond to the patterns of EC junctions, we performed photoconversion experiments and subsequently visualized adherens junctions by

immunofluorescence using an antibody against zf-VE-cadherin [5]. Consistently, we found that unicellular regions did not contain junctions (Fig. 1D,D'), whereas photoconverted cells nested within a multicellular region were demarcated by longitudinal lines of VE-cadherin (Fig. 1E,E'). To visualize endothelial cell contacts *in vivo* we generated a transgenic reporter line *UAS:EGFP-ZO1*$^{ubs5\text{-}6}$ (Fig. S1B). In double transgenic embryos (*fli1ep:GAL4ff*^{ubs2}*;UAS:EGFP-ZO1*^{ubs5}), we compared the localization of the EGFP-ZO1 fusion protein with the distribution of VE-cadherin and found that it specifically labels cell junctions, albeit in a mosaic fashion (Fig. S1C). Furthermore, we were able to confirm the heterogeneity in vascular architecture by the junctional patterns observed *in vivo* in *fli1ep:GAL4ff*^{ubs2}*;UAS:EGFP-ZO1*^{ubs5} transgenic embryos. In these embryos we found regions that had predominantly ring-shaped cell contacts (Fig. 1F) as well as regions that contained more complex junctional patterns (Fig. 1G). Thus, DLAVs (and also ISVs – data not shown) are heterogeneous in their architecture and can consist of different types of tubes: unicellular, multicellular tubes and tubes of mixed cellular arrangements.

To analyze the cellular dynamics of DLAV formation, we first focused on the initial events of contact formation between neighboring tip cells. From studies using immunofluorescent detection of ZO-1 we had previously proposed a model in which interactions between tip cells lead to generation of junctional spots at the contact sites [5]. These spots elaborate into rings as the cells increase their mutual surface area. Analysis of VE-cadherin protein revealed identical patterns (Fig. 2A-C). Since this sequence of events was inferred from observations in fixed tissues, we wanted to test this model in an *in vivo* situation by performing confocal time-lapse analyses on our EGFP-ZO1 reporter. In essence, the pattern of EGFP-ZO1 was congruent with our previous observations, thus confirming the above model (Fig. 2D-F; movie S1). Moreover, junctional remodeling is extremely dynamic – the transformation from spots to rings occurs within less than 40 minutes.

Whereas initiation of anastomosis appeared to be consistently associated with formation of ring-shaped junctions, the subsequent establishment of the DLAV showed considerably greater complexity and variety – in respect to (i) junctional remodeling, which corresponds to extensive cell rearrangements, (ii) the generation of a continuous endothelium with apical-basal polarity and (iii) lumen formation. After

analysis of 15 time-lapse movies representing 19 fusion events, we were able to discern two distinct junctional behaviors, which represent two alternative cellular mechanisms that underlie DLAV formation.

In some instances (7 events in 15 movies), we observed a mechanism that appears to be primarily driven by cell rearrangements (Fig. 3; movie S2). Here, cell contacts between at least 3 adjacent cells generate 2 (or more) junctional rings, which converge towards each other as the outer cells migrate over a central cell. This convergence ultimately results into novel contacts between the outer cells, the establishment of a new junction and the detachment of the medial cell at this site of contact (summarized in Fig. 5). Thus, the outcome of the process is the formation of a continuous apical surface concomitant with the fusion of local luminal spaces, which are contained within the junctional rings. In principle, this mechanism of luminal coalescence can act locally or, if occurring iteratively, may be used to lumenize longer stretches of tubes. Superficially, the mechanism we observe resembles cord hollowing mechanisms that have been described for the intestinal lumen in fish [6] and the dorsal aorta in mouse [7], both of which rely on *de novo* epithelial polarization and subsequent luminal coalescence to form a multicellular tube. Whereas the cellular mechanism of lumen coalescence in the dorsal aorta has not been described, lumen coalescence in the intestine has been. However, in details it appears different from the DLAV, as it seems to be driven by luminal expansion rather than cell rearrangements [6]. In contrast, a mechanism of remarkable similarity has been described for hollowing the notochord in the ascidian *Ciona intestinalis [8]*. In both systems, zebrafish DLAV and *Ciona* notochord, lumenization commences with the *de novo* establishment of apical domains at opposite sites of individual cells and is followed by cell movements and cell shape changes, which result in the formation of a continuous epithelium and the fusion of luminal spaces. To test, whether blood pressure is required for cell rearrangements during anastomosis, we blocked heartbeat by the injection of anti-sense morpholinos against cardiac troponin (*tnnt2a*) [9]. Whereas lumen formation in *tnnt2a* morphants proved difficult to monitor, we observed that the initial steps of anastomosis (i.e. the formation and elaboration of apical compartments) was relatively normal (see Fig S2A and movie S3). Further, cell movements appeared unaffected.

In the majority of time-lapse movies (12 events in 15 movies), we observed an alternate mechanism of vessel fusion that appears to be intrinsically connected to a different mechanism of lumen formation. In these instances, junctional rings did not move or extend towards each other, the cells exhibited much less migratory behavior and we did not find continuous adherens junctions along the vascular axis (Fig. 4, movie S4). Instead, the ECs maintained their junctional configuration throughout the process of lumenization. Imaging the dynamics of lumen formation *in vivo*, either by intravascular quantum dot injection or by lack of cytoplasmic mRFP, revealed that the lumen extended between two separate apical patches and joined them by a cell hollowing mechanism (Fig.4, Fig.S2B, movies S4 and S5, summarized in Fig.5). This mechanism leads to a transformation of the "tip cell" into a "fusion cell", which forms a unicellular tube containing an "intracellular" lumen. This was demonstrated by a blood cell serendipitously passing through the two junctional rings of a hollowed-out cell (insets in Fig. 4, movie S4).

The "fusion cell" of the DLAV may be considered analogous to the "doughnut cell" that is important for tubular fusion within the *Drosophila* tracheal system and eventually forms a seamless tube [10-12]. In the case of the "doughnut cell" it has been shown that the intracellular tube is generated by cell shape changes, which eventually lead to an intracellular membrane fusion [13]. Future experiments will show whether a similar mechanism is also used in the vertebrate vascular system. The cell shape changes, which occur during anastomosis, are far more drastic than those in the *Drosophila* tracheal system. We observed asymmetric cell shape changes, since the tip cell became hollowed in a proximal to distal direction - that is from the lumenized side. Furthermore, the direction of cell hollowing was independent of the anatomical orientation and occurred either in a ventral to dorsal or dorsal to ventral direction (compare Fig.4, S2B, S2C and movies S4, S5 and S6). In all cases, the lumen was formed in a continuous fashion and we did not detect isolated luminal spaces within the cell. These observations suggest that blood pressure may be a driving force for this type of anastomosis and vessel formation.

Using several combinations of labeling systems, we have shown that DLAVs and ISVs are both made up by different types of tubes, unicellular and multicellular. By observing cellular dynamics during anastomosis in vivo, we have further shown that

vascular anastomosis during DLAV formation can occur by very different morphogenetic mechanisms, either by cord hollowing processes generating a multicellular tube, or by a cell hollowing process resulting in a unicellular/seamless tube. In both cases, anastomosis is intrinsically connected with *de novo* lumen formation at the site of vessel fusion.

Here, we have studied the anastomosis of ISVs, which results in the formation of a new vessel, the DLAV. Accordingly, the principles outlined may also serve as a paradigm for vessel formation in general. It has previously been suggested that tubulogenesis may occur differently in various types of blood vessels [3, 14-18]. In general it appears that larger caliber multicellular tubes such as the mouse or zebrafish dorsal aorta use a cord hollowing mechanism [7, 16, 18], whereas small unicellular tubes use a cell hollowing mechanism [17, 19]. Previous *in vitro* studies in three dimensional culture systems have suggested that endothelial cell hollowing is driven by the intracellular coalescence of vacuoles [20, 21]. Concurring with this view, vacuole coalescence has also been proposed as the chief mechanism in the formation of unicellular ISVs in zebrafish embryos [17, 22]. In contrast, our *in vivo* studies show that cell hollowing during unicellular tube formation is driven rather by cell shape changes than by vacuole coalescence. These discrepancies to the earlier studies may be explained in several ways. Firstly, the dynamics of cell hollowing suggest that blood pressure plays an important role in cellular invagination. Several studies have recently demonstrated an important role for blood pressure in vascular remodeling [23-25]. *In vitro* cell culture systems, by design, do not provide blood pressure and ECs are not likely to show such drastic cell shape changes in this context. Secondly, imaging of cell shape changes requires a system that allows the identification of single cells. Our system of labeling endothelial cell junctions *in vivo* has enabled us to trace the outline and shapes of individual cells and to separate intracellular from extracellular spaces. These observations are in agreement with our microangiography experiments and strongly suggest that the early lumens that are generated during unicellular tube formation consist of extracellular lumens rather than large intracellular vacuoles. Our model does not preclude a significant contribution of vacuoles or vesicles to vascular lumen formation, such as expansion of apical membrane surfaces and of the extracellular vascular lumen.

Taken together, we describe two novel cellular mechanisms that govern vascular tube formation and anastomosis. These mechanisms although used by the same type of blood vessel employ very different cellular activities, cell rearrangements or cell invagination, respectively, to form and connect novel lumens, and therefore lead to vessels of distinct cellular architectures. Both mechanisms are used at a comparable rate of instances, suggesting a stochastic selection of the process. Future experiments will explore the parameters, such as blood pressure, vessel size and cell motility and number, which may influence the choice of mechanism.

Figure Legends

Figure 1:Anastomosis andheterogeneity of endothelial tubes.
(A) High-resolution movie (63x lens, 2x zoom, 2 minutes between time points) shows steps during DLAV formation. Tip cells reach the dorsal side of the embryo and send filopodia in anterior and posterior directions (00:18, arrow). The tip cells contact each other and form the DLAV (00:48). Later the lumen opens from the stalk and proceeds into the DLAV (arrow in 4:12 and 7:08).
Different vessel architectures represented in B-G, D' and E' are found in the ISV/DLAV.Single photoconverted cells (red) show a unicellular/seamless (B) and a multicellular arrangement (C). Inserts (i-iii) in (B) and (C) show a surface calculation (i), a sagittal cross section (ii) and the coronal cross section (iii) at the sites indicated by crosshair; single photoconverted cells (red) show a intracellular (D) and a extracellular arrangement (E). Corresponding VE-cadherin immunostainings are shown in (D') and (E'). Small rectangles (yellow) indicate regions of unicellular (D-D') and multicellular (E-E') tubes; a unicellular tube outlined by EGFP-ZO1 fusion protein is shown in (F), extracellular/intracellular and mixed arrangements represented by EGFP-ZO1 protein are shown in (G). The yellow arrow in (F) points at delocalized EGFP-ZO1 protein in the cell membrane. This mislocalization is most likely due to high levels of protein expressed in these cells. (B, C, D and E) High-resolution images (63x objective, 4x zoom) of 48hpf old embryos carrying a GAL4FF activatable UAS:Kaede transgene. Nuclei (n in figure) of single cells were converted by UV treatment. (F,G): High-resolution images (63x objective, 2x zoom) of 48hpf old embryos carrying the GAL4FF dependent UAS:EGFP-ZO1 (green) and UAS:mRFP (red) transgene. (D'),(E'): High-resolution images (63x objective, 2x zoom) of VE-cadherin immunostainings after photoconversion, cytoplasm (blue), α-VE-cadherin (green), photoconverted cells (red).

Figure 2: Initial contact formation during anastomosis. (A-C) VE-cadherin immunostainings of 30 hpf old fli:EGFP embryos. Spots, small and larger rings are shown in panel A, B and C respectively (see arrow). (D-F): picture series of supplementary movie S3 showing a time-lapse of a *fli:GAL4FF; UAS:mRFP; UAS:EGFP-ZO1* embryo (time: 1h20'). An initial contact spot of EGFP-ZO1(arrow in A) is elaborated into a small (arrow in B) and subsequently into a larger loop

(arrow in C), thereby stabilizing the fusion cell contact (see movie S1). The yellow arrow in (F) points to delocalized EGFP-ZO1 in the cell membrane (compare Fig. 1 and Fig. S1)

Figure 3: Multicellular lumen formation. Picture series from movie S2 showing a time-lapse of a *fli:GAL4FF; UAS:mRFP; UAS:EGFP-ZO1*embryo (time: 9h 20'). A tip cell has formed contacts with an adjacent tip cell (on the right) and has contact with a stalk cell, which results in two loops of EGFP-ZO1(arrow in A). These loops extend and eventually meet (B,C). A'-D' shows the junctional outline of participating cells (yellow: "central" cell, green: stalk cell, red: DLAV cell moving in from posterior (right)). The two initial cell contacts are shown in yellow/green and yellow/red, respectively. When stalk cell and the adjacent DLAV cell meet, they establish a new contact with "green/red" junctions (arrow in D, green/red line in D').

Figure 4: Anastomosis and fusion by cell hollowing. Picture series from supplementary movie S4 showing a time-lapse of a *fli:GAL4FF*^{ubs2}*; UAS:mRFP; UAS:EGFP-ZO1*^{ubs5} embryo (time: 10h 25'). A tip cell has formed initial contacts and subsequently forms loops of EGFP-ZO1 with its adjacent partner (arrow in A and B). The stalk shows a multicellular organization (two lines of EGFP-ZO1, arrowhead in B) and the lumen opens in this region (waved arrow in B). From (C) on the lumen invaginates into the fusion cell (follow arrow from C to E) and finally reaches the left loop of EGFP-ZO1, which is subsequently inflated (arrow in F). The lumen then continues to extend in the unlabeled fusion cell on the left (arrow in G). Right after, a red blood cell passes the newly formed intracellular lumen (follow arrowhead from G to J). Insets show the blood cell passing behind the junction (G) and once in front of the junction (H).

Figure 5: Distinct morphogenetic mechanisms of anastomosis and lumen formation in multicellular and unicellular blood vessels. (I) Neighboring tip cells deposit junctional proteins (VE-cadherin, ZO1) at the sites of contact formation (B). The contacted areas are expanded leading to a transformation of the initial junctional spots into rings. Individual tip cells are shown in green, blue and yellow, respectively). The ISV stalk can be either unicellular or multicellular. For simplicity,

a single adjoining stalk cell is shown in purple. Junctions are shown in two colors corresponding to the cell on either site of the cell contact.

From here, two different morphogenetic mechanisms lead to two different types of tubes i.e. unicellular/seamless tubes (II) or multicellular tubes (III). (II) A lumen, which has extended from the dorsal aorta into the stalk, invaginates into the "fusion/tip" cell (blue) (A). (The lumen is visualized in a lighter shade of the color of the surrounding cell). As the lumen reaches the distal end of the fusion cell (B), it merges with the previously formed apical membrane compartments at the contact sites, presumably by membrane fusion (C). (III) (A') to (C') show longitudinal sections along the black line shown in (A). Several cells (shown here in purple, blue and yellow) enlarge intercellular contact surfaces (A). Further cell rearrangements generate novel contacts between the purple and yellow cell (B) and lead to a local detachment of the blue cell at the novel contact site (C). As a result, two local compartments (blue/purple and blue/yellow) merge into a single multicellular lumen.

Experimental procedures

Construction of pT2fli1ep:GAL4FF vector

A PCR fragment containing the ORF of the GAL4-VP16 derivative Gal4FF (GAL4FF) was amplified from the pT2KhspGAL4FF vector [26, 27] using following primers (fwd pr. 5'-caccatgaagctactgtcttc-3' / rev pr. 5'-ttagttacccgggagcatatc-3') and directionally TOPO-cloned into the entry vector pENTR™/D-TOPO® (Invitrogen). The resulting pENTR:GAL4FF entry clone was recombined with the endothelial-specific destination vector pTolfli1epDest [28] via a Gateway LR reaction to yield the expression vector pTolfli1ep:GAL4FF.

Plasmid Construction

pT2UAS:EGFP-ZO1-cmlc:EGFP: A XhoI/AgeI 14xUASE1b fragment was PCR amplified using the following primers: (forward: 5'-GTGACCTCGAGAAGCTTAGGCCTCCAAGG-3' reverse 5'-GTATCACCGGTTCGAGGGAATTCGTGTGG-3'), cut and cloned via triple ligation together with an EGFP-humanZO1 fragment isolated from pG1UAS:EGFP-ZO1with AgeI/Asp718 into SalI/Asp718 cut vector pDestTol2CG2 (gift from Chi-Bin Chien).

pG1UAS:EGFP-hZO1: A XhoI/AgeI-cut 14xUASE1b fragment, generated by PCR using the following primers (fwd. pr. 5'-GTGACCTCGAGAAGCTTAGGCCTCCAAGG-3' rev. pr. 5'-GTATCACCGGTTCGAGGGAATTCGTGTGG-3') and the pBUASE1b vector (gift from Reinhard W. Köster) as a template, was cloned into pG1 flk-1:EGFP-ZO1which was digested with SalI and AgeI.

Generation of Tg(fli:GAL4FF;UAS:Kaede) transgenic fish

To generate and easily identify fish lines stably carrying the pTolfli1ep:GAL4FF driver construct 25 pg of tol2 transposase mRNA synthesized in vitro with the mMessage Machine Kit (Ambion) and 25 pg of pTofli1ep:GAL4FF plasmid DNA were co-injected into approximately 150 1-cell stage Tg(UAS:Kaede)^{rk8} embryos [29]. Injected embryos were visually screened under an epifluorescent microscope and animals with strong Kaede fluorescence in the developing vasculature were raised to adulthood to obtain putative G0 founders with mosaic transgenic germlines. G0

adults were individually out-crossed to Tg(UAS:Kaede)^{rk2} fish and their F1 progeny screened visually as described. Individual G0s that yielded progeny with vascular Kaede expression were selected to establish three independent Tg(fli1ep:GAL4FF) lines with the allele designations Tg(fli1ep:GAL4FF$^{UBS2,\ UBS3}$ and ^{UBS4}) (UBS3 and UBS4 were used in this study).

Generation of *Tg(UAS:EGFP-ZO1-cmlc:EGFP)* transgenic fish line

Approximately 150 embryos (EK/TL strain) were injected with pT2UAS:EGFP-ZO1-cmlc:EGFP at one cell stage. The cmlc2:EGFP cassette was used to facilitate the identification of transgenic carriers in the absence of Gal4 expression. Embryos were screened for transient cardiac EGFP expression between 24 hpf and 48 hpf. Embryos showing strong transient expression were selected and raised separately. G0 generation was crossed and screened for germ line transmission. We recovered 8 transgenic carriers displaying EGFP expression in the heart. Three carriers (Tg(UAS:EGFP-ZO1-cmlc:EGFP$^{UBS5,\ UBS6}$ and ^{UBS7}) showed mosaic GAL4FF dependent EGFP-ZO1expression in the vasculature and were used in this study.

Immunofluorescence and Live imaging

Antibody stainings

Antibody stainings were done as previously described with minor modifications [5]. The following antibodies were used: rabbit anti-zf-CDH5 [5] 1:1000; Alexa-568 goat anti-rabbit IgG, 1:1000; Alexa-568 goat anti-mouse IgG, 1:1000; Alexa-633 goat anti-mouse IgG, 1:1000 (All secondary antibodies were purchased from Invitrogen.). Images were taken with a Leica SP5 confocal microscope using a 63x glycerol immersion objective and analyzed using Imaris (Bitplane) and Image J software.

Photoconversion

To label individual ECs KAEDE photoconversion was done on a Leica Sp5 fluorescent microscope by 20-second exposures using a solid-state laser (405nm). At 2 dpf, when nuclei of individual ECs are easily discernible in ISVs having an inflated lumen, fli1ep:GAL4FF;UAS:Kaede transgenic embryos were anaesthetized with tricaine, mounted in 0.7% low melting agarose and a defined region of interest (ROI)

within individual nuclei was exposed to the violet light. Subsequently high resolution x,y,z stacks were acquired with a 63x glycerol immersion objective using the suggested slice thickness by the confocal software. Slice numbers ranged from 80 to 200 slices per stack.

In vivo time-lapse analysis

Triple transgenic embryos were selected using a Leica MZ FLIII fluorescent stereomicroscope. Embryos were selected for mRFP ensuring the presence of the fli1ep:GAL4FF and UAS:mRFP transgene and for the presence of the heart marker cmlc2:EGFP. Selected embryos were anaesthetized using tricaine and mounted in a 35 mm glass bottom petri dish (0.17 mm, MatTek), using 0.7% low melting agarose (Sigma) containing 0.01% tricaine and 0,003% PTU. Embryos were imaged overnight on a Leica Sp5 confocal microscope using a 63x glycerol immersion objective with a numerical aperture of 1.2 with additional zoom of 1-1.3x. In some cases resonance scanning with an optical zoom of 1.7 was used. All movies have an initial frame size of 512x512 pixels. Routinely, z-stack consisted of 50-80 slices with a step size of 0.8-1.0 µm. Stacks were taken every 5 minutes, unless noted differently.

Quantum Dot-injection

705 nm Quantum Dot (Invitrogen) were injected into the sinus venosus of mounted embryos at a concentration of 1:2. Special manufactured glass needles (Biomedical Instruments, Jena, Germany) with tip opening of 10 µm and beveled tip were utilized to reduce damage to the embryo.

Fish maintenance and stocks

Zebrafish were maintained at standard conditions [30]. Embryos were staged by hours post-fertilization (hpf) at 28.5 °C (Kimmel et al., 1995). Embryos derived from wild-type fish (AB/EK and EK/TL), Tg*(fli1ep:EGFP)*^{y1} [2], TG*(flk1:EGFP)*^{S843} [18], Tg(UAS:Kaede)^{rk8} [29], Tg(UAS:mRFP1) [26] and Tg(fli1ep:GAL4FF)^{UBS2,UBS3,UBS4} and Tg(UAS:EGFP-ZO1-cmlc:EGFP)$^{UBS5,\ UBS6,UBS7}$ (this study) were used.

Acknowledgments:

We thank Dr. Holger Gerhardt for continuous and valuable discussions, Dr. Koichi Kawakamifor providing tol2-plasmids and TG(UAS:mRFP) fish, Dr. Reinhard Köster for providing UAS-plasmids and members of the Affolter group for critically reading the manuscript. A.K. and A.L. are supported by a fellowship from the Werner-Siemens-Foundation (Zug). This work has been supported by the Kantons Basel-Stadt and Basel-Land and by a grant from the Swiss National Science Foundation to M.A.

References

1. Gerhardt, H., Golding, M., Fruttiger, M., Ruhrberg, C., Lundkvist, A., Abramsson, A., Jeltsch, M., Mitchell, C., Alitalo, K., Shima, D., et al. (2003). VEGF guides angiogenic sprouting utilizing endothelial tip cell filopodia. The Journal of Cell Biology *161*, 1163-1177.
2. Lawson, N.D., and Weinstein, B.M. (2002). In vivo imaging of embryonic vascular development using transgenic zebrafish. Developmental Biology *248*, 307-318.
3. Ellertsdóttir, E., Lenard, A., Blum, Y., Krudewig, A., Herwig, L., Affolter, M., and Belting, H.-G. (2010). Vascular morphogenesis in the zebrafish embryo. Developmental Biology *341*, 56-65.
4. Isogai, S., Lawson, N.D., Torrealday, S., Horiguchi, M., and Weinstein, B.M. (2003). Angiogenic network formation in the developing vertebrate trunk. Development *130*, 5281-5290.
5. Blum, Y., Belting, H.-G., Ellertsdottir, E., Herwig, L., Lüders, F., and Affolter, M. (2008). Complex cell rearrangements during intersegmental vessel sprouting and vessel fusion in the zebrafish embryo. Developmental Biology *316*, 312-322.
6. Bagnat, M., Cheung, I.D., Mostov, K.E., and Stainier, D.Y.R. (2007). Genetic control of single lumen formation in the zebrafish gut. Nat Cell Biol *9*, 954-960.
7. Strilic, B., Kucera, T., Eglinger, J., Hughes, M.R., Mcnagny, K.M., Tsukita, S., Dejana, E., Ferrara, N., and Lammert, E. (2009). The Molecular Basis of Vascular Lumen Formation in the Developing Mouse Aorta. Developmental Cell *17*, 505-515.
8. Dong, B., Horie, T., Denker, E., Kusakabe, T., Tsuda, M., Smith, W.C., and Jiang, D. (2009). Tube formation by complex cellular processes in Ciona intestinalis notochord. Developmental Biology *330*, 237-249.
9. Sehnert, A.J., Huq, A., Weinstein, B.M., Walker, C., Fishman, M., and Stainier, D.Y.R. (2002). Cardiac troponin T is essential in sarcomere assembly and cardiac contractility. Nat Genet *31*, 106-110.
10. Tanaka-Matakatsu, M., Uemura, T., Oda, H., Takeichi, M., and Hayashi, S. (1996). Cadherin-mediated cell adhesion and cell motility in Drosophila trachea regulated by the transcription factor Escargot. Development (Cambridge, England) *122*, 3697-3705.
11. Steneberg, P., Hemphälä, J., and Samakovlis, C. (1999). Dpp and Notch specify the fusion cell fate in the dorsal branches of the Drosophila trachea. Mech Dev *87*, 153-163.
12. Lee, S., and Kolodziej, P.A. (2002). The plakin Short Stop and the RhoA GTPase are required for E-cadherin-dependent apical surface remodeling during tracheal tube fusion. Development (Cambridge, England) *129*, 1509-1520.
13. Kakihara, K., Shinmyozu, K., Kato, K., Wada, H., and Hayashi, S. (2008). Conversion of plasma membrane topology during epithelial tube connection requires Arf-like 3 small GTPase in Drosophila. Mech Dev *125*, 325-336.
14. Strilić, B., Kučera, T., and Lammert, E. (2010). Formation of cardiovascular tubes in invertebrates and vertebrates. Cell. Mol. Life Sci., 1-10.

15. Zovein, A.C., Luque, A., Turlo, K.A., Hofmann, J.J., Yee, K.M., Becker, M.S., Fassler, R., Mellman, I., Lane, T.F., and Iruela-Arispe, M.L. (2010). Beta1 integrin establishes endothelial cell polarity and arteriolar lumen formation via a Par3-dependent mechanism. Developmental cell *18*, 39-51.
16. Herbert, S.P., Huisken, J., Kim, T.N., Feldman, M.E., Houseman, B.T., Wang, R.A., Shokat, K.M., and Stainier, D.Y.R. (2009). Arterial-venous segregation by selective cell sprouting: an alternative mode of blood vessel formation. Science *326*, 294-298.
17. Kamei, M., Saunders, W.B., Bayless, K.J., Dye, L., Davis, G.E., and Weinstein, B.M. (2006). Endothelial tubes assemble from intracellular vacuoles in vivo. Nature *442*, 453-456.
18. Jin, S.-W., Beis, D., Mitchell, T., Chen, J.-N., and Stainier, D.Y.R. (2005). Cellular and molecular analyses of vascular tube and lumen formation in zebrafish. Development *132*, 5199-5209.
19. Bayless, K.J., and Davis, G.E. (2002). The Cdc42 and Rac1 GTPases are required for capillary lumen formation in three-dimensional extracellular matrices. J Cell Sci *115*, 1123-1136.
20. Iruela-Arispe, M.L., and Davis, G.E. (2009). Cellular and molecular mechanisms of vascular lumen formation. Developmental Cell *16*, 222-231.
21. Folkman, J., and Haudenschild, C. (1980). Angiogenesis by capillary endothelial cells in culture. Trans Ophthalmol Soc U K *100*, 346-353.
22. Wang, Y., Kaiser, M.S., Larson, J.D., Nasevicius, A., Clark, K.J., Wadman, S.A., Roberg-Perez, S.E., Ekker, S.C., Hackett, P.B., Mcgrail, M., et al. (2010). Moesin1 and Ve-cadherin are required in endothelial cells during in vivo tubulogenesis. Development *137*, 3119-3128.
23. Nicoli, S., Standley, C., Walker, P., Hurlstone, A., Fogarty, K.E., and Lawson, N.D. (2010). MicroRNA-mediated integration of haemodynamics and Vegf signalling during angiogenesis. Nature *464*, 1196-1200.
24. Bussmann, J., Wolfe, S.A., and Siekmann, A.F. (2011). Arterial-venous network formation during brain vascularization involves hemodynamic regulation of chemokine signaling. Development (Cambridge, England).
25. Fujita, M., Cha, Y.R., Pham, V.N., Sakurai, A., Roman, B.L., Gutkind, J.S., and Weinstein, B.M. (2011). Assembly and patterning of the vascular network of the vertebrate hindbrain. Development (Cambridge, England).
26. Asakawa, K., Suster, M.L., Mizusawa, K., Nagayoshi, S., Kotani, T., Urasaki, A., Kishimoto, Y., Hibi, M., and Kawakami, K. (2008). Genetic dissection of neural circuits by Tol2 transposon-mediated Gal4 gene and enhancer trapping in zebrafish. Proc Natl Acad Sci USA *105*, 1255-1260.
27. Kawakami, K., Takeda, H., Kawakami, N., Kobayashi, M., Matsuda, N., and Mishina, M. (2004). A transposon-mediated gene trap approach identifies developmentally regulated genes in zebrafish. Developmental cell *7*, 133-144.
28. Villefranc, J.A., Amigo, J., and Lawson, N.D. (2007). Gateway compatible vectors for analysis of gene function in the zebrafish. Dev Dyn *236*, 3077-3087.
29. Hatta, K., Tsujii, H., and Omura, T. (2006). Cell tracking using a photoconvertible fluorescent protein. Nat Protoc *1*, 960-967.
30. Westerfield, M. (2000). The zebrafish book. A guide for the laboratory use of zebrafish (Danio rerio). 4th Edition, (Eugene: Univ. of Oregon Press).

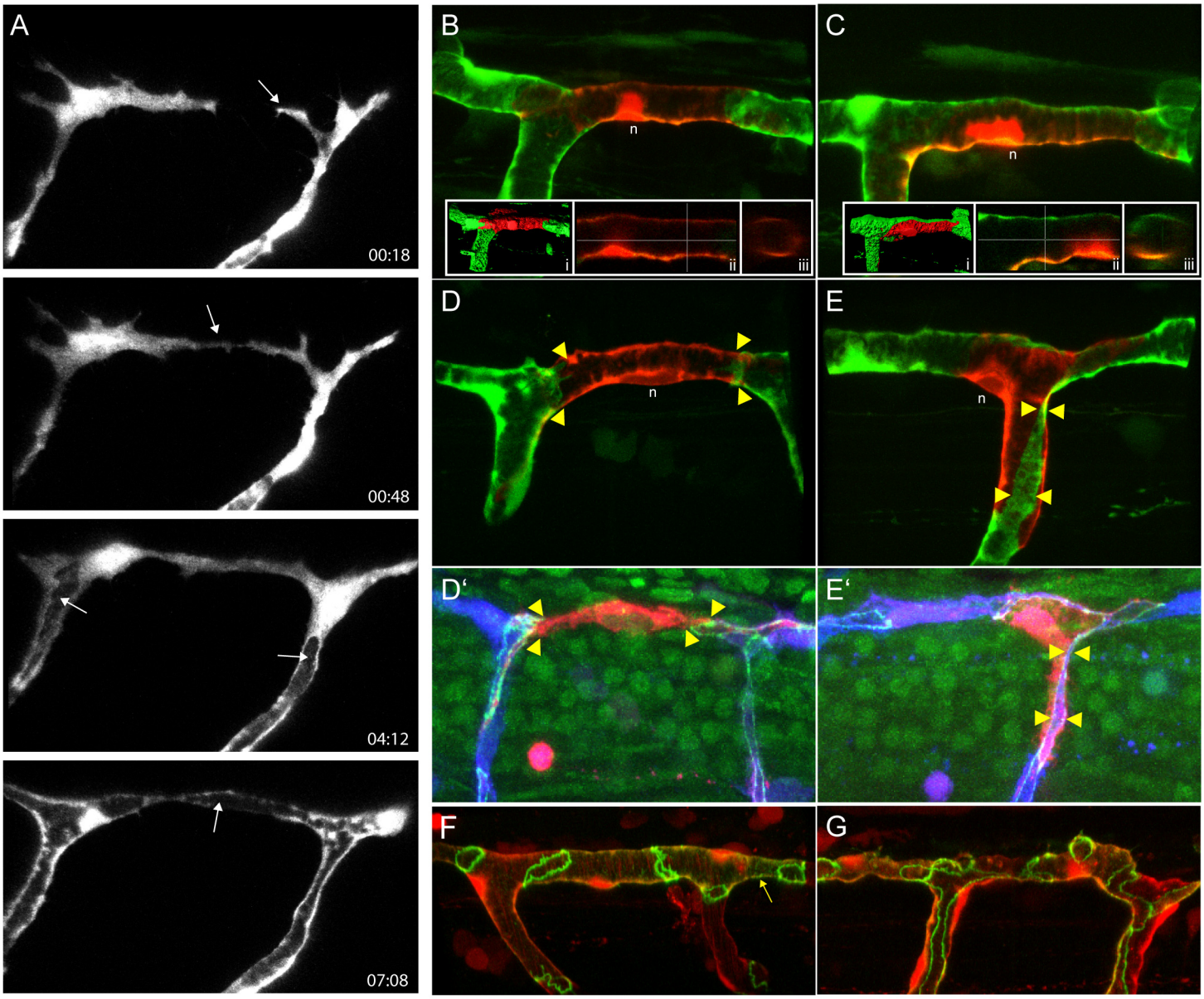

Herwig et al. Fig 1

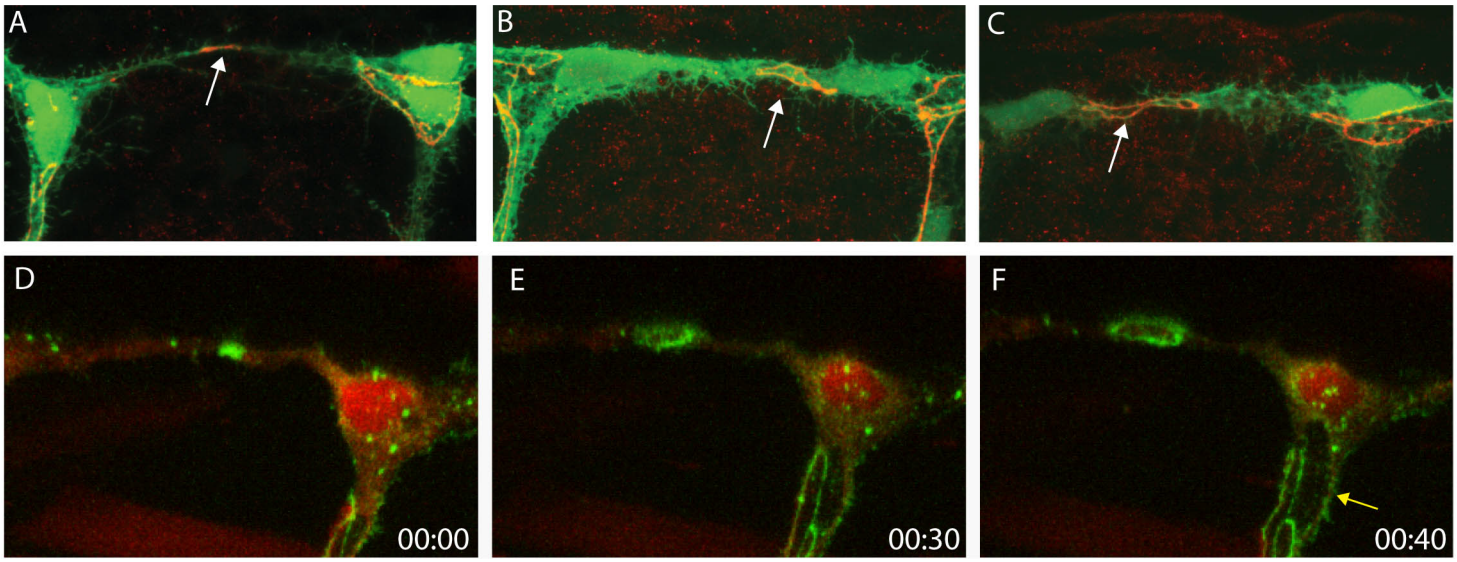

Herwig et al. Fig 2

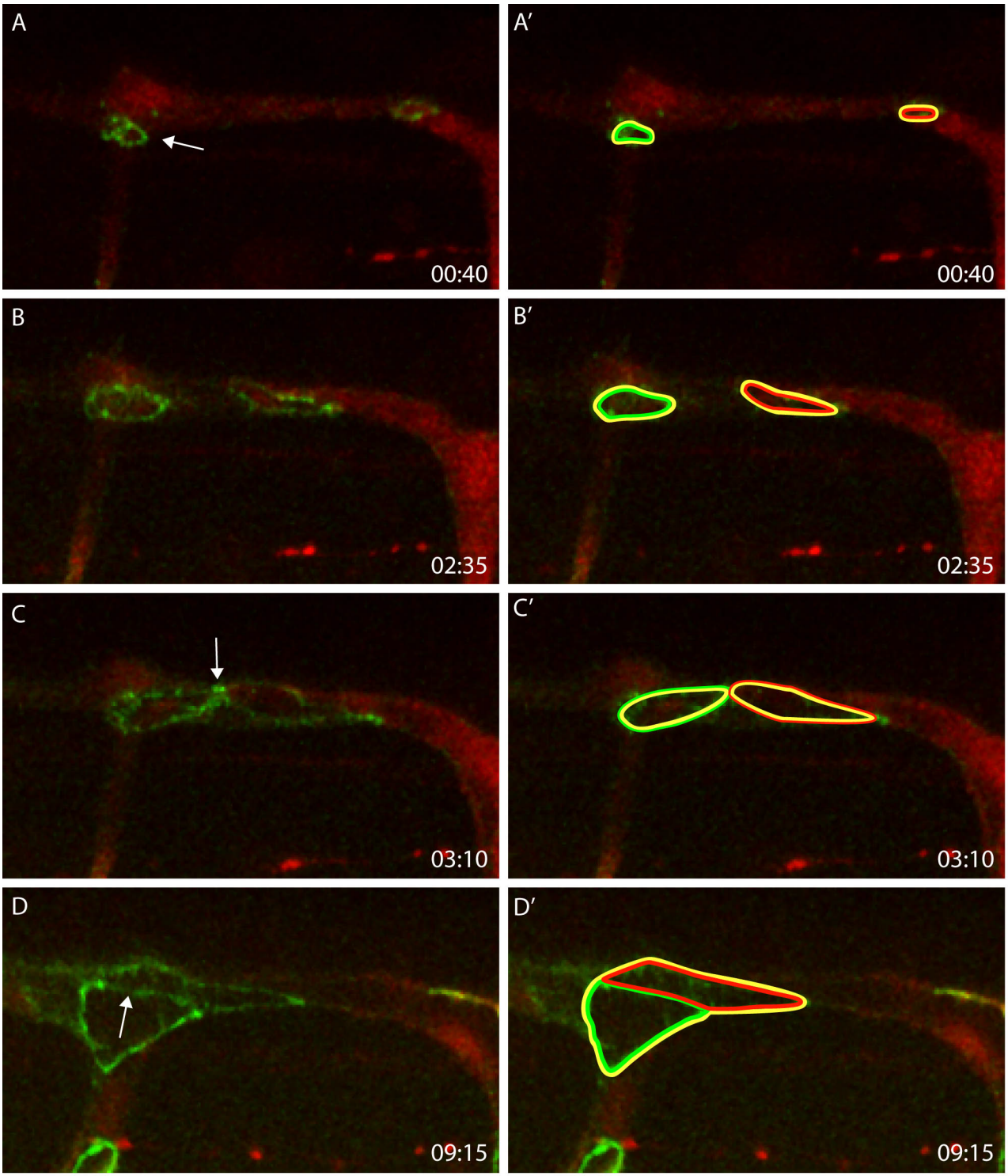

Herwig et al. Fig 3

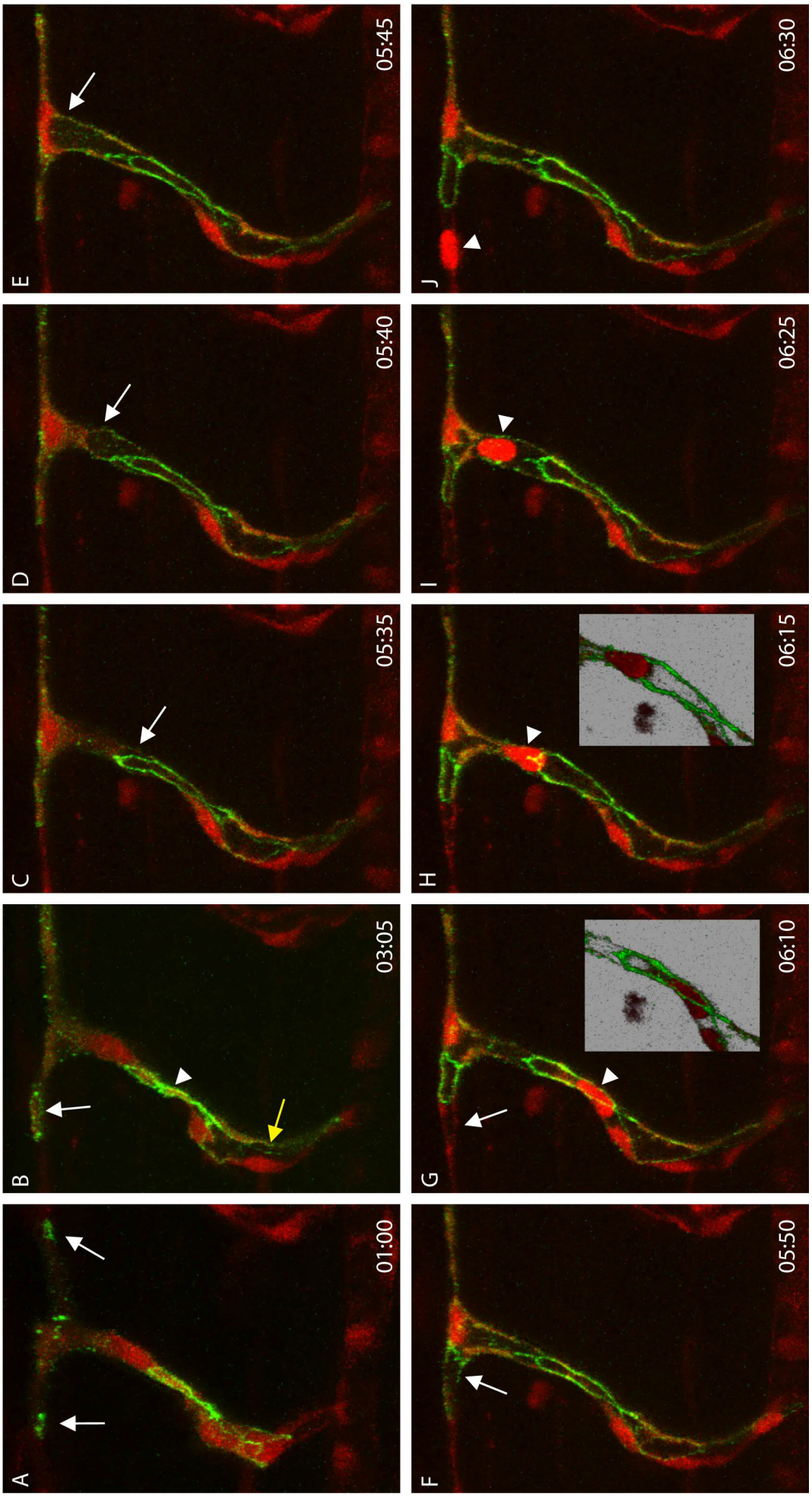

Herwig et al. Fig 4

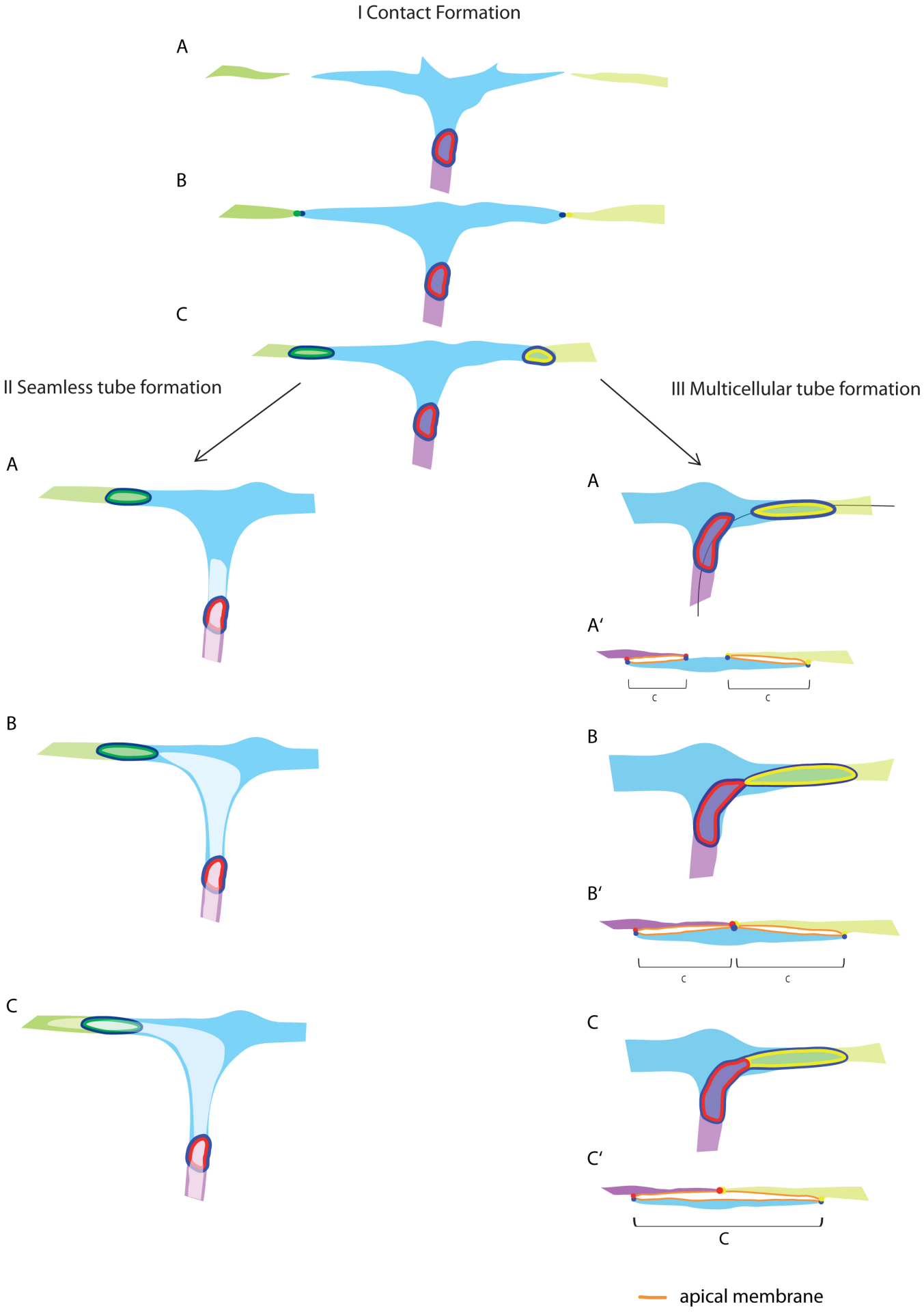

Herwig et al. Fig 5

5.1.2

Semaphorin-PlexinD1 Signaling Limits Angiogenic Potential via the VEGF Decoy Receptor sFlt1

Tomasz Zygmunt, Carl Michael Gay, Jordan Blondelle, Manvendra K. Singh, Kathleen McCrone Flaherty, Paula Casey Means, Lukas Herwig, Alice Krudewig, Heinz-Georg Belting, Markus Affolter, Jonathan A. Epstein and Jesus Torres-Vazquez

Developmental Cell 21, (1-14)
August 16, 2011, published online July 28, 2011

Contribution:
Together with Lukas Herwig I generated the pTol(*fli1ep*:gal4ff)^{ubs4} transgenic zebrafish line using the Gateway® system (Invitrogen™). We generated Figure S4G. I contributed to discussions during writing of the manuscript.

Developmental Cell
Article

Semaphorin-PlexinD1 Signaling Limits Angiogenic Potential via the VEGF Decoy Receptor sFlt1

Tomasz Zygmunt,[1,6] Carl Michael Gay,[1,6] Jordan Blondelle,[2] Manvendra K. Singh,[3,5] Kathleen McCrone Flaherty,[1] Paula Casey Means,[1] Lukas Herwig,[4] Alice Krudewig,[4] Heinz-Georg Belting,[4] Markus Affolter,[4] Jonathan A. Epstein,[3,5] and Jesús Torres-Vázquez[1,*]

[1]Department of Cell Biology, Helen L. and Martin S. Kimmel Center for Biology and Medicine at the Skirball Institute, New York University School of Medicine, New York, NY 10016, USA
[2]Université Diderot-Paris 7, Paris, France
[3]Department of Cell and Developmental Biology, Cardiovascular Institute, University of Pennsylvania, Philadelphia, PA 19104, USA
[4]Biozentrum, University of Basel, Ch-4056 Basel, Switzerland
[5]Institute for Regenerative Medicine, University of Pennsylvania, Philadelphia, PA 19104, USA
[6]These authors contributed equally to this work
*Correspondence: jesus.torres-vazquez@med.nyu.edu
DOI 10.1016/j.devcel.2011.06.033

SUMMARY

Sprouting angiogenesis expands the embryonic vasculature enabling survival and homeostasis. Yet how the angiogenic capacity to form sprouts is allocated among endothelial cells (ECs) to guarantee the reproducible anatomy of stereotypical vascular beds remains unclear. Here we show that Sema-PlxnD1 signaling, previously implicated in sprout guidance, represses angiogenic potential to ensure the proper abundance and stereotypical distribution of the trunk's segmental arteries (SeAs). We find that Sema-PlxnD1 signaling exerts this effect by antagonizing the proangiogenic activity of vascular endothelial growth factor (VEGF). Specifically, Sema-PlxnD1 signaling ensures the proper endothelial abundance of *soluble flt1* (*sflt1*), an alternatively spliced form of the VEGF receptor Flt1 encoding a potent secreted decoy. Hence, Sema-PlxnD1 signaling regulates distinct but related aspects of angiogenesis: the spatial allocation of angiogenic capacity within a primary vessel and sprout guidance.

INTRODUCTION

Blood vessels form a pervasive tubular network that distributes oxygen, nutrients, hormones, and immunity factors. The first blood vessels assemble de novo via EC coalescence or vasculogenesis. Later, they expand via angiogenesis, the growth of new blood vessels from preexisting ones. In some locales, this process is stereotypic and vascular sprouts form with evolutionarily conserved and organ-specific distribution, abundance and shapes (Carmeliet, 2005; Isogai et al., 2001; Isogai et al., 2003). For example, zebrafish SeAs sprout bilaterally from the trunk's aorta just anterior to each somite boundary (SB) (Figure 1A). SeA sprouts contain migratory, proliferative and filopodia-rich arterial angiogenic ECs molecularly distinct from the sedentary "phalanx" ECs remaining in the aorta (De Bock et al., 2009; Siekmann and Lawson, 2007; Torres-Vázquez et al., 2004). Normally, only aortic ECs near SBs acquire angiogenic capacity (Ahn et al., 2000; Childs et al., 2002). It is thought that nonendothelial paracrine VEGF signals promote angiogenic capacity, while Notch-mediated lateral inhibition between ECs antagonizes it (Phng and Gerhardt, 2009; Siekmann et al., 2008). However, the mRNA expression of *vegf-a* and Notch pathway genes is inconsistent with the distribution of SeA sprouts. *vegf-a* is not transcribed along SBs, but rather expressed dorsal to the aorta at both the flanking somites' centers and the hypochord, a midline endodermal cell row. Notch pathway genes are expressed continuously along the aorta or broadly through the body (Hogan et al., 2009b; Lawson et al., 2002; Leslie et al., 2007; Phng et al., 2009; Siekmann and Lawson, 2007) (C.M.G., J.B., and J.T.-V., unpublished data). Hence, other cascades likely modulate VEGF and/or Notch signaling at presprouting stages to enable the stereotypical allocation of angiogenic capacity within the aorta. Perturbing these unidentified cascades might change the SeA sprouts' reproducible number or distribution, the ratio of aortic ECs that acquire angiogenic capacity, and/or the responsiveness of these cells to angiogenic cues.

Besides VEGF and Notch activity, proper SeA development requires paracrine Sema-Plxn signaling. Type 3 semas (sema3s) are repulsive guidance cues secreted by somites. Sema3s direct SeA sprout pathfinding by modulating cytoskeletal dynamics via the endothelial Sema3-receptor PlxnD1. Hence, *sema3* or *plxnD1* inactivation yields similar SeA sprout pathfinding defects in zebrafish and mice (Gay et al., 2011). Two observations made in zebrafish make Sema-PlxnD1 signaling a candidate modulator of angiogenic capacity. First, *sema3* and *plxnD1* expression begins hours before SeAs sprout from the aorta at ~21 hr post-fertilization (hpf). Second, loss of Sema-PlxnD1 signaling induces ectopic SeA sprout launching (Childs et al., 2002; Torres-Vázquez et al., 2004).

In wild-type (WT) animals SeA sprouts grow dorsally with a chevron-like shape, bifurcate anteroposteriorly at the neural tube's roof level and interconnect with their ipsilateral neighbors at ~32 hpf forming the paired Dorsal Longitudinal Anastomotic Vessels (DLAVs) (Isogai et al., 2003). In contrast, in *plxnD1* (*out of bounds - obd*) mutants and *plxnD1* morphants, SeA sprouts are misshaped and interconnect ectopically with their ipsilateral

5.1.3

The novel transmembrane protein Tmem2 is essential for coordination of myocardial and endocardial morphogenesis

Roland Totong, Thomas Schell, Fabienne Lescroart, Lucile Ryckebüsch, Yi-Fan Lin, Tomas Zygmunt, Lukas Herwig, Alice Krudewig, Dafna Gershoony, Heinz-Georg Belting, Markus Affolter, Jesus Torres-Vazquez and Deborah Yelon

Developmental – in press

Contribution:
Together with Lukas Herwig I generated the pTol(*fli1ep*:gal4ff)^{ubs4} transgenic zebrafish line using the Gateway® system (Invitrogen™). I contributed to discussions during writing of the manuscript.

Development 138, 0000-0000 (2011) doi:10.1242/dev.064261
© 2011. Published by The Company of Biologists Ltd

The novel transmembrane protein Tmem2 is essential for coordination of myocardial and endocardial morphogenesis

Ronald Totong[1], Thomas Schell[1], Fabienne Lescroart[1], Lucile Ryckebüsch[2], Yi-Fan Lin[1,2], Tomasz Zygmunt[1], Lukas Herwig[3], Alice Krudewig[3], Dafna Gershoony[4], Heinz-Georg Belting[3], Markus Affolter[3], Jesús Torres-Vázquez[1] and Deborah Yelon[1,2,*]

SUMMARY

Coordination between adjacent tissues plays a crucial role during the morphogenesis of developing organs. In the embryonic heart, two tissues – the myocardium and the endocardium – are closely juxtaposed throughout their development. Myocardial and endocardial cells originate in neighboring regions of the lateral mesoderm, migrate medially in a synchronized fashion, collaborate to create concentric layers of the heart tube, and communicate during formation of the atrioventricular canal. Here, we identify a novel transmembrane protein, Tmem2, that has important functions during both myocardial and endocardial morphogenesis. We find that the zebrafish mutation *frozen ventricle* (*frv*) causes ectopic atrioventricular canal characteristics in the ventricular myocardium and endocardium, indicating a role of *frv* in the regional restriction of atrioventricular canal differentiation. Furthermore, in maternal-zygotic *frv* mutants, both myocardial and endocardial cells fail to move to the midline normally, indicating that *frv* facilitates cardiac fusion. Positional cloning reveals that the *frv* locus encodes Tmem2, a predicted type II single-pass transmembrane protein. Homologs of Tmem2 are present in all examined vertebrate genomes, but nothing is known about its molecular or cellular function in any context. By employing transgenes to drive tissue-specific expression of *tmem2*, we find that Tmem2 can function in the endocardium to repress atrioventricular differentiation within the ventricle. Additionally, Tmem2 can function in the myocardium to promote the medial movement of both myocardial and endocardial cells. Together, our data reveal that Tmem2 is an essential mediator of myocardial-endocardial coordination during cardiac morphogenesis.

KEY WORDS: Zebrafish, Heart development, Atrioventricular canal, Cardiac fusion

INTRODUCTION

The embryonic heart tube is initially a two-layered structure: the outer layer of muscular myocardium contracts to propel circulation and the inner layer of endothelial endocardium provides continuity with the rest of the vasculature. Myocardial and endocardial cells originate in neighboring regions of the lateral mesoderm (Schoenebeck et al., 2007). During the process of cardiac fusion, both cell types migrate medially in a synchronized fashion and merge at the midline to assemble the heart tube (Bussmann et al., 2007; Holtzman et al., 2007; Moreno-Rodriguez et al., 2006). At later stages, cardiac maturation involves remodeling of both juxtaposed layers during valve formation and trabeculation (Armstrong and Bischoff, 2004; Hinton and Yutzey, 2010; Sedmera et al., 2000). Despite the continual proximity of the myocardium and endocardium, little is known about the mechanisms that coordinate their development.

The coordination of myocardial and endocardial development has been particularly well established in the context of atrioventricular canal (AVC) formation. Both the myocardium and endocardium undergo specialized differentiation in order to create the characteristic morphology of the AVC and to establish the endocardial cushions that will remodel into the atrioventricular valve (Armstrong and Bischoff, 2004; Beis et al., 2005; Chi et al., 2008; Hinton and Yutzey, 2010). Several studies indicate that myocardial-endocardial communication regulates these spatially coincident events (Armstrong and Bischoff, 2004; Hinton and Yutzey, 2010). For example, chick explant experiments suggest that signal transduction between atrioventricular myocardium and atrioventricular endocardium induces endocardial cushion formation (Mjaatvedt et al., 1987). Although several signaling pathways have been implicated in promoting endocardial cushion development (Armstrong and Bischoff, 2004; Beis et al., 2005; Hinton and Yutzey, 2010), it is less clear which genes are responsible for attenuating these signals so as to spatially restrict atrioventricular differentiation.

Myocardial-endocardial coordination is also crucial during cardiac fusion. The synchronization of myocardial and endocardial migration suggests that both tissues respond to the same cues in the extracellular environment. Some cues may emanate from the endoderm: both myocardial and endocardial fusion are inhibited when endodermal specification or morphogenesis is disrupted (e.g. Holtzman et al., 2007; Kikuchi et al., 2001; Kupperman et al., 2000). Additionally, either diminished or excessive deposition of extracellular matrix (ECM) can hinder myocardial and endocardial movement (e.g. Arrington and Yost, 2009; Garavito-Aguilar et al., 2010; Trinh and Stainier, 2004). Furthermore, the myocardium and endocardium may impact the behavior of one another. Cardiomyocytes display aberrant migration patterns in the absence

[1]Developmental Genetics Program and Department of Cell Biology, Kimmel Center for Biology and Medicine, Skirball Institute of Biomolecular Medicine, New York University School of Medicine, New York, NY 10016, USA. [2]Division of Biological Sciences, University of California, San Diego, La Jolla, CA 92093, USA. [3]Biozentrum, University of Basel, CH-4056 Basel, Switzerland. [4]Department of Pharmacology, New York University School of Medicine, New York, NY 10016, USA.

*Author for correspondence (dyelon@ucsd.edu)

Accepted 18 July 2011

5.2 Generation of transgenic fish lines using the Gateway®/Tol2 system

The Gateway system is a rapid and highly efficient, restriction enzyme-free way to generate any desired vector for expression of a protein of interest. Instead of restriction enzymes, a so-called clonase enzyme mix catalyzes a site-specific recombination event between particular sequences called attachment sites (att sites). These are modified versions of the att sites the λ bacteriophage uses to integrate its genome into the bacterial host genome. The Gateway® system uses different variants of att sites to ensure directional cloning. In general, an entry vector contains a gene of interest flanked by specific att sites. These are used to integrate this gene into a destination vector containing different, but compatible att sites. This destination vector furthermore can harbor any feature to express the gene of interest (for example in *E.coli* or tissue culture cells). The entry and destination vectors can be distinguished by different selection markers.

An entry vector can be generated in three different ways (Fig. 6 A). First, a PCR fragment of the gene of interest has to be amplified using primers containing attB sites. This fragment is directly recombined into a pDONR vector containing attP sites via the BP clonase. Through this BP reaction attL sites are generated in the entry vector now containing the gene of interest. It should be noted that in the BP reaction the DNA fragment of interest is exchanged with a negative selection cassette present in the pDONR vector. This cassette contains the ccdB gene, whose expression is toxic for standard bacteria used in laboratories. Therefore, only entry vectors that contain a DNA fragment of interest can be amplified in bacteria. Second, the PCR fragment can be amplified using a 5` primer that contains a CACC overhang. This overhang is used for the directional integration of the fragment into the ENTR/TOPO vector via the topoisomerase. The ENTR/TOPO vector contains attL sites already. Third, conventional cloning via restriction enzyme digestion and ligation can also be used for the generation of an entry vector. In all cases the final entry vector contains the gene of interest flanked by attL sites. In the final step of gateway cloning, the LR reaction, the entry vector is

recombined with any destination vector (pDEST) of interest. Here, the LR clonase mediates the recombination between the attL sites in the entry vector and the attR sites in the pDEST vector (Fig. 6 A). The final expression plasmid contains the gene of interest flanked by attB sites and any feature to mediate expression. As this reaction can be performed with any desired destination vector, several expression plasmids can be generated simultaneously.

The system described above is applicable if the destination vectors already contain the desired promoter or tag of interest. Another way of creating a vector for the desired tissue-specific expression of a native or fusion protein is multisite Gateway cloning. Here, the simultaneous cloning of multiple DNA fragments in a specific order and orientation is performed. In our lab the three-way multisite Gateway system is used, where three different entry clones (5`, middle and 3` entry clone) containing the promoter, the gene of interest and the tag, respectively are recombined with each other (Fig. 6 B). The different entry clones are generated by the BP reaction described above. The final entry clones however all contain different versions of the attL and attR sites. These can only recombine with one other att site used in this system guaranteeing a defined order and orientation of entry clones (Fig. 6 B). Only the specific combination of recombination proteins of the LR Clonase II plus enzyme mix can perform this reaction. In summary, the three-way multisite Gateway system allows to combine any entry vectors of interest in any order possible, providing a large toolbox for expression vector generation.

In the past several methods have been used to generate transgenic fish lines, e.g. injection of linearized DNA (Thermes et al., 2002). However, the transmission efficiency using these methods is rather low making the generation of transgenic fish highly laborious (Davidson et al., 2003; Stuart et al., 1988; Stuart et al., 1990; Thermes et al., 2002). A drastic increase in transmission efficiency of zebrafish can be achieved by the so-called Tol2 system. This system is based on the Tol2 transposon from the medaka fish *Oryzias latipes* (Kawakami et al., 2004). In the Tol2 system the Tol2 transposase mediates the random integration of any sequence, which is flanked by inverted repeats called Tol2 sites (Kawakami et al., 2000; Kawakami et al., 2004). To generate transgenic fish via the Tol2 system, an

uncut plasmid containing the gene/sequence of interest between Tol2 sites is co-injected with mRNA coding for the Tol2 transposase (Fig. 7). After raising these embryos to adulthood, their progeny can be screened for the successful integration of the construct into the genome, for example by expression of a fluorescent marker (Fig. 7).

Two Tol2/Gateway kits have been generated for efficient cloning and integration of DNA constructs into the zebrafish genome. The first one contains the general toolbox of entry and destination vectors with different fluorescent and non-fluorescent tags as well as general promoters (Kwan et al., 2007). The second kit additionally contains destination vectors applicable for the expression within the blood vessel system of zebrafish embryos (e.g. plasmids already containing the endothelial specific promoter *fli1*) (Villefranc et al., 2007). Many of these vectors also possess the marker cmlc2:EGFP driving EGFP expression in the myocardium of the heart to facilitate the identification of transgenic fish.

For some experiments presented in this work, I generated several entry and expression vectors listed in Materials and Methods 4.3.2. The final expression vectors are designed either for the Gal4/UAS system or allow endothelial specific expression of a sequence of interest.

In order to determine the efficiency of the Tol2 system in my hands and with the conditions in our lab, I quantified the germline transmission for some of the constructs injected (fli1ep:mCherry, fli1ep:nlsmCherry, UAS:*cldn5b*EGFP;cmlc2EGFP). In total I screened the progeny of 77 individual crossed G_0 adult fish for the expression of the fluorescent or the heart marker (mCherry or *cmlc2*:EGFP) (min. n=80 embryos each cross). On average 45.3% of G_0 adult fish produced F_1 progeny showing the presence of the marker analyzed. In my hands, the transmission efficiency did not depend on the vector injected as all the constructs harbor the same vector backbone containing the elements for integration. These results correlate nicely with the published data for the germline transmission rate of about 50% using Tol2 (Kawakami et al., 2004).

As the genomic integration of DNA using the Tol2 system is random, it can lead to multiple insertions of the same plasmid. This fact can be easily

observed by various expression strengths of the fluorescent markers in F_2 embryos within one clutch. This observation is in agreement with the occurrence of multiple plasmid insertions using transposon-mediated DNA integration in other model organisms. For example, P-element-based random insertion of DNA into the *Drosophila* genome can lead to several simultaneous integration events (Venken and Bellen, 2007).

The occurrence of several expression levels of the fluorescent marker was observed in F_2 embryos derived from G_0 adults injected with protein-fusion constructs as well as UAS-constructs. However, in contrast to F_2 embryos carrying a protein-fusion transgene, expression of UAS-constructs in F_2 embryos can lead to a mosaic pattern (for example, EGFP was not observed in all ISVs although cross to *fli1* ep-Gal4ff fish). In general, embryos with the strongest expression and the least mosaicism were chosen to generate a stable transgenic line. The mosaic expression has been observed earlier and seems to be the result of epigenetic silencing of the 10xUAS cassette used in the corresponding UAS plasmids (Goll et al., 2009).

In summary, the Tol2 integration method combined with the Gateway cloning system provides a fast and efficient strategy to create a set of transgenic fish lines in a reasonable amount of time and labor.

A **The principle of Gateway cloning**

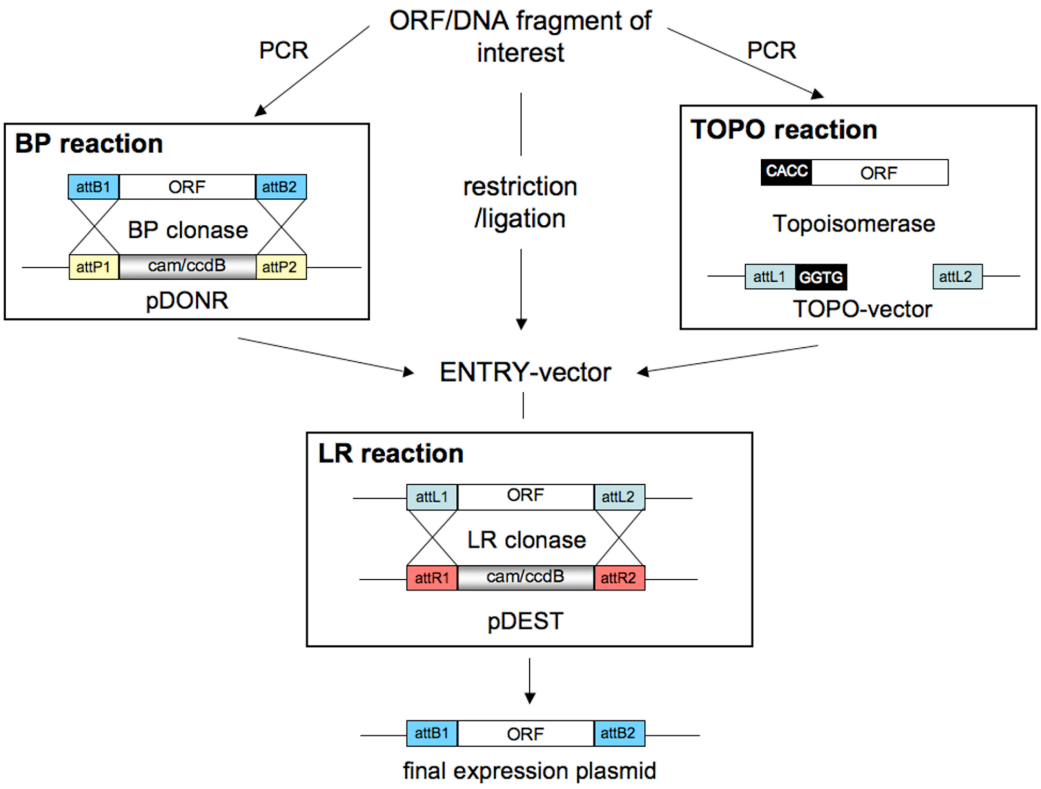

B **Three-way multisite Gateway cloning**

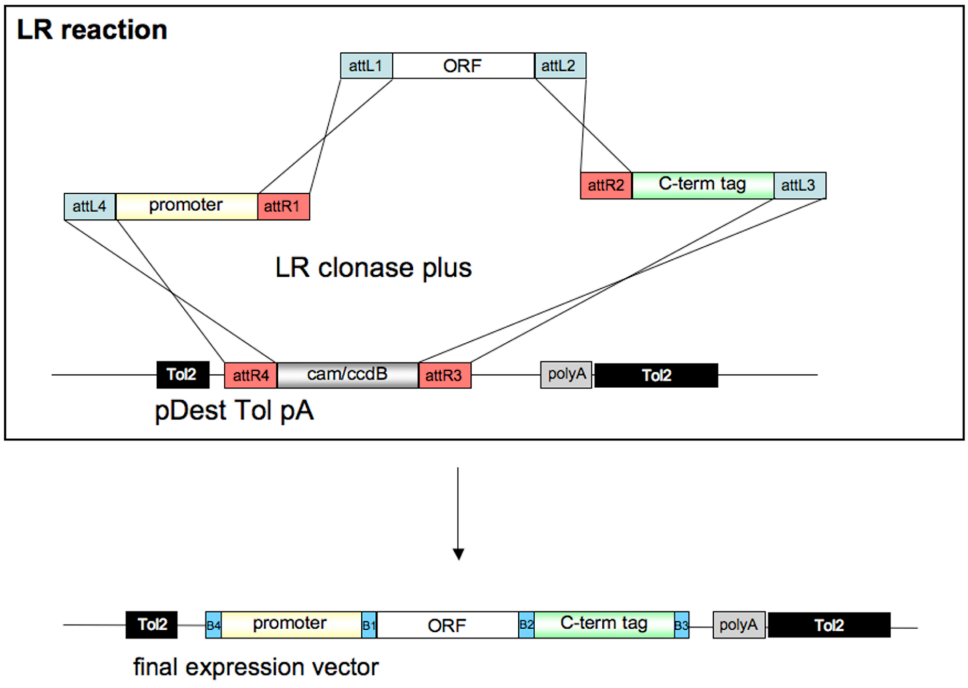

Figure 6: Schematic overview of the principles of Gateway and multisite Gateway cloning. (A) Entry vectors suitable for the Gateway system can be generated by a BP reaction (box on the left), by conventional restriction/ligation (arrow in the middle) or by TOPO cloning (box on the right). In a final LR reaction (box at the bottom) a LR clonase will mediate the exchange of a sequence of interest (here ORF) flanked by attL sites in the entry vector and a cassette flanked by attR sites in the pDEST vector. The resulting final expression plasmid contains the sequence of interest and all necessary features for expression of this sequence in the experimental model system of choice.
(B) In a three-way multisite Gateway experiment three different entry vectors (containing promoter, ORF and C-terminal tag) will integrate into a destination vector of choice at the same time. During the LR reaction the recombination of specific variations of attL sites only with compatible attR sites ensures the correct order of entry constructs. The resulting final expression vector contains all elements in the correct order. Modified after (Villefranc et al., 2007).

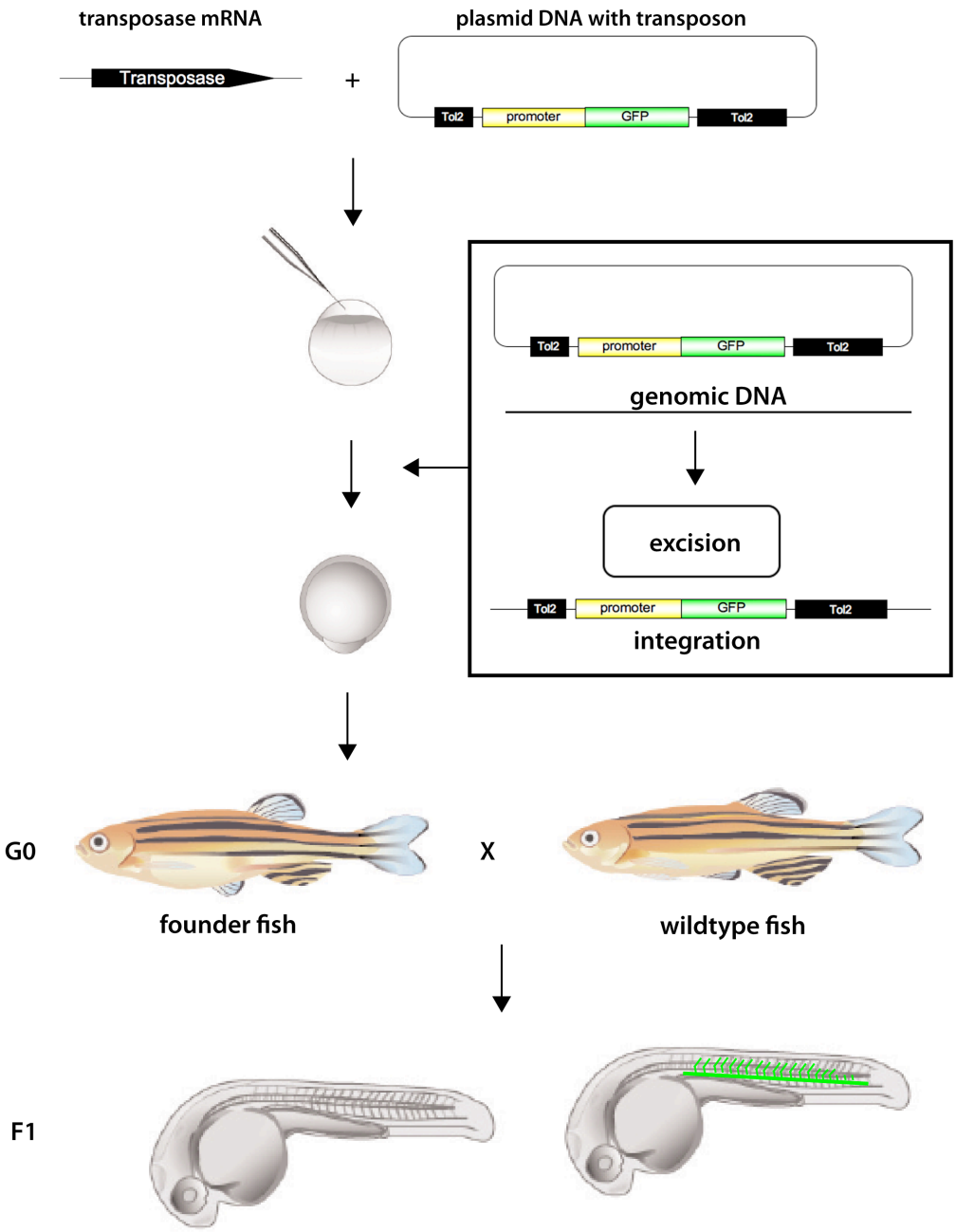

Figure 7: Schematic summary of the Tol2 system to create stable transgenic fish lines. Plasmids containing the desired sequences (here a specific promotor in front of a GFP coding region) flanked by Tol2 transposition sites are co-injected with mRNA encoding the Tol2 transposase into the one-cell stage of embryos. Here, the transposase mediates the integration of the injected plasmid into the genome. After growing the injected fish to adulthood (G0, founder fish), outcrossing to wild type fish allows to screen for the expression of the construct in the progeny (F1). Modified after Kawakami, 2007.

5.3 *Cldn5b* is a vascular-specific gene

A database search for junctional proteins that are expressed in a vascular specific fashion identified a transcript zgc:103419. Blast analysis revealed that this transcript is highly homologous to mammalian *claudin5*, which is specifically expressed in the vasculature.

Bioinformatic analysis shows that the zebrafish genome contains two *claudin5 (cldn5)* genes – *cldn5a* and *cldn5b* (Fig. 8 A, in collaboration with Bernhard Misof, Bonn, Germany). In contrast, non-fish vertebrate genomes ranging from frogs to humans possess only a single gene encoding a Claudin5 protein. *Cldn5a* and *cldn5b* DNA sequences are highly similar with 75% sequence identity. The corresponding proteins share 72% identity at the amino acid level (Suppl. Data 8, Fig. 1). These findings are consistent with the proposed genome duplication that occurred during early teleost evolution. All teleosts tested contained *cldn5* paralogs and genes within each paralogous group are more similar to each other than to any *cldn5* of the other paralog group.

In amphibians, avians and mammals *cldn5* is specifically expressed in the endothelial cells of the vascular system (Liebner et al., 2000; Morita et al., 1999). Expression analysis in zebrafish revealed that *cldn5a* mRNA is highly expressed in the embryonic nervous system, whereas *cldn5b* mRNA is restricted to the vasculature (Thisse, 2004).

To investigate the spatial and temporal differences of *cldn5b* and *cldn5a* expression during embryonic development in more detail, I analyzed mRNA expression using in situ hybridization at different embryonic stages (Fig. 8 B-I, Fig. 9). In contrast to the control sense probe, the antisense probe for *cldn5b* mRNA revealed a specific signal starting at around the 20-somite stage (Fig. 8 B-C vs. 8 D). At this stage a weak *cldn5b* signal is detectable in the head region as well as in a stripe along the trunk at the position of the forming aorta (arrows, Fig. 8 B). In 24hpf old embryos *cldn5b* is clearly expressed in blood vessels of the head (asterisks in Fig. 8 C and 8 E). In the vasculature *cldn5b* is transcribed by endothelial cells of the DA and the ISVs (Fig. 8 F-I, arrows in 8 F-G). Expression of *cldn5b* is also detected in the PCV, which starts at

around 28hpf and increases as development proceeds (Fig. 8 G-I, arrowheads). At 30 hpf signal intensity of the *cldn5b* antisense probe is comparable in PCV and DA (compare PCV and DA in Fig. 8 H). At later stages (30-36 hpf), the forming DLAV is also characterized by *cldn5b* expression (Fig. 8 H-I, asterisks).

In contrast to *cldn5b* expression, *cldn5a* mRNA is strongly transcribed in the brain and the spinal cord of the central nervous system throughout embryonic development (Fig. 9 A-E). Interestingly, *cldn5b* is enriched in the hindbrain (hb) and marks the midbrain-hindbrain boundary (Fig. 9 B, asterisk). At later stages, *cldn5a* is strongly expressed in the developing eye (Fig. 9 D-E, arrows in D). These findings are in agreement with a recent report showing that *cldn5a* is expressed in the brain and enriched in neuroepithelial cells adjacent to brain ventricles (Zhang et al., 2010). In younger embryos from 23 to 27 hpf weak *cldn5a* expression is detected in a stripe along the body axis beneath the spinal cord (sc) (Fig. 9 A-C). Higher magnification shows *cldn5a* expression in the DA (Fig. 9 A`-C`, arrows). However, detection of *cldn5a* mRNA in the DA is transient and lost in older embryos (Fig. 9 A`-C` vs. 9 D`-E`). At 30 hpf the *cldn5a* expression is undetectable in the DA while concomitantly *cldn5a* mRNA is transcribed in the spinal cord at similar levels than before (Fig. 9 D` vs 9 C`). Taken together, although *cldn5a* is transiently expressed in the DA, *cldn5b* appears to be a vasculature-specific *cldn5* gene during embryonic stages.

To definitely confirm that *cldn5b* mRNA is indeed expressed in endothelial cells, I visualized at the same time *cldn5b* mRNA and *fli1* mRNA - which is specifically expressed endothelial cells - via double-fluorescent in situ hybridization. Applying the tyramide signal amplification (TSA) system *cldn5b* mRNA was visualized with tetramethylrodamine (TMR) and *fli1* transcripts with fluorescein isothiocyanate (FITC) (Fig. 10). Analysis of embryos at 24 hpf shows that the *cldn5b* and *fli1* messages are indeed co-expressed (Fig. 10 A`-A``). This clearly demonstrates that *cldn5b* is expressed in endothelial cells of the developing vasculature. During development the expression of many genes varies between mRNA and protein level. While mRNA expression tends to be more stable, the expression of proteins is more dynamic. In order to analyze the expression pattern and specific subcellular localization of

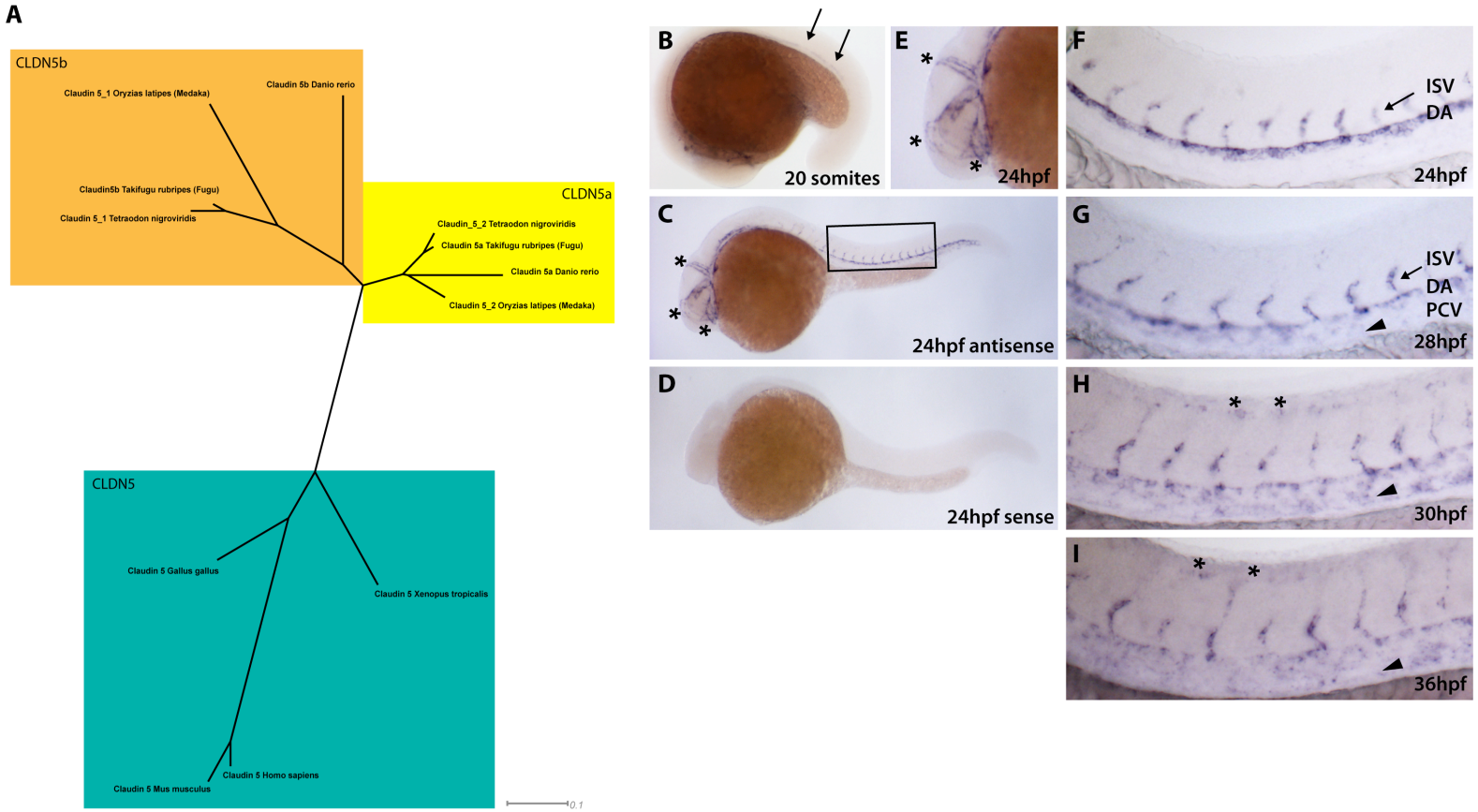

Figure 8: *Cldn5b* expression is restricted to the vasculature. (A) Cladogram comparing *cldn5* of vertebrates and representatives of the teleost lineage. (B-I) Expression analysis of *cldn5b* mRNA. All images are shown with lateral view and rostral to left. While the antisense probe shows a clear signal (C), the sense probe does not anything (D). *Cldn5b* mRNA is expressed from the 20 somite stage onwards (B). At 24hpf it is expressed in the DA, the ISVs and in vessels of the head (C, E, F). At this stage no *cldn5b* mRNA is expressed in the PCV (F), its expression increases though over time (G-I). Details see in main text.

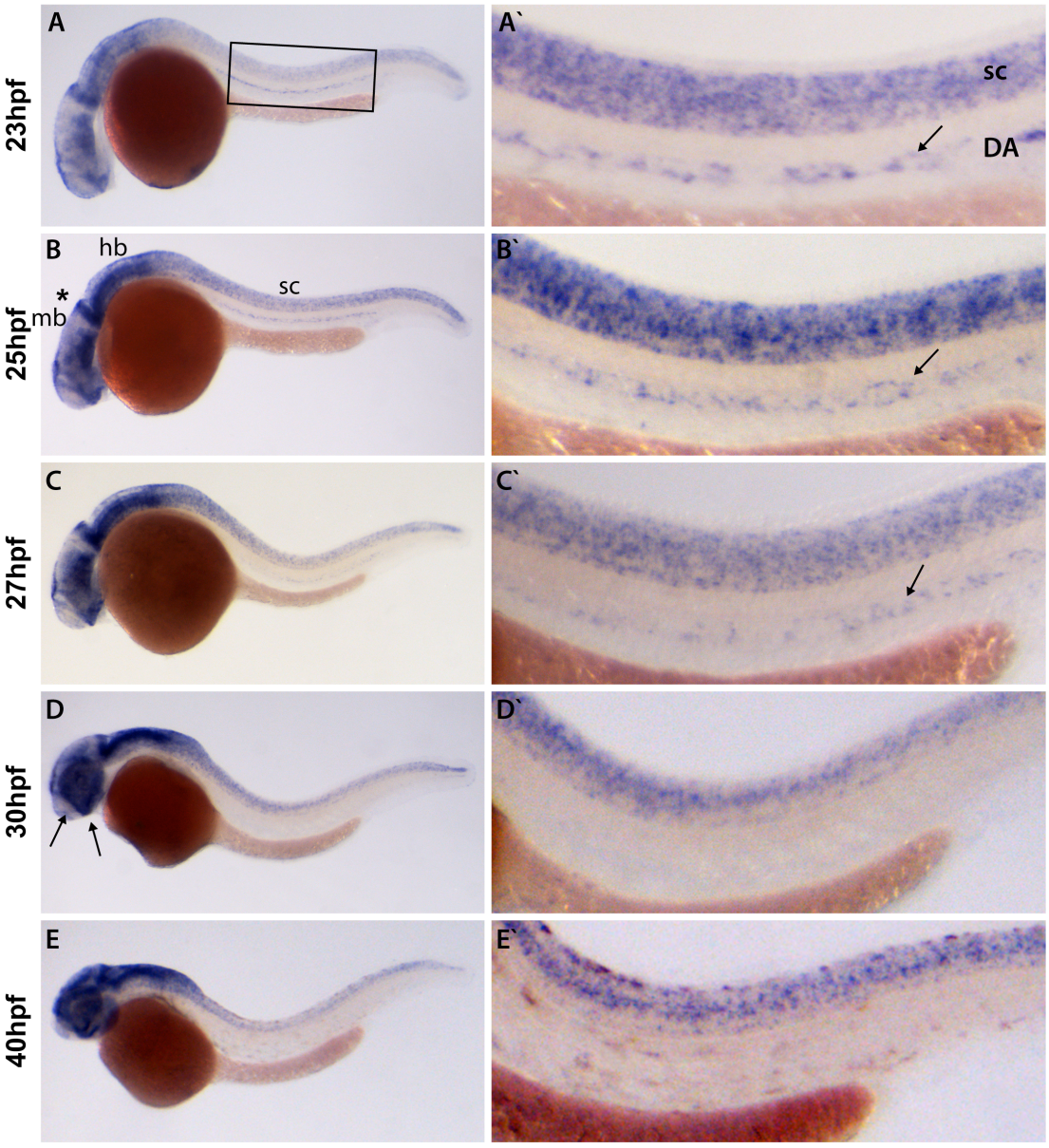

Figure 9: *Cldn5a* is highly expressed in the nervous system and temporally in the DA. (A-E`) Analysis of *cldn5a* mRNA expression. (A-E) Whole mount lateral view, (A`-E`) close-up view of region indicated by box in A. (A-E) *Cldn5a* is expressed in the brain and spinal cord. It is enriched in the hindbrain and highly expressed in the midbrain/hindbrain boundary (asterisk B). (A`-C`) Weak transient expression of *cldn5a* mRNA in DA (arrows). (D`-E`) Expression of *cldn5a* in DA is lost. DA: dorsal aorta, fb: forebrain, hb: hindbrain, mb: midbrain, sc: spinal cord.

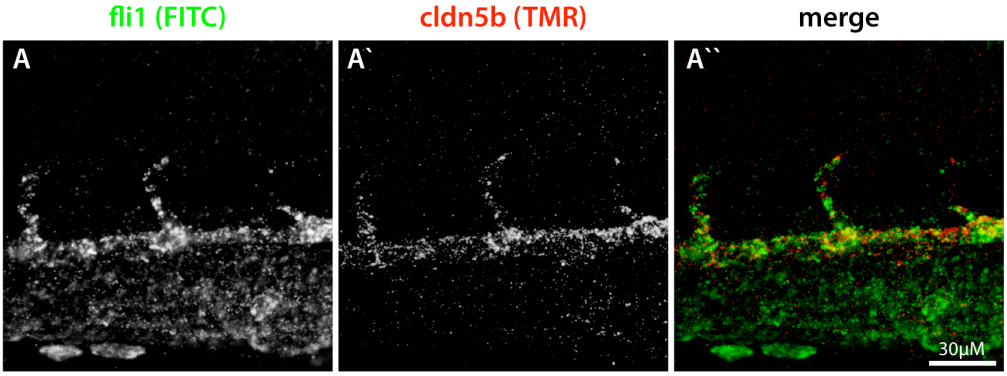

Figure 10: *Cldn5b* mRNA colocalizes with *fli1a* mRNA. (A-A``) Double fluorescent in situ hybridization in 24hpf embryos shows that *fli1* (visualized by FITC, green) and *cldn5b* (visualized by TMR, red) are co-expressed in the endothelial cells of the vasculature.

Cldn5b protein, different peptide antibodies were raised in rabbit and guinea pig against two epitopes in the zebrafish Cldn5b protein. These epitopes have the least similarity in aminoacid sequence with other Cldn proteins (Suppl. Data 8, Fig. 1). To test the antibodies` ability to recognize Cldn5b protein, I performed costainings for VE-cadherin (VE-cad) or ZO-1 protein with each of the peptide antibodies. I tested different staining protocols as well as different antibody concentrations. Compared to the efficient staining of VE-cad or ZO-1, none of the peptide antibodies recognizes Cldn5b protein (compare Suppl. Data 8, Fig. 2 A` vs A``). Therefore, I tested another Cldn5 antibody that is commercially available. It is raised against the C-terminus of the human Cldn5 protein. This antibody apparently recognizes both Cldn5 protein isoforms in endothelial cells as well as the neural tube and colocalizes with VE-cad in a junction-like pattern (Suppl. Data 8, Fig. 3).

Therefore, I used this antibody to visualize the expression pattern of Cldn5 during the development of ISVs in the zebrafish embryo. I performed immunohistochemical stainings for Cldn5 (green) and VE-cad (red) at different stages of ISV formation (Fig. 11). The embryos used for these experiments also expressed cytoplasmic EGFP under the control of the *fli1a* promoter (Fig. 11 A, E, I, M). During all timepoints analyzed Cldn5 signal can be observed in the aorta as well as in the neural tube (Fig. 11 C, G, K, O, S) and at later stages Cldn5 protein is also expressed in the ISVs. Within the ECs Cldn5 colocalizes with VE-cadherin at cell junctions (Fig. 11 L, P, T). However,

Cldn5 is almost absent from the PCV; only in some embryos a very weak signal can be observed (arrowhead in Fig. 11 G). Interestingly, in the vast majority of ISVs Cldn5 could not be detected during sprout formation and outgrowth (arrows in Fig. 11 C, D). At 24 hpf, when the vessels have started to grow dorsally, most ISVs lack Cldn5 protein expression (arrows in Fig. 10 G, H). Only with further progression of ISV formation, Cldn5 protein becomes detectable in all cells of the ISVs (arrows in Fig. 11 K, L; Fig. 11 O, P, S, T).
To analyze the different expression patterns of Cldn5 and VE-cad during ISV outgrowth in more detail, I detected Cldn5 (green) and VE-cad (red) expression in cross sections of *fli1a*:EGFP (blue) expressing embryos (Fig. 12). To better visualize Cldn5b expression in cross sections, I masked the staining of Cldn5 and VE-cad outside of the vasculature using the surface rendering and masking option in the Imaris® imaging software (Bitplane, Fig. 12 I-L vs M-P). Between 22hpf and 26hpf Cldn5 is only weakly expressed in the ISVs compared to the aorta (compare arrows in Fig. 12 C, D; G, H; K, L vs arrowheads). The expression level of VE-cad is similar between aorta and ISVs (Fig. 12 B, F, J).
Taken together, Cldn5b protein is localized in endothelial cell junctions in the ECs of the aorta. *Cldn5b* mRNA and protein seem to have different expression patterns. While the mRNA is localized in all ECs of the ISVs, Cldn5b protein is removed from cell junctions during sprout formation, when ECs are undergoing extensive remodeling. However, it becomes redeployed during later stages of ISV and DLAV formation, suggesting a role for blood vessel maturation and/or stabilization.

5.4 Analysis of the effects of *cldn5b* knock-down on angiogenesis

To investigate the requirement of *cldn5b* during the process of angiogenesis, I depleted *cldn5b* function by anti-sense morpholino (MO) injections. Knock-down via MO injection is an established method to evaluate the molecular functions of a particular gene (Summerton, 2007). These “RNA-type”

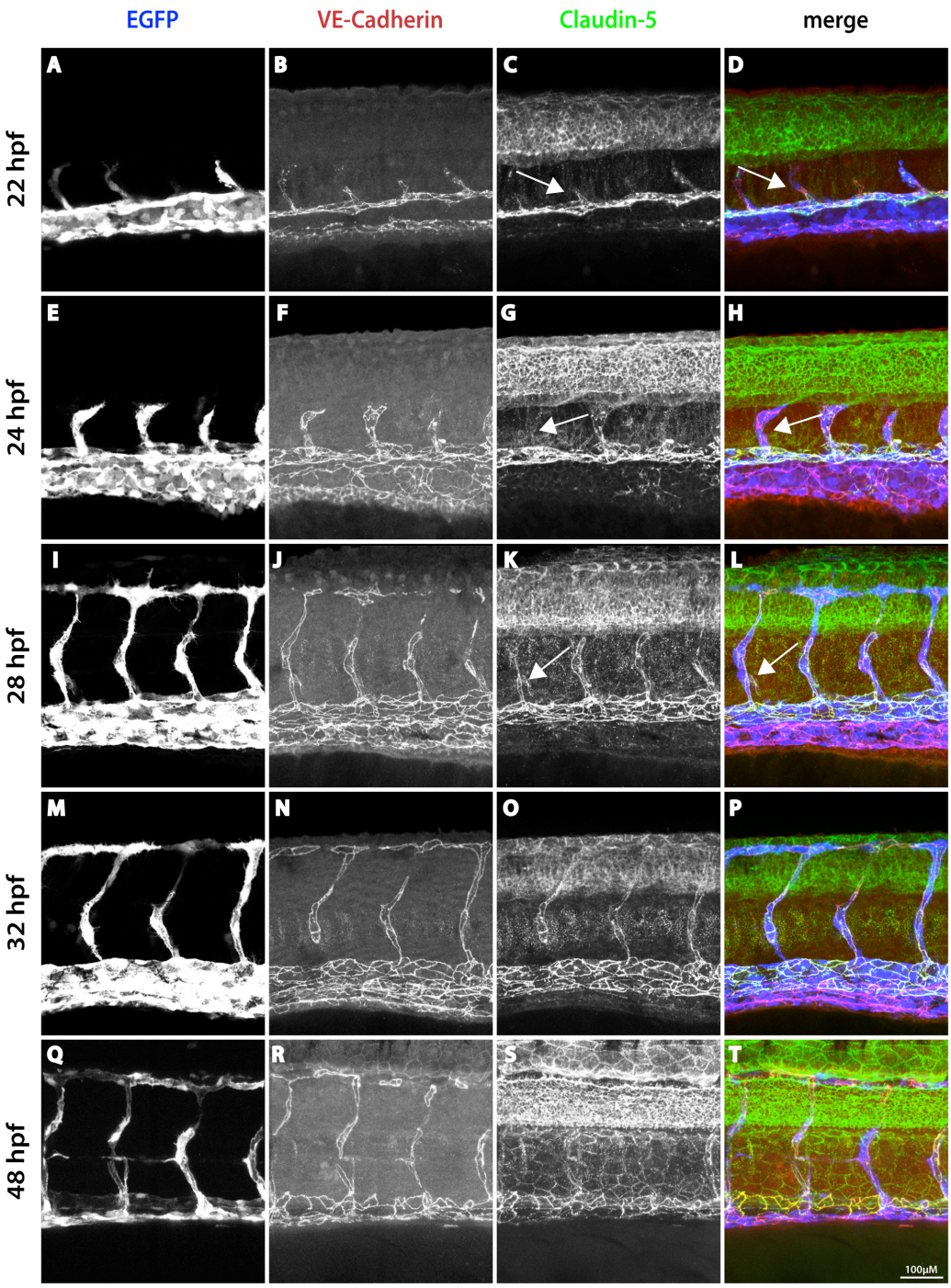

Figure 11: Cldn5 expression is downregulated in early ISV sprouts. (A-T) Immuno-histochemical analysis of Cldn5 (green) localization in respect to the adherens junction marker VE-cadherin (red) in *fli1a*:EGFP (blue) expressing embryos. VE-cadherin is expressed in all endothelial cells throughout the ISV formation process (B, F, J, N, R). Cldn5 is not expressed in sprouts of 22hpf and 24hpf old embryos (C, D, G, H), however gets upregulated in all cells of the ISV in older embryos (K, O, S).

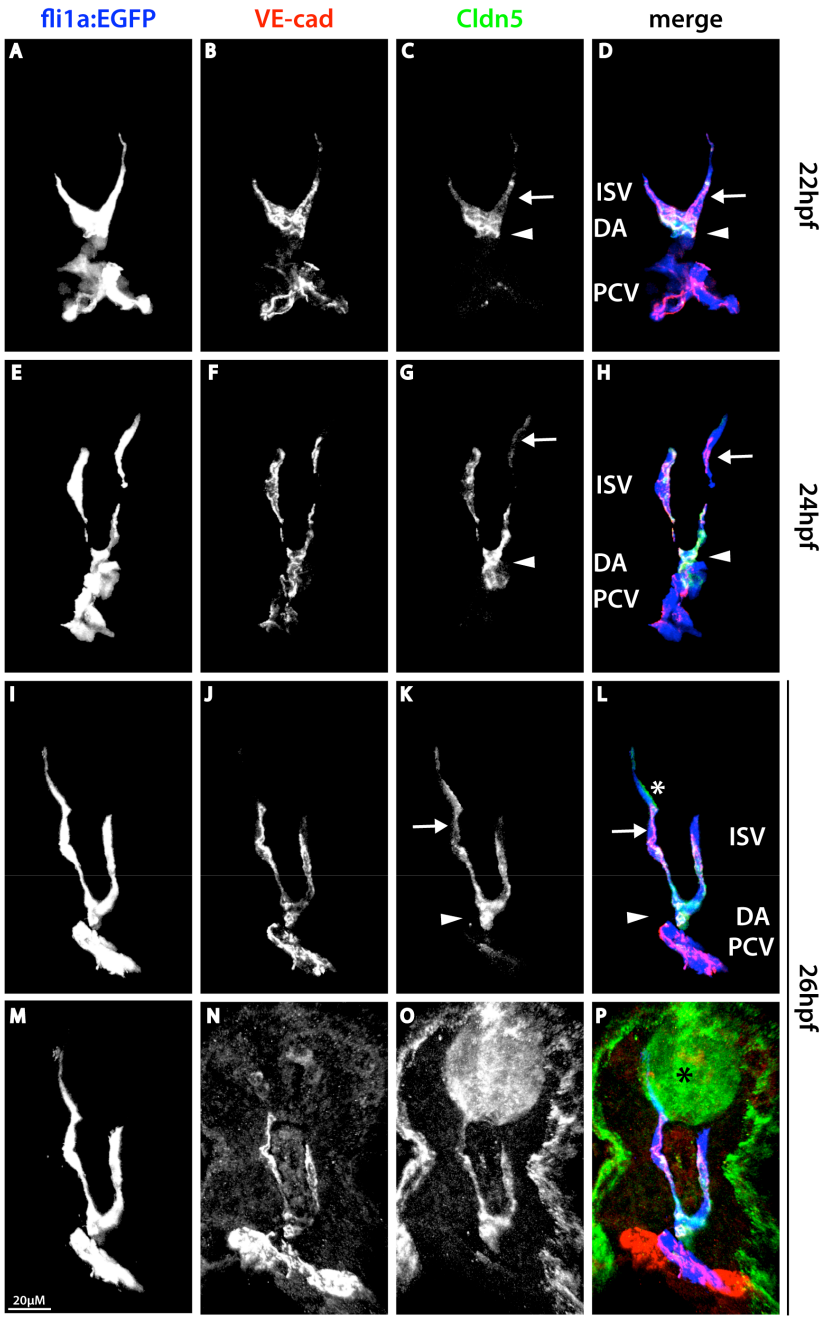

Figure 12: Differential localization of VE-cadherin and Cldn5. (A-P) Cross sections of transgenic *fli1a*:EGFP (blue) expressing embryos stained for Cldn5 (green) and VE-cadherin (red). (A-L) Surface rendering and masking for better visualization of the vasculature; (M-P) Original cross section of I-L. (B, F, J) VE-cadherin is expressed at the same level in aorta and ISVs. (C, G) Cldn5 is weakly expressed in the ISVs compared to the aorta. Also at later stages Cldn5 is expressed stronger in aorta and ventral ISV than in the tip of the ISV (K, L). (* L) Please note: fluorescence signal originates from the neural tube.

molecules bind to a specific RNA and through this either block its splicing or translation leading to a downregulation of the corresponding protein. MOs are injected into one-cell stage embryos and the subsequent knock-down is analyzed in the developmental stages of interest. Usually one translation- and one splice- blocking MO are used in parallel to validate the specificity of the MO knockdown. Because the *cldn5b* ORF only consists of one exon I used two different translation-blocking MOs. After testing the efficacy of the two different MOs, I decided to use morpholino #2 for all subsequent experiments (MO2; also see end of this sections). For phenotypic analysis of the *cldn5b* knock-down on ISV formation I concomitantly visualized the vasculature by *fli1a*:EGFP expression in these embryos. To show the efficacy of the MO knock-down, I looked for the absence of *cldn5b* mRNA as well as Cldn5b protein in MO injected embryos. For this purpose I compared in situ hybridization for *cldn5b* mRNA on standard control MO (std ctrl MO) injected as well as *cldn5b* MO injected embryos (Fig. 13). In control animals a robust mRNA signal can be observed in the aorta and ISVs (arrow and arrowhead in Fig. 13 A). In contrast, the mRNA expression level is strongly reduced in *cldn5b* MO injected animals probably caused by an enhanced instability of the mRNA, driven by error prone RNA degradation (compare arrowhead and arrow in Fig. 13 B vs A). To evaluate the effects of the *cldn5b* MO knock-down on the protein level, I performed immunohistochemical stainings for Cldn5 (green) and VE-cad (red) in injected and uninjected *fli1a*:EGFP (blue) expressing embryos (Fig. 14). As shown above, in uninjected and std ctrl MO injected embryos, Claudin 5 protein is expressed in the neural tube (Fig. 14 A``, B``) as well as in stripes along the axis of the ISVs, colocalizing with VE-cad protein in the aorta and the ISVs (Fig. 14 A-B```). Upon injection of *cldn5a* MO, the Cldn5 signal in the neural tube is lost. The remaining signal in the vasculature represents Cldn5b protein expression in the aorta and ISVs (Fig. 14 C``, C```). In contrast, injection of *cldn5b* leads to a loss of Cldn5 protein in the ISVs (arrowheads in Fig. 14 D``, D```) and a weaker signal in the aorta compared to control embryos (asterisks in Fig. 14 D``, D```). This indicates that the remaining signal in the neural tube (arrow Fig. 14 D``) and aorta (asterisk in Fig. 14 D``, D```) represent Cldn5a expression. The expression level of VE-cad in these embryos stays like in control embryos (compare Fig.

14 D` vs A`, B`). Embryos treated with both *cldn5a* and *cldn5b* MO lack Cldn5 protein expression completely (Fig. 14 E``, E```). The lack of expression in the aorta and ISVs (asterisks Fig. 14 E``, E``` and arrowheads Fig. 14 E``, E```) as well as in the neural tube (arrows in Fig. 14 E``, E```) shows the efficient knock-down of *cldn5a* and *cldn5b* via MO injection. Furthermore, these results demonstrate that the α-human Cldn5 antibody specifically recognizes Cldn5a and Cldn5b protein.

Interestingly, the knock-down of *cldn5b* leads to an irregular ISV patterning in contrast to *cldn5a* MO injected embryos where the ISV pattern is indistinguishable from wild type fish (see next section). It is important to note that the injection of MOs often causes cell death in some tissues, which is prevented by the simultaneous injection of *p53* MO (Robu et al., 2007). Also in *cldn5a* MO injected animals, cell death occurs in the nervous system. Therefore, the injection is always performed with simultaneous injection of *p53* MO in order to prevent this cell death (data not shown). The injection of *cldn5b* MO does not cause any cells death (data not shown). Furthermore, the concomitant injection of *p53* MO with *cldn5b* MO does not alter the outcome of the phenotype and has therefore not been further used (data not shown). As mentioned above, I tested the efficacy of two different *cldn5b* MO both ablating translation of this gene. In a pre-screen I determined the most efficient concentration for each of the MOs by comparing their effect on the outgrowth of ISVs (sequences in Suppl. Data 8, list 1). In a further screen these MOs were compared to each other (Suppl. Data 8, Fig. 4). MO2 at a concentration of 0.2mM causes the stronger phenotype and was therefore used in all the following experiments.

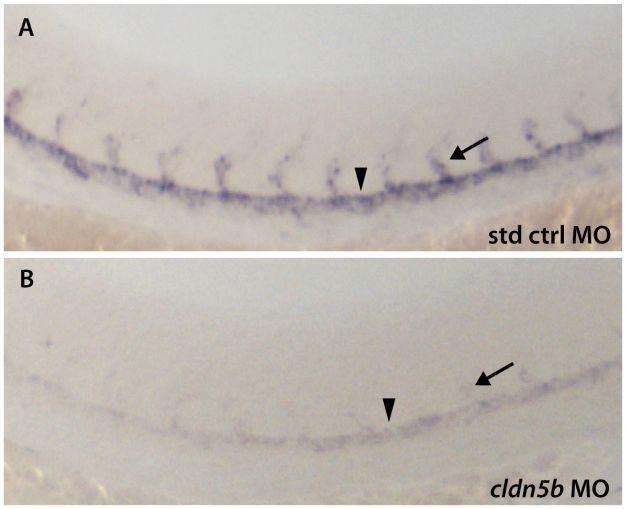

Figure 13: Efficient knock-down of *cldn5b* mRNA by MO injection. (A, B) Analysis of in situ hybridization for *cldn5b* in standard control MO (0.2 mM, A) and *cldn5b* MO (0.2 mM, B) injected 24hpf zebrafish embryos. Lateral view, rostral to left. Injection of *cldn5b* MO leads to a strong reduction of *cldn5b* mRNA in the ISVs (compare arrows in A and B) and the aorta (compare arrowheads in A and B).

Figure 14: Efficient knock-down of Cldn5b protein expression upon MO knock-down. (A-E``') Confocal images of 27hpf *fli1a*:EGFP (blue) expressing zebrafish embryos stained for Cldn5 (green) and VE-cadherin (red) and injected with the indicated MOs on the left. Cldn5 is expressed in the vasculature and the neural tube in control embryos (arrows in A``, B``) indicating the recognition of both Cldn5b and Cldn5a by the human Cldn5 antibody. Depletion of *cldn5a* leads to the absence of staining in the neural tube (arrows in C``, C'''). *Cldn5b* MO injection causes depletion of Cldn5 staining in the ISVs (arrows in D``, D''') and reduction in the aorta (asterisks in D``, D'''). Knock-down of both *cldn5b* and *cldn5a* abolishes antibody staining in the neural tube (arrowheads in E``, E'''), the DA (asterisks in E``, E''') and the ISVs (arrows in E``, E'''). ●unspecific VE-cadherin staining in the pronephric duct. MO concentrations injected: *cldn5b* - 0.2 mM; *cldn5a* - 0.2 mM; *p53* - 0.5 mM; std ctrl - 0.5 mM.

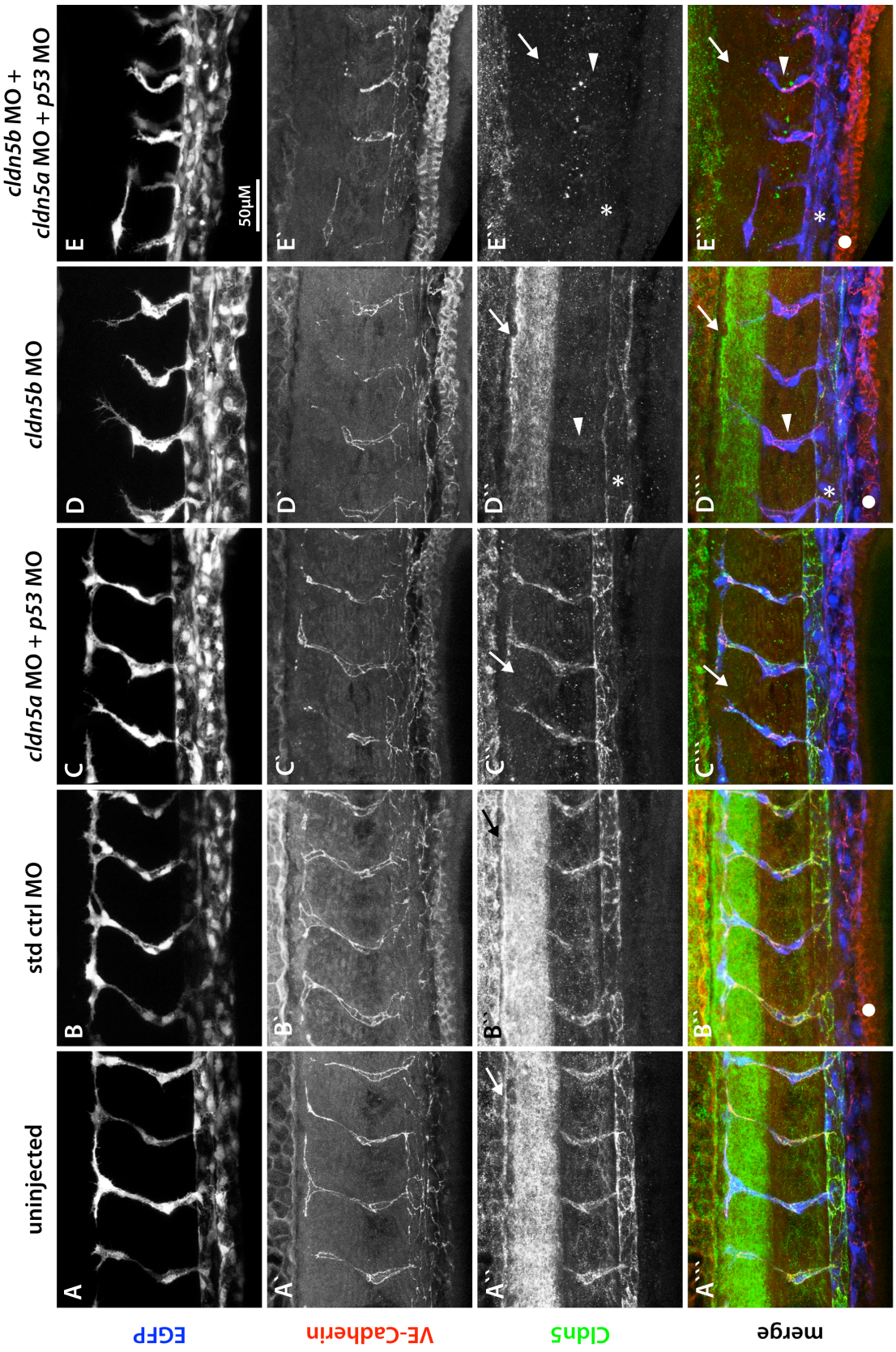
uninjected
std ctrl MO
cldn5a MO + p53 MO
cldn5b MO
cldn5b MO +
cldn5a MO + p53 MO
A
B
C
D
E
A`
B`
C`
D`
E`
A``
B``
C``
D``
E``
A```
B```
C```
D```
E```
50µM
EGFP
VE-Cadherin
Cldn5
merge

5.4.1 Leaky vessels in *cldn5b* knock-down embryos cause hemorrhages

As mentioned above, the ISV pattern in *cldn5b* MO injected embryos looks irregular. To study the general effect of *cldn5b* knock-down on embryonic development, I analyzed the overall anatomy of 54hpf old embryos. In order to do so, I compared *cldn5b* MO injected animals with uninjected embryos (Fig. 15). Compared to control fish, *cldn5b* MO injected embryos show no gross anatomical defects (compare Fig. 15 A vs B, C). However, in some embryos the heart developed edema shown by an enlarged cardiac sac and/or showed an elongated and thin morphology (arrowhead in Fig. 15 F vs D, E). Additionally, in many cases *cldn5b* MO injected embryos showed expanded hindbrain regions (arrow in Fig. 15 E) that were often accompanied by accumulations of blood (data not shown). These hemorrhages were also visible in the head outside of the brain (arrow in Fig. 15 F) as well as in other regions of the embryo (data not show, see next section). The trunk and tail regions of *cldn5b* MO injected embryos are morphologically indistinguishable from wildtype embryos (compare Fig. 15 H, I, K, L vs G, J).

In uninjected and std ctrl MO injected embryos blood flow is visible in the axial vessels as well as in the ISVs at 48hpf (see Suppl. movie 1 and 2). Most *cldn5b* MO injected embryos show blood flow in the axial vessels, but lack it in the ISVs (Suppl. movie 3). However, in these embryos rarely blood flow is visible also in the ISVs (data not shown). Furthermore, mainly in embryos showing heart edema or elongated hearts, blood flow was missing completely (Suppl. movie 4) or slow (data not shown).

As shown in the previous experiments, *cldn5b* knock-down causes hemorrhages. As Cldn5 is known for its sealing function of the blood-brain barrier (BBB) (Nitta et al., 2003), I wanted to investigate further the role of *cldn5b* in sealing vessels in the zebrafish embryo. Using fish that express *fli1a*:EGFP (green) and *gata1*:dsRed marking erythrocytes in red, I compared the effect of *cldn5b* MO knock-down on the number of hemorrhages in uninjected and ctrl MO injected animals (50hpf, Fig. 16). Some embryos of the *gata1*:dsRed transgenic line show expression of dsRed positive cells at the

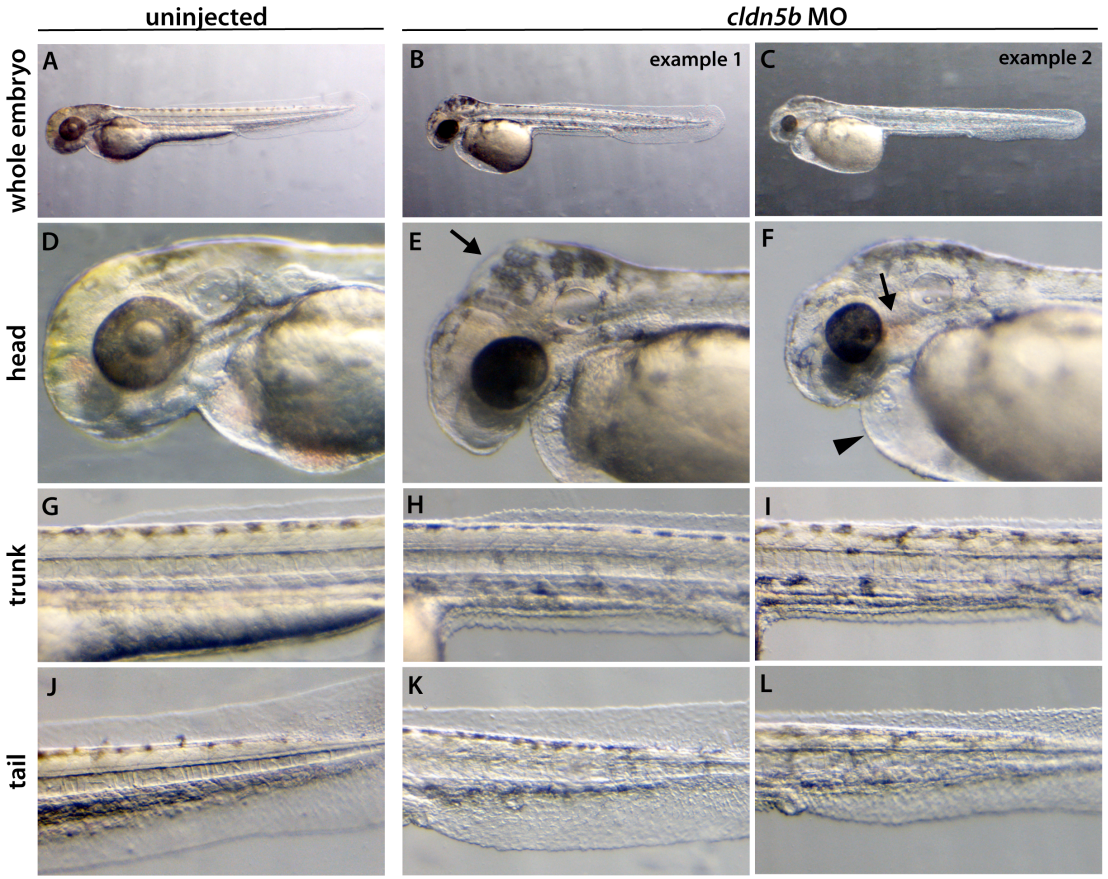

Figure 15: *Cldn5b* MO knock-down causes hemorrhages and heart edema. (A-L) Comparison of wildtype (A, D, G, J) with *cldn5b* MO injected embryos (example1 (B, E, H, K), example2 (C, F, I, L)). Lateral view, rostral to the left. The overall anatomy of *cldn5b* morphants (B, C) is normal compared to wildtype embryos (A). *Cldn5b* morphants have enlarged heads (arrow, E) and show edema of the heart (arrowhead, F) as well as hemorrhages in different parts of the body (arrow, F) compared to uninjected embryos (D). The anatomy of the trunk and tail of *cldn5b* morphants (H, I, K, L) is unaltered compared to wildtype embryos (G, J).

level of the notochord resembling a part of the expression pattern of this particular *gata1* promoter (see arrowheads Fig. 16 F). These dsRed positive cells were not taken into account when counting the hemorrhages: instead clusters of dsRed positive cells outside of this expression pattern were counted. Compared to control embryos, which do not reveal any hemorrhages in the trunk and tail (wt: n=39; std ctrl MO: n=28 embryos), more than 37% of *cldn5b* morphants show one and more hemorrhages in the trunk and over 40% show hemorrhages in the tail (37.8% and 43.2%, n= 37 embryos; compare Fig. 16 B, C, E, F vs H, I). In the head more then 50% of uninjected embryos show hemorrhages, while less than 5% of std ctrl MO (std ctrl MO) injected embryos showed hemorrhages in the head (53.8% and 3.6%, compare Fig. 16 A with D). In contrast, *cldn5b* MO injection causes hemorrhages in more than 60% of the embryos (64.9%, Fig. 16 G, J). In the specific example shown, the *cldn5b* morphant shows a strong reduction of erythrocyte number, which is probably caused by the loss of heart beat and blood flow and the subsequent accumulation of blood cells in one region of the embryonic body (data not shown).

These data suggest a sealing function of *cldn5b*. To gain insights into the dynamics of this process, I visualized ECs and blood cells in living zebrafish embryos and compared the effect of *clnd5b* knock-down (Suppl. movie 7) with uninjected (Suppl. movie 5) and std ctrl MO injected embryos (Suppl. movie 6) (Fig. 17). The analysis started at around 33hpf. At this stage blood flow in uninjected fish and control morphants is visible in the axial vessels, but not yet in the ISVs. At roughly 38 hpf, a few blood cells start to enter the ISVs and soon later blood flow starts in these vessels (653`, 788`, upper panel, Fig. 17). Compared to control embryos the ISV morphology in *cldn5b* morphants is severely altered with premature stopping of sprout outgrowth. Lumen formation, however, is not affected. In this particular example almost no ISV is connected to the neighboring vessel. Also in *cldn5b* morphants blood flow is visible at 33hpf, but blood cells start to enter the ISVs earlier than in control embryos (compare 425` lower panel with 425` upper and middle panel, Fig. 17). They accumulate in the vessel and burst out of the tip of the ISV (arrows in lower panel, 425`- 475`, Fig. 17). The

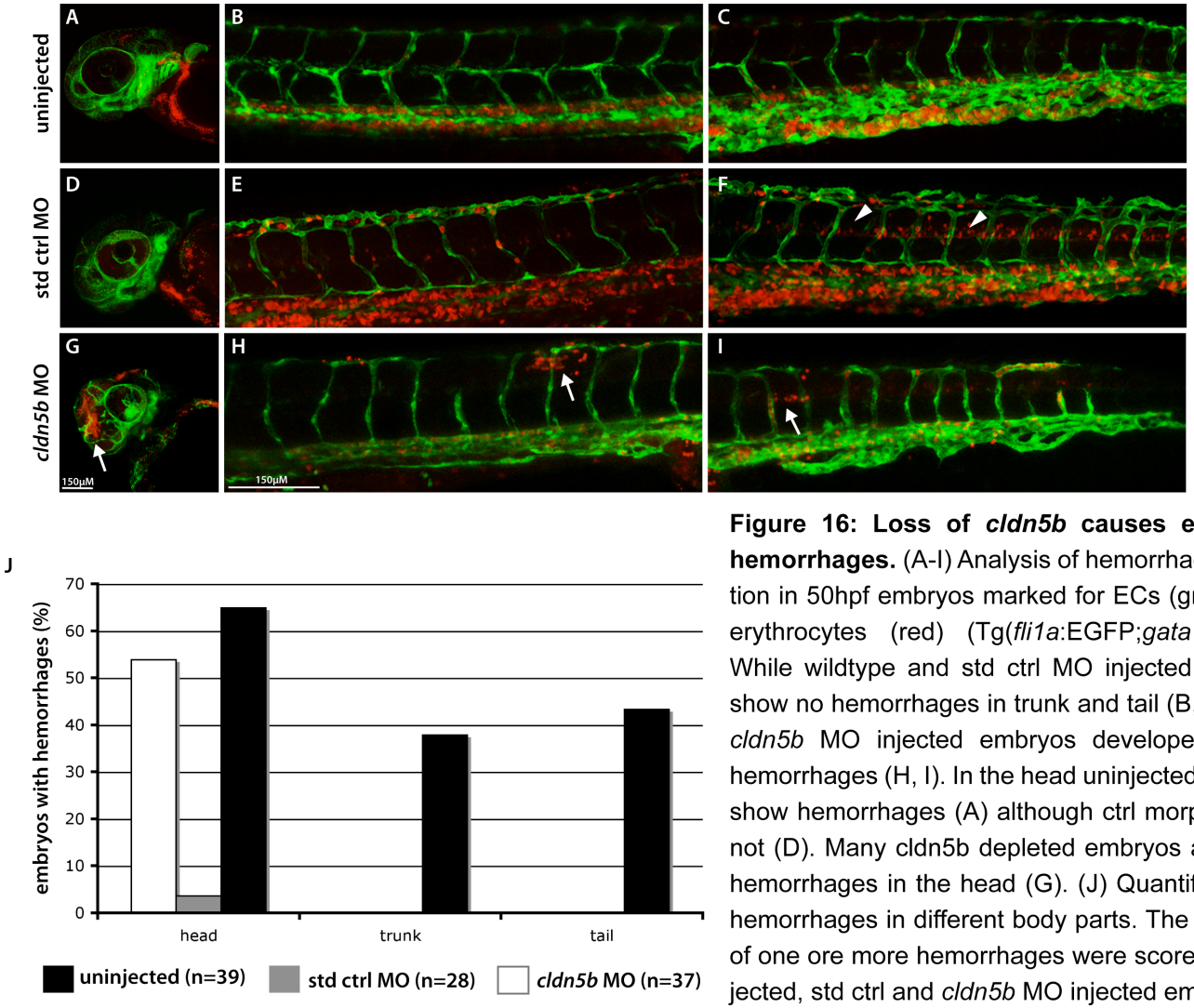

Figure 16: Loss of *cldn5b* causes excessive hemorrhages. (A-I) Analysis of hemorrhage formation in 50hpf embryos marked for ECs (green) and erythrocytes (red) (Tg(*fli1a*:EGFP;*gata1*:dsRed). While wildtype and std ctrl MO injected embryos show no hemorrhages in trunk and tail (B, C, E, F), *cldn5b* MO injected embryos developed severe hemorrhages (H, I). In the head uninjected embryos show hemorrhages (A) although ctrl morphants do not (D). Many cldn5b depleted embryos also have hemorrhages in the head (G). (J) Quantification of hemorrhages in different body parts. The presence of one ore more hemorrhages were scored in uninjected, std ctrl and *cldn5b* MO injected embryos.

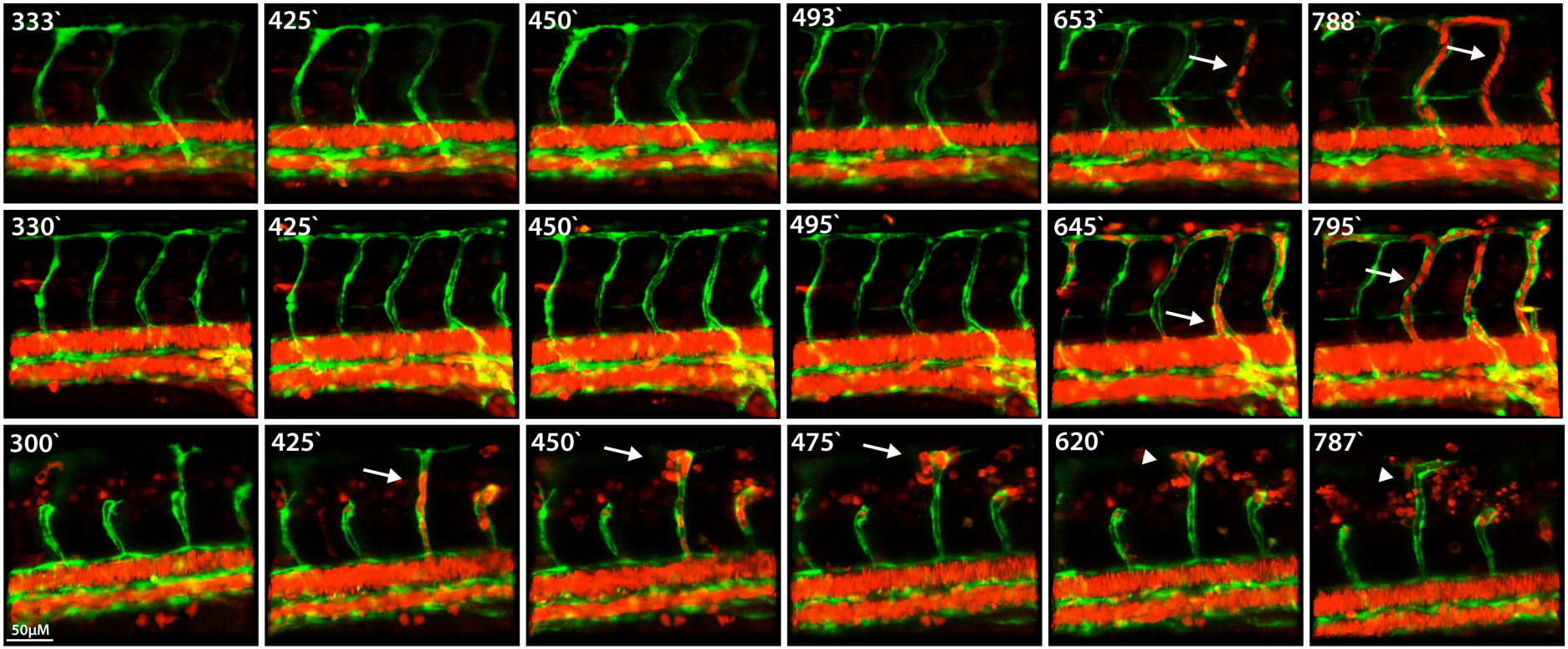

Figure 17: *Cldn5b* MO knock-down causes blood leakage in ISVs. Still pictures from confocal time-lapse movies (Suppl. movies 5-7) of embryos expressing *fli1a*:EGFP (green) and *gata1*:dsRed (red). At 33 hpf blood flow is observed in the DA and PCV of all embryos. After 11 hrs, blood flow also starts in the ISVs in uninjected embryos and control morphants (upper and middle panel). In *cldn5b* MO injected embryos (lower panel), erythrocytes enter the ISVs, but explode out into the body cavity (arrows).

erythrocytes then disperse in the surrounding tissue (arrowheads, lower panel, 620`, 787`, Fig. 17). This shows that the MO mediated knock-down of *cldn5b* decreases the vessel integrity causing severe hemorrhages to occur.

5.4.2 *Cldn5b* is required for vessel outgrowth and stability

As already mentioned before, vessel outgrowth is impaired in *cldn5b* function depleted embryos. To investigate this phenotype in more detail, I analyzed the ISV formation at different stages (Fig. 18). Using *fli1a*:EGFP expressing embryos, I compared *cldn5b* MO injected embryos to std ctrl morphants. In control embryos ISVs start to form at 22hpf and grow along the segment boundary until they reach the middle of the horizontal myoseptum (HMS) (indicated in red in Fig. 18 A, B, Fig. 18 E). From here on they do not follow the segment boundary anymore, but grow straight in the dorsal direction. At the roof of the neural tube the ISVs ramify into anterior and posterior directions and connect to the neighboring ISVs (Fig. 18 G). Until 48 hpf these vessels develop into functional tubes (Fig. 18 K). Very rarely ISV outgrowth is delayed in control morphants, which is corrected for in all of the cases until 48hpf (Fig. 18 K). In *cldn5b* MO injected embryos the initial ISV formation and outgrowth is indistinguishable from control morphants with all ISVs growing posteriorly and some reaching the level of the HMS (compare arrows in Fig. 18 C vs B). However, at 25hpf when in control morphants the ISV grow beyond the level of the HMS, most of the morphant vessels show an arrest of growth (compare arrows in Fig. 18 F vs E). At 30hpf, although many ISVs are still halted (arrow in Fig. 18 H), individual ISVs start to extend protrusions and grow beyond the middle of the HMS. These, however, are very thin extensions that seem to harbor only a small part of the cell content (arrowhead in Fig. 18 H). At 35 hpf, whereas in control embryos most of the ISVs are connected within the DLAV, in *cldn5b* MO injected animals only single vessels have reached the roof of the neural tube while many are still halted at the HMS (arrowheads and arrow in Fig. 18 J). Most vessels eventually grow further posteriorly, but often the anatomy is aberrant. In some vessels e.g. protrusions emerge that grow anteriorly and posteriorly at the

level of the HMS (orange arrowheads in Fig. 18 J). Furthermore, the connections of many vessels to the aorta become very thin (green arrowheads in Fig. 18 J). At 48hpf the DLAV is only partially made with several connections missing between neighboring ISVs (asterisks in Fig. 18 L). Some ISVs are still arrested at the level of the HMS, which is never seen at this stage in control embryos (compare arrow in Fig. 18 L vs K). Furthermore, the connections between the ISV and DA are very thin (green arrowhead in Fig. 18 L). Analyzing ISV/DLAV formation reveals that the knock-down of *cldn5b* via MO injection leads not only to a halt of ISV outgrowth, but also to vessel instability.

To analyze the dynamics of the morphological defects occurring in *cldn5b* morphants, I documented ISV outgrowth and DLAV formation in living embryos via time-lapse analysis (Fig. 19). In uninjected (Suppl. movie 8) and std ctrl MO injected animals (Suppl. movie 9) (A-E; F-J) ISVs have grown to the roof of the neural tube and ramified anteriorly and posteriorly (arrows in Fig 19 F, G). Eventually a functional vascular network is formed (Fig. 19 C-E). In contrast, in *cldn5b* MO injected embryos (Suppl. movie 10), an arrested growth is seen in most of the ISVs (arrow in Fig. 19 K), which eventually grow beyond the HMS. A connected DLAV is never made in this particular example (arrows Fig. 19 M, N), although an individual ISV grows posteriorly and seems to connect to the neighboring ISV, this connection is not maintained (asterisks Fig. 19 M-O). Interestingly, the ventral connection between ISV and DA starts to be very thin (arrowhead Fig. 19 M) and breaks completely with further development (arrowheads in Fig. 19 N, O), a phenotype never observed in control animals (arrow in Fig. 19 H). In other movies of a *cldn5b* MO injected embryo this loss of connection between the aorta and the ISV can be seen, too (Suppl. movie 11 and movie 12). Interestingly, in one of these embryos at a later timepoint the ventral end of one detached vessel gets contacted by a secondary sprout coming from the vein and subsequently makes a full connection via this sprout to the PCV (Suppl. movie 12).

To determine the frequency of the morphological defects described above, I quantified the ISV outgrowth, missing connections within the DLAV and the detachment of ISVs from the DA in std ctrl and *clnd5b* MO injected animals.

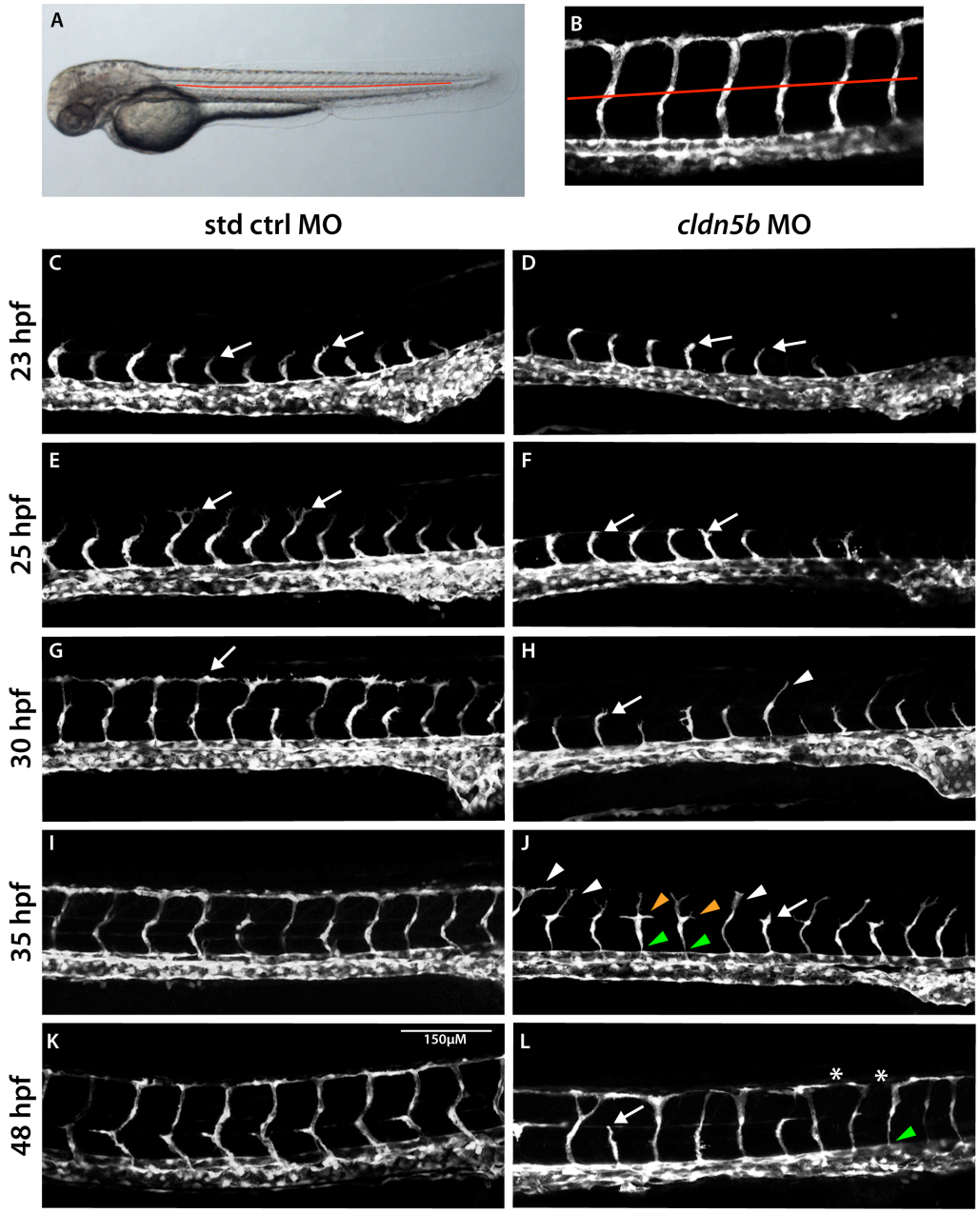

Figure 18: *Cldn5b* MO knock-down causes delay in vessel outgrowth and vessel instability. (A,B) Marking (red) of the horizontal myoseptum in a 48hpf embryo and in relation to the ISVs in a 34hpf embryo. (C-L) Images of Tg(*fli1a*:EGFP) embryos injected with std ctrl MO and *cldn5b* MO at different stages of development. Compared to std ctrl MO injected embryos (C, E, G, I, K), *cldn5b* morphants (D, F, H, J, L) show a delay in vessel growth from the level of the horizontal myoseptum on (compare arrows in C vs D, F). Neighboring ISVs do not always connect within the DLAV (asterisk in L) and connections between the ISV and the DA remain thin or break (green arrowheads in J, L).

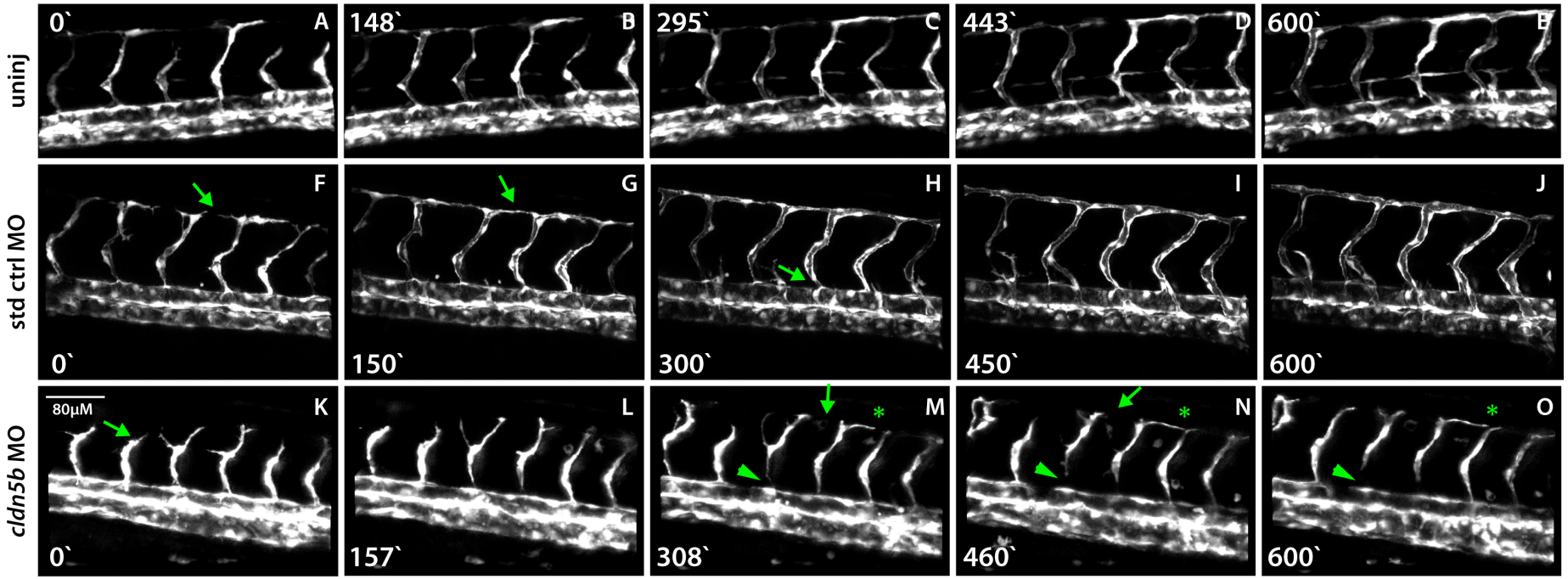

Figure 19: *Cldn5b* MO knock-down causes halting of outgrowth and vessel instability. (A-O) Still pictures from confocal time-lapse movies of uninjected (A-E, Suppl. movie 8), control MO injected (F-J, Suppl. movie 9) and *cldn5b* MO injected (K-O, Suppl. movie 10) embryos expressing *fli1a*:EGFP starting at 26hpf. (A-J) ISVs in control embryos connect to neighboring ISVs and form luminized circuits. (K-O) *Cldn5b* MO injected embryos show a delay in vessel outgrowth from the horizontal myoseptum onwards (arrow in K), a lack of connection within the DLAV (arrow in M, N) and detachment of ISVs from the DA (arrowheads in M-O).

The ISV growth defect was quantified by counting the growth of ISVs beyond the HMS at different developmental stages (HMS indicated in red in Fig. 18 A, B; Fig. 20 A). In uninjected embryos (dark grey bars Fig. 20 A) on average 7 vessels grow further than the HMS at 24hpf (7.3/10 vessels +/-2.5, n=20 embryos). At this stage the anterior vessels have grown further, while posterior vessels have not reached or have just reached the HMS. In *cldn5b* morphants however almost no vessel has grown further than the HMS (0.1/10 vessels +/-0.2, n=20 embryos). This reflects the growth defects shown in Fig. 18 F. At 30hpf on average 6 vessels (5.6/10 vessels +/-2, n=20 embryos) grows beyond the HMS compared to almost all of the vessels in control embryos (9.8/10 vessels +/-0.5, n=20 embryos) indicating a growth stop of vessels at the HMS. The number of vessels growing further than the HMS increases, but never reaches the number of control embryos. At 48hpf e.g. all vessels in std ctrl morphants have grown further (10/10 vessels +/-0, n=20 embryos) and on average 8 vessels grew beyond the HMS in *cldn5b* MO injected embryos (8.1/10 vessels +/-0.3, n=20 embryos). Taken together, compared to control animals, a significant number of ISVs in *cldn5b* morphants halts its outgrowth at the HMS (compare Fig. 20 B, B` vs C, C`). The phenotype of missing connections within the DLAV was quantified by counting the DLAV connections between individual ISVs in ctrl as well as *cldn5b* morphants. In 44% of the DLAV connections a continuous assembly of neighboring ISVs was missing at 48hpf (4.4/10 vessels, n=27 embryos), which never occurred in control morphants (0/10 vessels, n=20 embryos) (compare Fig. 20 E, E` vs D, D`). Furthermore, 24% of all ISVs counted detached from the DA, which is never observed in control animals at this time point (2.4/10 vessels, n=27 embryos; compare Fig. 20 F, F` vs D, D`). Interestingly, this phenotype can be observed only from roughly 35hpf onwards, as in 36hpf old *cldn5b* MO injected embryos 10% of ISVs are detached from the aorta (1/10 vessels, n=20 embryos).

As described above, some *cldn5b* MO injected embryos show reduced or absent bloodflow. Although the blockage of blood flow does not influence the primary network formation in wildtype animals, the ISVs do develop enlargements and ramifications in the dorsal part of the vessels at later timepoints (Isogai et al., 2003). Because most *cldn5b* morphants display

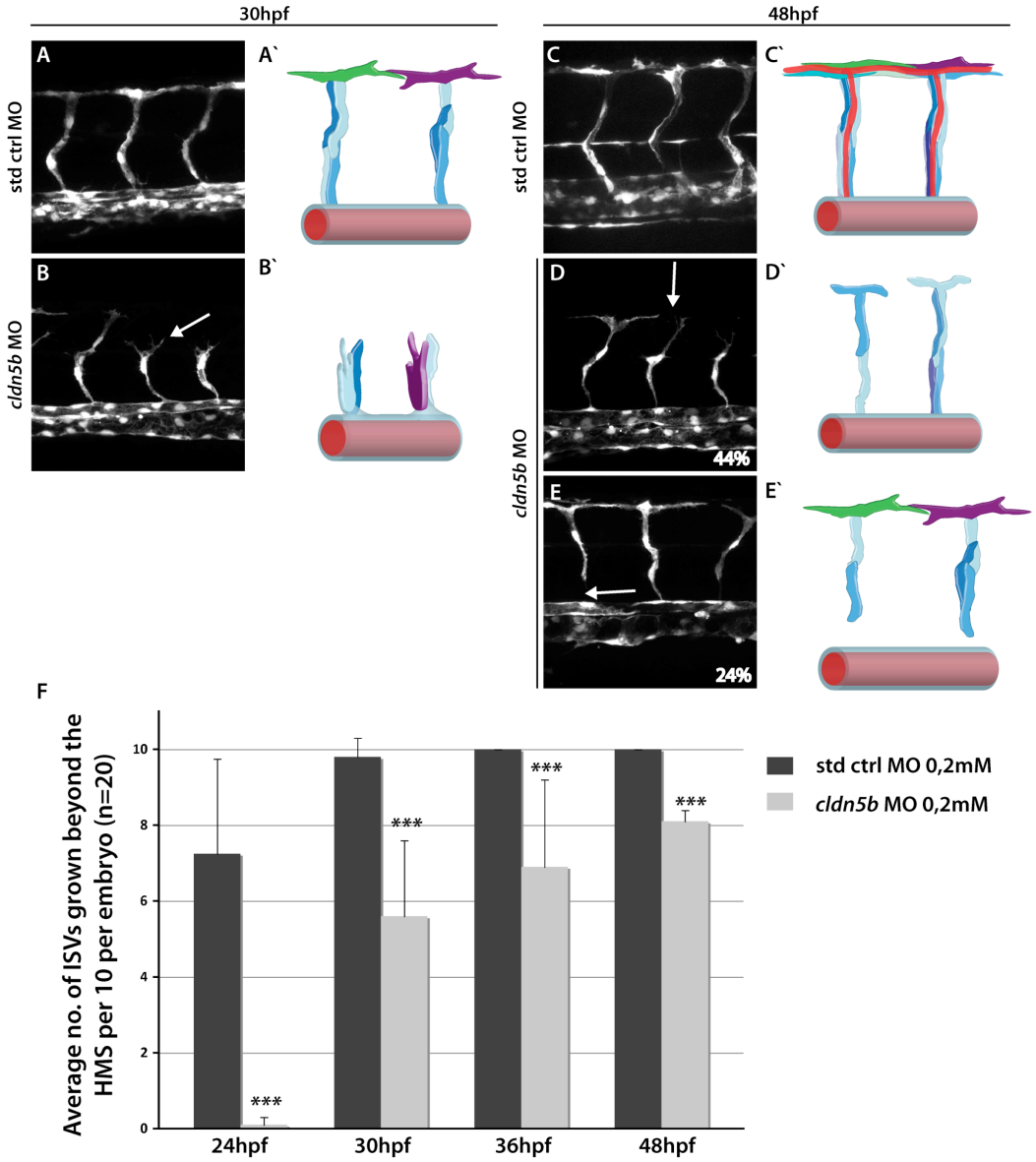

Figure 20: *Cldn5b* knock-down causes vessel halting and instability. (A-E) Confocal images of std ctrl and *cldn5b* MO injected embryos expressing Tg(*fli1a:EGFP*) (30hpf A, B; 48hpf C, D, E) and the corresponding schematics (A`- E`). (F) Quantification of ISVs grown beyond HMS at different timpoints. Compared to control morphants (A, A`), *cldn5b* MO injected embryos show a significant degree of vessels halting at the HMS (B, B` and F). Quantification of missing DLAV connections and detachment from DA bottom right in C, D, E. At 48hpf 44% of vessels in *cldn5b* morphants are not connected within DLAV (D, D`) and 24% of ISVs are detached from the DA (E, E`) compared to 0% in control morphants (C, C`). HMS: horizontal myoseptum. *** indicate p<0.001 (ANOVA).

normal blood flow and show all of the observed phenotypes described above, the absence of blood flow does not seem to influence the outcome of the phenotype. Nevertheless, I performed an experiment, in which I quantified the occurrence of altered ISV formation in embryos with normal, slow and absent blood flow (example of ISV detachment in Suppl. Data 8, Fig. 5, data not shown). These experiments show no clear correlation between the penetrance of the ISV phenotype and the absence or presence of blood flow in *cldn5b* morphants.

In summary, three different phenotypes can be observed in *cldn5b* morphants, the arrest of vessel outgrowth at the HMS, the missing connections within the DLAV as well as the detachment of ISVs from the DA.

5.4.3 *Cldn5b* and *cldn5a* do not function redundantly during ISV formation

As shown before (see chapter 5.2), *cldn5a* is expressed mainly in the nervous system, but between 23 hpf and 27 hpf it is also expressed in the DA. To analyze the role for *cldn5a* in ISV formation, I performed knock-down experiments for *cldn5a*, *cldn5b* and both concomitantly and quantified the resulting phenotypes (Fig. 21). In control embryos the ISVs have grown to the roof of the neural tube and are connected to their neighbors at 36hpf (arrow Fig. 21 A). As described above, in *cldn5b* morphants the ISVs have stopped growing at the HMS or are not connected to neighboring ISVs at this stage (arrow Fig. 21 B). *Cldn5a* morphants, however, show none of these phenotypes with all ISVs connected to their neighbors (arrow Fig. 21 C). Upon injection of both *cldn5a* and *cldn5b* MO, the ISV phenotype observed resembles that of *cldn5b* morphants (Fig. 21 D). The quantification of these phenotypes revealed a non-significant difference between *cldn5b* and *cldn5b*/*cldn5a* double morphants (Fig. 21 E, F).

During the analysis of *cldn5a* and *cldn5b* function on ISV formation, I found that the morphology of the CV is altered in many embryos. First, they show a reduction of the dorso-ventral length of the CV. More interesting, the CV and DA are sometimes fused to one large vessel. In wildtype embryos the CV

plexus arises through cell sprouting, migration and anastomosis, which are governed by complex cell rearrangement events (Choi et al., 2011), which ultimately leads to the formation of a complex network of loops. In order to investigate the morphology of the CV in more detail I compared cross-sections of the CV in std ctrl MO, *cldn5b*, *cldn5a* and *cldn5a* + *cldn5b* MO injected embryos (Fig. 22). Furthermore, I quantified the fusion of CV and DA in these embryos. In control embryos the CV shows a complex plexus, which is divided into many tubes at both anterior and posterior positions (Fig. 22 A, A`, A``). In *cldn5b* MO injected embryos, however, the length of the CV is highly reduced (Fig. 22 B). Cross sections in the anterior and posterior part of the CV show that it completely lacks the complexity of a control embryos` CV. Here it is composed of one vessel only (Fig. 22 B`, B``). The frequency of this phenotype was not analyzed, but is estimated to occur in at least half of the morphants. However, the CV and DA are separated vessels in all embryos observed (vessel fusion in 0% of embryos, 0/29 embryos). Also in *cldn5a* morphants the CV plexus is highly altered in morphology. The formation of a complex CV plexus is only observed in roughly 20% of the embryos. Furthermore, *cldn5a* morphants resemble the fusion of CV and DA that is never observed in control MO injected embryos (compare Fig. 22 C`` with A` and A``). This phenotype occurs in ~18% of the embryos (7/38 embryos). In contrast, double morphants show a much stronger phenotype. The dorso-ventral tube of the CV is often very thin and the CV and DA are fused in ~53% of the embryos (24/45 embryos, Fig. 22 D, D`, D``). It should be noted that more *cldn5a* morphants than *cldn5b* morphants show a lack of blood flow in the axial vessels (29% vs 10%; n= 38, n= 29). In double MO injected embryos the lack of blood flow can be observed in 27% of the embryos. Therefore, *cldn5a* and *cldn5b* do not resemble overlapping functions in determining blood flow. However, there seems to be a correlation between the absence/reduction of blood flow and the fusion of CV/DA. In *cldn5a* morphants 100% of the embryos with a fused CV/DA show a loss or reduction of blood flow (7/7 embryos). In double morphants 62.5% of the embryos without separated CV and DA lack blood flow, but 37.5% of these embryos do have blood flow. In summary, *cldn5b* and *cldn5a* function non-redundantly

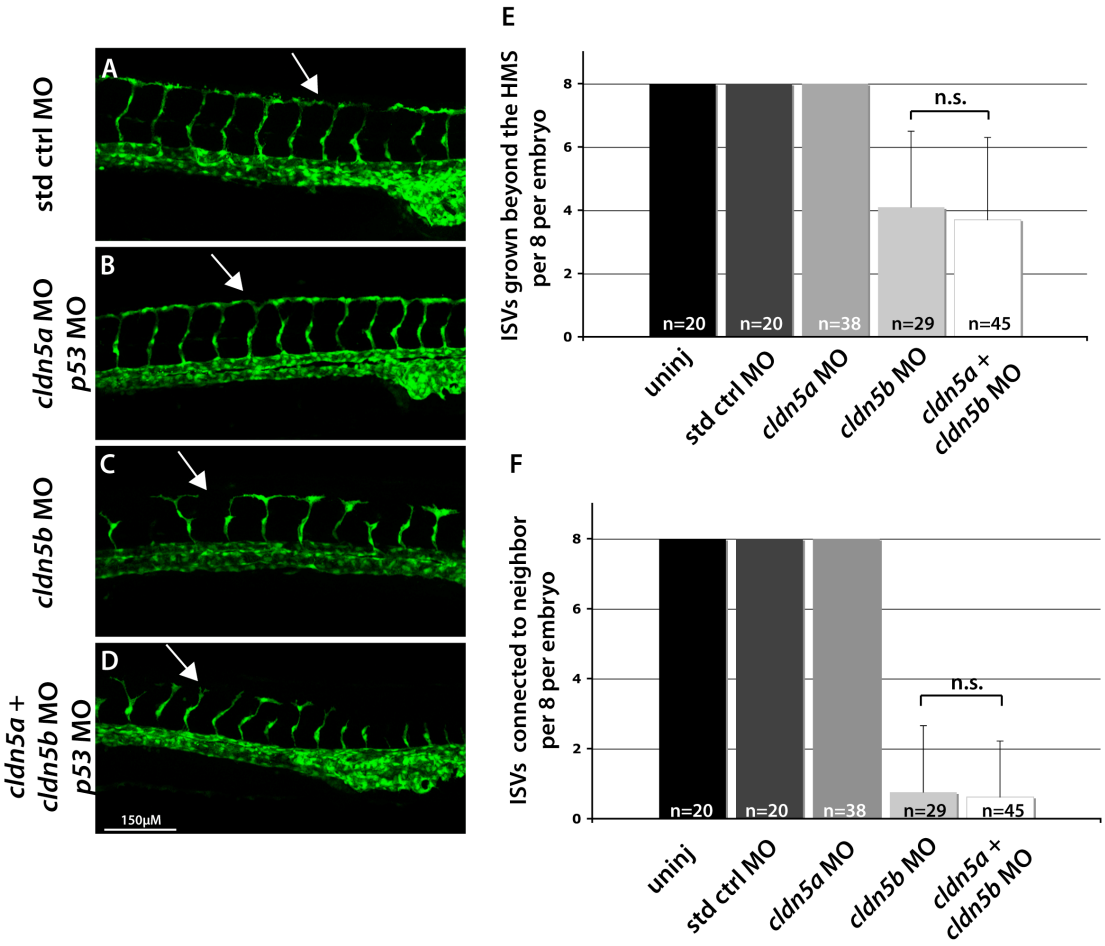

Figure 21: Non-redundant functions of *cldn5b* and *cldn5a* in ISV formation. (A-D) Confocal images of *fli1a*:EGFP expressing 30hpf old fish injected with *cldn5b*, *cldn5a* or both MOs, respectively. Compared to control MO injected animals (A), *cldn5b* MO injection causes vessels to halt from the notochord onwards (C). Knock-down of *cldn5a* does not result in any ISV morphology phenotype (C). Knock-down of both *cldn5b* and *cldn5a* at the same time causes the same phenotype as in *cldn5b* morphants (D). (E) Quantification of ISVs grown beyond the notochord. (F) Quantification of ISVs connected to neighbor. For both quantifications eight vessels above the yolk extension were counted. Embryo number is indicated in the graphs. Error bars represent SEM. No significant difference for both phenotypes between *cldn5b* and double morphants was observed (n.s.; ANOVA). HMS: horizontal myoseptum.

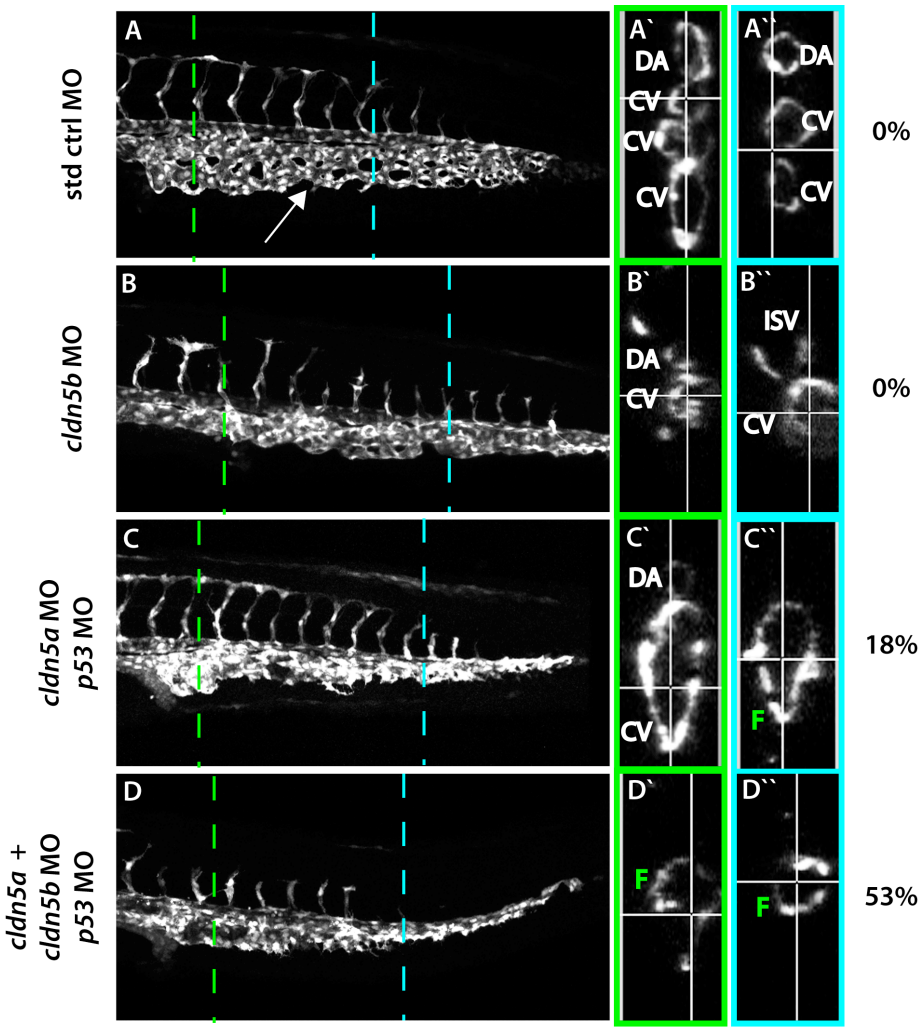

Figure 22: Fusion of CV and DA in *cldn5b/cldn5a* double knock-down. (A-D``) Confocal images of the CV plexus in 30hpf old *fli1a*:EGFP expressing embryos injected with *cldn5b*, *cldn5a* and both MOs. (A`) Transverse section in the anterior part of the CV marked by a green dashed line in A. (A``) Transverse section in the posterior part of the CV marked by a blue dashed line in A. Control morphants show a highly complex network of vessels in the CV (A-A``). *Cldn5b* morphants lack this complexity with only one vessel building the CV (B-B``). In *cldn5a* morphants next to the lack of CV complexity, the DA and CV are not separated in parts of the CV (C-C``). This phenoype is much stronger in *cldn5b* and *cldn5a* MO injected embryos (D-D``). Quantification of fused DA and CV shown right of each panel. CV: caudal vein, DA: dorsal aorta, F: fused DA and CV, ISV: intersegmental vessel.

during ISV formation. However, in the context of CV plexus formation *cldn5b* and *cldn5a* have common functions. The organization of the CV into many loops and the separation of the CV from the DA are processes that require the concomitant functions of *cldn5b* and *cldn5a* functions.

5.5 Normal cellular rearrangement in *cldn5b* morphants

As described above, *cldn5b* knock-down stops ISV outgrowth at the HMS and delays or inhibits fusion of neighboring vessels resulting in the detachment of ISVs from the DA. One reason for this phenotype to occur might be the lack of cellular rearrangement. Furthermore, the expression and localization of other junctional proteins in *cldn5b* morphants might be altered. To test this hypothesis, I analyzed the localization of VE-cad and ZO-1. This is not only a means to study the cell outlines and the hence visualized ISV architecture, but also the expression levels of other junctional proteins (Fig. 23). In std ctrl morphants, VE-cad and ZO-1 are localized in stripes along the axis of the ISV displaying its` multicellular architecture (Fig. 23 A-D). At newly formed connections between neighboring ISVs, a ring of VE-cad and ZO-1 marks the contact area between two contacting cells (asterisk Fig. 23 B). *Cldn5b* MO injected animals, despite showing defects in ISV outgrowth, display a VE-cad and ZO-1 distribution comparable to control embryos (Fig. 23 E-H). The ISVs show single and double lines along the dorso-ventral axis (arrows in Fig. 23 F). Additionally, a ring of junctions can be seen at the contact area between two connecting ISVs (asterisk in Fig. 23 F). These data are in agreement with the fact, that a lumen is formed within the stunted ISVs of *cldn5b* morphants.
Furthermore, the level of expression of both VE-cad and ZO-1 are not altered compared to control embryos (compare Fig. 23 B vs F and C vs G).
These data indicate, that *cldn5b* does not influence cellular rearrangement in the ISV. It also has no impact on the localization and expression level of VE-cad and ZO-1.

5.6 Expression of Cldn5b:EGFP does not rescue the morphant phenotype

Knock-down of gene functions by MO injection is known to be very specific. However, the risk of non-specific binding of the MO persists. In order to prove the specificity of the phenotype caused by *cldn5b* MO injection, I performed two rescue approaches. One method is the coinjection of MO together with the mRNA encoding the respective gene. The other approach is the endothelial specific expression of a Cldn5b:EGFP fusion construct.

To ensure a proper rescue by *cldn5b* mRNA injection in *cldn5b* morphants, I injected a mRNA that was resistant to the MO. To visualize the successful injection of mRNA, I coinjected *cldn5b* together with *mKate* mRNA. However, the injection of these high concentrations of mRNA caused severe morphological defects in many embryos. Therefore, I injected *mKate* mRNA alone to analyze whether protein expression via the injection of mRNA is possible in my hands (Fig. 24 A-D``). The injection of *mKate* mRNA into one cell stage embryos, leads to a weak expression of *mKate* protein in the stages of 80% epiboly and 24hpf of embryogenesis (Fig. 24 A, C`-C``). In contrast, the injection of the control *cldn5b* mRNA does not cause any fluorescent signal in the living embryo (Fig. 24 B, arrow in D`-D``). These data show that it is possible with the protocols I used to ubiquitously express a protein via mRNA injections. Therefore, I used the same parameters to express *cldn5b* mRNA alone (Fig. 24 E-G). I injected *cldn5b* mRNA into one cell stage embryos and stained for Cldn5 protein in 24 hpf old embryos. In uninjected embryos, Cldn5 antibody staining is seen in the vasculature as well as in the neural tube (Cldn5b panel, Fig. 24 E). In the vasculature it colocalizes with VE-cad (VE-cad and merge panel in Fig. 24 E, E). The injection of *cldn5b* mRNA into wildtype embryos shows the same expression pattern with no obvious increase in expression level compared to uninjected embryos (compare arrows in green panel of Fig. 24 F vs E). The coinjection of *cldn5b* mRNA together with the MO did not show any enhancement of Cldn5 protein expression, either (compare arrows green panel of Fig. 24 G vs E). In these embryos, the phenotype caused by *cldn5b* MO injection was not rescued (Fig.

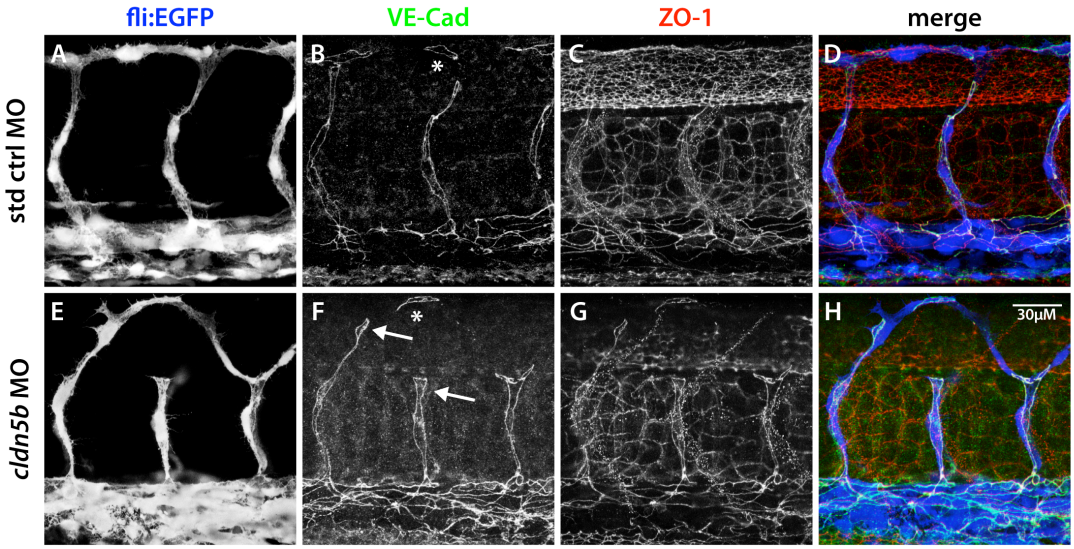

Figure 23: *Cldn5b* does not influence rearrangement in ISVs. (A-H) Immuno-histochemical staining for VE-cad (B, F; green) and ZO-1 (C, D; red) in 30hpf *fli1a*:EGFP (A, E, blue) expressing embryos injected with std ctrl (A-D) or *cldn5b* MO (E-H). In *cldn5b* morphants VE-cad and ZO-1 localize to junction-like lines along the axis of the ISV like in control morphants (arrows F, G vs B, C). Also new connections between ISVs resemble junctional rings (compare asterisks in F vs B).

24 G; data not shown). In summary, the injection of *cldn5b* mRNA does not induce the expression of Cldn5b protein and does not rescue the morphant phenotype.

In the second rescue approach I wanted to express a Cldn5b:EGFP fusion construct in the endothelial cells of *cldn5b* morphants using the Gal4/UAS system. Thus, I generated a transgenic UAS:cldn5b:EGFP line (Appendix 9.3) and crossed it to the driver line *fli1ep*:Gal4ff (this study, Appendix 9.1) leading to the expression of Cldn5b:EGFP in all ECs of the progeny. The *fli1ep*:Gal4ff line also harbors a UAS:mRFP construct for the concomitant visualization of the cytoplasm in endothelial cells. For the analysis of the potential rescue ability of the Cldn5b:EGFP fusion protein, I compared control embryos with *cldn5b* MO injected embryos in Cdln5b:EGFP expressing and non-expressing fish (Fig. 25). In control embryos the expression of the Cldn5b:EGFP fusion protein did not cause any ISV formation defect (compare Fig. 25 E-H vs A-D and M-P vs I-L). The injection of *cldn5b* MO causes an ISV outgrowth and connection phenotype, which cannot be rescued with the specific Cldn5b:EGFP expression in ECs (compare Fig. 25 Q-T vs U-X). To evaluate the rescue ability of the Cldn5b:EGFP fusion protein in further detail, I quantified the number of ISVs connecting to neighboring ISVs (Fig. 26). In control embryos 100% of the ISVs are connected within the DLAV (8/8) in Cldn5b:EGFP expressing (wt: n=88; std ctrl MO: n=72 vessels) and non-expressing embryos (wt: n= 72; std ctrl MO: n= 48 vessels). In contrast, embryos injected with *cldn5b* MO and not expressing the fusion construct present only 2 connections within the DLAV (2/8 connections; n= 96 vessels). The siblings expressing Cldn5b:EGFP do show a slight increase in vessel connections (3.5/8 connections; n= 152 vessels), this is however not significantly different to non-expressing embryos (Fig. 26).

In summary, the expression of the UAS:cldn5b:EGFP fusion construct does not rescue the *cldn5b* MO induced phenotype.

Figure 24: Insufficient expression of Cldn5b protein by mRNA injection. (A-D``) Expression of mKate protein in *fli1a*:EGFP expressing living embryos after *mKate* mRNA injection (A, C) compared to control *cldn5b* mRNA injected embryos (B, D) at 80% epiboly (A, B) and 24hpf (C, D) respectively. Upon injection of *mKate* mRNA, a red fluorescent signal can be observed (A, C`) compared to the absent fluorescent signal upon *cldn5b* mRNA injection (B, D`). (E-G) Immunohistochemical stainings for VE-cadherin and Cldn5 in uninjected (E), *cldn5b* mRNA injected (F) and *cldn5b* mRNA and MO injected embryos (G). The injection of *cldn5b* mRNA does not lead to the expression of Cldn5b protein (compare arrows in E vs F and G).

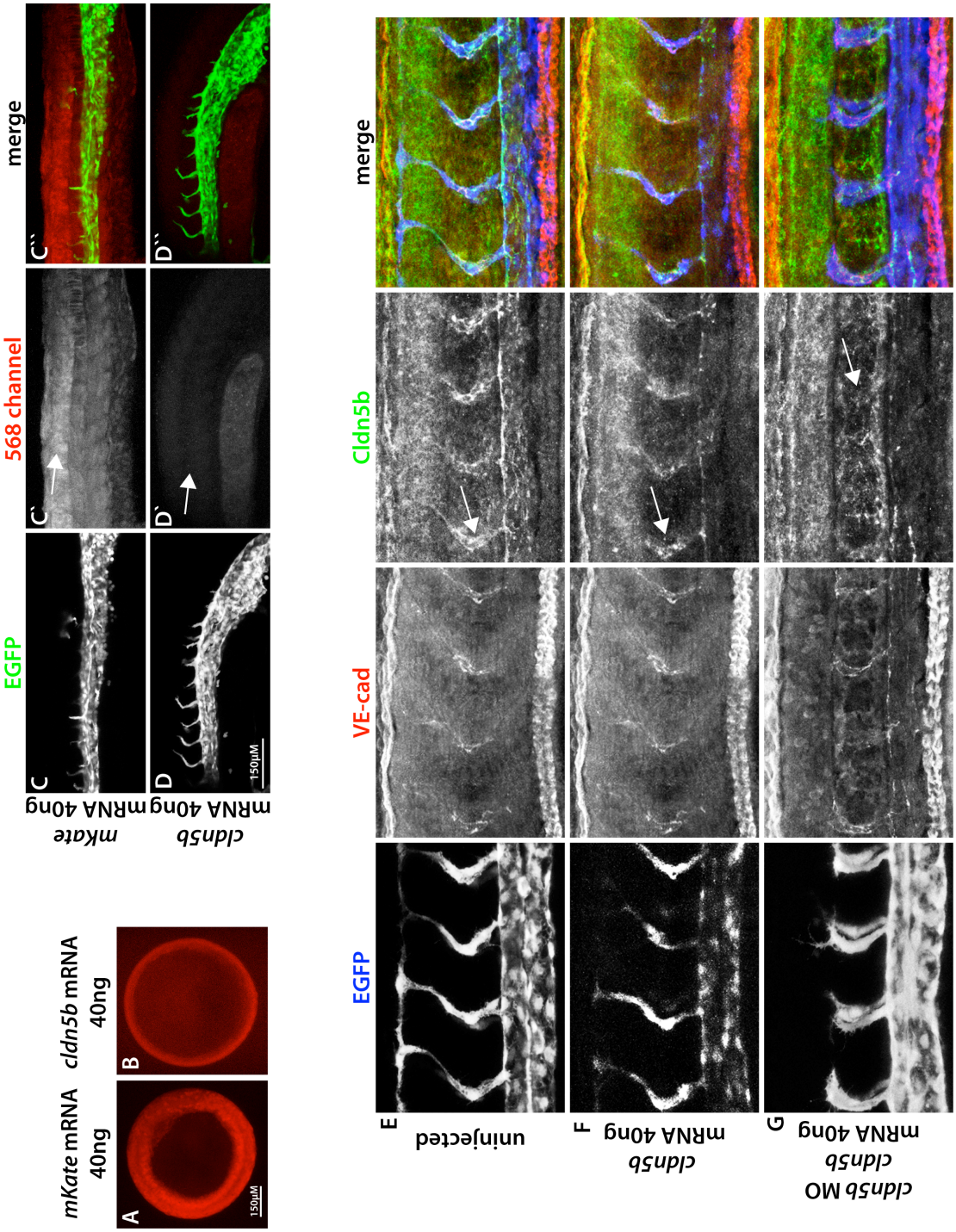
EGFP
VE-cad
Cldn5b
merge
E uninjected
F cldn5b mRNA 40ng
G cldn5b MO cldn5b mRNA 40ng
EGFP
568 channel
merge
C cldn5b mRNA 40ng
D mKate mRNA 40ng
150µM
A mKate mRNA 40ng
B cldn5b mRNA 40ng
150µM

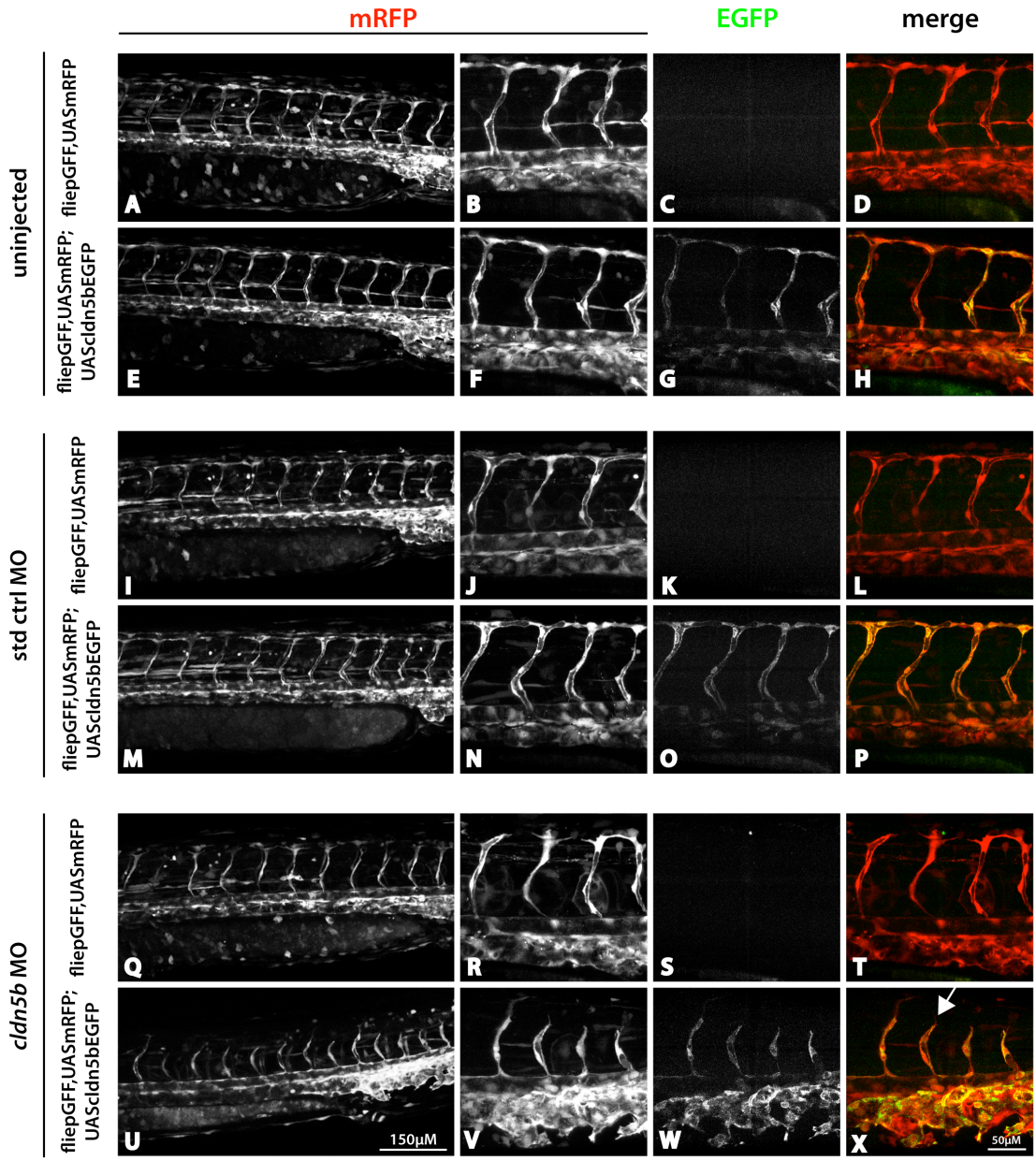

Figure 25: Expression of a Cldn5b:EGFP fusion does not rescue the *cldn5b* morphant phenotype. (A-X) Comparison of uninjected, std ctrl MO and *cldn5b* MO injected 36hpf old embryos transgenic for *fliep*:Gal4ff;UAS:mRFP (A-D, I-L, Q-T) and for *fliep*:Gal4ff;UAS:mRFP (red); UAS:*cldn5b*EGFP (green) (E-H, M-P, U-X). Embryos expressing UAS:*cldn5b*:EGFP do not show any ISV formation phenotype compared to non-expressing embryos in control embryos (compare E-H vs A-D; M-P vs I-L). *Cdln5b* MO injection causes vessels to halt or not connect to neighboring ISVs (Q, R, T). This phenotype cannot be rescued by the expression of Cldn5b:EGFP (U-X; arrow in X).

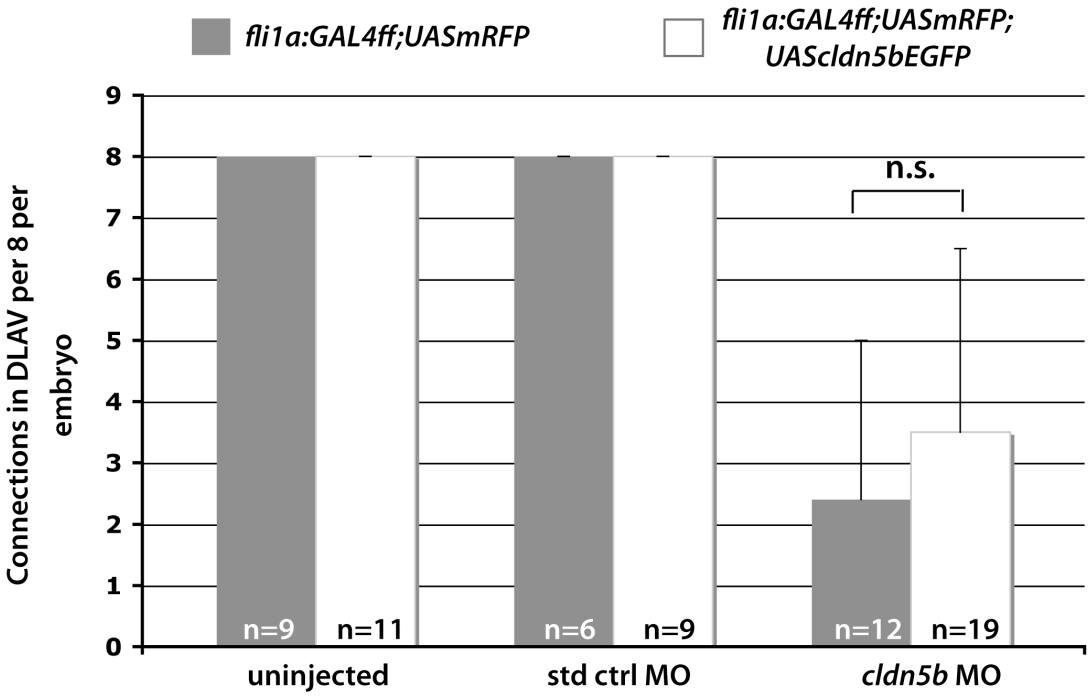

Figure 26: Fail to make connections in DLAV in *cldn5b* morphants cannot be rescued by the expression of Cldn5b:EGFP. Quantitative analysis of DLAV connections in uninjected, std ctrl MO and *cldn5b* MO injected embryos; comparison between UAS:*cldn5b*:EGFP expressing and non-expression 36hpf embryos. The expression of Cldn5b:EGFP does not alter ISV formation in control embryos. Upon injection of *cldn5b* MO ISVs do not connect to neighbors. The expression of Cldn5b:EGFP does not rescue this phenotype. Differences are not specific (n.s.; ANOVA).

5.7 Reduced cell number and cell proliferation in *cldn5b* morphants – a cause for ISV formation defects?

During the analysis of ISV formation in *cldn5b* morphants I observed a decrease in cell number compared to control embryos. To investigate this phenotype in more detail I generated a transgenic line for *fli1ep*:nlsmCherry expressing a nuclear version of mCherry in all ECs (Appendix 9.2). Using this transgenic line I compared the number of nuclei in ISVs between uninjected, ctrl MO and *cldn5b* MO injected embryos (Fig. 27 A-C, D) by counting the nuclei in 8 vessels above the yolk extension. Uninjected and ctrl MO injected embryos revealed an average number of 5.7 nuclei per ISV at 56hpf (uninj.: 5.7 +/- 1 nuclei, n=53 vessels; std ctrl MO: 5.7 +/- 0.76 nuclei, n=56; Fig. 27 A, B, D). This number was ranging from 3 to 6 nuclei per ISV with 29% containing 3 nuclei and 43% containing 6 nuclei per ISV (Fig. 27 E). In contrast, in *cldn5b* morphants the cell number per ISV is significantly altered. Here, embryos harbor on average only 4.1 nuclei per ISV (4.1 +/- 0.79 nuclei, n= 102 vessels; Fig. 27 C, D). The nuclei number in these morphants ranges from 0 to 5 with the majority of 50% of the ISVs harboring 2 nuclei (purple asterisks in Fig. 27 C, E). Taken together, *cldn5b* morphants clearly show a reduced cell number in the ISVs, the majority of which contains 2 nuclei only.

The reduction in cell number can have different causes. Either cell proliferation is decreased or less cells migrate into the ISV or both events happen simultaneously. In order to study the cause for the reduced cell number, I performed time-lapse analysis on *fli1a*:moesin-EGFP; *fli1ep*:nls-mCherry expressing uninjected and MO injected fish (Fig. 28). In these movies the cell nuclei entering and dividing within the ISV were analyzed and quantified by marking every red nucleus employing the manual tracking function of ImageJ (Fig. 28 A`, B`, C). In uninjected embryos (Suppl. movie 13 and movie 14) between 3 and 4 cells enter the ISVs from the DA on average (3.5 +/- 1.22 nuclei; n=6 ISVs). Of these 3-4 cells, roughly one cell divides within the ISV (1.2 +/- 1 divisions, n=6 ISVs, Fig. 28 C). In *cldn5b* MO injected embryos (Suppl. movie 15 and movie 16) a significant

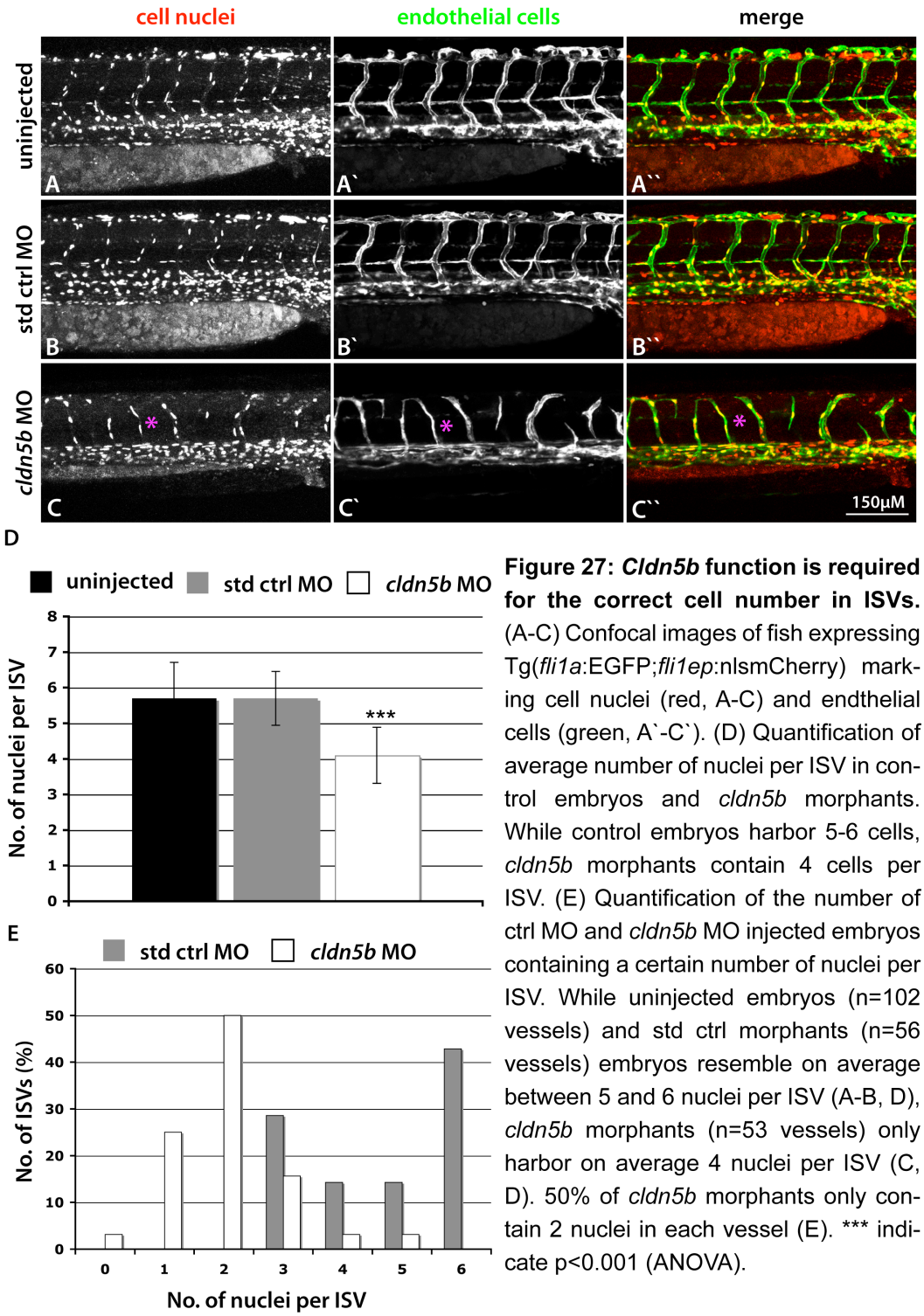

Figure 27: *Cldn5b* function is required for the correct cell number in ISVs. (A-C) Confocal images of fish expressing Tg(*fli1a*:EGFP;*fli1ep*:nlsmCherry) marking cell nuclei (red, A-C) and endthelial cells (green, A`-C`). (D) Quantification of average number of nuclei per ISV in control embryos and *cldn5b* morphants. While control embryos harbor 5-6 cells, *cldn5b* morphants contain 4 cells per ISV. (E) Quantification of the number of ctrl MO and *cldn5b* MO injected embryos containing a certain number of nuclei per ISV. While uninjected embryos (n=102 vessels) and std ctrl morphants (n=56 vessels) embryos resemble on average between 5 and 6 nuclei per ISV (A-B, D), *cldn5b* morphants (n=53 vessels) only harbor on average 4 nuclei per ISV (C, D). 50% of *cldn5b* morphants only contain 2 nuclei in each vessel (E). *** indicate p<0.001 (ANOVA).

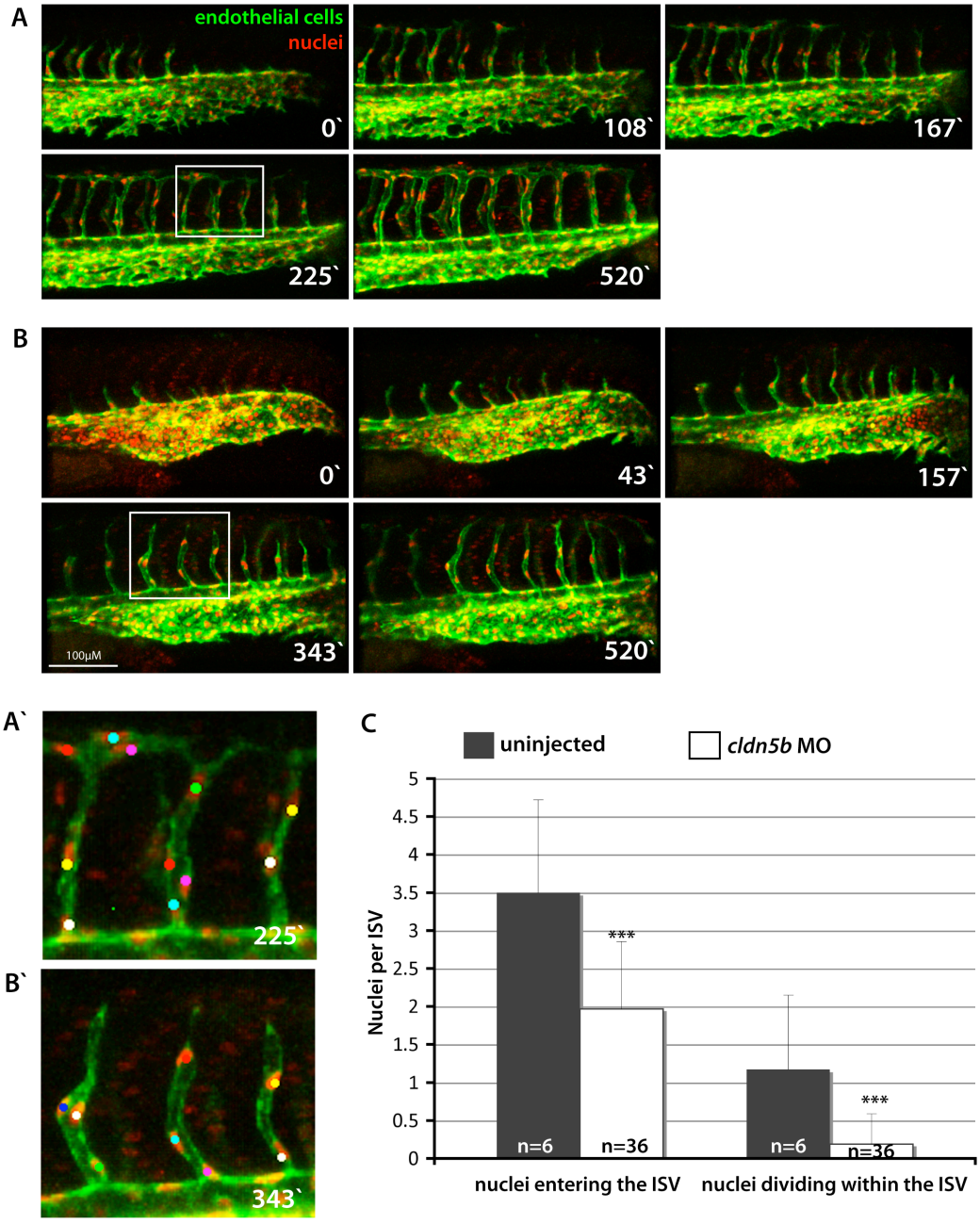

Fig. 28: Less cells proliferate in and enter the ISV in *cldn5b* morphants. Still pictures of confocal time-lapse movies of *fli1a*:moesin:EGFP;*fli1a*:nlsmCherry expressing embryos. Uninjected embryos (A, Suppl. movie 13), *cldn5b* MO injected (B, Suppl movie 15). Start of movie: 24hpf; end of movie: 32.6hpf. (A`-B`) Close-up view of box in A and B. Nuclei were counted by marking with the manuel tracking function (ImageJ) (see dots; Suppl. movie 14, 16). (C) Quantification of cell nuclei entering and dividing within the ISVs. In *cldn5b* morphants less cells enter the ISV than in wildtype embryos (2 vs 3.5) and less cell proliferate within the ISVs (0.2 vs 1.2). *** indicate $p<0.001$ (ANOVA).

decrease of cells entering can be observed (2 +/- 0.9 cell nuclei, n=36 ISVs) of which almost no cell divides within the ISV (0.2 +/- 0.4 divisions, n=36 ISVs; Fig. 28 C).

It should be noted that the total numbers of cell nuclei within an ISV vary between experiments (Fig. 27 vs Fig. 28). The total numbers in Fig. 27 were obtained in the trunk. The movies of Fig. 28 were taken in the tail region at a stage when major morphology changes do not occur anymore allowing for easier time-lapse analysis.

Taken together, *cldn5b* morphants show a reduced number of cells per ISV resulting from less cells entering and dividing within the ISV.

5.8 VE-cadherin is necessary for cell rearrangement during ISV formation

In the previous chapters I have shown the functional analysis of the tight junction protein Cldn5b during angiogenesis. It is required for the ISV outgrowth, fusion to neighboring vessels and the connection to the DA. This indicates that normal tight junction function is required for ISV formation and maintenance. Tight junction proteins are not the only ones mediating cell-cell contacts. Adherens junctions are known for the initial contact formation between cells and the maintenance of this contact. To study the role of AJs during the process of angiogenesis I looked at the function of the EC-specific VE-cad. Therefor, I used MO knock-down approaches as well as a mutant lacking *VE-cad* function (generated in the lab, Heinz-Georg Belting, unpublished). The effects of the *VE-cad* knock-out were analyzed by performing time-lapse analysis on wildtype and homozygous mutant animals expressing *fli1a*:EGFP (Fig. 29). In wildtype embryos (Suppl. movie 17) the ISVs grow dorsally, connect to their neighboring ISVs and eventually form the final network of vessels (Fig. 29 A-G). On the other hand, in *VE-cad* mutants (Suppl. movie 18) the initial outgrowth of cells occurs normal (arrows in Fig. 29 H). With further progression of ISV formation, connections that have been made between the ISVs and the DLAV become very thin and

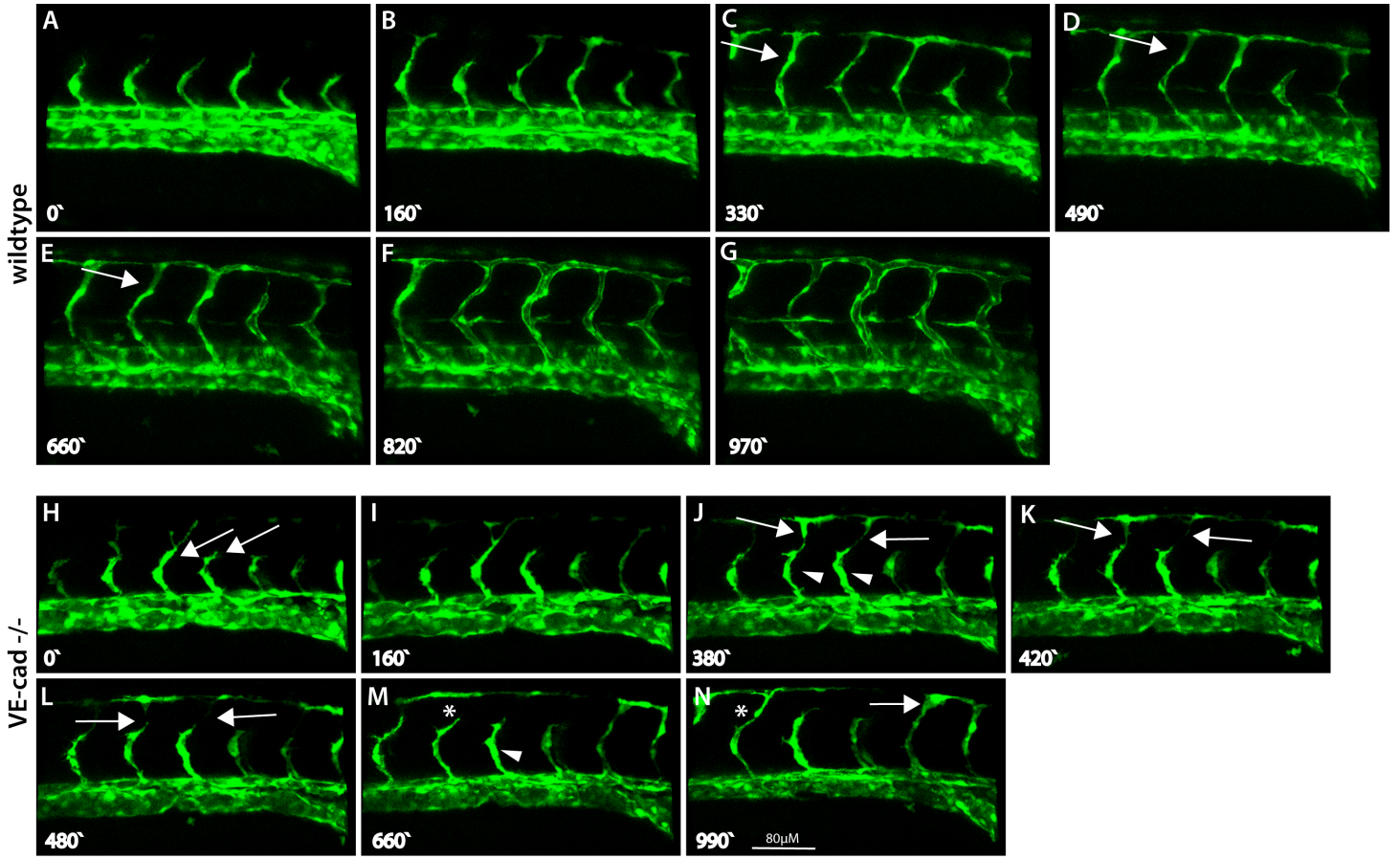

Figure 29: VE-cadherin is necessary for EC rearrangement in angiogenesis. Still pictures of time-lapse movies in wildtype (A-G; Suppl. movie 17) and homozygous *VE-cadherin* mutants (H-N; Suppl. movie18) expressing *fli1a*:EGFP. Start of movie 24hpf. Compared to wildtype embryos, *VE-cad* mutants develop thin connections between the ISV and DLAV (arrows J) that break off (K, L). These however partially reconnect to the DLAV (asterisks M, N). The mutants show accumulation of ECs in the ventral part of ISVs (arrowheads J, M).

disrupt (see arrows in Fig. 29 J-L). In some vessels these connections are reestablished (asterisks Fig. 29 M, N). Interestingly, it seems that many cells accumulate at the ventral part of the ISV (arrowhead in Fig. 29 J, M). Indeed, further experiments in which cell nuclei and junctional proteins were marked show a concentration of stalk cells in the ventral part of the ISV (personal communication, Heinz-Georg Belting). Furthermore, over time the dorsal part of the ISV flattens consisting only of one cell (arrowhead Fig. 29 N, also see arrows Fig. 30 C, personal communication, Heinz-Georg Belting). These data indicate a role for VE-cad in the rearrangement of ECs to form the final architecture of the ISV.

5.8.1 *VE-cadherin* and *Claudin5* function non-redundantly during ISV formation

The analysis of *cldn5b* morphant embryos indicates that *cldn5b* is important for vessel outgrowth and vessel stability in the ventral part of the ISV. *VE-cad* however is necessary for the rearrangement of cells and vessel stability in the dorsal part of the ISV. Adherens junctions are know to be required for the expression and proper localization of tight junction components (St Johnston and Ahringer; Taddei et al., 2008). To study a putative functional relationship between AJ and TJ, I injected *VE-cad* and *cldn5b* MO into *fli1a*:EGFP expressing embryos (Fig. 30). In this experiment I kept the *VE-cad* MO concentration constant and used an increasing concentration of *cldn5b* MO. This experiment was performed shortly before the mutant was generated and characterized. VE-cad morphants show a phenotype similar to VE-cad mutants, albeit a bit milder (H.-G. B., personal communication). Compared to uninjected and std ctrl MO injected embryos at 48hpf, *VE-cad* MO injected fish show very thin connections within the DLAV (compare red arrow in Fig. 30 C vs 30 A, B). Furthermore, the dorsal part of the ISV appears flattened compared to control embryos (compare red arrowheads Fig. 30 C vs 30 A, B). Double morphants show phenotypic defects characteristic for the knock-out of *VE-cad* and *cldn5b*. The VE-cad phenotype was not enhanced by the increased *cldn5b* MO injection. In addition these embryos show a detachment

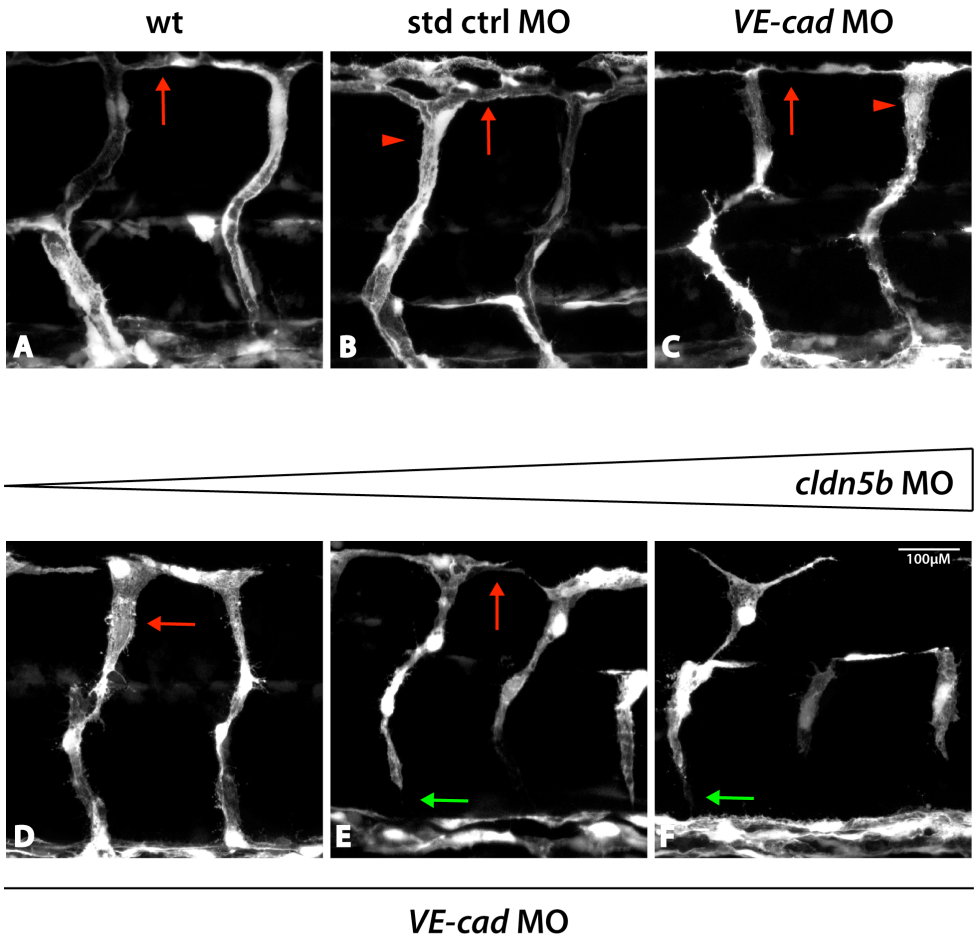

Figure 30: *VE-cadherin* and *cldn5b* act differently in ISV fomation. (A-F) Confocal images of 48hpf old *fli1a*:EGFP expressing fish injected with *VE-cad* MO and increasing concentrations of *cldn5b* MO. Knock-down of VE-cad leads thin connections in the DLAV and flattening of the dorsal ISV (0.2 mM MO concentration; C). Coinjection of *cldn5b* MO does not enhance this phenotype with any concnetration used (MO concentration 0.1, 0.2, 0.4 mM); additionally, the detachment of ISVs from the DA can be observed (E,F).

of ISVs from the DA, a phenotype caused by the knock-down of *cldn5b* alone (green arrows, Fig. 30 E, F; compare to Fig. 19). These analyses strongly suggest that VE-cad and Cldn5b control different steps in ISV development independently and function non-redundantly in this context.

5.8.2 VE-cadherin does not influence Cldn5 expression and localization *in vivo*

Although it appears that *VE-cad* and *cldn5b* have different functions during primary vessel formation, it has been shown in endothelial cell culture that *VE-cad* blocks the transcriptional repression of the *cldn5* locus in a β-catenin/FoxO1/TCF4-dependent manner (Taddei et al., 2008), suggesting a tight linking of expression of Cldn5 and VE-cad *in vitro*. Whether VE-cad displays a similar function on Cldn5b expression *in vivo*, was analyzed by studying the expression and localization of Cldn5b protein in animals deficient for VE-cad (Fig. 31). In wildtype and heterozygous animals VE-cad expression is clearly visible in ISVs in a junctional pattern (arrows in Fig. 31 B, F). As expected homozygous VE-cad mutants lack VE-cad protein and display the ISV phenotype as described in Fig. 29. Cldn5 protein is found in the DA and ISVs in all genetic backgrounds at a comparable level to wildtype levels (compare arrows in Fig. 31 C, G, K). Furthermore, Cldn5 protein clearly localizes at cell junctions throughout individual ISVs as has been described in Fig. 11. Even in VE-cad deficient ISVs showing thin extensions and connection between two cells, Cdln5 is visible at these contact points (arrowheads in Fig. 31 K). Please note, that all genotypes were subsequently verified by PCR and restriction analysis. In summary, VE-cad does not influence the expression and localization of Cldn5 protein *in vivo*.

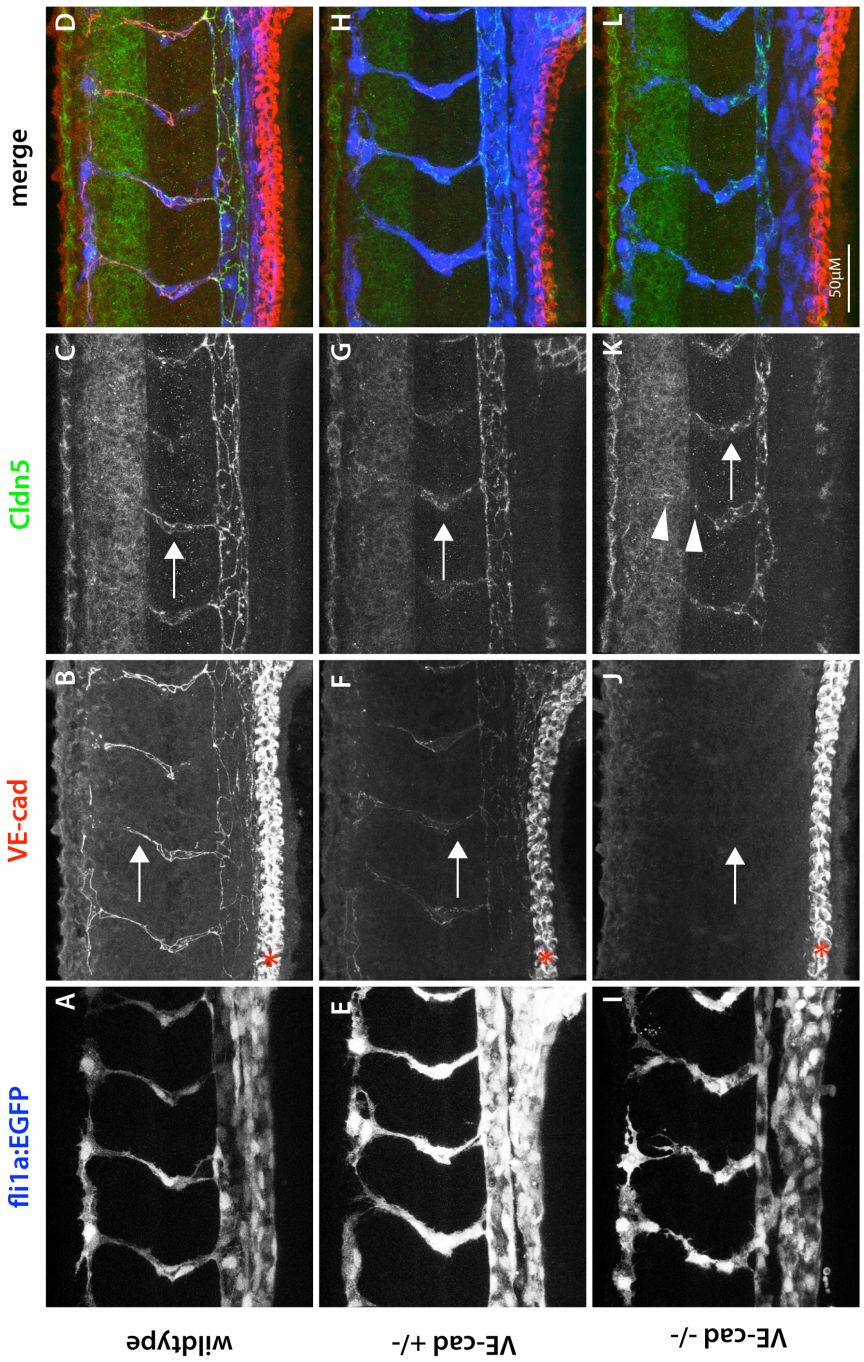

Figure 31: VE-cad does not influence Cldn5 protein expression. (A-L) Confocal images of immunohistochemical stainings for VE-cad and Cldn5 on 30hpf old *fli1a*:EGFP expressing embryos. Homozygous VE-cadherin mutants lack VE-cad protein expression (compare J vs B, F). Cldn5 protein expression is found in comparable levels in all genetic backgrounds (compare C, G, K). * unspecific VE-Cad staining in the pronephric duct.

5.9 Generation and analysis of a *cldn5b* mutant

While injection of cldn5b anti-sense morpholinos generated vascular specific defects in the zebrafish embryos, rescue of the phenotype by RNA or DNA injections proved to be difficult. Therefore, I cannot exclude that the observed morphant phenotypes are due to off-target effects (see discussion). Therefore, to analyze cldn5b function at the genetic level, I generated a genomic mutant fish line using the Zinc-Finger Nuclease (ZFN) system (Doyon et al., 2008; Ekker, 2008; Meng et al., 2008). This Zinc-Finger is a hybrid protein consisting of the Zinc-Finger domain as well as the FokI Nuclease. The ZFN is designed as an obligate heterodimer, each monomer contains 3 zincfinger modules and one half of the FokI nuclease domain. Heterodimerization of these monomers generates an active endonuclease with a DNA recognition sequence of 28 nucleotides on each side of the nuclease domain. The size of this recognition sequence ensures very rare restriction events – ideally the target size exists only once in the zebrafish genome. The double-strand break in the DNA generated by the ZFN is repaired by error-prone non-homologous end-joining. This leads to the generation of deletions or insertions.

The *cldn5b* transcript consists of one exon of 654bp containing the entire open reading frame. Therefore, the Zinc-Finger Nuclease was designed to cut close to the start codon (Fig. 32). I tested the knock-out ability of the ZFN by transiently expressing the nuclease in embryos by mRNA injection and performing PCR analysis on the genomic DNA of 1-2 day old embyos. Sequence analysis revealed a HinfI restriction site in immediate proximity of the ZFN cutting site. Therefore a potential mutation in this region may generate a restriction enzyme polymorphism presenting the HinfI site (Fig. 32 A). A PCR on the region of interest and the subsequent digestion of the PCR product with HinfI uncovered a mutation within the *cldn5b* locus. While the PCR product generated on DNA from uninjected embryos could be digested with HinfI, the PCR product from ZFN injected embryos could only partially be digested. Sequencing of the non-digestable PCR product revealed a 2bp

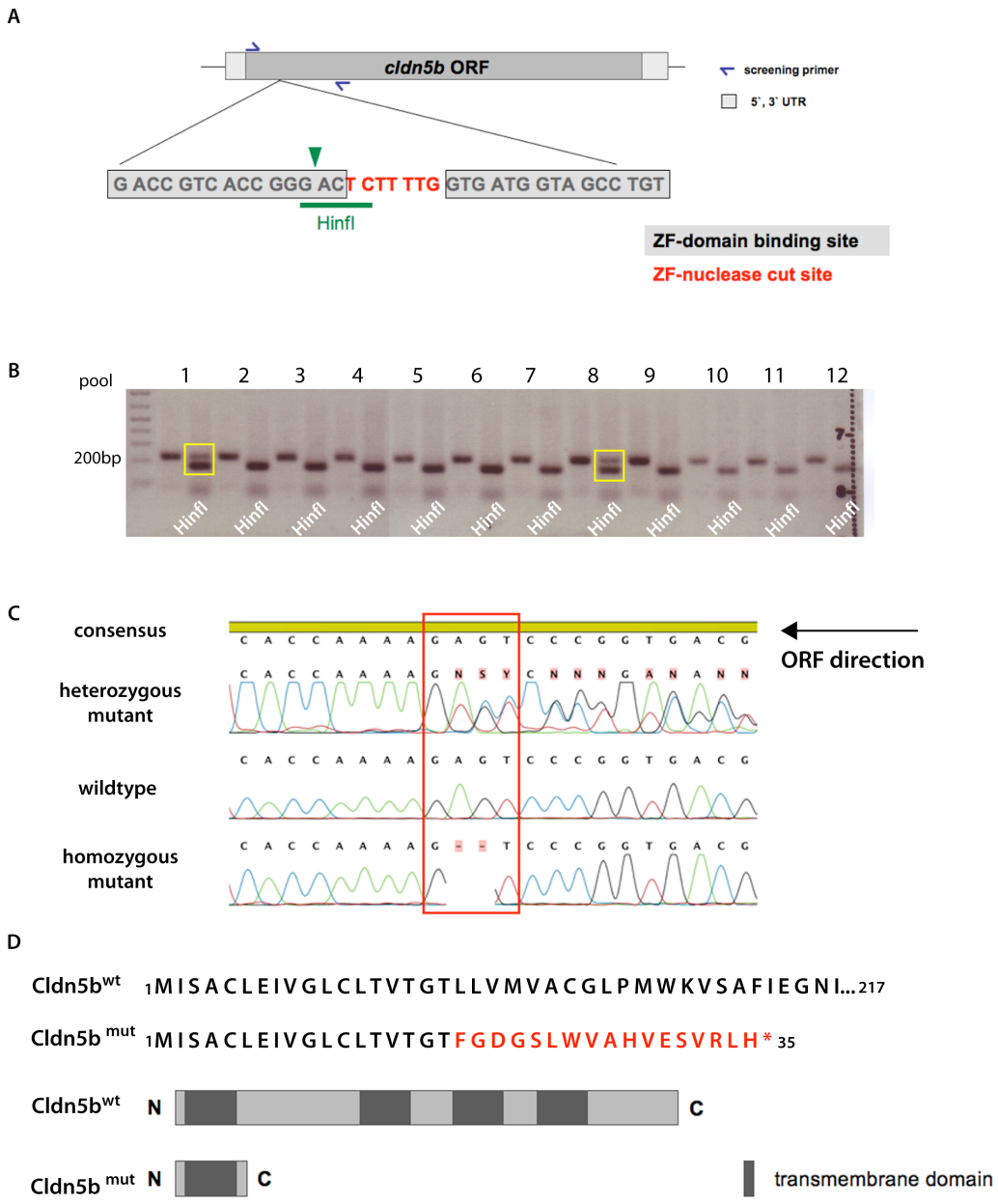

Figure 32: Generation of a *cldn5b* mutant. (A) Binding and cut site of the Zinc-Finger Nuclease (ZFN) in the *cldn5b* ORF. A potential mutation can be found by the restriction enzyme polymorphism of HinfI. (B) Pools of genomic DNA were used for PCR amplifying the region of interest and subsequently digest with HinfI. Undigested bands reveal a mutation in the sequence tested. (C) Positively screened fish harbored a 2bp deletion compared to the wildtype sequence. (D) This deletion leads to a frameshift in the DNA sequence and therefore a premature stop in the protein resulting in a truncated version of the protein.

deletion within the cut site of the ZFN. Therefore, the ZFN is effective in generating mutations in the *cldn5b* locus *in vivo*.

To isolate a mutation in the germline, I injected ZFN mRNA into embryos and raised them to adulthood. The offspring of this G_0 fish was analyzed for a HinfI polymorphism as described above (for a detailed protocol please see 4.3.15). In total 80 embryos per G_0 fish were pooled to groups of 5 and analyzed for the absence/presence of HinfI restriction. Out of 24 screened adult fish, 4 showed a mutation in the offspring and therefore carried germ cells with a mutation in *cldn5b* (example of restriction enzyme digestion in Fig. 32 B). All embryos derived from these 4 G_0 fish carried the same 2bp deletion (Fig. 32 C). At the transcript level this deletion leads to a frameshift and a premature translational stop at aa35 (Fig. 32 D). This stop codon is located within the region coding for the first transmembrane domain of the protein. This should lead to the formation of a truncated Cldn5b protein lacking all but the first transmembrane domain (Fig. 32 D).

Progeny of the identified G_0 fish were raised to adulthood and screened for the *cldn5b* mutation by performing PCR/restriction analysis on genomic DNA derived from fin clip biopsies (also see protocol in 4.3.15). Individual fish containing the HinfI polymorphism were used to generate a mutant fish line for *cldn5b*.

In summary, the Zinc-Finger Nuclease system was used to generate a mutations in *cldn5b* in zebrafish. 4 independently isolated alleles showed an identical 2bp deletion in the 5` region of the *cldn5b* ORF leading to the generation of a premature stop, which ablates 84% of the protein.

5.9.1 Efficient knock-out in *cldn5b* mutants

To verify the *cldn5b* knock-out, I analyzed the Cldn5b protein expression in wildtype, heterozygous and homozygous siblings of *cldn5b* mutants. The mutation in the *cldn5b* gene of these animals should lead to a strongly truncated version of the Cldn5b protein. The anti-human Cldn5 antibody used for this experiment recognizes an epitope at the C-terminus of the protein.

Based on the molecular analysis of the mutation, this epitope should be deleted in *cldn5b* homozygous mutants.

The analysis for *cldn5b* knock-out was performed in mutants expressing *fli1a*:EGFP and injected with the *cldn5a* MO for better visualization of Cldn5b protein only (Fig. 33). In wildtype and *cldn5b*$^{+/ubs11}$ fish, Cldn5b is expressed at the junctions of the ISVs and aorta as described in section 5.2 (arrows in Fig. 33 C, G, D, H). In contrast, in *cldn5b*$^{ubs11/ubs11}$ embryos Cldn5 can not be detected (arrow in Fig. 33 K, L). VE-cad protein, however, is expressed in a similar level in all genetic backgrounds (Fig. 33 B, F, J).

These data indicate, that the knock-out in *cldn5b* mutants effectively abrogates Cldn5b at the protein level.

5.9.2 *Cldn5b* mutant embryos show an overall normal anatomy

To study the general effect of the *cldn5b* knock-out on embryonic development, I analyzed the overall anatomy of *cldn5b* mutants (Fig. 34). Compared to wildtype and *cldn5b*$^{+/ubs11}$ embryos, *cldn5b*$^{ubs11/ubs11}$ reveal an overall indistinguishable anatomy at 24hpf of development (compare Fig. 34 A, B vs C). No gross anatomical defects can be observed in these embryos. They also do not show any developmental delay (Fig. 34 C). Also at 33hpf the overall anatomy of *cldn5b*$^{ubs11/ubs11}$ embryos is similar from *cldn5b*$^{+/ubs11}$ fish (compare Fig. 34 E vs D).

When analyzing the overall anatomy of the *cldn5b* mutant siblings, I found that the majority of embryos within one clutch showed bloodflow in the axial vessels. However, very few embryos were lacking blood flow throughout the body. Most of these embryos were missing blood flow at different time points during development. While some lacked blood flow at 1 dpf, others were missing blood flow at 2 dpf. Interestingly, all of these embryos however regained blood flow within a few hours. From the third dpf onwards, all embryos showed normal blood flow.

To test whether transient defects in blood flow are associated with the mutation in *cldn5b,* I generated short movies of heart beat and blood flow

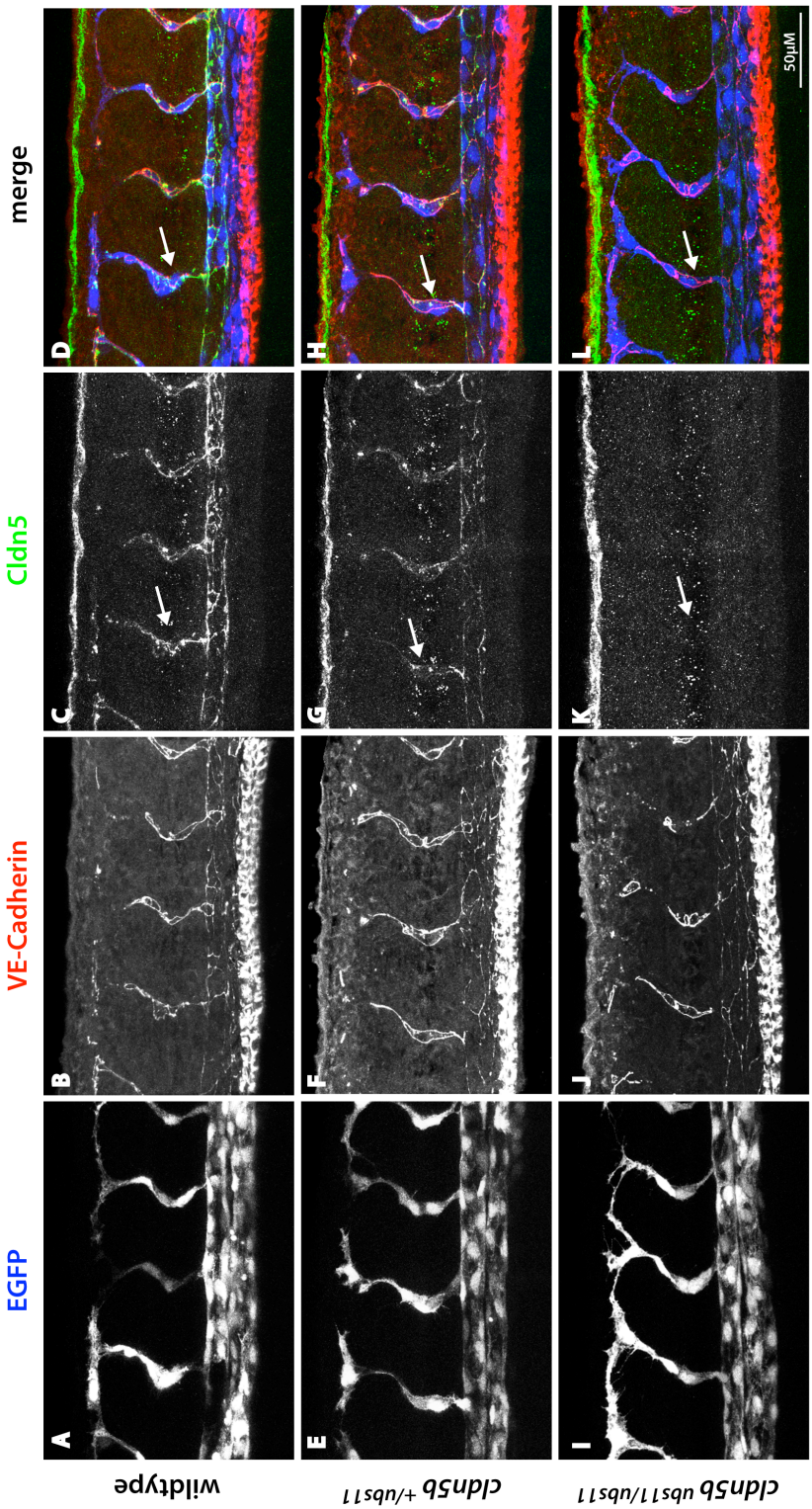

Figure 32: Efficient knock-down in *cldn5b* mutants. (A-L) Confocal images of transgenic Tg(fli1a:eGFP) embryos injected with *cldn5a* MO and stained for VE-cadherin and Cldn5. Wildtype and heterozyous embryos show a clear expression of Cldn5b protein in ISVs and DA (C, G). Homozygous *cldn5b* mutants lack Cldn5b protein expression (K,L). The VE-cadherin expression level however is similar in all genetic backgrounds (B, F, I). Images were taken with the same settings.

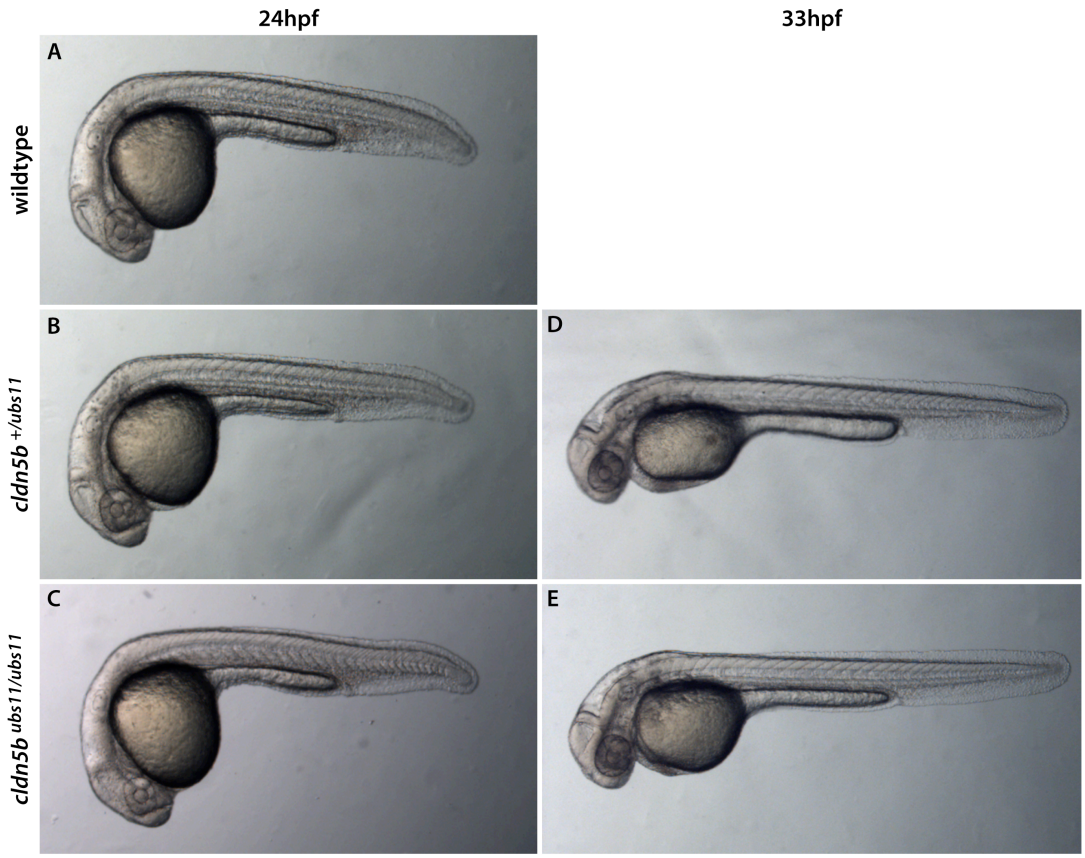

Figure 33: *Cldn5b* mutants do not show obvious anatomical defects. (A-E) Wildtype, heterozygous and homozygous *cldn5b* mutant embryos at 24hpf and 33hpf. Homozygous mutant embryos develop normally compared to heterozygous and wt siblings (compare C vs A, B and E vs D).

under the binocular microscope in *cldn5b* mutant siblings (Suppl. movies 19-29). In most *cldn5b*$^{+/ubs11}$ embryos heart beat and blood flow is clearly visible at 24hpf as well as 33hpf (Suppl. movies 19 – 22). In a few *cldn5b*$^{+/ubs11}$ embryos blood flow was missing though throughout the embryo (data not shown). In one particular example shown in the Suppl. movie 23, the heart beat looked similar to wildtype embryos. In contrast to other cldn5b mutant siblings missing bloodflow, this embryo showed blood flow in the main vessels of the head. Interestingly, the embryo, however, lacked blood flow in the trunk vessels completely (Suppl. movie 24). This was caused by a shunt in the head region where the two LDA merge to one DA. The heart beat and blood flow of the majority of *cldn5b*$^{ubs11/ubs11}$ embryos analyzed resembled that of wildtype animals (Suppl. movie 25 - 27). It should be noted, that *cldn5b*$^{ubs11/ubs11}$ embryos that showed blood flow in the axial vessels, always presented blood flow also in the ISVs at later timepoints comparable to wildtype embryos (data not shown). However, a few *cldn5b*$^{ubs11/ubs11}$ animals were lacking blood flow completely, although the heart was pumping (Suppl. movie 28, 29).

Taken together, most homozygous mutant animals showed blood flow in the axial vessels and ISVs comparable to wildtype embryos. However, very few embryos were missing blood flow over a short period of time.

All embryos of a clutch develop into larval stages. If however, homozygous fish survive until adulthood has to be determined in further experiments.

5.9.3 ISVs develop normally in *cldn5b* mutants

The knock-down of *cldn5b* via MO injections causes strong ISV formation defects with vessels halting during outgrowth, failing to connect to neighbors and detaching from the DA (see chapter 5.3.2). It could be shown for *cldn5b* mutants, that these embryos clearly lack Cldn5b protein expression in the vasculature (see chapter 5.8.1). Therefore, I analyzed the effect of *cldn5b* knock-out on the formation of ISVs. For this, I compared the morphology of ISVs in *fli1a*:EGFP expressing *cldn5b* mutant siblings at different developmental stages (Fig. 35). In wildtype embryos of 30hpf the ISVs have

started to grow in anterior and posterior directions. They have partially built a continuous connection within the DLAV (Fig. 35 A, arrow in Fig. 35 B). *Cldn5b*$^{+/ubs11}$ animals reveal the same ISV pattern as in wildtype embryos (compare Fig. 35 D vs A and arrows in E vs B). To my surprise and in contrast to *cldn5b* knock-down embryos, also the ISVs in *cldn5b*$^{ubs11/ubs11}$ animals have started to ramify anteriorly and posteriorly at the roof of the neural tube (arrows in Fig. 35 H). They also form a partially connected DLAV resembling the morphology of wildtype embryos (compare Fig. 35 G, H vs A, B). At 50hpf the ISVs in wildtype and *cldn5b*$^{+/ubs11}$ embryos have build a fully developed circuit. At this point also the parachordal chain (PAC) is visible (asterisk in Fig. 35 C). Interestingly, embryos homozygous for the *cldn5b* mutation also show a complete circuit of ISVs and DLAVs (Fig. 35 I). They have also developed the PAC vessels at this timepoint (asterisk in Fig. 35 I). This stands in stark contrast to the phenotypes observed in *cldn5b* morphant embryos (compare to Fig. 18).

In summary, *cldn5b* knock-out does not seem to influence the process of angiogenesis in the context of ISV formation.

Also for *cldn5b* mutants the analysis of the dynamics of ISV formation was performed via time-lapse analysis (Fig. 36). In wildtype embryos (Suppl. movie 30) as well as in *cldn5b*$^{+/ubs11}$ animals (Suppl. movie 31) the ISVs have started to grow anteriorly and posteriorly after reaching the roof of the neural tube at 26hpf (Fig. 36 A, F). In contrast, in *cldn5b*$^{ubs11/ubs11}$ animals (Suppl. movie 32) the ISVs have not reached the neural tube roof yet and have partially grown to the level of the HMS only (compare Fig. 36 K vs A, F). When in wildtype and *cldn5b*$^{+/ubs11}$ embryos the ISVs start to connect to neighboring ISVs, in *cldn5b*$^{ubs11/ubs11}$ embryos some ISVs still have not grown further than the HMS (compare arrows Fig. 36 L vs K, compare Fig. 36 L vs B, G). These vessels however do grow further dorsally and start to connect to neighboring ISVs (Fig. 36 M, N). However, not all vessels connect within the DLAV, which is never observed in wildtype and *cldn5b*$^{+/ubs11}$ embryos (arrow Fig. 36 O, compare Fig. 36 O vs E, J). As in wildtype and cldn5b$^{+/ubs11}$ embryos, secondary sprouts emerge and build a PAC (asterisks in Fig. 36 J, O). It should be mentioned that the delay of ISV outgrowth in *cldn5b* mutants cannot be compared to the halting of vessels in *cldn5b* morphants. In the

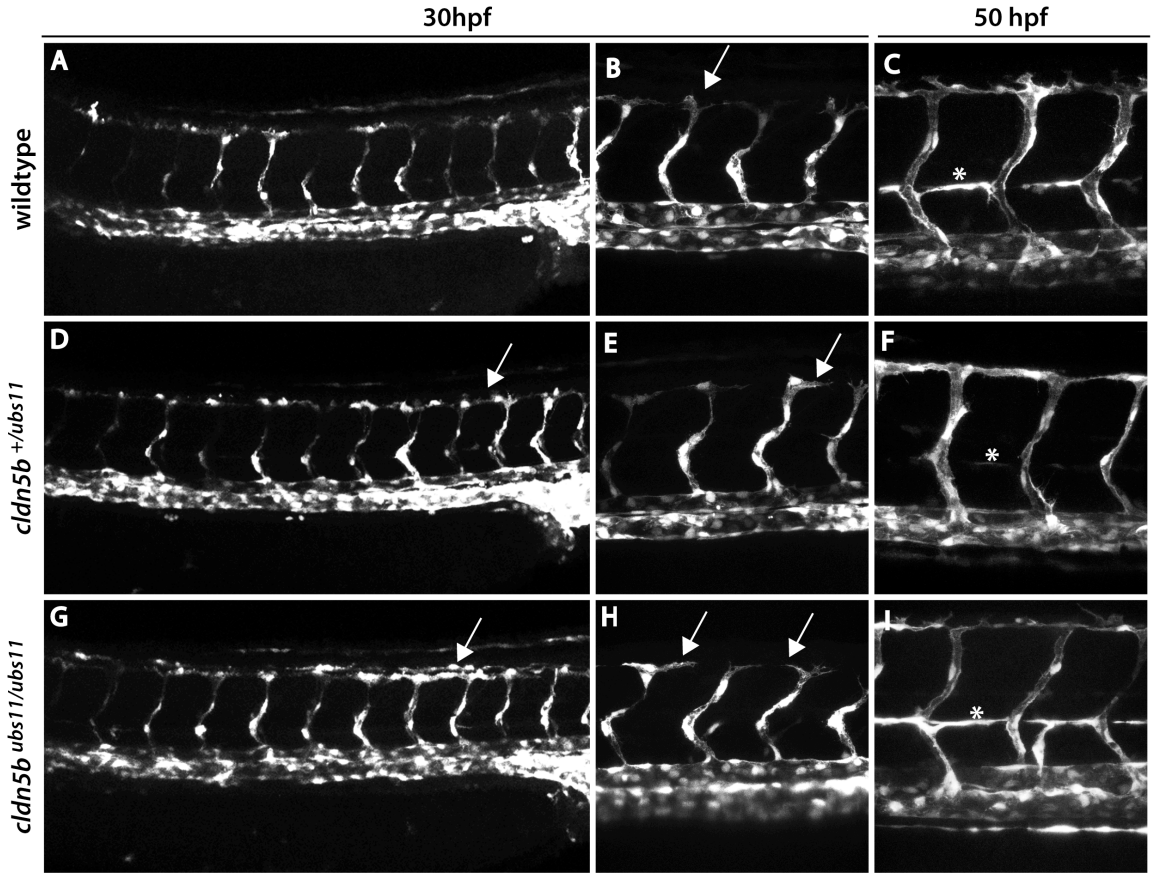

Figure 35: Normal development of ISVs in *cldn5b* mutants. (A-I) C*ldn5b* mutant siblings expressing *fli1a*:EGFP at 30hpf (A, B, D, E, G, H) and 50hpf (C, F, I). Wildtype embryos and heterozygous cldn5b mutants reveal ISVs that started to grow anteriorly and posteriorly above the neural roof and have partially connected to their neighbros at 30 hpf (A, B, D, E). Embryos deficient for *cldn5b* also show a normal development of ISVs (G, H). Also at 50hpf *cldn5b* homozygous mutants show an ISV architecture comparable to wildtype and *cldn5b* heterozygous animals (I vs C, F).*: parachordal chain (PAC).

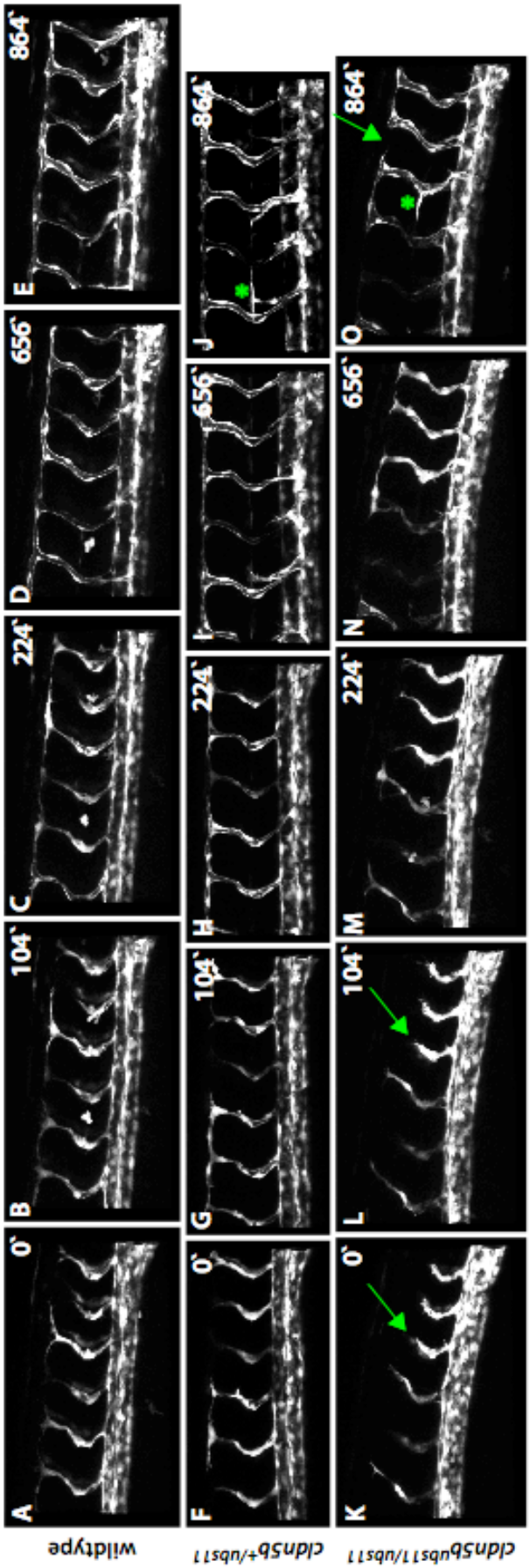

Figure 36: Movies of *cldn5b* mutants reveal a delay in vessel formation. (A-O) Still pictures of time-lapse movies (Suppl. movies 30-32) of *cldn5b* mutant siblings expressing *fli1a*:EGFP starting at 26hpf. (A-J) Formation of ISVs in wildtype and heterozygous *cldn5b* mutant embryos. (K-O) Formation of ISVs in homozygous *cldn5b* mutants. In these animals ISV formation is slowed down, compared to wildtype and heterozgous *cldn5b* mutant siblings (compare A-D, F-J vs K-O). Although some vessels halt at the HMS, they soon grow further dorsally (K-L). Neighboring vessels in the DLAV connect later than in control embryos, of which some ISVs never connect in the DLAV (compare O vs E, J).

latter the ISVs halt for a much longer time than in *cldn5b*$^{ubs11/ubs11}$ embryos. More embryos are needed to be looked at for a statistical evaluation to be made.

5.9.4 *Cldn5b* is not required for the organization of ZO-1

As described above ZO-1 binds to the C-terminus of Cldn proteins. The localization of ZO-1 to tight junctions depends on Cldn proteins in cell culture experiments (Itoh et al., 1999a; McCarthy et al., 2000). To investigate if ZO-1 localization also depends on Claudin 5 *in vivo*, I analyzed the ZO-1 expression in *cldn5b* mutants (Fig. 37). Wildtype and *clnd5b*$^{+/ubs11}$ sibling show ZO-1 localization in a junctional fashion within the ISVs as well as the axial vessels (Fig. 37 A, B). But also *cldn5b*$^{ubs11/ubs11}$ animals resemble a ZO-1 staining that is comparable to wildtype (compare Fig. 37 C vs A). The level of expression does not seem to be altered compared to wildtype siblings. Furthermore, also 50hpf embryos show a distribution and expression level of ZO-1 that is resembling wildtype expression (data not shown). Further analysis on Cldn1 for example might indicate if other tight junction components are altered in expression in *cldn5b* mutant embryos. Also, stainings for VE-cad will give insights into the role of Cldn5b on adherens junction formation in the vasculature.

The ZO-1 expression also gives information about the architecture of the ISVs. In wildtype embryos as well as *cldn5b*$^{+/ubs11}$ animals ZO-1 is expressed in stripes along the axis of the ISVs. Furthermore at 30hpf it localizes to spots and rings within the DLAV. These represent the contact area between two neighboring cells that connect to each other (arrows in Fig. 37 A``, B``). In *cldn5b*$^{ubs11/ubs11}$ mutants lines of ZO-1 expression are also visible in the ISVs. Also the DLAV resembles dots and rings of ZO-1 expression (arrows in Fig. 37 C``). Therefore, the cellular architecture and rearrangement within the ISV and during the formation of the DLAV in *cldn5b* mutants is comparable to wildtype. Further analysis with markers specifically expressed in the vasculature like VE-cad will give further insights into this.

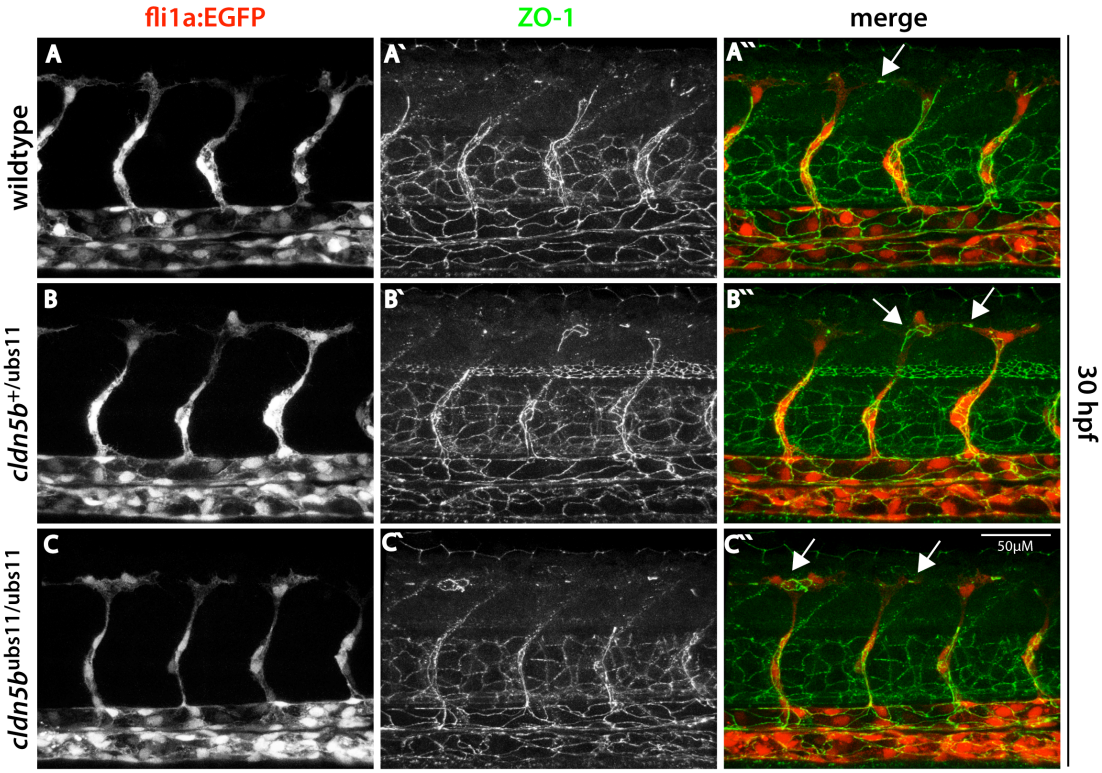

Figure 37: Cldn5b is not required for ZO-1 localization. (A-C) Confocal images of immunohistochemical stainings for ZO-1 (green) in *cldn5b* mutant siblings expressing *fli1a*:EGFP (red). The expression of ZO-1 in homozygous *cldn5b* mutant embryos at 30hpf is comparable to that of wildtype and heterozygous mutant embryos (compare C vs A, B). Images were taken with the same settings.

5.9.5 The *cldn5b* mutant phenotype cannot be enhanced by additional *cldn5b* MO knock-down

As shown above *cldn5b* mutants do present a very weak phenotype during the process of angiogenesis, although Cldn5b protein is completely absent (see chapter 5.8.1). The knock-down via MO injection, however, shows a strong phenotype in ISV formation. This phenotype could be caused by a non-specific effect of the MO. However, Cldn5b protein expression is lacking in *cldn5b* morphants. Therefore, under the assumption, that the MO knock-down phenotype was specific, several scenarios could lead to the absence of a phenotype in *cldn5b* mutants. One of these possibilities is the maternal contribution of Cldn5b protein during embryonic development. No *cldn5b* mRNA and protein could be observed in early stages of development or in *cldn5b* knock-out embryos, respectively. However, a weak maternal expression that is beneath the detection level of in situs and antibody stainings, could be present in later embryos.

Therefore, I wanted to analyze the effect of inhibiting the putative maternal expression of Cldn5b. By using suboptimal concentrations of *cldn5b* MO (0.05 mM) this maternal expression is inhibited partially without causing the strong phenotype described in Fig. 18. In this experiment, the outgrowth of ISVs as well as their fusion in the DLAV was quantified in *fli1a*:EGFP expressing *cldn5b* mutant siblings (Fig. 38, Fig. 39). Std ctrl MO injected wildtype, *cldn5b*$^{+/ubs11}$ and *cldn5b*$^{ubs11/ubs11}$ embryos showed a normal outgrowth of ISVs as 100% of the vessels have grown beyond the HMS and connected within the DLAV at 30hpf (arrows in Fig. 38 A, C, E; wt: n=10; het: n=60; hom: n=30 vessels, Fig. 39 A, B). The injection of *cldn5b* MO causes even at low concentrations (0.05mM) a strong phenotype in ISV outgrowth in wildtype embryos. Although all vessels counted grew further than the HMS, none of these vessels connected within the DLAV (arrow Fig. 38 B, Fig. 39 A, B). In contrast, the injection of *cldn5b* MO in heterozygous and homozygous mutants causes on average more vessels do halt at the level of the HMS compared to wildtype embryos (arrow Fig. 38 D; 7.7 and 8/10 vessels,

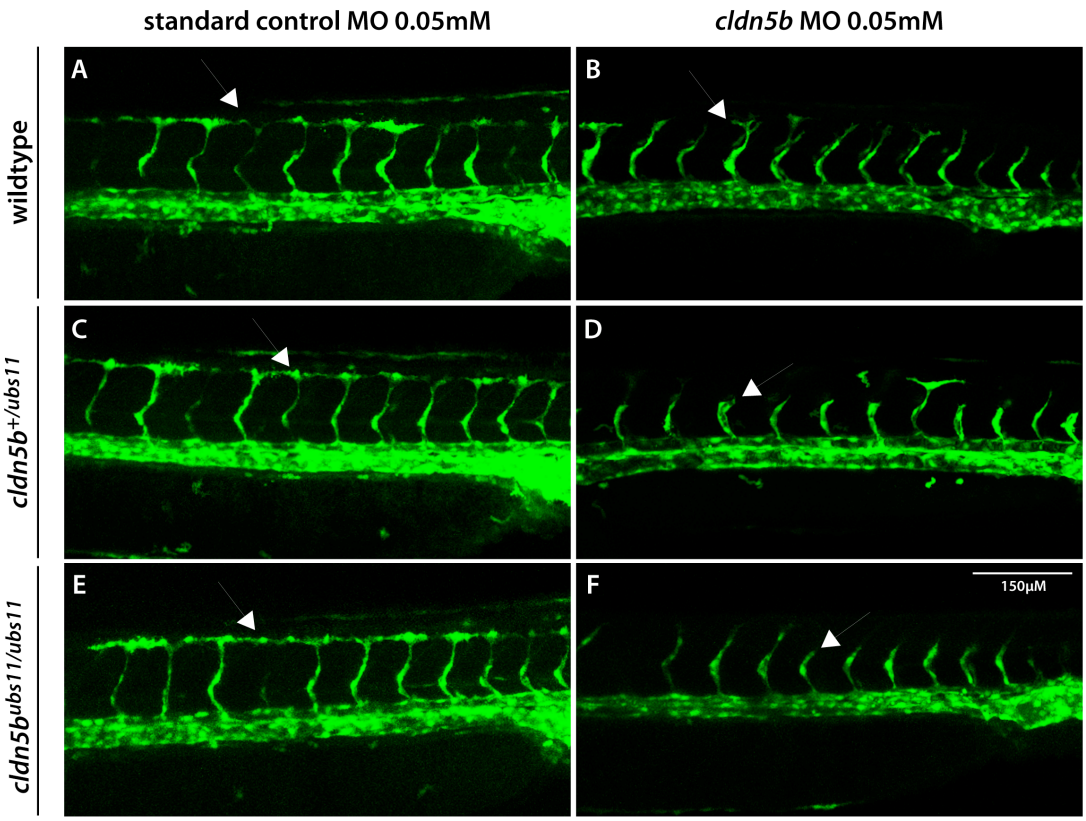

Figure 38: Maternal contribution of *cldn5b* function in *cldn5b* mutants? (A-F) Comparison of ISV outgrowth and DLAV connection in *fli1a*:EGFP expressing embryos injected with ctrl MO and a suboptimal concentration of *cldn5b* MO. (A, C, E) In ctrl MO injected wildtype, heterozygous and homozygous *cldn5b* mutants the ISVs have grown beyond the notochord and have connected to the neighboring ISVs at 30hpf. (B, D, F) In *cldn5b* MO injected embryo the majority of vessels has grown further than the level of the notochord, but has not connected within the DLAV in wildtype and *cldn5b* heterozygous and homozygous embryos.

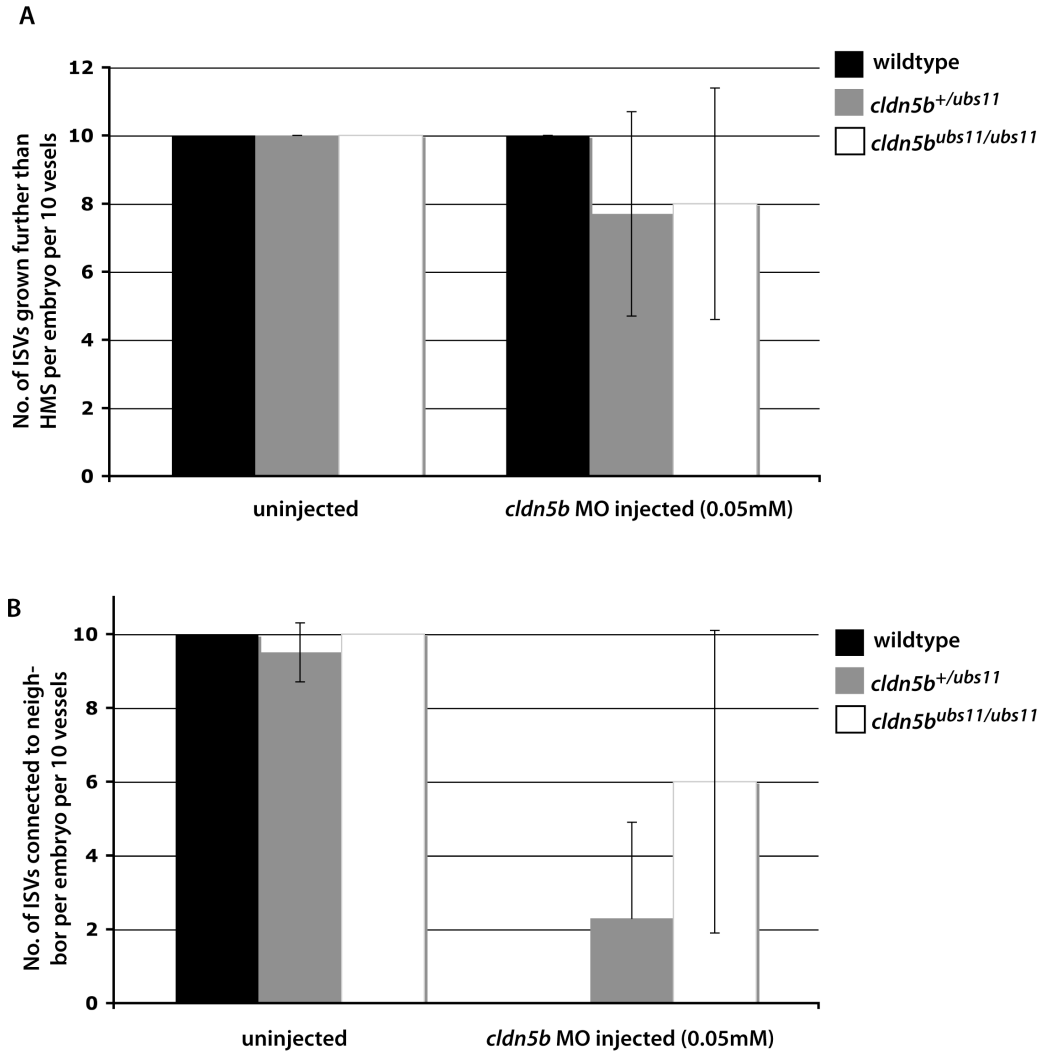

Figure 39: Maternal contribution of *cldn5b* during angiogenesis? (A) Quantification of ISVs grown beyond HMS in *fli1a*:EGFP expresssing *cldn5b* mutant siblings. The potential maternal gene expression was inhibited by the injection of a suboptimal *cldn5b* MO concentration (0.05 mM). Although heterozgyous and homozygous *cldn5b* mutants injected with the MO showed a stronger phenotype than wildtype embryos, the significance could not be determined. (B) Quantification of ISVs connected in the DLAV. Experiment was performed as in A. Here the wildtype embryo injected with *cldn5b* MO showed a stronger phenotype than *cldn5b* het/hom embryos. The lack of wildtype siblings does not allow any conclusion about the presence of maternal contribution.

respectively; Fig. 39 A). But it causes less vessels to connect to neighboring vessels in the DLAV (arrow Fig. 38 F; 2.3 and 6/10 vessels, respectively, Fig. 39 B). From these experiments so far no conclusions about a putative maternal contribution can be made. Further repetitions of this experiment will answer the effect of maternal contribution on the development of the ISVs.

5.9.6 *Cldn5a* knock-down does not cause any angiogenesis phenotype in *cldn5b* mutants

Cldn5a is expressed in the DA for a period of time, when ISVs grow dorsally and form the DLAV (see chapter 5.2). As described above, knock-down of *cldn5a* alone does not cause any phenotype during ISV formation. However, *cldn5a* is responsible for CV plexus formation as well as the DA/CV separation in conjunction with *cldn5b*. Therefore, I analyzed the effect of *cldn5a* MO knock-down on ISV and DA/CV formation in *cldn5b* mutants (Fig. 40). In std ctrl MO injected embryos ISV outgrowth above the level of the HMS occurs the same in wildtype, *cldn5b*$^{+/ubs11}$ and *cldn5b*$^{ubs11/ubs11}$ siblings (Fig. 40 A-C, Fig. 41 A). However, at this stage of development not all ISVs made connections in the DLAV (arrows in Fig. 40 A; wt 8.5 +/- 0.7; het 9.4 +/- 1.3; hom 10 +/- 0; Fig. 41 B). Upon *cldn5a* MO injection, the number of ISVs grown beyond the HMS decreases slightly in wildtype embryos (9.8 +/- 0.5 vessels per 10 vessels). Although *cldn5b*$^{ubs11/ubs11}$ embryos show a slight enhancement of the outgrowth phenotype, the difference to wildtype embryos is not significant (arrow Fig. 40 F; 9.3 +/- 0.5 vessels per 10; Fig. 41 A). Also the impact of *cldn5a* MOs on *cldn5b* mutants on the number connections within the DLAV is not significantly different to wildtype or *cldn5b*$^{+/ubs11}$ animals (Fig. 40 F vs D, E; 8.7 +/- 1.9 vs 8.8 +/- 1.3 and 8.2 +/- 2.4 vessels per 10, respectively; Fig. 41 B).

Furthermore, I analyzed the effect of *cldn5a* MO knock-down on the formation of the CV plexus (Fig. 41 A` - F`). For this, the number of embryos with an altered CV plexus and a possible fusion between DA and CV was quantified (Fig. 41 C). In std ctrl MO injected *cldn5b*$^{ubs11/ubs11}$ embryos, CV plexus

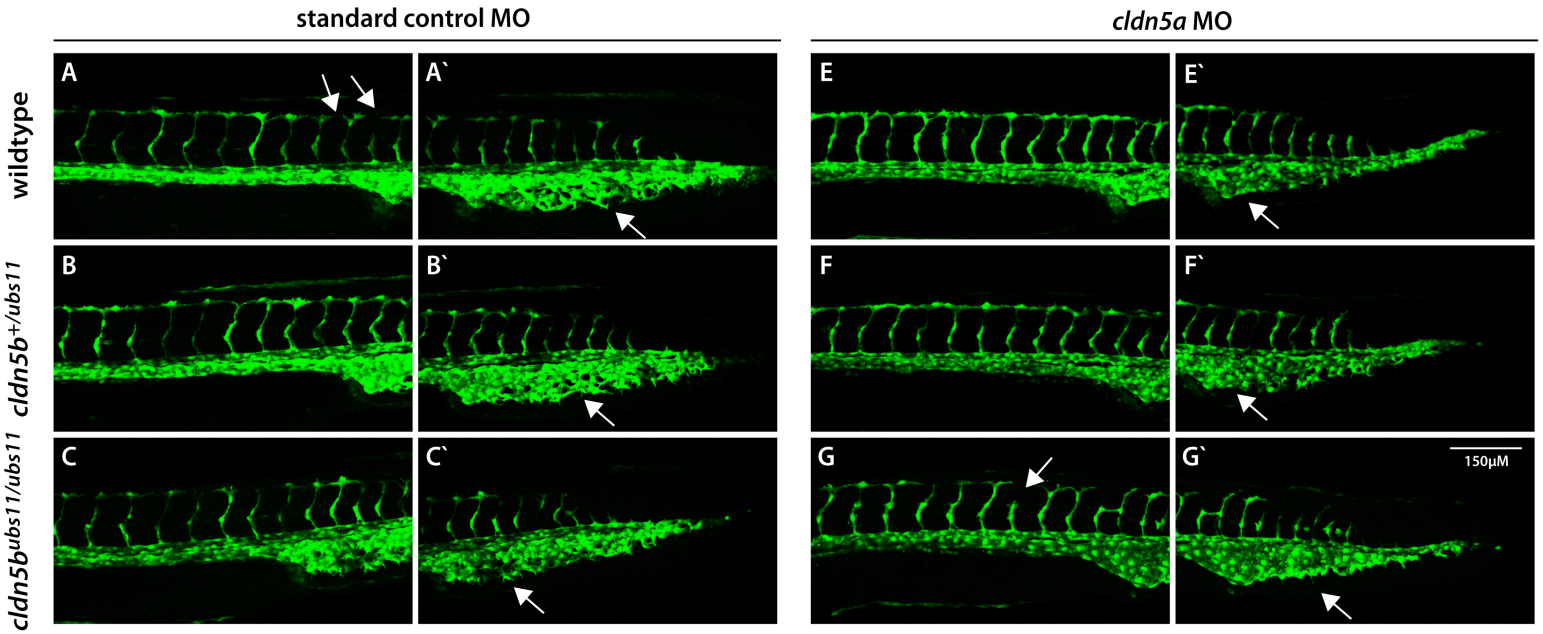

Figure 40: Normal angiogenesis in *cldn5b*/*cldn5a* double knock-down embryos. Confocal images of *fli1a*:EGFP expressing embryos wildtype, heterozygous or homozygous for the *cldn5b* mutation injected with std ctlr MO or *cldn5a* MO. *Cldn5b* mutants and their wildtype and heterozygous siblings do not reveal any abnormalities in ISV formation at 30hpf when injected with std ctrl MO (A-C). The down-regulation of *cldn5a* does not alter ISV outgrowth or the frequency of connections to neighboring ISVs in all genetic backgrouns (D-F). The rearangement of the CV plexus is normal in *cldn5b* mutant sibling injected with std ctrl MO (A`, B`, C`). Injection of *cldn5a* MO causes a severe reduction of CV plexus complexity in all genetic backgrounds (D`, E`, F`). A difference between wildtype animals and homozygous *cldn5b* mutants cannot be observed (F` vs D`). A fusion of DA and CV is never observed.

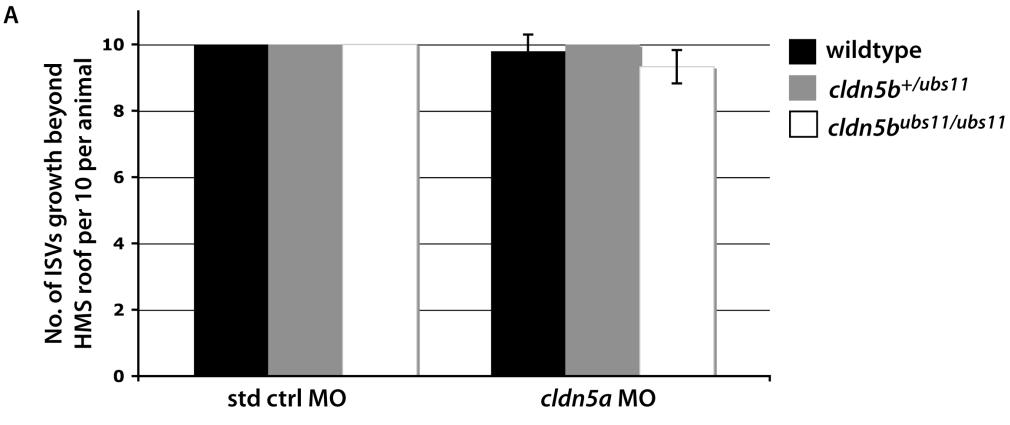

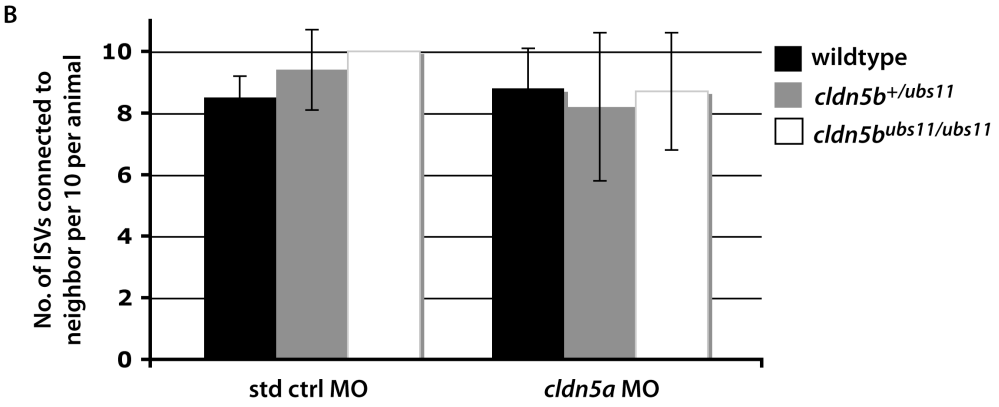

C

Number of embryos with a lack in CV complexity

	wt	het	hom
std ctrl MO	0%	0%	0%
cldn5a MO	100%	80%	100%

Figure 41: *Cldn5a* MO knock-down does not alter ISV outgrowth in *cldn5b* mutants. (A) Quantification of ISVs grown beyond the HMS in 27hpf embryos. Although less ISVs grow further than the HMS in *cldn5a* MO injected animals compared to ctrl MO injected embryos, the difference between homozygous *cldn5b* mutants and wildtype animals is neglectable. (B) Quantification of vessels connecting to neighboring ISVs in 27hpf embryos. At this stage not all ISVs have connected to neighbors in wildtype embryos. The knock-down of *cldn5a* does not increase the number of vessels without connection. (C) Quantification of number of embryos with low complexity CV plexuses. Ctrl MO injected animals show a normal development of the CV plexus. Upon injection of *cldn5a* MO almost all embryos independent of the genetic background lack CV plexus complexity.

formation occurs in a comparable manner as in wildtype and heterozygous animals (compare Fig. 40 C` vs A`, B`; Fig. 41 C). In contrast, the injection of *cldn5a* MO causes a loss of complexity within the CV plexus of all genotypic backgrounds analyzed (compare arrows in Fig. 40 D`, E`, F` with arrows in Fig. 40 A`, B`, C`, Fig. 41 C). The fusion of DA and CV was never observed in either std ctrl MO or *cldn5a* MO injected mutant siblings.

Taken together, these data show that *cldn5a* does not work in conjunction with *cldn5b* in the mutant background during ISV and DA/CV formation.

6. Discussion

During blood vessel development cell-cell contacts mediate adhesion between migrating and rearranging endothelial cells during blood vessel generation and maturation. Although the cell contacts in endothelial cells underlie dynamic changes, the adhesion governed by these cell contacts has to be maintained over a certain threshold to ensure tissue integrity.

Cell contacts in endothelial cells consist to a large extent of adherens junctions and tight junctions, which are composed of different protein complexes (Bazzoni and Dejana, 2004; Ebnet, 2008). Whereas adherens junctions are thought to establish and maintain cellular contacts, tight junctions form selective barriers between cells to control paracellular transport (Anderson and Van Itallie, 2009; Baum and Georgiou, 2011; Ebnet, 2008; Van Itallie and Anderson, 2004a; Van Itallie and Anderson, 2006). Although much is known about the molecular composition of junctional protein complexes (Ebnet, 2008; Hartsock and Nelson, 2008) and the behavior in cell culture experiments has been intensely studied (Matsuda et al., 2004; Perryn et al., 2008; Sasaki et al., 2003), only little is known about the exact role of adherens and tight junctions during development of the vasculature *in vivo*.

In this project, I focused on the functional analysis of the tight junction specific protein Claudin5b during the formation of intersegmental vessels (ISVs) in the zebrafish embryo. Cldn5b is an endothelial specific Claudin and Claudins are necessary for the formation and maintenance of tight junctions (Furuse, 2010; Krause et al., 2008).

6.1 Dynamics of Cldn5b protein expression correlate with the need for adhesion during ISV outgrowth

In the first part of this section I will discuss the expression of *cldn5b* in the context of the different stages of ISV development. Later on I will discuss the phenotype of the *cldn5b* knock-down in this process.

At sprout formation and early EC outgrowth, the DA epithelium has just formed (Herbert et al., 2009; Jin et al., 2005). It is generally assumed that the overall adhesion between cells that grow out and cells that remain in the DA has to be decreased. Many studies showed the importance of the right level of adhesion during migratory behaviors of single cells and groups of cells (Arboleda-Estudillo et al., 2010; Jeon et al., 2009; Patel and Brunton, 2009). The reduction of adhesion strength between cells could be achieved by the downregulation or by the re-localization of junctional components. In sprouting ISVs Cldn5b protein is not or only weakly expressed compared to the DA. Given the prominent role of Cldn5 as a component of tight junctions in forming strong connections between adjacent cells, the temporal downregulation of Cldn5b protein in migrating ECs could lead to a lowered cell-cell adhesion as suggested in other studies (Furuse, 2010; Krause et al., 2008). Interestingly, it was shown that a reduction of Cldn5 protein expression in cultured mammalian ECs and in the mouse brain vasculature is triggered by the presence of VEGF-A, a key regulator of vessel growth (Argaw et al., 2009). The observation that the level of *cldn5b* mRNA remains the same in the ISV sprouts strongly suggests regulation at the protein level in these cells.

After the initial downregulation of Cldn5b protein expression during sprout formation, it gets upregulated again and maintained during ISV formation. This upregulation coincides with the further outgrowth of ISVs and the entering of more cells from the DA into the ISV. Here, an increase of cell-cell contact strength among ISV cells would prevent vessel disruption. Several studies showed that a certain level of adhesion is needed for tissue integrity and morphogenesis (Classen et al., 2005; Levayer et al., 2011).

One would assume, that the lack of Cldn5b protein in early ISV sprouts would not cause any sprout formation defect as Cldn5b protein expression is lowered anyway. Indeed, in *cldn5b* morphants, early sprout formation and outgrowth is not altered. In these animals, the early outgrowth of ECs is comparable to wildtype embryos.

The earliest phenotype observed in *cldn5b* morphants occurs when in wildtype Cldn5b protein expression gets upregulated again. In these embryos, ISV outgrowth is arrested for a few hours at the level of the horizontal myoseptum (HMS). Stalling of sprout outgrowth has been observed in a

number of mutants and morphants (Bignon et al., 2011; Brown et al., 2010; Ernkvist et al., 2009; Wu et al., 2011). Therefore, it is likely that many factors can cause this phenotype. However, one factor that might have a big impact on the halting of ISVs at the HMS is the reduction of total cell number in ISVs of *cldn5b* morphants. It was observed, that fewer cells entered the ISV and fewer cells divided within the ISV. Therefore, in *cldn5b* morphants next to the loss of adhesion between the migrating ECs, the ISVs might halt their outgrowth, because not enough cells enter the ISV and follow the migration of the tip cells.

How could Cldn5b influence cell proliferation? Several tight junction proteins are known to bind to the actin cytoskeleton (Wittchen et al., 1999; Wittchen et al., 2000). It was shown in several studies that defects in F-actin formation influence cell proliferation and cytokinesis (Pollard, 2010; Skau et al., 2011; Sun et al., 2011; Vavylonis et al., 2008). To study whether the actin cytoskeleton is altered upon *cldn5b* knock-down, MO injections into fish expressing a live-actin marker can be performed. Interestingly, some tight junction proteins such as ZO proteins, JAM-A and ZONAB are known to regulate cell proliferation directly (Balda and Matter, 2009; Capaldo et al., 2011; Nava et al., 2011). In particular, for the ZO-1 associated protein ZONAB it was shown, that it translocates to the nucleus and activates the expression of cell-cycle dependent genes (Balda et al., 2003; Balda and Matter, 2000; Sourisseau et al., 2006). It would be interesting to test, whether in *cldn5b* morphants the localization of these proteins is altered, which would indicate a potential link to the observed cell proliferation defect. A very similar phenotype as observed in *cldn5b* morphants was shown for zebrafish embryos depleted for *Notch-regulated-ankyrin-repeat protein* (*nrarp*) and *lymphoid enhancer factor 1* (*lef1*) function (Phng et al., 2009). The ISVs in these embryos show detachment and regression from the DA similarly to the observations in *cldn5b* morphants (discussed below). In contrast to Phng et al., I have found additionally, that the ISVs in *nrarp* morphants also halt at the HMS (data not shown). Interestingly, *nrarp* morphants reveal a strong reduction of cell number per ISV (Phng et al., 2009). It was shown that Nrarp expression is induced by Notch, which in turn inhibits Notch signaling, but also increases Wnt signaling by inducing Lef1/βcatenin expression. The authors suggest that

nrarp regulates cell proliferation by limiting Notch-dependent cell cycle arrest and by increasing Lef1/Wnt signaling-dependent CyclinD1 expression. The very similar phenotypes in both *nrarp* and *cldn5b* morphant embryos raises the possibility that these genes might act synergistically during ISV formation. It will be very interesting to study the effect of cell number reduction on the architecture and formation of ISVs in wildtype animals. This could be achieved by the general block of cell proliferation within an animal or by laser ablation of single cells within an ISV. Another less invasive method to reduce cell number in the ISVs would be the expression of proapoptotic genes in an EC-specific manner using for example the Gal4/UAS system. This approach has been used successfully in *Drosophila* by expression of the proapoptotic genes *hid* and *reaper* (Bergantinos et al., 2010; Wu et al., 2010; Yorozu et al., 2009). Furthermore, an increase of cell number could be achieved by the injection of a *p27* MO, which has been shown to block cell cycle arrest (Komatsu et al., 2011; Polyak et al., 1994).

After the initial sprouting of the ISV and the temporary halting of migration in *cldn5b* morphant embryos, the ECs of the ISV do eventually migrate further. This indicates, that the attractive signal persists. When migrating into anterior and posterior directions above the neural tube, the ISVs do partially not make connections between neighboring ISVs in the dorsal-longitudinal-anastomotic vessel (DLAV). Also here a reduction of cell number might prevent the ECs from joining in the DLAV. However, one can assume that in wildtype embryos a certain migratory behavior in these cells ensures the fusion of the neighboring ISVs. It was shown for cultured MDCK cells that the lack of the tight junction protein Occludin inhibits migration in a wound healing assay. Furthermore, this protein is responsible for the polarization of the migrating cell (Du et al., 2010). In wildtype zebrafish embryos, Cldn5b localizes to the points of first contact between cells migrating towards each other. Therefore, the lack of Cldn5b could either directly or indirectly fulfill a similar function as Occludin in regulating the migratory behavior of ECs and in guiding the connection of ECs in the DLAV.

It might be assumed, that during ISVs outgrowth in wildtype embryos the tip cells creates a pulling force on every cell of the ISV. For the dorsal branch in the *Drosophila* tracheal system strong pulling forces of the tip cells as well as

tensile forces on the whole branch were recently shown (Caussinus et al., 2008). Here, the laser ablation of connections between the stalk cells and the main branch caused a fast constriction of the remaining cells. Furthermore, for groups of migrating epithelial cells mechanical stress such as pulling forces were shown to be distributed over many cells within the epithelium. This distribution is mediated by cell-cell contacts between the cells (Tambe et al., 2011). Similar pulling forces as well as mechanical stress might be assumed to be present within the ISV. Especially in ISVs consisting of two cells only, these appear very thin and stretched. This might indicate that a high load of mechanical tension is imposed on these cells. Finally, *cldn5b* morphants showed a detachment of many ISVs from the DA at a timepoint, when a vascular loop of ISV and DLAV has been formed already in wildtype embryos. This observation suggests that the pulling forces of the tip cell might dramatically increase and a connection between the ISV and DA cannot be maintained anymore.

Interestingly, the level of Cldn5 expression in wildtype embryos is much higher at the base of the connection between the ISV and the DA than within the ISV itself. Therefore, a loss of Cldn5b protein expression at this connection might loosen the contact between ISV and DA. These observations correlate with the finding, that in *cldn5b* morphants a detachment of cells always occurs at the contact point between ISV and DA. This might indicate an important function for Cldn5 in anchoring the ISV to the DA.

The majority of studies about Cldn proteins as the core components of tight junctions have revealed a function in building a sealing barrier of epithelia (Alexandre et al., 2005; Amasheh et al., 2002; Anderson and Van Itallie, 2009; Furuse, 2010; Furuse et al., 2002; Nitta et al., 2003; Van Itallie and Anderson, 2006). Interestingly, a few reports also show that Cldn function could be linked to morphogenetic processes (Bagnat et al., 2007; Moriwaki et al., 2007; Siddiqui et al., 2010). Cldn15 function is necessary for the coalescence of lumen of the zebrafish gut and Cldn4 and Cldn6 were shown to be important for blastocoel cavity expansion in mouse embryos (Bagnat et al., 2007; Moriwaki et al., 2007). However, the morphogenesis defect in the gut is also linked to the regulated paracellular ion transport within the epithelium (Bagnat

et al., 2007). In *cldn5b* morphants the defects in ISV formation occur prior to lumen formation. This raises the question whether the function in this process of *cldn5b* is mediated by paracellular transport or the more likely direct regulation of differential cell adhesion. This for the first time suggests a role for a Cldn in a morphogenetic process.

6.2 Cldn5b and VE-cadherin have different expression patterns and functions

Cadherins were shown to have a function in regulating cell dynamics during morphogenetic processes. During the process of tip cell fusion in the *Drosophila* tracheal system, the lack of Drosophila epithelial (DE) - cadherin leads to a failure in tip cell adhesion and fusion (Tanaka-Matakatsu et al., 1996). For vertebrate ECs VE-cadherin was shown to inhibit angiogenesis by repressing VEGFR-2 internalization and by limiting Rac1-dependent migration of ECs (Abraham et al., 2009; Lampugnani et al., 2006). However, VE-cadherin also may have proangiogenic functions as it facilitates the EC rearrangements in mouse allantoid cultures (Perryn et al., 2008). It can be assumed that during zebrafish development VE-cadherin exerts a similar function during angiogenic processes.

In this study as well as in experiments performed by Heinz-Georg Belting in the lab, we found, that during ISV formation in *VE-cadherin* mutant ECs are arrested in the ventral part of the ISV. Furthermore, connections between cells in the dorsal part of the ISV and the DLAV cannot always be maintained and get disrupted. However, the disrupted connection between ISVs re-established again. Antibody stainings for ZO-1 in *VE-cadherin* mutants showed an absence of ZO-1 localization in the dorsal part of the ISVs, indicating that here the ISV is constituted of one cell only compared to wildtype (Heinz-Georg Belting, unpublished data). These data suggest that VE-cadherin is necessary for the rearrangement of cells during the highly dynamic process of angiogenesis. This can be supported by other studies, in which VE-cadherin function was analyzed in the vasculature of zebrafish. The

knock-down of VE-cadherin via MO injections caused the loss of vessel integrity as well as a lack of lumen formation in ISVs (Wang et al., 2010). Furthermore, the process of anastomosis in neighboring ISVs is highly impaired (Montero-Balaguer et al., 2009).

In contrast, in *cldn5b* knock-down embryos such phenotypes could not be observed. Here, ZO-1 and VE-cadherin stainings showed that the cellular architecture within ISVs resembles that of wildtype embryos. Cells are arranged in a side-by-side pattern shown by the linear fashion of junctional protein localization along the whole axis of ISVs. These data indicate, that Cldn5b and VE-cadherin might have different functions during the highly dynamic process of ISV formation. Also, the simultaneous knock-down of *VE-cadherin* and *cldn5b* shown in this study does not reveal any redundant functions, but rather leads to additive effects.

However, in cultured murine ECs a functional connection between the VE-cadherin and Cldn5 was shown (Taddei et al., 2008). Here, VE-cadherin induces Cldn5 expression mediated by the Tcf4/FoxO1/β-catenin-complex (Taddei et al., 2008). *In vivo* in VE-cadherin mutant embryos we still detect Cldn5 protein expression that is comparable to wildtype siblings. Therefore, significant differences between *in vitro* and *in vivo* data for Cldn5 protein expression upon VE-cadherin knock-down were observed. They propose that another level of complexity might be responsible for the regulation of Cldn5 protein expression *in vivo*.

In summary, the analysis of the adherens junction specific protein VE-cadherin and the tight junction specific protein Cldn5b suggests different functions during the process of angiogenesis (Fig. 42). The DA is a fully developed epithelium expressing VE-cadherin as well as Cldn5b. However, upon sprout formation, the ECs that sprout form the DA epithelium have to loosen their adhesion to the cells of the DA and become migratory. Therefore, in these early sprouts Cldn5b gets downregulated compared to the expression level in the DA. In early ISV sprouts VE-cadherin mediates the rearrangement of ECs for the proper formation of the ISV. Loss of VE-cadherin function inhibits this dynamic cell behavior leading to the accumulation of cells in the ventral part of the ISV. As ISV formation proceeds Cldn5b gets upregulated

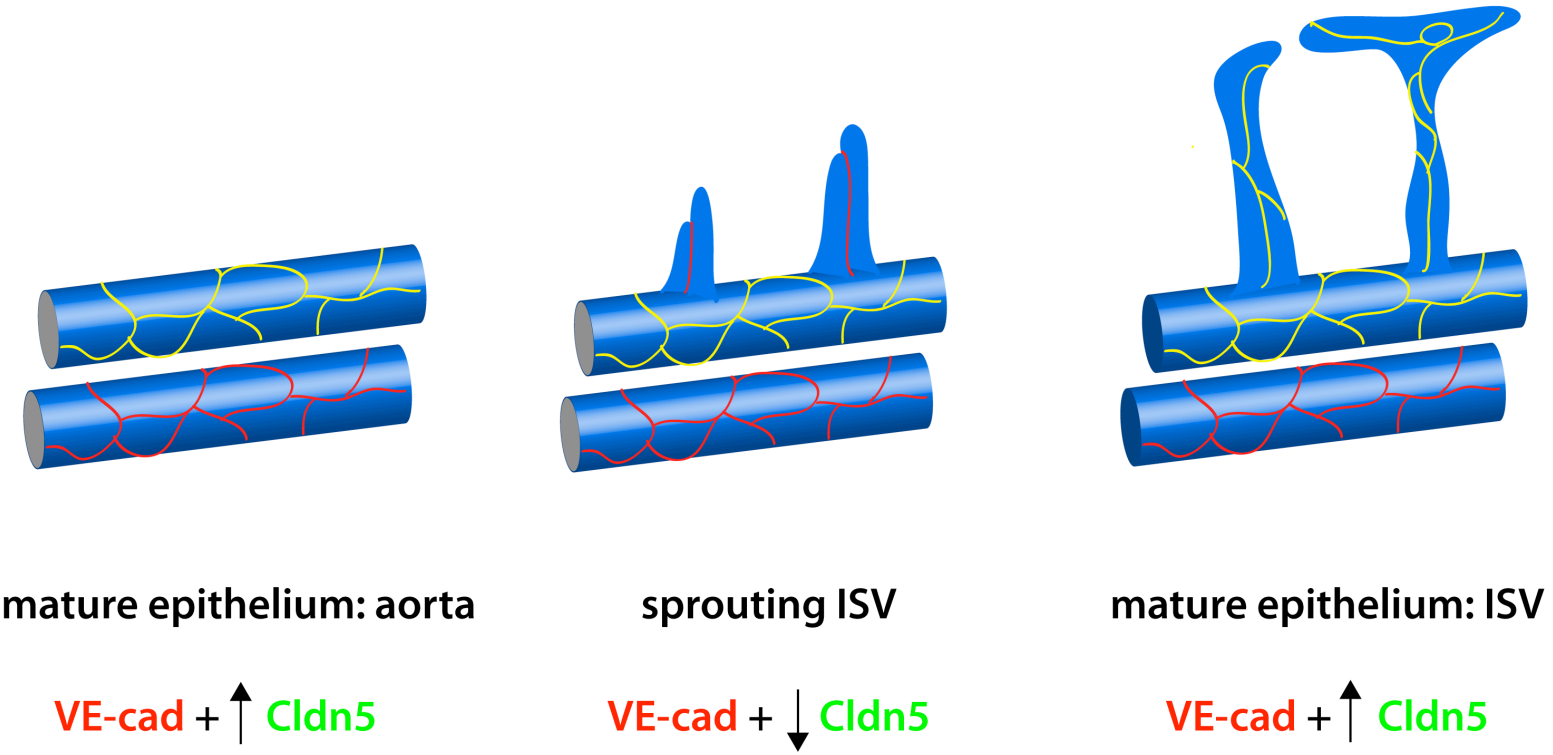

Figure 42: Schematic representation of VE-cadherin and Cldn5 expression in sprouting ISVs. In the mature epithelium of the aorta, VE-cad and Cldn5 are expressed. Upon initiation of sprouting ECs adopt a migratory behavior and have to leave the aorta epithelium. Now Cldn5 is downregulated. As soon as a functional epithelium has to be generated in the ISVs, they upregulate Cldn5 again.

again and maintained. At later stages during ISV maturation, Cldn5b might mediate the maintenance of vessel stability and connectivity to the DA.

6.3 *Cldn5b* mutants lack a clear angiogenesis phenotype

In order to specifically delete *cldn5b* function, I generated a *cldn5b* mutant fish line using Zinc-Finger Nucleases (ZFN). In these mutants a 2bp deletion leads to a frame shift and a premature stop codon, which encodes a strongly truncated protein. Interestingly, the exact same 2bp deletion was observed in all four mutant fish found as well as in the fish transiently expressing the ZFN. The generation of the same mutation has been observed in other instances as well (personal communication of Nathan Lawson to H. B.). It may be influenced by the nucleotide composition surrounding the cleavage site. It would be desirable to use a different ZFN against *cldn5b* to generate an allele different from the existing one. However, due to the small size of the *cldn5b* ORF it may be difficult to find an optimal target sequence. Very recently a novel method to generate knock-outs in zebrafish has been described (Sander et al., 2011; Zhang et al., 2011). This could also be used to generate another allele for *cldn5b*.

In agreement with the genetics, a complete loss of Cldn5b protein was observed in these mutants. They represent the first knock-out of the key component of tight junctions in fish and provide a great tool to study the role of a Cldn protein during angiogenesis. Surprisingly, *cldn5b* zebrafish mutants do only show a very weak phenotype regarding the morphogenesis of ISV formation. Compared to *cldn5b* morphants, no delay in outgrowth or vessel detachment was observed. Only when analyzing this process via time-lapse imaging, a weak delay of outgrowth as well as the lack of a few connections between neighboring ISVs was observed. Furthermore, also the expression of the junctional component ZO-1 revealed an expression pattern comparable to wildtype embryos.

Why do the different techniques of *cldn5b* knock-down/out show such a big discrepancy in phenotype penetrance?

In *cldn5b* morphants protein expression of Cldn5b is completely absent, while Cldn5a protein is still expressed. Furthermore, the knock-down using two different MOs for *cldn5b* generated the same phenotype. These data suggest a specific knock-down of *cldn5b* via MO injection. However, the knock-down via MO injections is not always entirely specific. Therefore, I wanted to further prove the specificity of the MO-mediated *cldn5b* knock-down by performing rescue experiments. The rescue of MO phenotypes using mRNA injections is an established method used in zebrafish developmental biology (Kappler et al., 2004; Labalette et al., 2011; Zhang et al., 2010). However, in this study Cldn5b could not be successfully expressed from the injected mRNA.

It was observed that the injection of a MO itself might cause aggravated p53 levels in the injected embryos (personal communication Nathan Lawson to H.B.). This transcription factor induces apoptosis of cells and might therefore account for a possible secondary effect of MO injections (Brady et al., 2011; Wu and Levine, 1994). However, in this study I observed, that the concomitant injection of *p53* MO and *cldn5b* MO does not change the phenotype penetrance (data not shown).

Additionally, the Gal4/UAS system was applied as a second approach to rescue the MO-associated defects. By crossing transgenic fish carrying a UAS:*cldn5b*:EGFP construct to *fli1ep*:Gal4ff fish the specific expression of the Cldn5b:EGFP fusion protein in ECs was achieved. Although expression of the fusion protein was observed (Suppl. Data 8, Fig. 3), no rescue activity could be assigned to the expression of Cldn5b:EGFP. Several reasons might account for the missing rescue ability of the *cldn5b*:EGFP construct. First, the construct is driven by the *fli1* promoter, whose expression pattern does not entirely overlap with the normal *cldn5b* expression. Second, the expression via the Gal4/UAS system might lead to a higher expression level of Cldn5b than would be present in wildtype embryos. The exact protein level might be important for the rescue of the phenotype. Third, the position of the tag used for monitoring the expression might have a big impact on the function of the protein by changing its expression pattern or localization. In this case the

EGFP tag was added to the C-terminus of Cldn5b. It was shown before, that fluorescent tags to the C-terminus of Cldn proteins do not to alter their localization to the junctions (Furuse et al., 1998). However, compared to Cldn5b protein marked via antibody stainings, the Cldn5b:EGFP protein is rather expressed in the cytoplasm than at the junctions (Suppl. Data 8, Fig. 3). Additionally, it was shown that ZO-1 cannot be recruited to tight junctions, if the C-terminus of Cldn proteins is “blocked” by a fluorescent tag (Sasaki et al., 2003). These data strongly suggest that the Cldn5b:EGFP protein fusion is not functional.
Finally, although Cldn5b protein expression is completely absent in *cldn5b* morphants, it cannot be completely excluded that the MO used in these experiments exerts unspecific effects. Furthermore, the presentation of a very weak phenotype in *cldn5b* mutants could indicate, that the gene may not be strictly required during ISV formation, but may still have a function.

It should be noted, that Cldn5 is known for its function in forming the blood-brain barrier (BBB) as well as blood-retinal barrier (BRB) (Jeong et al., 2008; Nitta et al., 2003; Virgintino et al., 2004; Xie et al., 2010). One could speculate that *cldn5b* exerts the same function during vessel sealing in the zebrafish vasculature. Indeed, a leakage of erythrocytes from the ISVs was observed in *cldn5b* morphant embryos. If this holds true for the mutant embryos has to be determined in future experiments using *fli1a*:EGFP;*gata1*:dsRed fish. Additionally, the injection of fluorescently labeled dextrans or Quantum dots into the functional blood vessel system will give further insights into the role of *cldn5b* in vessel sealing.

Assuming however, that the MO-mediated knock-down of *cldn5b* is specific, several reasons might account for the low phenotype penetrance during ISV formation in *cldn5b* mutants. It should be noted that a small part of the Cldn5b protein is still expressed in *cldn5b* mutants. This could adopt a function that might partially rescue the phenotype. However, the N-terminus in Claudins has not been reported to have any functional relevance. Furthermore, it was shown in mice that different strains of mice can exhibit strikingly different phenotypes (Baribault et al., 1994; Baribault et al., 1993; Jelcick et al., 2011;

Kent et al., 1997; Rozmahel et al., 1996). Also in zebrafish this issue has been started to be addressed (Bretaud et al., 2011). Therefore, it will be desirable to analyze the *cldn5b* mutation in a different zebrafish strain.

Furthermore, in ECs compensatory mechanisms could mask the *cldn5b* knock-out phenotype. An acute knock-down in MO injected embryos could lead to a different cellular response than in embryos lacking a gene from the beginning.

A few studies show that the maternal effect of genes can last until late into embryogenesis in zebrafish and other model organisms (Franks et al., 2006; Kotani and Kawakami, 2008; Wagner et al., 2004). Also in *cldn5b* mutants a maternal contribution could compensate for the loss of zygotic *cldn5b* function. Although no *cldn5b* mRNA was detected in early stages of development, the level of expression could be under the detection threshold of the in situ hybridization. Initial experiments inhibiting *cldn5b* translation of potential maternal mRNA in *cldn5b* mutants did not lead to clear conclusions. In this direction, it would be interesting to know, if homozygous *cldn5b* mutants survive until adulthood. If these fish exist, a series of experiments will clarify if a maternal contribution exists and what its putative effect on *cldn5b* function during angiogenesis is.

Another compensatory mechanism that could mask the function of *cldn5b* might be the functional redundancy with other tight junction proteins, especially Cldns. These might be either upregulated or function redundantly without being upregulated. The compensation for the loss of certain genes during development has been observed in several examples (FitzPatrick et al., 2002; Gupta et al., 2006; McAnally and Yampolsky, 2009; Stenberg et al., 2009). Despite the high sequence similarity Cldn5a does not mask *cldn5b* loss of function. Antibody stainings do not show a clear upregulation of Cldn5a in *cldn5b* mutants (data not shown). More importantly, the injection of *cldn5a* MO into *cldn5b* mutants does not lead to an increase in phenotype. Beside Cldn5b other Cldns are among other tissues also expressed in ECs such as Cldn1, Cldn3, Cldn12 and Cdln15 (Kiuchi-Saishin et al., 2002; Leach et al., 2002; Liebner et al., 2000; Lievano et al., 2006; Wolburg et al., 2003). These could therefore be functionally redundant to *cldn5b* function and mask the *cldn5b* loss of function. Future experiments will determine whether the

lack of *cldn5b* influences the expression level of these Cldns. Furthermore, knock-out studies of these *cldns* will address their putative role during angiogenesis.

6.4 Conclusions

In this study, I have analyzed the role of *cldn5b* during the process of ISV formation, by anti-sense morpholino injections and by generation of a *cldn5b* mutant. MO-mediated knock-down of *cldn5b* causes defects in ISV outgrowth and blood vessel stability. In addition, I have found that cell proliferation is impaired in *cldn5b* morphants, raising the possibility that the correct cell number of ECs is important for ISV formation. These findings for the first time point to functions for a Claudin protein in the control of vascular morphogenesis.

Using Zinc-Finger Nuclease technology I was able to generate a fish line that contains a lesion in the genomic locus of *cldn5b*. This frameshift mutation leads to the expression of a truncated protein product. Phenotypic analysis reveals significant discrepancies between *cldn5b* mutant and morphant embryos. In contrast to the morphants, the *claudin* mutant phenotype is much weaker and less penetrant. The cause of these discrepancies is not known but may be accounted for by compensation through protein redundancy or by off-target effects of the morpholinos. Further detailed analyses including mutants of other tight junction proteins will be required to delineate the exact function of tight junctions during vascular morphogenesis.

7. Contribution to further publication

Vascular morphogenesis in the zebrafish embryo

Elin Ellertsdottir, Anna Lenard, Yannick Blum, Alice Krudewig, Lukas Herwig, Markus Affolter, Heinz-Georg Belting

Developmental Biology 341 (56-65)
May 01, 2010

Contribution:
I contributed to discussions during writing of the manuscript.

Developmental Biology 341 (2010) 56–65

Contents lists available at ScienceDirect

Developmental Biology

journal homepage: www.elsevier.com/developmentalbiology

Review

Vascular morphogenesis in the zebrafish embryo

Elín Ellertsdóttir, Anna Lenard, Yannick Blum, Alice Krudewig, Lukas Herwig, Markus Affolter, Heinz-Georg Belting *

Department of Cell Biology, Biozentrum der Universität Basel, Klingelbergstrasse 70, CH-4056 Basel, Switzerland

ARTICLE INFO

Article history:
Received for publication 11 September 2009
Revised 28 October 2009
Accepted 28 October 2009
Available online 3 November 2009

Keywords:
Angiogenesis
Vasculogenesis
Branching morphogenesis
Cell migration
Lumen formation
Development
Zebrafish

ABSTRACT

During embryonic development, the vertebrate vasculature is undergoing vast growth and remodeling. Blood vessels can be formed by a wide spectrum of different morphogenetic mechanisms, such as budding, cord hollowing, cell hollowing, cell wrapping and intussusception. Here, we describe the vascular morphogenesis that occurs in the early zebrafish embryo. We discuss the diversity of morphogenetic mechanisms that contribute to vessel assembly, angiogenic sprouting and tube formation in different blood vessels and how some of these complex cell behaviors are regulated by molecular pathways.

© 2009 Elsevier Inc. All rights reserved.

Introduction

Branched tubular organs, such as the insect tracheal system or the vertebrate cardiovascular system, kidney or lung, are found throughout the animal kingdom. Formation of such tubular networks from precursor cells or tissues involves a variety of morphogenetic processes, such as tube formation, elongation, branching and fusion. These processes are brought about by complex cellular behaviors, which include cell polarization, cell migration, cell rearrangements, cell shape changes and cell division. Although tubular organs are extremely diverse in anatomy and function, the cellular activities that govern tube formation and branching morphogenesis appear to be quite similar (Baer et al., 2009; Andrew and Ewald, 2010). In this review, we describe the current understanding of blood vessel formation in the early zebrafish embryo. We are placing special emphasis on the morphogenetic processes that contribute to vascular development and discuss the regulatory components that accompany these events.

In vertebrates, the cardiovascular system constitutes a highly ramified network of tubes that transports gas, nutrients, hormones and metabolites throughout the body. It also has important roles in the regulation of homeostasis and wound healing and is involved in the pathology of numerous diseases including cancer and inflammation (Carmeliet, 2003). The cardiovascular system emerges as one of the first organs during embryonic development and retains morphogenetic plasticity in adult life. Blood vessels are an integral component of all organs and are vital not only for their function but also for their formation during embryonic development (Nikolova and Lammert, 2003; Red-Horse et al., 2007; Sakaguchi et al., 2008). Blood vessels are highly diverse: they differ in size and are specialized depending on their function and the tissue or organ they are embedded in (Aird, 2007; Rocha and Adams, 2009). In general, they consist of an inner epithelium (endothelium) lining the lumen; depending on the type of vessel, this endothelium is surrounded by a basal lamina and by mural cells, such as pericytes and smooth muscle cells, which both support and regulate the function of the endothelium (Armulik et al., 2005).

Over the last decade, the molecular pathways controlling vascular development have attracted much attention, and a large number of key molecules has been identified that regulate different aspects of blood vessel morphogenesis. The basic frameworks of the vascular anatomy are conserved among vertebrates, which makes it possible to assign homologies between distinct blood vessels and to directly compare the formation of these vessels in different vertebrate species (Isogai et al., 2001; see Fig. 1). The zebrafish embryo has proven to be a useful model to study vascular morphogenesis in vivo. The vasculature can be easily visualized using a variety of labeling techniques, such as endothelial specific expression of fluorescent protein or by microangiography (Fig. 1). Its small size, experimental accessibility, optical clarity and rapid development allow to observe cellular activities, such as cell migration, cellular rearrangements and cell divisions, as they occur during blood vessel formation in the embryo. It is also possible to follow cardiovascular mutant phenotypes for several days because oxygenation of the early zebrafish embryo does

* Corresponding author.
E-mail address: heinz-georg.belting@unibas.ch (H.-G. Belting).

0012-1606/$ – see front matter © 2009 Elsevier Inc. All rights reserved.
doi:10.1016/j.ydbio.2009.10.035

8. Supplementary Data

8.1 Supplementary Figures

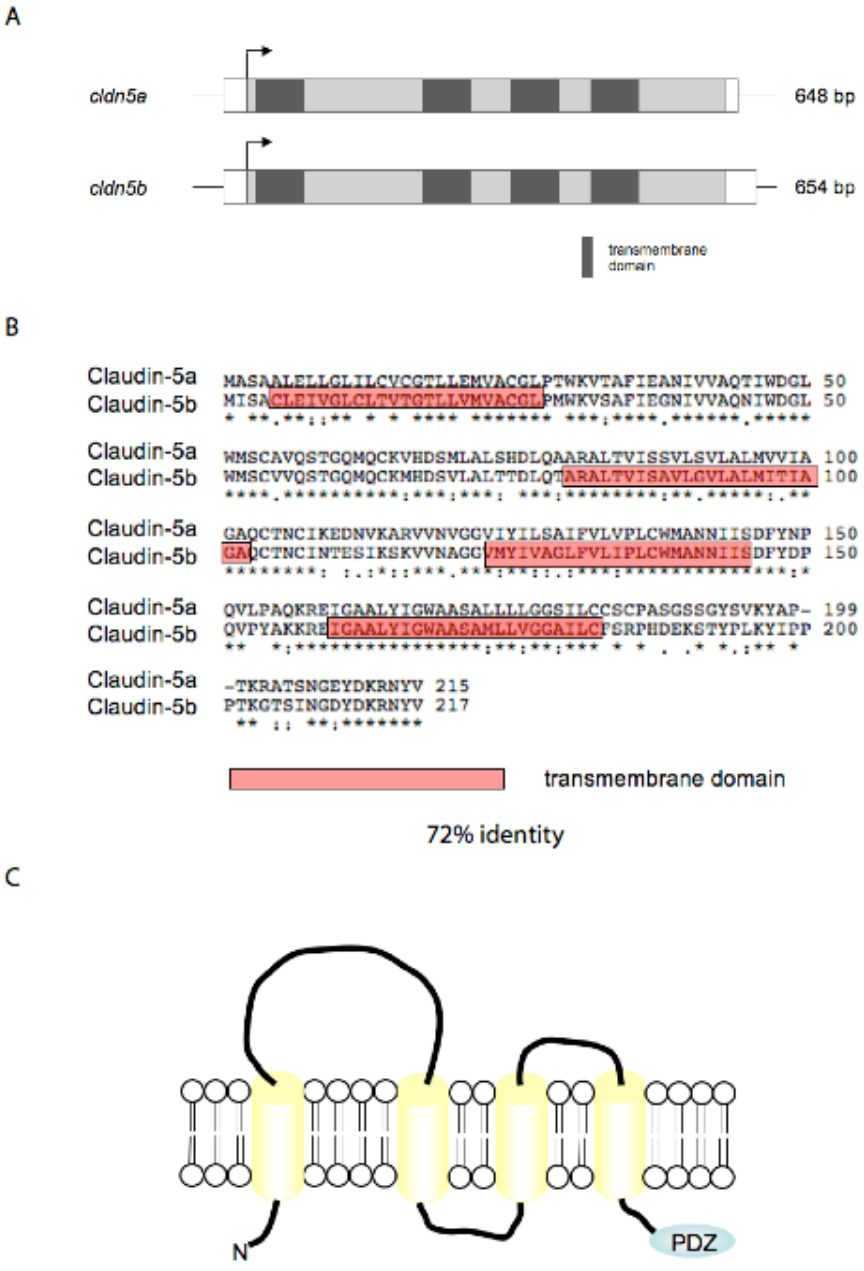

Supplementary Figure 1: Hihgly identical protein sequence of Cldn5a and Cldn5b. (A) Schematic representation of *cldn5a* and *cldn5b* ORF. (B) Alignment with "Clustal 2.0.12 multiple sequence alignment" of Cldn5a and Cldn5b protein sequences. These proteins share 72% of aminoacids. (C) Schematic representation of Cldn5b protein within the plasma membrane.

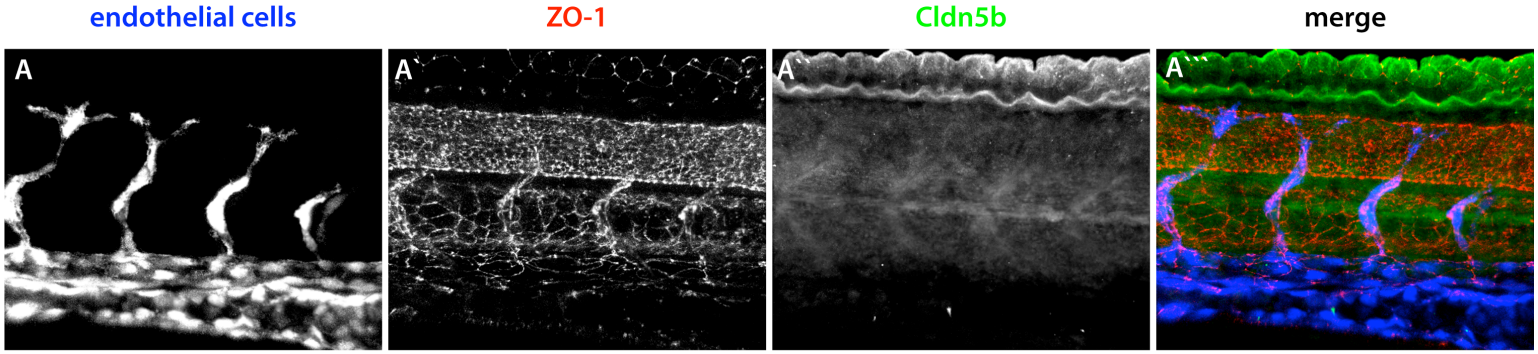

B

MISACLEIVGLCLTVTGTLLVMVACGLPMWKVSAFIEGNIVVAQNIWDGL 50
WMSCVVQSTGQMQCKMHDSVLALTTDLQTARALTVISAVLGVLALMITIA 100
GAQCTNCINTESIKSKVVNAGGVMYIVAGLFVLIPLCWMANNIISDFYDP 150
QVPYAKKREIGAALYIGWAASAMLLVGGAILCFSRPHDEKSTYPLKYIPPP 200
TKGTSINGDYDKRNYV 217

Supplementary Figure 2: Representative antibody staining for one of four Cldn5b specific peptide antibodies. (A) Immunohistochemical staining with rabbit anti-Cldn5b antibody (green, A`) and ZO-1 (red, A`) in fli1a:EGFP expressing fish (blue, A). (B) Epitopes the antibodies were raised against (yellow box). Four different peptide antibodies were raised against the Cldn5b protein, two in rabbit and two in guineapig. For each of the antibodies three different concentrations and two different fixation methods were tested. All antibodies gave a high background staining especially in the muscles and epidermis, but none of them stained Cldn5b protein in the ECs.

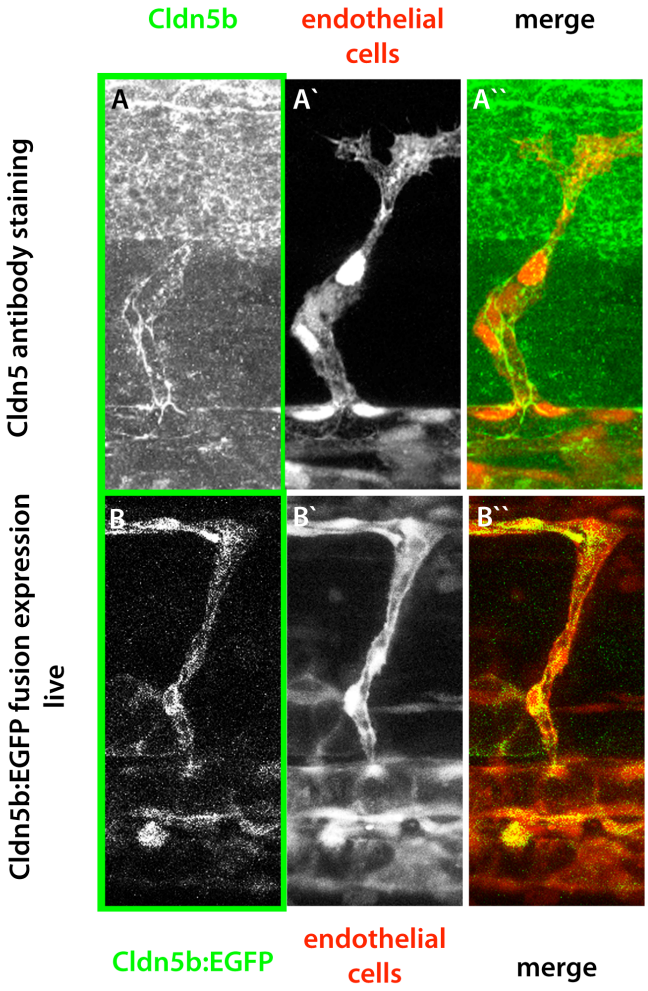

Supplementary Figure 3: Unlike the Cldn5b junctional staining using a human Cldn5 antibody, a Cldn5b:EGFP fusion protein does not localize to junctions. (A-A``) Antibody staining using the human Cldn5 antibody (green, A) in a *fli1a*:EGFP expressing embryo (red, A`). The antibody recognizes Cldn5b in the vasculature and Cldn5a in the neural tube. (B-B``) Living embryo expressing UAS:cldn5b:EGFP (green, B) in the background of *fli1a*:Gal4ff; UAS:mRFP (red, B`). Compared to the antibody staining Cldn5b:EGFP does not localize to the junctions (compare green box; A vs B).

Supplementary Figure 4: *Cldn5b* MO2 is more efficient than MO1. (A) Schematic representation of MO1 and MO2 binding sites to *cldn5b* translational start site. (B-M) Confocal images (B-E; H-L) and statistical comparison (F, G, M) of phenotypic strengths in *cldn5b* MO1 and MO2 injected fli1a:EGFP expressing fish. For evaluation of the MO strengths, the halting of ISVs at the level of the HMS (F, 30hpf) and the missing connections within the DLAV (G, 36hpf) were counted in 8 vessels per animal. *Cldn5b* MO2 injection causes more vessels with these phenotypes (F, G). Also at 52hpf MO2 caused more ISVs per embryo to show a lack of connection within the DLAV (M). HMS: horizontal myoseptum

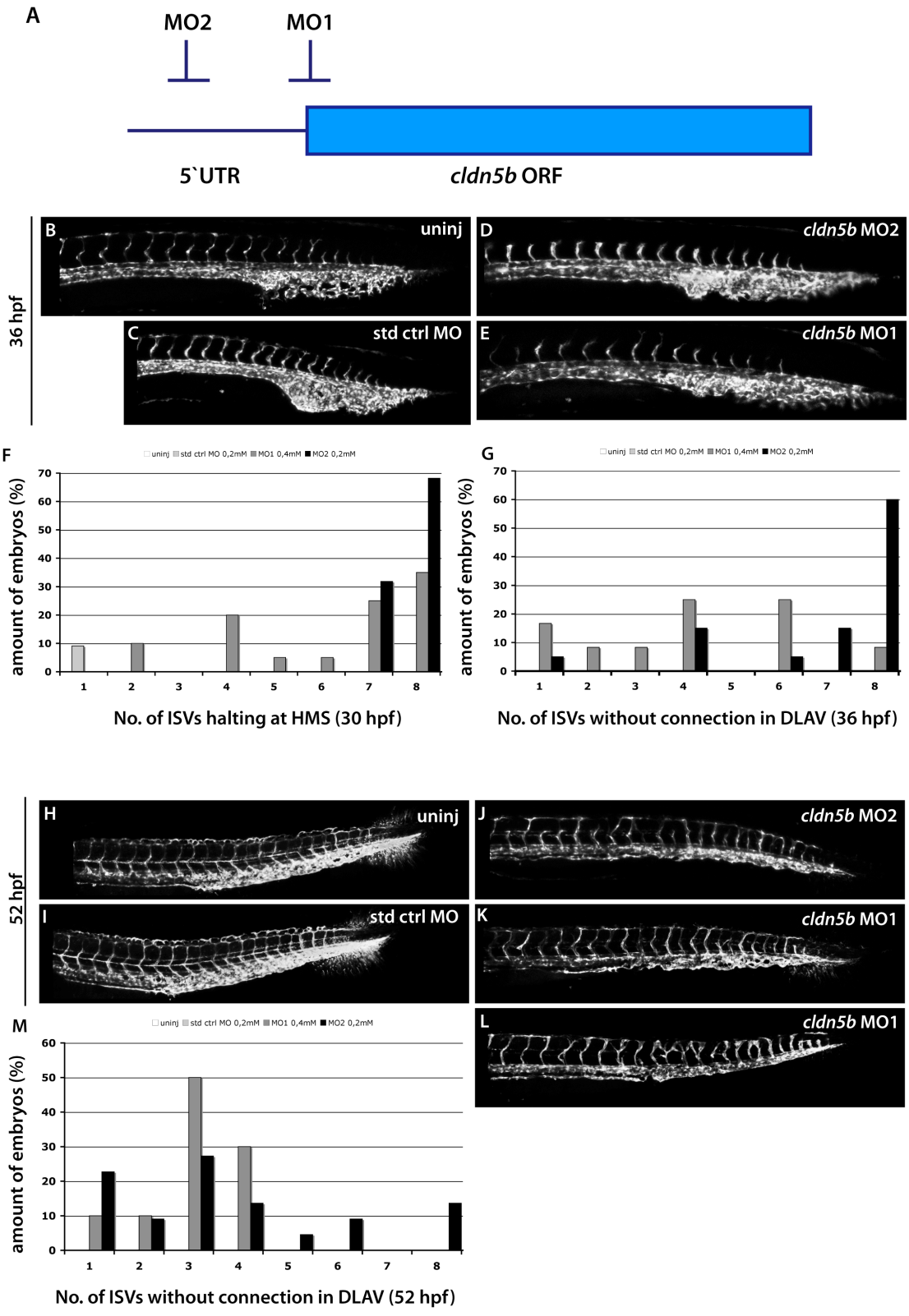
A
MO2
MO1
5`UTR
cldn5b ORF
36 hpf
B
uninj
C
std ctrl MO
D
cldn5b MO2
E
cldn5b MO1
F
uninj std ctrl MO 0,2mM MO1 0,4mM MO2 0,2mM
amount of embryos (%)
No. of ISVs halting at HMS (30 hpf)
G
uninj std ctrl MO 0,2mM MO1 0,4mM MO2 0,2mM
amount of embryos (%)
No. of ISVs without connection in DLAV (36 hpf)
52 hpf
H
uninj
I
std ctrl MO
J
cldn5b MO2
K
cldn5b MO1
L
cldn5b MO1
M
uninj std ctrl MO 0,2mM MO1 0,4mM MO2 0,2mM
amount of embryos (%)
No. of ISVs without connection in DLAV (52 hpf)

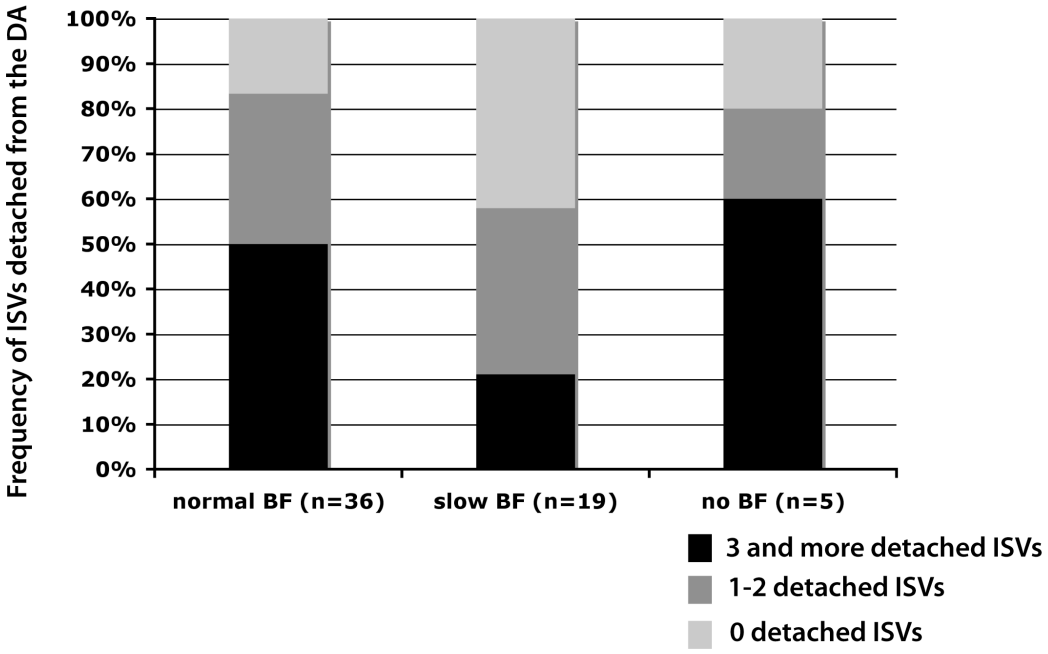

Supplementary Figure 5: The lack of blood flow does not influence the phenotypic penetrance in *cldn5b* morphants. Correlation between normal, slow and no blood flow and the detachment of ISVs from the aorta. Detached ISVs were counted in embryos expressing fli1a:EGFP. 50% of embryos with normal blood flow display 3 and more detached ISVs and less than 20% show no detached ISV from the aorta. Compared to that roughly 20% of embryos with slow blood flow have 3 and more detached ISVs and more than 40% of these embryos show no detached ISV. In embryos without any blood flow, 60% of the embryos reveal 3 and more detached ISVs and 20% without detached ISVs. A clear correlation between the phenotype strengths and the presence/absence of blood flow can therfore not be made. BF= blood flow.

8.2 Supplementary Lists

8.2.1 Supplementary list 1 of primers

name	sequence (5`-> 3`)
GFF for	CACCATGAAGCTACTGTCTTC
GFF rev	TTAGTTACCCGGGAGCATATC
CACC cldn5b for	CACCATGATTTCTGCATGTCTGG
cldn5b rev	GATAAACGAAACTACGTCTGA
cldn5b rev wo stop	CTATGATAAACGAAACTACGTC
p3EattB2cldn5bfor	GGGGACAGCTTTCTTGTACAAAGTGGAGATGATTTCTGCATGTCTGGAG
p3EattB3cldn5brev	GGGGACAACTTTGTATAATAAAGTTGCTCAGACGTAGTTTCGTTTATCATAG
mKate for EcoRI rescue	GGAATTCCATGGTGAGCGAGCTGATTAAG
mKate rev XbaI rescue	GCTCTAGATCTGTGCCCCAGTTTGCTAGG
Claudin5b for EcoRI rescue	GGAATTCCATGATTTCTGCATGTCTGG
Claudin5b rev XbaI rescue	GCTCTAGAGACGTAGTTTCGTTTATC
screening primer HinfI cldn5b for	ATGATTTCTGCATGTCTGGAGATTGTTGcACTCTG
screening primer HinfI cldn5b rev	CAGCGCCAGGACAGAGTgGTGCAT

8.2.2 Supplementary list 2 of morpholinos

name	sequence	reference
cldn5b MO1	CCAGACATGCAGAAATCATATTTGC	this study
cldn5b MO2	TCAGAAGCAGCAGAAGTGTCTCTAC	this study
cldn5a MO	AGGCCATCGCTTTCTTTTCCCACTC	Zhang et al., 2010
standard control MO	CCTCTTACCTCAGTTACAATTTATA	
p53 MO	GCGCCATTGCTTTGCAAGAATTG	Robu et al., 2007

9. Appendix

9.1 Generation of the *fli1ep*:gal4ff construct

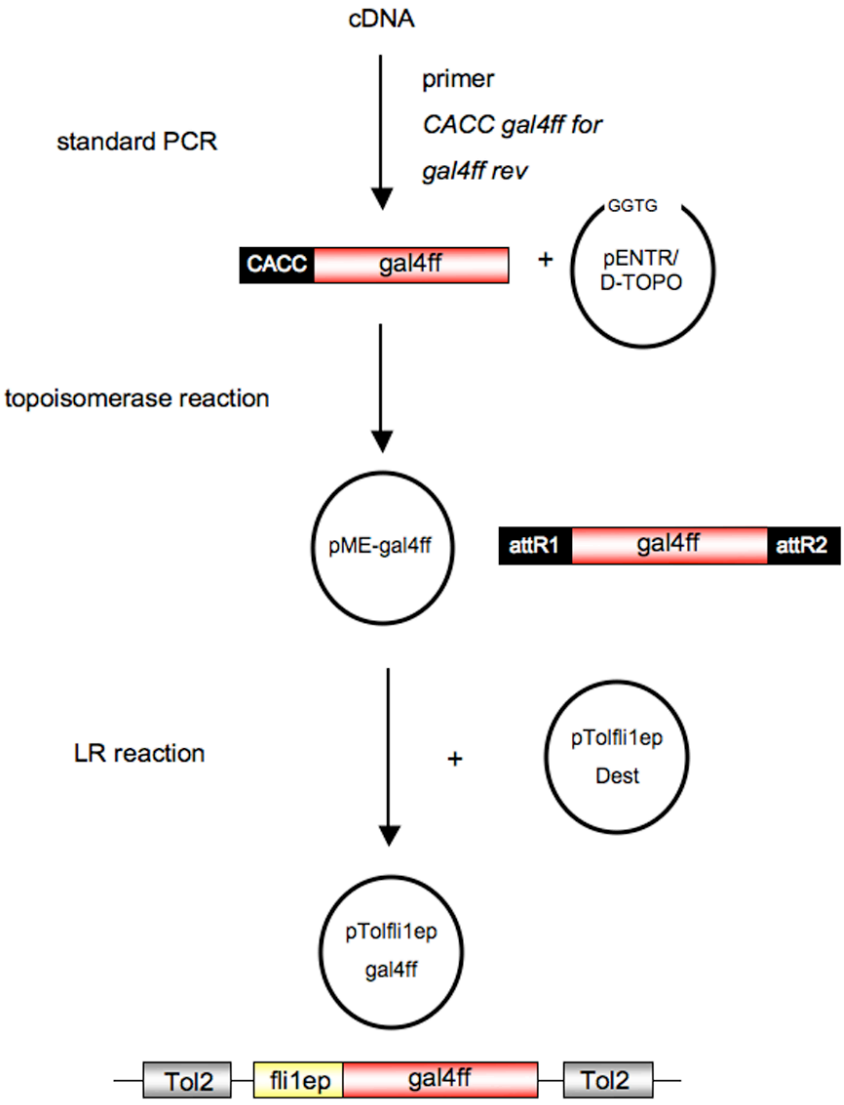

9.2 Generation of the *fli1ep*:nlsmCherry construct

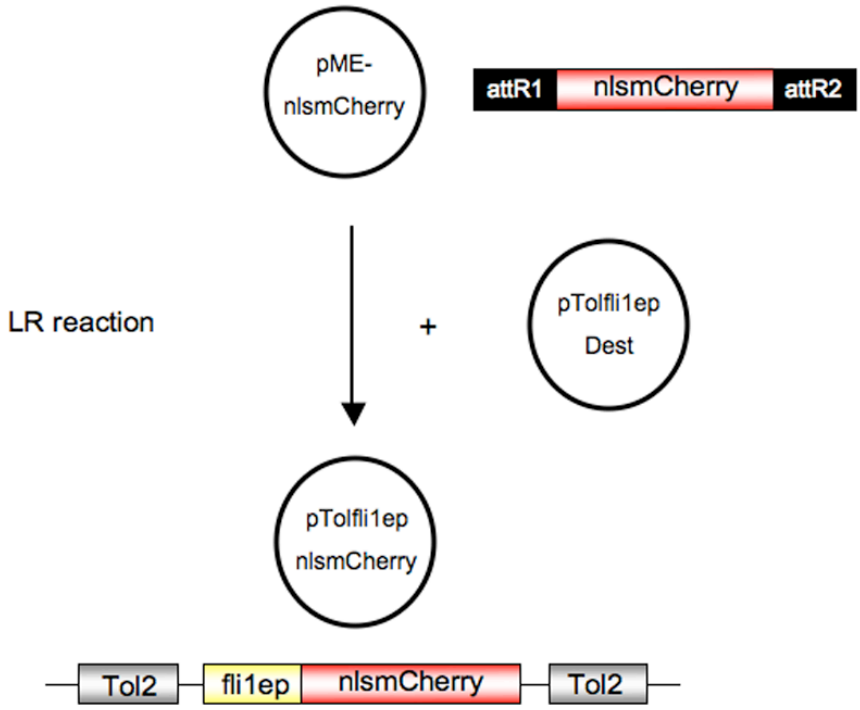

9.3 Generation of the UAS:*cldn5b*:EGFP construct

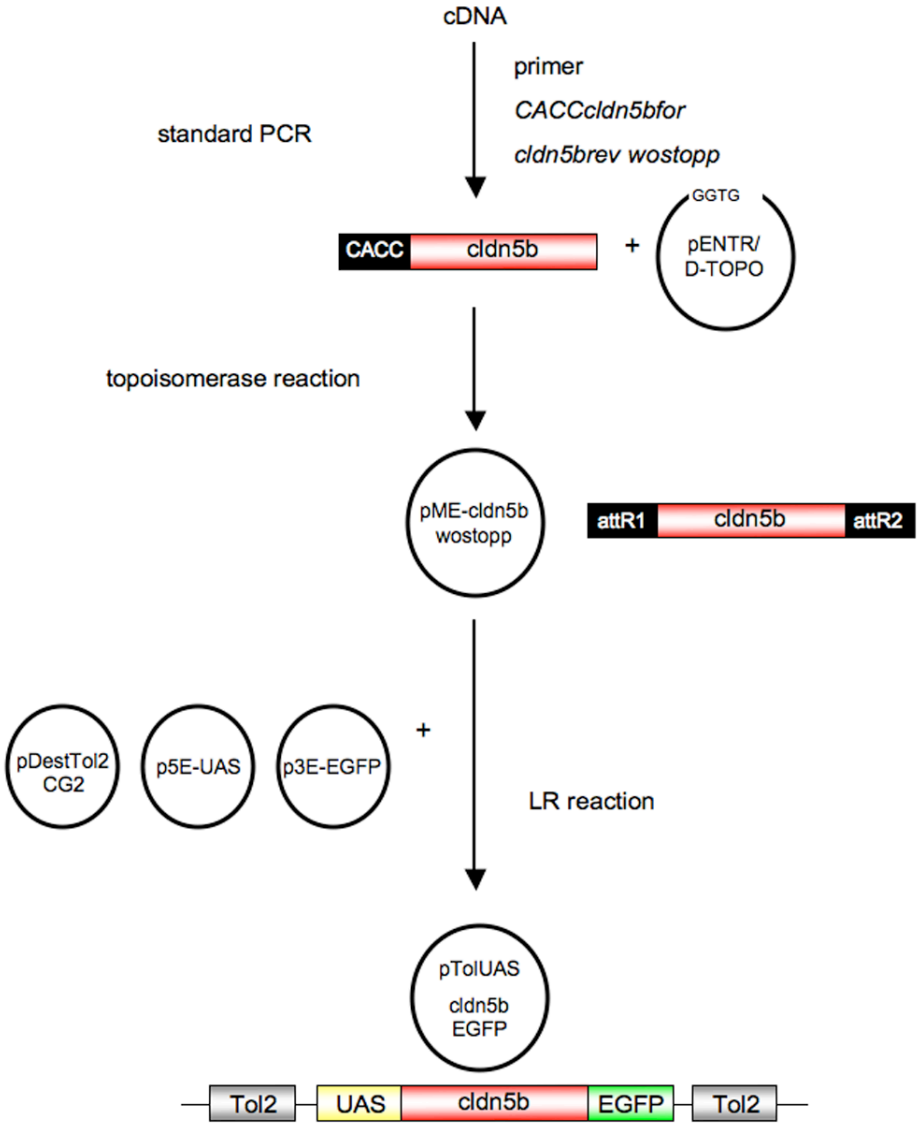

10. References

Abraham, S., Yeo, M., Montero-Balaguer, M., Paterson, H., Dejana, E., Marshall, C. J. and Mavria, G. (2009). VE-Cadherin-mediated cell-cell interaction suppresses sprouting via signaling to MLC2 phosphorylation. *Curr Biol* **19**, 668-74.

Adams, C. L., Nelson, W. J. and Smith, S. J. (1996). Quantitative analysis of cadherin-catenin-actin reorganization during development of cell-cell adhesion. *J Cell Biol* **135**, 1899-911.

Alexandre, M. D., Lu, Q. and Chen, Y. H. (2005). Overexpression of claudin-7 decreases the paracellular Cl- conductance and increases the paracellular Na+ conductance in LLC-PK1 cells. *J Cell Sci* **118**, 2683-93.

Amasheh, S., Meiri, N., Gitter, A. H., Schoneberg, T., Mankertz, J., Schulzke, J. D. and Fromm, M. (2002). Claudin-2 expression induces cation-selective channels in tight junctions of epithelial cells. *J Cell Sci* **115**, 4969-76.

Anderson, J. M. and Van Itallie, C. M. (2009). Physiology and function of the tight junction. *Cold Spring Harb Perspect Biol* **1**, a002584.

Ando-Akatsuka, Y., Yonemura, S., Itoh, M., Furuse, M. and Tsukita, S. (1999). Differential behavior of E-cadherin and occludin in their colocalization with ZO-1 during the establishment of epithelial cell polarity. *J Cell Physiol* **179**, 115-25.

Aono, S. and Hirai, Y. (2008). Phosphorylation of claudin-4 is required for tight junction formation in a human keratinocyte cell line. *Exp Cell Res* **314**, 3326-39.

Arabzadeh, A., Troy, T. C. and Turksen, K. (2006). Role of the Cldn6 cytoplasmic tail domain in membrane targeting and epidermal differentiation in vivo. *Mol Cell Biol* **26**, 5876-87.

Arboleda-Estudillo, Y., Krieg, M., Stuhmer, J., Licata, N. A., Muller, D. J. and Heisenberg, C. P. (2010). Movement directionality in collective migration of germ layer progenitors. *Curr Biol* **20**, 161-9.

Argaw, A. T., Gurfein, B. T., Zhang, Y., Zameer, A. and John, G. R. (2009). VEGF-mediated disruption of endothelial CLN-5 promotes blood-brain barrier breakdown. *Proc Natl Acad Sci U S A* **106**, 1977-82.

Asakawa, K. and Kawakami, K. (2008). Targeted gene expression by the Gal4-UAS system in zebrafish. *Dev Growth Differ* **50**, 391-9.

Asakura, T., Nakanishi, H., Sakisaka, T., Takahashi, K., Mandai, K., Nishimura, M., Sasaki, T. and Takai, Y. (1999). Similar and differential behaviour between the nectin-afadin-ponsin and cadherin-catenin systems during the formation and disruption of the polarized junctional alignment in epithelial cells. *Genes Cells* **4**, 573-81.

Autiero, M., Waltenberger, J., Communi, D., Kranz, A., Moons, L., Lambrechts, D., Kroll, J., Plaisance, S., De Mol, M., Bono, F. et al. (2003). Role of PlGF in the intra- and intermolecular cross talk between the VEGF receptors Flt1 and Flk1. *Nat Med* **9**, 936-43.

Baer, M. M., Chanut-Delalande, H. and Affolter, M. (2009). Cellular and molecular mechanisms underlying the formation of biological tubes. *Curr Top Dev Biol* **89**, 137-62.

Bagnat, M., Cheung, I. D., Mostov, K. E. and Stainier, D. Y. (2007). Genetic control of single lumen formation in the zebrafish gut. *Nat Cell Biol* **9**, 954-60.

Balda, M. S., Garrett, M. D. and Matter, K. (2003). The ZO-1-associated Y-box factor ZONAB regulates epithelial cell proliferation and cell density. *J Cell Biol* **160**, 423-32.

Balda, M. S. and Matter, K. (2000). The tight junction protein ZO-1 and an interacting transcription factor regulate ErbB-2 expression. *EMBO J* **19**, 2024-33.

Balda, M. S. and Matter, K. (2009). Tight junctions and the regulation of gene expression. *Biochim Biophys Acta* **1788**, 761-7.

Baribault, H., Penner, J., Iozzo, R. V. and Wilson-Heiner, M. (1994). Colorectal hyperplasia and inflammation in keratin 8-deficient FVB/N mice. *Genes Dev* **8**, 2964-73.

Baribault, H., Price, J., Miyai, K. and Oshima, R. G. (1993). Mid-gestational lethality in mice lacking keratin 8. *Genes Dev* **7**, 1191-202.

Baum, B. and Georgiou, M. (2011). Dynamics of adherens junctions in epithelial establishment, maintenance, and remodeling. *J Cell Biol* **192**, 907-17.

Bazzoni, G. and Dejana, E. (2004). Endothelial cell-to-cell junctions: molecular organization and role in vascular homeostasis. *Physiol Rev* **84**, 869-901.

Behr, M., Riedel, D. and Schuh, R. (2003). The claudin-like megatrachea is essential in septate junctions for the epithelial barrier function in Drosophila. *Dev Cell* **5**, 611-20.
Bellomo, D., Headrick, J. P., Silins, G. U., Paterson, C. A., Thomas, P. S., Gartside, M., Mould, A., Cahill, M. M., Tonks, I. D., Grimmond, S. M. et al. (2000). Mice lacking the vascular endothelial growth factor-B gene (Vegfb) have smaller hearts, dysfunctional coronary vasculature, and impaired recovery from cardiac ischemia. *Circ Res* **86**, E29-35.
Bellusci, S., Grindley, J., Emoto, H., Itoh, N. and Hogan, B. L. (1997). Fibroblast growth factor 10 (FGF10) and branching morphogenesis in the embryonic mouse lung. *Development* **124**, 4867-78.
Ben-Yosef, T., Belyantseva, I. A., Saunders, T. L., Hughes, E. D., Kawamoto, K., Van Itallie, C. M., Beyer, L. A., Halsey, K., Gardner, D. J., Wilcox, E. R. et al. (2003). Claudin 14 knockout mice, a model for autosomal recessive deafness DFNB29, are deaf due to cochlear hair cell degeneration. *Hum Mol Genet* **12**, 2049-61.
Ben-Ze'ev, A. and Geiger, B. (1998). Differential molecular interactions of beta-catenin and plakoglobin in adhesion, signaling and cancer. *Curr Opin Cell Biol* **10**, 629-39.
Bergantinos, C., Corominas, M. and Serras, F. (2010). Cell death-induced regeneration in wing imaginal discs requires JNK signalling. *Development* **137**, 1169-79.
Bienz, M. and Clevers, H. (2000). Linking colorectal cancer to Wnt signaling. *Cell* **103**, 311-20.
Bignon, M., Pichol-Thievend, C., Hardouin, J., Malbouyres, M., Brechot, N., Nasciutti, L., Barret, A., Teillon, J., Guillon, E., Etienne, E. et al. (2011). Lysyl oxidase-like protein-2 regulates sprouting angiogenesis and type IV collagen assembly in the endothelial basement membrane. *Blood*.
Blum, Y., Belting, H. G., Ellertsdottir, E., Herwig, L., Luders, F. and Affolter, M. (2008). Complex cell rearrangements during intersegmental vessel sprouting and vessel fusion in the zebrafish embryo. *Dev Biol* **316**, 312-22.
Bouvree, K., Larrivee, B., Lv, X., Yuan, L., DeLafarge, B., Freitas, C., Mathivet, T., Breant, C., Tessier-Lavigne, M., Bikfalvi, A. et al. (2008). Netrin-1 inhibits sprouting angiogenesis in developing avian embryos. *Dev Biol* **318**, 172-83.
Brady, C. A., Jiang, D., Mello, S. S., Johnson, T. M., Jarvis, L. A., Kozak, M. M., Kenzelmann Broz, D., Basak, S., Park, E. J., McLaughlin, M. E. et al. (2011). Distinct p53 transcriptional programs dictate acute DNA-damage responses and tumor suppression. *Cell* **145**, 571-83.
Bretaud, S., Macraild, S., Ingham, P. W. and Bandmann, O. (2011). The Influence of the Zebrafish Genetic Background on Parkinson's Disease-Related Aspects. *Zebrafish*.
Brown, L. A., Rodaway, A. R., Schilling, T. F., Jowett, T., Ingham, P. W., Patient, R. K. and Sharrocks, A. D. (2000). Insights into early vasculogenesis revealed by expression of the ETS-domain transcription factor Fli-1 in wild-type and mutant zebrafish embryos. *Mech Dev* **90**, 237-52.
Brown, L. J., Alawoki, M., Crawford, M. E., Reida, T., Sears, A., Torma, T. and Albig, A. R. (2010). Lipocalin-7 is a matricellular regulator of angiogenesis. *PLoS One* **5**, e13905.
Bussmann, J., Bos, F. L., Urasaki, A., Kawakami, K., Duckers, H. J. and Schulte-Merker, S. (2010). Arteries provide essential guidance cues for lymphatic endothelial cells in the zebrafish trunk. *Development* **137**, 2653-7.
Bussmann, J., Wolfe, S. A. and Siekmann, A. F. (2011). Arterial-venous network formation during brain vascularization involves hemodynamic regulation of chemokine signaling. *Development* **138**, 1717-26.
Capaldo, C. T., Koch, S., Kwon, M., Laur, O., Parkos, C. A. and Nusrat, A. (2011). Tight function zonula occludens-3 regulates cyclin D1-dependent cell proliferation. *Mol Biol Cell* **22**, 1677-85.
Cardoso, W. V. and Lu, J. (2006). Regulation of early lung morphogenesis: questions, facts and controversies. *Development* **133**, 1611-24.
Carmeliet, P., Ferreira, V., Breier, G., Pollefeyt, S., Kieckens, L., Gertsenstein, M., Fahrig, M., Vandenhoeck, A., Harpal, K., Eberhardt, C. et al. (1996). Abnormal blood vessel development and lethality in embryos lacking a single VEGF allele. *Nature* **380**, 435-9.
Carmeliet, P., Lampugnani, M. G., Moons, L., Breviario, F., Compernolle, V., Bono, F., Balconi, G., Spagnuolo, R., Oosthuyse, B., Dewerchin, M. et al. (1999). Targeted deficiency or cytosolic truncation of the VE-cadherin gene in mice impairs VEGF-mediated endothelial survival and angiogenesis. *Cell* **98**, 147-57.

Carmeliet, P., Moons, L., Luttun, A., Vincenti, V., Compernolle, V., De Mol, M., Wu, Y., Bono, F., Devy, L., Beck, H. et al. (2001). Synergism between vascular endothelial growth factor and placental growth factor contributes to angiogenesis and plasma extravasation in pathological conditions. *Nat Med* **7**, 575-83.
Caussinus, E., Colombelli, J. and Affolter, M. (2008). Tip-cell migration controls stalk-cell intercalation during Drosophila tracheal tube elongation. *Curr Biol* **18**, 1727-34.
Chappell, J. C., Taylor, S. M., Ferrara, N. and Bautch, V. L. (2009). Local guidance of emerging vessel sprouts requires soluble Flt-1. *Dev Cell* **17**, 377-86.
Chico, T. J., Ingham, P. W. and Crossman, D. C. (2008). Modeling cardiovascular disease in the zebrafish. *Trends Cardiovasc Med* **18**, 150-5.
Childs, S., Chen, J. N., Garrity, D. M. and Fishman, M. C. (2002). Patterning of angiogenesis in the zebrafish embryo. *Development* **129**, 973-82.
Choi, J., Mouillesseaux, K., Wang, Z., Fiji, H. D., Kinderman, S. S., Otto, G. W., Geisler, R., Kwon, O. and Chen, J. N. (2011). Aplexone targets the HMG-CoA reductase pathway and differentially regulates arteriovenous angiogenesis. *Development* **138**, 1173-81.
Chun, T. H., Sabeh, F., Ota, I., Murphy, H., McDonagh, K. T., Holmbeck, K., Birkedal-Hansen, H., Allen, E. D. and Weiss, S. J. (2004). MT1-MMP-dependent neovessel formation within the confines of the three-dimensional extracellular matrix. *J Cell Biol* **167**, 757-67.
Classen, A. K., Anderson, K. I., Marois, E. and Eaton, S. (2005). Hexagonal packing of Drosophila wing epithelial cells by the planar cell polarity pathway. *Dev Cell* **9**, 805-17.
Cleaver, O. and Krieg, P. A. (1998). VEGF mediates angioblast migration during development of the dorsal aorta in Xenopus. *Development* **125**, 3905-14.
Colegio, O. R., Van Itallie, C., Rahner, C. and Anderson, J. M. (2003). Claudin extracellular domains determine paracellular charge selectivity and resistance but not tight junction fibril architecture. *Am J Physiol Cell Physiol* **284**, C1346-54.
Coultas, L., Chawengsaksophak, K. and Rossant, J. (2005). Endothelial cells and VEGF in vascular development. *Nature* **438**, 937-45.
Crosby, C. V., Fleming, P. A., Argraves, W. S., Corada, M., Zanetta, L., Dejana, E. and Drake, C. J. (2005). VE-cadherin is not required for the formation of nascent blood vessels but acts to prevent their disassembly. *Blood* **105**, 2771-6.
Davidson, A. E., Balciunas, D., Mohn, D., Shaffer, J., Hermanson, S., Sivasubbu, S., Cliff, M. P., Hackett, P. B. and Ekker, S. C. (2003). Efficient gene delivery and gene expression in zebrafish using the Sleeping Beauty transposon. *Dev Biol* **263**, 191-202.
Dejana, E. (2004). Endothelial cell-cell junctions: happy together. *Nat Rev Mol Cell Biol* **5**, 261-70.
del Toro, R., Prahst, C., Mathivet, T., Siegfried, G., Kaminker, J. S., Larrivee, B., Breant, C., Duarte, A., Takakura, N., Fukamizu, A. et al. (2010). Identification and functional analysis of endothelial tip cell-enriched genes. *Blood* **116**, 4025-33.
Detrich, H. W., 3rd, Kieran, M. W., Chan, F. Y., Barone, L. M., Yee, K., Rundstadler, J. A., Pratt, S., Ransom, D. and Zon, L. I. (1995). Intraembryonic hematopoietic cell migration during vertebrate development. *Proc Natl Acad Sci U S A* **92**, 10713-7.
Doyon, Y., McCammon, J. M., Miller, J. C., Faraji, F., Ngo, C., Katibah, G. E., Amora, R., Hocking, T. D., Zhang, L., Rebar, E. J. et al. (2008). Heritable targeted gene disruption in zebrafish using designed zinc-finger nucleases. *Nat Biotechnol* **26**, 702-8.
Du, D., Xu, F., Yu, L., Zhang, C., Lu, X., Yuan, H., Huang, Q., Zhang, F., Bao, H., Jia, L. et al. (2010). The tight junction protein, occludin, regulates the directional migration of epithelial cells. *Dev Cell* **18**, 52-63.
Dudek, S. M. and Garcia, J. G. (2001). Cytoskeletal regulation of pulmonary vascular permeability. *J Appl Physiol* **91**, 1487-500.
Ebnet, K. (2008). Organization of multiprotein complexes at cell-cell junctions. *Histochem Cell Biol* **130**, 1-20.
Ebnet, K., Suzuki, A., Horikoshi, Y., Hirose, T., Meyer Zu Brickwedde, M. K., Ohno, S. and Vestweber, D. (2001). The cell polarity protein ASIP/PAR-3 directly associates with junctional adhesion molecule (JAM). *EMBO J* **20**, 3738-48.
Eichmann, A., Le Noble, F., Autiero, M. and Carmeliet, P. (2005). Guidance of vascular and neural network formation. *Curr Opin Neurobiol* **15**, 108-15.
Ekker, S. C. (2008). Zinc finger-based knockout punches for zebrafish genes. *Zebrafish* **5**, 121-3.
Ellertsdottir, E., Lenard, A., Blum, Y., Krudewig, A., Herwig, L., Affolter, M. and Belting, H. G. (2010). Vascular morphogenesis in the zebrafish embryo. *Dev Biol* **341**, 56-65.

Elvert, G., Kappel, A., Heidenreich, R., Englmeier, U., Lanz, S., Acker, T., Rauter, M., Plate, K., Sieweke, M., Breier, G. et al. (2003). Cooperative interaction of hypoxia-inducible factor-2alpha (HIF-2alpha) and Ets-1 in the transcriptional activation of vascular endothelial growth factor receptor-2 (Flk-1). *J Biol Chem* **278**, 7520-30.
Eriksson, J. and Lofberg, J. (2000). Development of the hypochord and dorsal aorta in the zebrafish embryo (Danio rerio). *J Morphol* **244**, 167-76.
Ernkvist, M., Luna Persson, N., Audebert, S., Lecine, P., Sinha, I., Liu, M., Schlueter, M., Horowitz, A., Aase, K., Weide, T. et al. (2009). The Amot/Patj/Syx signaling complex spatially controls RhoA GTPase activity in migrating endothelial cells. *Blood* **113**, 244-53.
Fanning, A. S., Jameson, B. J., Jesaitis, L. A. and Anderson, J. M. (1998). The tight junction protein ZO-1 establishes a link between the transmembrane protein occludin and the actin cytoskeleton. *J Biol Chem* **273**, 29745-53.
Farquhar, M. G., Palade, G.E. (1963). Junctional complexes in various epithelia. *J Cell Biol* **17**, 375-412.
Ferrara, N., Carver-Moore, K., Chen, H., Dowd, M., Lu, L., O'Shea, K. S., Powell-Braxton, L., Hillan, K. J. and Moore, M. W. (1996). Heterozygous embryonic lethality induced by targeted inactivation of the VEGF gene. *Nature* **380**, 439-42.
FitzPatrick, D. R., Ramsay, J., McGill, N. I., Shade, M., Carothers, A. D. and Hastie, N. D. (2002). Transcriptome analysis of human autosomal trisomy. *Hum Mol Genet* **11**, 3249-56.
Fong, G. H., Rossant, J., Gertsenstein, M. and Breitman, M. L. (1995). Role of the Flt-1 receptor tyrosine kinase in regulating the assembly of vascular endothelium. *Nature* **376**, 66-70.
Fong, G. H., Zhang, L., Bryce, D. M. and Peng, J. (1999). Increased hemangioblast commitment, not vascular disorganization, is the primary defect in flt-1 knock-out mice. *Development* **126**, 3015-25.
Fraisl, P., Mazzone, M., Schmidt, T. and Carmeliet, P. (2009). Regulation of angiogenesis by oxygen and metabolism. *Dev Cell* **16**, 167-79.
Franks, D. M., Izumikawa, T., Kitagawa, H., Sugahara, K. and Okkema, P. G. (2006). C. elegans pharyngeal morphogenesis requires both de novo synthesis of pyrimidines and synthesis of heparan sulfate proteoglycans. *Dev Biol* **296**, 409-20.
Furuse, M. (2010). Molecular basis of the core structure of tight junctions. *Cold Spring Harb Perspect Biol* **2**, a002907.
Furuse, M., Fujita, K., Hiiragi, T., Fujimoto, K. and Tsukita, S. (1998). Claudin-1 and -2: novel integral membrane proteins localizing at tight junctions with no sequence similarity to occludin. *J Cell Biol* **141**, 1539-50.
Furuse, M., Hata, M., Furuse, K., Yoshida, Y., Haratake, A., Sugitani, Y., Noda, T., Kubo, A. and Tsukita, S. (2002). Claudin-based tight junctions are crucial for the mammalian epidermal barrier: a lesson from claudin-1-deficient mice. *J Cell Biol* **156**, 1099-111.
Furuse, M., Sasaki, H. and Tsukita, S. (1999). Manner of interaction of heterogeneous claudin species within and between tight junction strands. *J Cell Biol* **147**, 891-903.
Gelfand, M. V., Hong, S. and Gu, C. (2009). Guidance from above: common cues direct distinct signaling outcomes in vascular and neural patterning. *Trends Cell Biol* **19**, 99-110.
Gerhardt, H., Golding, M., Fruttiger, M., Ruhrberg, C., Lundkvist, A., Abramsson, A., Jeltsch, M., Mitchell, C., Alitalo, K., Shima, D. et al. (2003). VEGF guides angiogenic sprouting utilizing endothelial tip cell filopodia. *J Cell Biol* **161**, 1163-77.
Gering, M., Rodaway, A. R., Gottgens, B., Patient, R. K. and Green, A. R. (1998). The SCL gene specifies haemangioblast development from early mesoderm. *EMBO J* **17**, 4029-45.
Ghabrial, A. S. and Krasnow, M. A. (2006). Social interactions among epithelial cells during tracheal branching morphogenesis. *Nature* **441**, 746-9.
Gitler, A. D., Lu, M. M. and Epstein, J. A. (2004). PlexinD1 and semaphorin signaling are required in endothelial cells for cardiovascular development. *Dev Cell* **7**, 107-16.
Goll, M. G., Anderson, R., Stainier, D. Y., Spradling, A. C. and Halpern, M. E. (2009). Transcriptional silencing and reactivation in transgenic zebrafish. *Genetics* **182**, 747-55.
Goodenough, D. A. and Revel, J. P. (1970). A fine structural analysis of intercellular junctions in the mouse liver. *J Cell Biol* **45**, 272-90.
Gorfinkiel, N. and Arias, A. M. (2007). Requirements for adherens junction components in the interaction between epithelial tissues during dorsal closure in Drosophila. *J Cell Sci* **120**, 3289-98.

Gu, C., Yoshida, Y., Livet, J., Reimert, D. V., Mann, F., Merte, J., Henderson, C. E., Jessell, T. M., Kolodkin, A. L. and Ginty, D. D. (2005). Semaphorin 3E and plexin-D1 control vascular pattern independently of neuropilins. *Science* **307**, 265-8.
Gumbiner, B., Stevenson, B. and Grimaldi, A. (1988). The role of the cell adhesion molecule uvomorulin in the formation and maintenance of the epithelial junctional complex. *J Cell Biol* **107**, 1575-87.
Guo, D., Jia, Q., Song, H. Y., Warren, R. S. and Donner, D. B. (1995). Vascular endothelial cell growth factor promotes tyrosine phosphorylation of mediators of signal transduction that contain SH2 domains. Association with endothelial cell proliferation. *J Biol Chem* **270**, 6729-33.
Guo, R., Sakamoto, H., Sugiura, S. and Ogawa, M. (2007). Endothelial cell motility is compatible with junctional integrity. *J Cell Physiol* **211**, 327-35.
Gupta, V., Parisi, M., Sturgill, D., Nuttall, R., Doctolero, M., Dudko, O. K., Malley, J. D., Eastman, P. S. and Oliver, B. (2006). Global analysis of X-chromosome dosage compensation. *J Biol* **5**, 3.
Harrington, L. S., Sainson, R. C., Williams, C. K., Taylor, J. M., Shi, W., Li, J. L. and Harris, A. L. (2008). Regulation of multiple angiogenic pathways by Dll4 and Notch in human umbilical vein endothelial cells. *Microvasc Res* **75**, 144-54.
Hartsock, A. and Nelson, W. J. (2008). Adherens and tight junctions: structure, function and connections to the actin cytoskeleton. *Biochim Biophys Acta* **1778**, 660-9.
Haskins, J., Gu, L., Wittchen, E. S., Hibbard, J. and Stevenson, B. R. (1998). ZO-3, a novel member of the MAGUK protein family found at the tight junction, interacts with ZO-1 and occludin. *J Cell Biol* **141**, 199-208.
Heicklen-Klein, A., McReynolds, L. J. and Evans, T. (2005). Using the zebrafish model to study GATA transcription factors. *Semin Cell Dev Biol* **16**, 95-106.
Hellstrom, M., Phng, L. K., Hofmann, J. J., Wallgard, E., Coultas, L., Lindblom, P., Alva, J., Nilsson, A. K., Karlsson, L., Gaiano, N. et al. (2007). Dll4 signalling through Notch1 regulates formation of tip cells during angiogenesis. *Nature* **445**, 776-80.
Herbert, S. P., Huisken, J., Kim, T. N., Feldman, M. E., Houseman, B. T., Wang, R. A., Shokat, K. M. and Stainier, D. Y. (2009). Arterial-venous segregation by selective cell sprouting: an alternative mode of blood vessel formation. *Science* **326**, 294-8.
Herzog, Y., Guttmann-Raviv, N. and Neufeld, G. (2005). Segregation of arterial and venous markers in subpopulations of blood islands before vessel formation. *Dev Dyn* **232**, 1047-55.
Hiratsuka, S., Nakao, K., Nakamura, K., Katsuki, M., Maru, Y. and Shibuya, M. (2005). Membrane fixation of vascular endothelial growth factor receptor 1 ligand-binding domain is important for vasculogenesis and angiogenesis in mice. *Mol Cell Biol* **25**, 346-54.
Hogan, B. M., Bos, F. L., Bussmann, J., Witte, M., Chi, N. C., Duckers, H. J. and Schulte-Merker, S. (2009). Ccbe1 is required for embryonic lymphangiogenesis and venous sprouting. *Nat Genet* **41**, 396-8.
Huang, C. C., Wang, T. C., Lin, B. H., Wang, Y. W., Johnson, S. L. and Yu, J. (2009). Collagen IX is required for the integrity of collagen II fibrils and the regulation of vascular plexus formation in zebrafish caudal fins. *Dev Biol* **332**, 360-70.
Hurov, J. B., Watkins, J. L. and Piwnica-Worms, H. (2004). Atypical PKC phosphorylates PAR-1 kinases to regulate localization and activity. *Curr Biol* **14**, 736-41.
Ikenouchi, J., Umeda, K., Tsukita, S. and Furuse, M. (2007). Requirement of ZO-1 for the formation of belt-like adherens junctions during epithelial cell polarization. *J Cell Biol* **176**, 779-86.
Ishizaki, T., Chiba, H., Kojima, T., Fujibe, M., Soma, T., Miyajima, H., Nagasawa, K., Wada, I. and Sawada, N. (2003). Cyclic AMP induces phosphorylation of claudin-5 immunoprecipitates and expression of claudin-5 gene in blood-brain-barrier endothelial cells via protein kinase A-dependent and -independent pathways. *Exp Cell Res* **290**, 275-88.
Isogai, S., Horiguchi, M. and Weinstein, B. M. (2001). The vascular anatomy of the developing zebrafish: an atlas of embryonic and early larval development. *Dev Biol* **230**, 278-301.
Isogai, S., Lawson, N. D., Torrealday, S., Horiguchi, M. and Weinstein, B. M. (2003). Angiogenic network formation in the developing vertebrate trunk. *Development* **130**, 5281-90.
Itoh, M., Furuse, M., Morita, K., Kubota, K., Saitou, M. and Tsukita, S. (1999a). Direct binding of three tight junction-associated MAGUKs, ZO-1, ZO-2, and ZO-3, with the COOH termini of claudins. *J Cell Biol* **147**, 1351-63.

Itoh, M., Morita, K. and Tsukita, S. (1999b). Characterization of ZO-2 as a MAGUK family member associated with tight as well as adherens junctions with a binding affinity to occludin and alpha catenin. *J Biol Chem* **274**, 5981-6.
Jakobsson, L., Franco, C. A., Bentley, K., Collins, R. T., Ponsioen, B., Aspalter, I. M., Rosewell, I., Busse, M., Thurston, G., Medvinsky, A. et al. (2010). Endothelial cells dynamically compete for the tip cell position during angiogenic sprouting. *Nat Cell Biol* **12**, 943-53.
Jargiello, D. M. and Caplan, A. I. (1983). The fluid flow dynamics in the developing chick wing. *Prog Clin Biol Res* **110 Pt A**, 143-54.
Jelcick, A. S., Yuan, Y., Leehy, B. D., Cox, L. C., Silveira, A. C., Qiu, F., Schenk, S., Sachs, A. J., Morrison, M. A., Nystuen, A. M. et al. (2011). Genetic variations strongly influence phenotypic outcome in the mouse retina. *PLoS One* **6**, e21858.
Jeon, T. J., Lee, S., Weeks, G. and Firtel, R. A. (2009). Regulation of Dictyostelium morphogenesis by RapGAP3. *Dev Biol* **328**, 210-20.
Jeong, J. Y., Kwon, H. B., Ahn, J. C., Kang, D., Kwon, S. H., Park, J. A. and Kim, K. W. (2008). Functional and developmental analysis of the blood-brain barrier in zebrafish. *Brain Res Bull* **75**, 619-28.
Jin, S. W., Beis, D., Mitchell, T., Chen, J. N. and Stainier, D. Y. (2005). Cellular and molecular analyses of vascular tube and lumen formation in zebrafish. *Development* **132**, 5199-209.
Kallianpur, A. R., Jordan, J. E. and Brandt, S. J. (1994). The SCL/TAL-1 gene is expressed in progenitors of both the hematopoietic and vascular systems during embryogenesis. *Blood* **83**, 1200-8.
Kappler, J. A., Starr, C. J., Chan, D. K., Kollmar, R. and Hudspeth, A. J. (2004). A nonsense mutation in the gene encoding a zebrafish myosin VI isoform causes defects in hair-cell mechanotransduction. *Proc Natl Acad Sci U S A* **101**, 13056-61.
Kawakami, K. (2007). Tol2: a versatile gene transfer vector in vertebrates. *Genome Biol* **8 Suppl 1**, S7.
Kawakami, K., Shima, A. and Kawakami, N. (2000). Identification of a functional transposase of the Tol2 element, an Ac-like element from the Japanese medaka fish, and its transposition in the zebrafish germ lineage. *Proc Natl Acad Sci U S A* **97**, 11403-8.
Kawakami, K., Takeda, H., Kawakami, N., Kobayashi, M., Matsuda, N. and Mishina, M. (2004). A transposon-mediated gene trap approach identifies developmentally regulated genes in zebrafish. *Dev Cell* **7**, 133-44.
Kearney, J. B., Ambler, C. A., Monaco, K. A., Johnson, N., Rapoport, R. G. and Bautch, V. L. (2002). Vascular endothelial growth factor receptor Flt-1 negatively regulates developmental blood vessel formation by modulating endothelial cell division. *Blood* **99**, 2397-407.
Kendall, R. L. and Thomas, K. A. (1993). Inhibition of vascular endothelial cell growth factor activity by an endogenously encoded soluble receptor. *Proc Natl Acad Sci U S A* **90**, 10705-9.
Kent, G., Iles, R., Bear, C. E., Huan, L. J., Griesenbach, U., McKerlie, C., Frndova, H., Ackerley, C., Gosselin, D., Radzioch, D. et al. (1997). Lung disease in mice with cystic fibrosis. *J Clin Invest* **100**, 3060-9.
Kiuchi-Saishin, Y., Gotoh, S., Furuse, M., Takasuga, A., Tano, Y. and Tsukita, S. (2002). Differential expression patterns of claudins, tight junction membrane proteins, in mouse nephron segments. *J Am Soc Nephrol* **13**, 875-86.
Klambt, C., Glazer, L. and Shilo, B. Z. (1992). breathless, a Drosophila FGF receptor homolog, is essential for migration of tracheal and specific midline glial cells. *Genes Dev* **6**, 1668-78.
Komatsu, Y., Kaartinen, V. and Mishina, Y. (2011). Cell cycle arrest in node cells governs ciliogenesis at the node to break left-right symmetry. *Development* **138**, 3915-20.
Kotani, T. and Kawakami, K. (2008). Misty somites, a maternal effect gene identified by transposon-mediated insertional mutagenesis in zebrafish that is essential for the somite boundary maintenance. *Dev Biol* **316**, 383-96.
Krause, G., Winkler, L., Mueller, S. L., Haseloff, R. F., Piontek, J. and Blasig, I. E. (2008). Structure and function of claudins. *Biochim Biophys Acta* **1778**, 631-45.
Krause, G., Winkler, L., Piehl, C., Blasig, I., Piontek, J. and Muller, S. L. (2009). Structure and function of extracellular claudin domains. *Ann N Y Acad Sci* **1165**, 34-43.
Kwan, K. M., Fujimoto, E., Grabher, C., Mangum, B. D., Hardy, M. E., Campbell, D. S., Parant, J. M., Yost, H. J., Kanki, J. P. and Chien, C. B. (2007). The Tol2kit: a multisite

gateway-based construction kit for Tol2 transposon transgenesis constructs. *Dev Dyn* **236**, 3088-99.
Labalette, C., Bouchoucha, Y. X., Wassef, M. A., Gongal, P. A., Le Men, J., Becker, T., Gilardi-Hebenstreit, P. and Charnay, P. (2011). Hindbrain patterning requires fine-tuning of early krox20 transcription by Sprouty 4. *Development* **138**, 317-26.
Lamont, R. E., Lamont, E. J. and Childs, S. J. (2009). Antagonistic interactions among Plexins regulate the timing of intersegmental vessel formation. *Dev Biol* **331**, 199-209.
Lampugnani, M. G., Orsenigo, F., Gagliani, M. C., Tacchetti, C. and Dejana, E. (2006). Vascular endothelial cadherin controls VEGFR-2 internalization and signaling from intracellular compartments. *J Cell Biol* **174**, 593-604.
Lampugnani, M. G., Zanetti, A., Breviario, F., Balconi, G., Orsenigo, F., Corada, M., Spagnuolo, R., Betson, M., Braga, V. and Dejana, E. (2002). VE-cadherin regulates endothelial actin activating Rac and increasing membrane association of Tiam. *Mol Biol Cell* **13**, 1175-89.
Larrivee, B., Freitas, C., Trombe, M., Lv, X., Delafarge, B., Yuan, L., Bouvree, K., Breant, C., Del Toro, R., Brechot, N. et al. (2007). Activation of the UNC5B receptor by Netrin-1 inhibits sprouting angiogenesis. *Genes Dev* **21**, 2433-47.
Lawson, N. D., Scheer, N., Pham, V. N., Kim, C. H., Chitnis, A. B., Campos-Ortega, J. A. and Weinstein, B. M. (2001). Notch signaling is required for arterial-venous differentiation during embryonic vascular development. *Development* **128**, 3675-83.
Lawson, N. D., Vogel, A. M. and Weinstein, B. M. (2002). sonic hedgehog and vascular endothelial growth factor act upstream of the Notch pathway during arterial endothelial differentiation. *Dev Cell* **3**, 127-36.
Lawson, N. D. and Weinstein, B. M. (2002). In vivo imaging of embryonic vascular development using transgenic zebrafish. *Dev Biol* **248**, 307-18.
Le, T. L., Yap, A. S. and Stow, J. L. (1999). Recycling of E-cadherin: a potential mechanism for regulating cadherin dynamics. *J Cell Biol* **146**, 219-32.
Leach, L., Babawale, M. O., Anderson, M. and Lammiman, M. (2002). Vasculogenesis, angiogenesis and the molecular organisation of endothelial junctions in the early human placenta. *J Vasc Res* **39**, 246-59.
Legan, P. K., Collins, J. E. and Garrod, D. R. (1992). The molecular biology of desmosomes and hemidesmosomes: "what's in a name"? *Bioessays* **14**, 385-93.
Leslie, J. D., Ariza-McNaughton, L., Bermange, A. L., McAdow, R., Johnson, S. L. and Lewis, J. (2007). Endothelial signalling by the Notch ligand Delta-like 4 restricts angiogenesis. *Development* **134**, 839-44.
Leung, D. W., Cachianes, G., Kuang, W. J., Goeddel, D. V. and Ferrara, N. (1989). Vascular endothelial growth factor is a secreted angiogenic mitogen. *Science* **246**, 1306-9.
Levayer, R., Pelissier-Monier, A. and Lecuit, T. (2011). Spatial regulation of Dia and Myosin-II by RhoGEF2 controls initiation of E-cadherin endocytosis during epithelial morphogenesis. *Nat Cell Biol* **13**, 529-40.
Liao, E. C., Paw, B. H., Oates, A. C., Pratt, S. J., Postlethwait, J. H. and Zon, L. I. (1998). SCL/Tal-1 transcription factor acts downstream of cloche to specify hematopoietic and vascular progenitors in zebrafish. *Genes Dev* **12**, 621-6.
Liao, W., Bisgrove, B. W., Sawyer, H., Hug, B., Bell, B., Peters, K., Grunwald, D. J. and Stainier, D. Y. (1997). The zebrafish gene cloche acts upstream of a flk-1 homologue to regulate endothelial cell differentiation. *Development* **124**, 381-9.
Liebner, S., Kniesel, U., Kalbacher, H. and Wolburg, H. (2000). Correlation of tight junction morphology with the expression of tight junction proteins in blood-brain barrier endothelial cells. *Eur J Cell Biol* **79**, 707-17.
Lievano, S., Alarcon, L., Chavez-Munguia, B. and Gonzalez-Mariscal, L. (2006). Endothelia of term human placentae display diminished expression of tight junction proteins during preeclampsia. *Cell Tissue Res* **324**, 433-48.
Lints, T. J., Parsons, L. M., Hartley, L., Lyons, I. and Harvey, R. P. (1993). Nkx-2.5: a novel murine homeobox gene expressed in early heart progenitor cells and their myogenic descendants. *Development* **119**, 419-31.
Liu, F., Walmsley, M., Rodaway, A. and Patient, R. (2008). Fli1 acts at the top of the transcriptional network driving blood and endothelial development. *Curr Biol* **18**, 1234-40.
Lobov, I. B., Renard, R. A., Papadopoulos, N., Gale, N. W., Thurston, G., Yancopoulos, G. D. and Wiegand, S. J. (2007). Delta-like ligand 4 (Dll4) is induced by VEGF as a negative regulator of angiogenic sprouting. *Proc Natl Acad Sci U S A* **104**, 3219-24.

Lohela, M., Bry, M., Tammela, T. and Alitalo, K. (2009). VEGFs and receptors involved in angiogenesis versus lymphangiogenesis. *Curr Opin Cell Biol* **21**, 154-65.
Lu, X., Le Noble, F., Yuan, L., Jiang, Q., De Lafarge, B., Sugiyama, D., Breant, C., Claes, F., De Smet, F., Thomas, J. L. et al. (2004). The netrin receptor UNC5B mediates guidance events controlling morphogenesis of the vascular system. *Nature* **432**, 179-86.
Matsuda, M., Kubo, A., Furuse, M. and Tsukita, S. (2004). A peculiar internalization of claudins, tight junction-specific adhesion molecules, during the intercellular movement of epithelial cells. *J Cell Sci* **117**, 1247-57.
Matter, K. and Balda, M. S. (2003). Signalling to and from tight junctions. *Nat Rev Mol Cell Biol* **4**, 225-36.
McAnally, A. A. and Yampolsky, L. Y. (2009). Widespread transcriptional autosomal dosage compensation in Drosophila correlates with gene expression level. *Genome Biol Evol* **2**, 44-52.
McCarthy, K. M., Francis, S. A., McCormack, J. M., Lai, J., Rogers, R. A., Skare, I. B., Lynch, R. D. and Schneeberger, E. E. (2000). Inducible expression of claudin-1-myc but not occludin-VSV-G results in aberrant tight junction strand formation in MDCK cells. *J Cell Sci* **113 Pt 19**, 3387-98.
McNeill, H., Ryan, T. A., Smith, S. J. and Nelson, W. J. (1993). Spatial and temporal dissection of immediate and early events following cadherin-mediated epithelial cell adhesion. *J Cell Biol* **120**, 1217-26.
Meng, X., Noyes, M. B., Zhu, L. J., Lawson, N. D. and Wolfe, S. A. (2008). Targeted gene inactivation in zebrafish using engineered zinc-finger nucleases. *Nat Biotechnol* **26**, 695-701.
Metzger, R. J., Klein, O. D., Martin, G. R. and Krasnow, M. A. (2008). The branching programme of mouse lung development. *Nature* **453**, 745-50.
Mineta, K., Yamamoto, Y., Yamazaki, Y., Tanaka, H., Tada, Y., Saito, K., Tamura, A., Igarashi, M., Endo, T., Takeuchi, K. et al. (2011). Predicted expansion of the claudin multigene family. *FEBS Lett* **585**, 606-12.
Montero-Balaguer, M., Swirsding, K., Orsenigo, F., Cotelli, F., Mione, M. and Dejana, E. (2009). Stable vascular connections and remodeling require full expression of VE-cadherin in zebrafish embryos. *PLoS One* **4**, e5772.
Morita, K., Sasaki, H., Furuse, M. and Tsukita, S. (1999). Endothelial claudin: claudin-5/TMVCF constitutes tight junction strands in endothelial cells. *J Cell Biol* **147**, 185-94.
Moriwaki, K., Tsukita, S. and Furuse, M. (2007). Tight junctions containing claudin 4 and 6 are essential for blastocyst formation in preimplantation mouse embryos. *Dev Biol* **312**, 509-22.
Nava, P., Capaldo, C. T., Koch, S., Kolegraff, K., Rankin, C. R., Farkas, A. E., Feasel, M. E., Li, L., Addis, C., Parkos, C. A. et al. (2011). JAM-A regulates epithelial proliferation through Akt/beta-catenin signalling. *EMBO Rep* **12**, 314-20.
Nicoli, S., Standley, C., Walker, P., Hurlstone, A., Fogarty, K. E. and Lawson, N. D. (2010). MicroRNA-mediated integration of haemodynamics and Vegf signalling during angiogenesis. *Nature* **464**, 1196-200.
Nitta, T., Hata, M., Gotoh, S., Seo, Y., Sasaki, H., Hashimoto, N., Furuse, M. and Tsukita, S. (2003). Size-selective loosening of the blood-brain barrier in claudin-5-deficient mice. *J Cell Biol* **161**, 653-60.
Ooshio, T., Fujita, N., Yamada, A., Sato, T., Kitagawa, Y., Okamoto, R., Nakata, S., Miki, A., Irie, K. and Takai, Y. (2007). Cooperative roles of Par-3 and afadin in the formation of adherens and tight junctions. *J Cell Sci* **120**, 2352-65.
Park, J. E., Chen, H. H., Winer, J., Houck, K. A. and Ferrara, N. (1994). Placenta growth factor. Potentiation of vascular endothelial growth factor bioactivity, in vitro and in vivo, and high affinity binding to Flt-1 but not to Flk-1/KDR. *J Biol Chem* **269**, 25646-54.
Park, K. W., Crouse, D., Lee, M., Karnik, S. K., Sorensen, L. K., Murphy, K. J., Kuo, C. J. and Li, D. Y. (2004). The axonal attractant Netrin-1 is an angiogenic factor. *Proc Natl Acad Sci U S A* **101**, 16210-5.
Park, K. W., Urness, L. D., Senchuk, M. M., Colvin, C. J., Wythe, J. D., Chien, C. B. and Li, D. Y. (2005). Identification of new netrin family members in zebrafish: developmental expression of netrin 2 and netrin 4. *Dev Dyn* **234**, 726-31.
Patel, H. and Brunton, V. G. (2009). Loss of FrmA leads to increased cell-cell adhesion and impaired multi-cellular development of Dictyostelium cells. *Cell Mol Life Sci* **66**, 145-55.
Perryn, E. D., Czirok, A. and Little, C. D. (2008). Vascular sprout formation entails tissue deformations and VE-cadherin-dependent cell-autonomous motility. *Dev Biol* **313**, 545-55.

Pham, V. N., Lawson, N. D., Mugford, J. W., Dye, L., Castranova, D., Lo, B. and Weinstein, B. M. (2007). Combinatorial function of ETS transcription factors in the developing vasculature. *Dev Biol* **303**, 772-83.
Phng, L. K. and Gerhardt, H. (2009). Angiogenesis: a team effort coordinated by notch. *Dev Cell* **16**, 196-208.
Phng, L. K., Potente, M., Leslie, J. D., Babbage, J., Nyqvist, D., Lobov, I., Ondr, J. K., Rao, S., Lang, R. A., Thurston, G. et al. (2009). Nrarp coordinates endothelial Notch and Wnt signaling to control vessel density in angiogenesis. *Dev Cell* **16**, 70-82.
Piontek, J., Winkler, L., Wolburg, H., Muller, S. L., Zuleger, N., Piehl, C., Wiesner, B., Krause, G. and Blasig, I. E. (2008). Formation of tight junction: determinants of homophilic interaction between classic claudins. *FASEB J* **22**, 146-58.
Pollard, S. M., Parsons, M. J., Kamei, M., Kettleborough, R. N., Thomas, K. A., Pham, V. N., Bae, M. K., Scott, A., Weinstein, B. M. and Stemple, D. L. (2006). Essential and overlapping roles for laminin alpha chains in notochord and blood vessel formation. *Dev Biol* **289**, 64-76.
Pollard, T. D. (2010). Mechanics of cytokinesis in eukaryotes. *Curr Opin Cell Biol* **22**, 50-6.
Polyak, K., Lee, M. H., Erdjument-Bromage, H., Koff, A., Roberts, J. M., Tempst, P. and Massague, J. (1994). Cloning of p27Kip1, a cyclin-dependent kinase inhibitor and a potential mediator of extracellular antimitogenic signals. *Cell* **78**, 59-66.
Powell, D. W. (1981). Barrier function of epithelia. *Am J Physiol* **241**, G275-88.
Reyes, J. L., Lamas, M., Martin, D., del Carmen Namorado, M., Islas, S., Luna, J., Tauc, M. and Gonzalez-Mariscal, L. (2002). The renal segmental distribution of claudins changes with development. *Kidney Int* **62**, 476-87.
Ribeiro, C., Neumann, M. and Affolter, M. (2004). Genetic control of cell intercalation during tracheal morphogenesis in Drosophila. *Curr Biol* **14**, 2197-207.
Risau, W. (1997). Mechanisms of angiogenesis. *Nature* **386**, 671-4.
Risau, W. and Flamme, I. (1995). Vasculogenesis. *Annu Rev Cell Dev Biol* **11**, 73-91.
Roberts, D. M., Kearney, J. B., Johnson, J. H., Rosenberg, M. P., Kumar, R. and Bautch, V. L. (2004). The vascular endothelial growth factor (VEGF) receptor Flt-1 (VEGFR-1) modulates Flk-1 (VEGFR-2) signaling during blood vessel formation. *Am J Pathol* **164**, 1531-5.
Robu, M. E., Larson, J. D., Nasevicius, A., Beiraghi, S., Brenner, C., Farber, S. A. and Ekker, S. C. (2007). p53 activation by knockdown technologies. *PLoS Genet* **3**, e78.
Rozmahel, R., Wilschanski, M., Matin, A., Plyte, S., Oliver, M., Auerbach, W., Moore, A., Forstner, J., Durie, P., Nadeau, J. et al. (1996). Modulation of disease severity in cystic fibrosis transmembrane conductance regulator deficient mice by a secondary genetic factor. *Nat Genet* **12**, 280-7.
Ruffer, C. and Gerke, V. (2004). The C-terminal cytoplasmic tail of claudins 1 and 5 but not its PDZ-binding motif is required for apical localization at epithelial and endothelial tight junctions. *Eur J Cell Biol* **83**, 135-44.
Ruhrberg, C., Gerhardt, H., Golding, M., Watson, R., Ioannidou, S., Fujisawa, H., Betsholtz, C. and Shima, D. T. (2002). Spatially restricted patterning cues provided by heparin-binding VEGF-A control blood vessel branching morphogenesis. *Genes Dev* **16**, 2684-98.
Sander, J. D., Dahlborg, E. J., Goodwin, M. J., Cade, L., Zhang, F., Cifuentes, D., Curtin, S. J., Blackburn, J. S., Thibodeau-Beganny, S., Qi, Y. et al. (2011). Selection-free zinc-finger-nuclease engineering by context-dependent assembly (CoDA). *Nat Methods* **8**, 67-9.
Sasaki, H., Matsui, C., Furuse, K., Mimori-Kiyosue, Y., Furuse, M. and Tsukita, S. (2003). Dynamic behavior of paired claudin strands within apposing plasma membranes. *Proc Natl Acad Sci U S A* **100**, 3971-6.
Sato, T., Fujita, N., Yamada, A., Ooshio, T., Okamoto, R., Irie, K. and Takai, Y. (2006). Regulation of the assembly and adhesion activity of E-cadherin by nectin and afadin for the formation of adherens junctions in Madin-Darby canine kidney cells. *J Biol Chem* **281**, 5288-99.
Shalaby, F., Rossant, J., Yamaguchi, T. P., Gertsenstein, M., Wu, X. F., Breitman, M. L. and Schuh, A. C. (1995). Failure of blood-island formation and vasculogenesis in Flk-1-deficient mice. *Nature* **376**, 62-6.
Shaye, D. D., Casanova, J. and Llimargas, M. (2008). Modulation of intracellular trafficking regulates cell intercalation in the Drosophila trachea. *Nat Cell Biol* **10**, 964-70.

Sheldon, R., Moy, A., Lindsley, K., Shasby, S. and Shasby, D. M. (1993). Role of myosin light-chain phosphorylation in endothelial cell retraction. *Am J Physiol* **265**, L606-12.
Shen, L., Weber, C. R. and Turner, J. R. (2008). The tight junction protein complex undergoes rapid and continuous molecular remodeling at steady state. *J Cell Biol* **181**, 683-95.
Siddiqui, M., Sheikh, H., Tran, C. and Bruce, A. E. (2010). The tight junction component Claudin E is required for zebrafish epiboly. *Dev Dyn* **239**, 715-22.
Siekmann, A. F. and Lawson, N. D. (2007). Notch signalling limits angiogenic cell behaviour in developing zebrafish arteries. *Nature* **445**, 781-4.
Siekmann, A. F., Standley, C., Fogarty, K. E., Wolfe, S. A. and Lawson, N. D. (2009). Chemokine signaling guides regional patterning of the first embryonic artery. *Genes Dev* **23**, 2272-7.
Simionescu, M., Simionescu, N. and Palade, G. E. (1975). Segmental differentiations of cell junctions in the vascular endothelium. The microvasculature. *J Cell Biol* **67**, 863-85.
Simon, A. M. and Goodenough, D. A. (1998). Diverse functions of vertebrate gap junctions. *Trends Cell Biol* **8**, 477-83.
Sirotkin, H., Morrow, B., Saint-Jore, B., Puech, A., Das Gupta, R., Patanjali, S. R., Skoultchi, A., Weissman, S. M. and Kucherlapati, R. (1997). Identification, characterization, and precise mapping of a human gene encoding a novel membrane-spanning protein from the 22q11 region deleted in velo-cardio-facial syndrome. *Genomics* **42**, 245-51.
Skau, C. T., Courson, D. S., Bestul, A. J., Winkelman, J. D., Rock, R. S., Sirotkin, V. and Kovar, D. R. (2011). Actin filament bundling by fimbrin is important for endocytosis, cytokinesis, and polarization in fission yeast. *J Biol Chem* **286**, 26964-77.
Sourisseau, T., Georgiadis, A., Tsapara, A., Ali, R. R., Pestell, R., Matter, K. and Balda, M. S. (2006). Regulation of PCNA and cyclin D1 expression and epithelial morphogenesis by the ZO-1-regulated transcription factor ZONAB/DbpA. *Mol Cell Biol* **26**, 2387-98.
St Johnston, D. and Ahringer, J. (2010). Cell polarity in eggs and epithelia: parallels and diversity. *Cell* **141**, 757-74.
Stemple, D. L., Solnica-Krezel, L., Zwartkruis, F., Neuhauss, S. C., Schier, A. F., Malicki, J., Stainier, D. Y., Abdelilah, S., Rangini, Z., Mountcastle-Shah, E. et al. (1996). Mutations affecting development of the notochord in zebrafish. *Development* **123**, 117-28.
Stenberg, P., Lundberg, L. E., Johansson, A. M., Ryden, P., Svensson, M. J. and Larsson, J. (2009). Buffering of segmental and chromosomal aneuploidies in Drosophila melanogaster. *PLoS Genet* **5**, e1000465.
Stevenson, B. R., Siliciano, J. D., Mooseker, M. S. and Goodenough, D. A. (1986). Identification of ZO-1: a high molecular weight polypeptide associated with the tight junction (zonula occludens) in a variety of epithelia. *J Cell Biol* **103**, 755-66.
Stork, T., Engelen, D., Krudewig, A., Silies, M., Bainton, R. J. and Klambt, C. (2008). Organization and function of the blood-brain barrier in Drosophila. *J Neurosci* **28**, 587-97.
Stuart, G. W., McMurray, J. V. and Westerfield, M. (1988). Replication, integration and stable germ-line transmission of foreign sequences injected into early zebrafish embryos. *Development* **103**, 403-12.
Stuart, G. W., Vielkind, J. R., McMurray, J. V. and Westerfield, M. (1990). Stable lines of transgenic zebrafish exhibit reproducible patterns of transgene expression. *Development* **109**, 577-84.
Suchting, S., Freitas, C., le Noble, F., Benedito, R., Breant, C., Duarte, A. and Eichmann, A. (2007). The Notch ligand Delta-like 4 negatively regulates endothelial tip cell formation and vessel branching. *Proc Natl Acad Sci U S A* **104**, 3225-30.
Summerton, J. E. (2007). Morpholino, siRNA, and S-DNA compared: impact of structure and mechanism of action on off-target effects and sequence specificity. *Curr Top Med Chem* **7**, 651-60.
Sun, S. C., Wang, Z. B., Xu, Y. N., Lee, S. E., Cui, X. S. and Kim, N. H. (2011). Arp2/3 complex regulates asymmetric division and cytokinesis in mouse oocytes. *PLoS One* **6**, e18392.
Sutherland, D., Samakovlis, C. and Krasnow, M. A. (1996). branchless encodes a Drosophila FGF homolog that controls tracheal cell migration and the pattern of branching. *Cell* **87**, 1091-101.

Suzuki, A., Hirata, M., Kamimura, K., Maniwa, R., Yamanaka, T., Mizuno, K., Kishikawa, M., Hirose, H., Amano, Y., Izumi, N. et al. (2004). aPKC acts upstream of PAR-1b in both the establishment and maintenance of mammalian epithelial polarity. *Curr Biol* **14**, 1425-35.
Suzuki, A., Ishiyama, C., Hashiba, K., Shimizu, M., Ebnet, K. and Ohno, S. (2002). aPKC kinase activity is required for the asymmetric differentiation of the premature junctional complex during epithelial cell polarization. *J Cell Sci* **115**, 3565-73.
Taddei, A., Giampietro, C., Conti, A., Orsenigo, F., Breviario, F., Pirazzoli, V., Potente, M., Daly, C., Dimmeler, S. and Dejana, E. (2008). Endothelial adherens junctions control tight junctions by VE-cadherin-mediated upregulation of claudin-5. *Nat Cell Biol* **10**, 923-34.
Takahashi, K., Nakanishi, H., Miyahara, M., Mandai, K., Satoh, K., Satoh, A., Nishioka, H., Aoki, J., Nomoto, A., Mizoguchi, A. et al. (1999). Nectin/PRR: an immunoglobulin-like cell adhesion molecule recruited to cadherin-based adherens junctions through interaction with Afadin, a PDZ domain-containing protein. *J Cell Biol* **145**, 539-49.
Takahashi, T., Yamaguchi, S., Chida, K. and Shibuya, M. (2001). A single autophosphorylation site on KDR/Flk-1 is essential for VEGF-A-dependent activation of PLC-gamma and DNA synthesis in vascular endothelial cells. *EMBO J* **20**, 2768-78.
Takai, Y., Miyoshi, J., Ikeda, W. and Ogita, H. (2008). Nectins and nectin-like molecules: roles in contact inhibition of cell movement and proliferation. *Nat Rev Mol Cell Biol* **9**, 603-15.
Tambe, D. T., Hardin, C. C., Angelini, T. E., Rajendran, K., Park, C. Y., Serra-Picamal, X., Zhou, E. H., Zaman, M. H., Butler, J. P., Weitz, D. A. et al. (2011). Collective cell guidance by cooperative intercellular forces. *Nat Mater* **10**, 469-75.
Tammela, T., Zarkada, G., Wallgard, E., Murtomaki, A., Suchting, S., Wirzenius, M., Waltari, M., Hellstrom, M., Schomber, T., Peltonen, R. et al. (2008). Blocking VEGFR-3 suppresses angiogenic sprouting and vascular network formation. *Nature* **454**, 656-60.
Tanaka-Matakatsu, M., Uemura, T., Oda, H., Takeichi, M. and Hayashi, S. (1996). Cadherin-mediated cell adhesion and cell motility in Drosophila trachea regulated by the transcription factor Escargot. *Development* **122**, 3697-705.
Thermes, V., Grabher, C., Ristoratore, F., Bourrat, F., Choulika, A., Wittbrodt, J. and Joly, J. S. (2002). I-SceI meganuclease mediates highly efficient transgenesis in fish. *Mech Dev* **118**, 91-8.
Thisse, B., Thisse, C. (2004). Fast Release Clones: A High Throughput Expression Analysis, (ed.: ZFIN Direct Data Submission.
Thisse, C. and Zon, L. I. (2002). Organogenesis--heart and blood formation from the zebrafish point of view. *Science* **295**, 457-62.
Tiklova, K., Senti, K. A., Wang, S., Graslund, A. and Samakovlis, C. (2010). Epithelial septate junction assembly relies on melanotransferrin iron binding and endocytosis in Drosophila. *Nat Cell Biol* **12**, 1071-7.
Torres-Vazquez, J., Gitler, A. D., Fraser, S. D., Berk, J. D., Van, N. P., Fishman, M. C., Childs, S., Epstein, J. A. and Weinstein, B. M. (2004). Semaphorin-plexin signaling guides patterning of the developing vasculature. *Dev Cell* **7**, 117-23.
Tu, C. T., Yang, T. C. and Tsai, H. J. (2009). Nkx2.7 and Nkx2.5 function redundantly and are required for cardiac morphogenesis of zebrafish embryos. *PLoS One* **4**, e4249.
Uemura, T., Oda, H., Kraut, R., Hayashi, S., Kotaoka, Y. and Takeichi, M. (1996). Zygotic Drosophila E-cadherin expression is required for processes of dynamic epithelial cell rearrangement in the Drosophila embryo. *Genes Dev* **10**, 659-71.
van Hinsbergh, V. W. and Koolwijk, P. (2008). Endothelial sprouting and angiogenesis: matrix metalloproteinases in the lead. *Cardiovasc Res* **78**, 203-12.
Van Itallie, C., Rahner, C. and Anderson, J. M. (2001). Regulated expression of claudin-4 decreases paracellular conductance through a selective decrease in sodium permeability. *J Clin Invest* **107**, 1319-27.
Van Itallie, C. M. and Anderson, J. M. (2004a). The molecular physiology of tight junction pores. *Physiology (Bethesda)* **19**, 331-8.
Van Itallie, C. M. and Anderson, J. M. (2004b). The role of claudins in determining paracellular charge selectivity. *Proc Am Thorac Soc* **1**, 38-41.
Van Itallie, C. M. and Anderson, J. M. (2006). Claudins and epithelial paracellular transport. *Annu Rev Physiol* **68**, 403-29.
Van Itallie, C. M., Fanning, A. S. and Anderson, J. M. (2003). Reversal of charge selectivity in cation or anion-selective epithelial lines by expression of different claudins. *Am J Physiol Renal Physiol* **285**, F1078-84.

Van Itallie, C. M., Gambling, T. M., Carson, J. L. and Anderson, J. M. (2005). Palmitoylation of claudins is required for efficient tight-junction localization. *J Cell Sci* **118**, 1427-36.
Vavylonis, D., Wu, J. Q., Hao, S., O'Shaughnessy, B. and Pollard, T. D. (2008). Assembly mechanism of the contractile ring for cytokinesis by fission yeast. *Science* **319**, 97-100.
Venken, K. J. and Bellen, H. J. (2007). Transgenesis upgrades for Drosophila melanogaster. *Development* **134**, 3571-84.
Villefranc, J. A., Amigo, J. and Lawson, N. D. (2007). Gateway compatible vectors for analysis of gene function in the zebrafish. *Dev Dyn* **236**, 3077-87.
Virgintino, D., Errede, M., Robertson, D., Capobianco, C., Girolamo, F., Vimercati, A., Bertossi, M. and Roncali, L. (2004). Immunolocalization of tight junction proteins in the adult and developing human brain. *Histochem Cell Biol* **122**, 51-9.
Vogeli, K. M., Jin, S. W., Martin, G. R. and Stainier, D. Y. (2006). A common progenitor for haematopoietic and endothelial lineages in the zebrafish gastrula. *Nature* **443**, 337-9.
Wagner, D. S., Dosch, R., Mintzer, K. A., Wiemelt, A. P. and Mullins, M. C. (2004). Maternal control of development at the midblastula transition and beyond: mutants from the zebrafish II. *Dev Cell* **6**, 781-90.
Wang, H. U., Chen, Z. F. and Anderson, D. J. (1998). Molecular distinction and angiogenic interaction between embryonic arteries and veins revealed by ephrin-B2 and its receptor Eph-B4. *Cell* **93**, 741-53.
Wang, S., Li, X., Parra, M., Verdin, E., Bassel-Duby, R. and Olson, E. N. (2008). Control of endothelial cell proliferation and migration by VEGF signaling to histone deacetylase 7. *Proc Natl Acad Sci U S A* **105**, 7738-43.
Wang, Y., Kaiser, M. S., Larson, J. D., Nasevicius, A., Clark, K. J., Wadman, S. A., Roberg-Perez, S. E., Ekker, S. C., Hackett, P. B., McGrail, M. et al. (2010). Moesin1 and Ve-cadherin are required in endothelial cells during in vivo tubulogenesis. *Development* **137**, 3119-28.
Warga, R. M., Kane, D. A. and Ho, R. K. (2009). Fate mapping embryonic blood in zebrafish: multi- and unipotential lineages are segregated at gastrulation. *Dev Cell* **16**, 744-55.
Watson, C. J. and Khaled, W. T. (2008). Mammary development in the embryo and adult: a journey of morphogenesis and commitment. *Development* **135**, 995-1003.
Weinstein, B. M. (2005). Vessels and nerves: marching to the same tune. *Cell* **120**, 299-302.
Weinstein, B. M., Stemple, D. L., Driever, W. and Fishman, M. C. (1995). Gridlock, a localized heritable vascular patterning defect in the zebrafish. *Nat Med* **1**, 1143-7.
Wen, H., Watry, D. D., Marcondes, M. C. and Fox, H. S. (2004). Selective decrease in paracellular conductance of tight junctions: role of the first extracellular domain of claudin-5. *Mol Cell Biol* **24**, 8408-17.
Westerfield, M. (2000). The zebrafish book. A guide for the laboratory use of zebrafish Danio rerio, (ed.: Univ. of Oregon Press, Eugene.
Whitelaw, E., Tsai, S. F., Hogben, P. and Orkin, S. H. (1990). Regulated expression of globin chains and the erythroid transcription factor GATA-1 during erythropoiesis in the developing mouse. *Mol Cell Biol* **10**, 6596-606.
Wilcox, E. R., Burton, Q. L., Naz, S., Riazuddin, S., Smith, T. N., Ploplis, B., Belyantseva, I., Ben-Yosef, T., Liburd, N. A., Morell, R. J. et al. (2001). Mutations in the gene encoding tight junction claudin-14 cause autosomal recessive deafness DFNB29. *Cell* **104**, 165-72.
Wittchen, E. S., Haskins, J. and Stevenson, B. R. (1999). Protein interactions at the tight junction. Actin has multiple binding partners, and ZO-1 forms independent complexes with ZO-2 and ZO-3. *J Biol Chem* **274**, 35179-85.
Wittchen, E. S., Haskins, J. and Stevenson, B. R. (2000). Exogenous expression of the amino-terminal half of the tight junction protein ZO-3 perturbs junctional complex assembly. *J Cell Biol* **151**, 825-36.
Wolburg, H., Wolburg-Buchholz, K., Kraus, J., Rascher-Eggstein, G., Liebner, S., Hamm, S., Duffner, F., Grote, E. H., Risau, W. and Engelhardt, B. (2003). Localization of claudin-3 in tight junctions of the blood-brain barrier is selectively lost during experimental autoimmune encephalomyelitis and human glioblastoma multiforme. *Acta Neuropathol* **105**, 586-92.
Wu, C., Agrawal, S., Vasanji, A., Drazba, J., Sarkaria, S., Xie, J., Welch, C. M., Liu, M., Anand-Apte, B. and Horowitz, A. (2011). Rab13-dependent trafficking of RhoA is required for directional migration and angiogenesis. *J Biol Chem* **286**, 23511-20.

Wu, J. N., Nguyen, N., Aghazarian, M., Tan, Y., Sevrioukov, E. A., Mabuchi, M., Tang, W., Monserrate, J. P., White, K. and Brachmann, C. B. (2010). grim promotes programmed cell death of Drosophila microchaete glial cells. *Mech Dev* **127**, 407-17.
Wu, V. M., Schulte, J., Hirschi, A., Tepass, U. and Beitel, G. J. (2004). Sinuous is a Drosophila claudin required for septate junction organization and epithelial tube size control. *J Cell Biol* **164**, 313-23.
Wu, X. and Levine, A. J. (1994). p53 and E2F-1 cooperate to mediate apoptosis. *Proc Natl Acad Sci U S A* **91**, 3602-6.
Xia, P., Aiello, L. P., Ishii, H., Jiang, Z. Y., Park, D. J., Robinson, G. S., Takagi, H., Newsome, W. P., Jirousek, M. R. and King, G. L. (1996). Characterization of vascular endothelial growth factor's effect on the activation of protein kinase C, its isoforms, and endothelial cell growth. *J Clin Invest* **98**, 2018-26.
Xie, J., Farage, E., Sugimoto, M. and Anand-Apte, B. (2010). A novel transgenic zebrafish model for blood-brain and blood-retinal barrier development. *BMC Dev Biol* **10**, 76.
Yaniv, K., Isogai, S., Castranova, D., Dye, L., Hitomi, J. and Weinstein, B. M. (2006). Live imaging of lymphatic development in the zebrafish. *Nat Med* **12**, 711-6.
Yee, C. S., Chandrasekhar, A., Halloran, M. C., Shoji, W., Warren, J. T. and Kuwada, J. Y. (1999). Molecular cloning, expression, and activity of zebrafish semaphorin Z1a. *Brain Res Bull* **48**, 581-93.
Yorozu, S., Wong, A., Fischer, B. J., Dankert, H., Kernan, M. J., Kamikouchi, A., Ito, K. and Anderson, D. J. (2009). Distinct sensory representations of wind and near-field sound in the Drosophila brain. *Nature* **458**, 201-5.
You, L. R., Lin, F. J., Lee, C. T., DeMayo, F. J., Tsai, M. J. and Tsai, S. Y. (2005). Suppression of Notch signalling by the COUP-TFII transcription factor regulates vein identity. *Nature* **435**, 98-104.
Yu, A. S., Enck, A. H., Lencer, W. I. and Schneeberger, E. E. (2003). Claudin-8 expression in Madin-Darby canine kidney cells augments the paracellular barrier to cation permeation. *J Biol Chem* **278**, 17350-9.
Zeissig, S., Burgel, N., Gunzel, D., Richter, J., Mankertz, J., Wahnschaffe, U., Kroesen, A. J., Zeitz, M., Fromm, M. and Schulzke, J. D. (2007). Changes in expression and distribution of claudin 2, 5 and 8 lead to discontinuous tight junctions and barrier dysfunction in active Crohn's disease. *Gut* **56**, 61-72.
Zhang, F., Cong, L., Lodato, S., Kosuri, S., Church, G. M. and Arlotta, P. (2011). Efficient construction of sequence-specific TAL effectors for modulating mammalian transcription. *Nat Biotechnol* **29**, 149-53.
Zhang, J., Piontek, J., Wolburg, H., Piehl, C., Liss, M., Otten, C., Christ, A., Willnow, T. E., Blasig, I. E. and Abdelilah-Seyfried, S. (2010). Establishment of a neuroepithelial barrier by Claudin5a is essential for zebrafish brain ventricular lumen expansion. *Proc Natl Acad Sci U S A* **107**, 1425-30.
Zhong, T. P., Childs, S., Leu, J. P. and Fishman, M. C. (2001). Gridlock signalling pathway fashions the first embryonic artery. *Nature* **414**, 216-20.
Zhong, T. P., Rosenberg, M., Mohideen, M. A., Weinstein, B. and Fishman, M. C. (2000). gridlock, an HLH gene required for assembly of the aorta in zebrafish. *Science* **287**, 1820-4.

Lebenslauf - Alice Krudewig

Geburtsdatum:	25.09.1981
Geburtsort:	Bocholt, Deutschland
Eltern:	Klaus Krudewig, Monika Krudewig geb. Haschke

Schulbildung

1988 – 1992	Grundschule Bocholt
1992 – 2001	Mariengymnasium Bocholt, Abitur

Studium

10/ 2001 – 07/2004	Grundstudium des Diplomstudiengangs Biologie an der WWU Münster, Deutschland
08/ 2004 – 01/2005	Studium der Biologie an der Macquarie University, Sydney, Australien
02/2005 – 12/2006	Hauptstudium des Diplomstudiengangs Biologie an der WWU Münster, Deutschland Diplomarbeit am Institut für Neuro- und Verhaltensbiologie, Arbeitsgruppe Prof. Dr. Christian Klämbt
01/2007 – 07/2007	Wissenschaftliche Arbeit am Institut für Neuro- und Verhaltensbiologie, Arbeitsgruppe Prof. Dr. Christian Klämbt

Promotion

9/2007 – 9/2012	Promotionsstudiengang an der Universität Basel, Biozentrum, Arbeitsgruppe Prof. Dr. Markus Affolter; Koreferent und PhD comittee: Prof. Dr. Rolf Zeller; PhD comittee: Prof. Dr. Anne Spang Werner-Siemens Stipendium

Basel, den